

Terrapin Rocket Team Project Honu

Team 121 Project Technical Report to the 2024 Spaceport America Cup

Michael Mallamaci*, Sunjum Mehta†, Andrew Bean‡, Nathan Roy§, Sophie Jack¶, Matthew Chou||, Varun Unnithan**, Joseph Hauerstein††, Cooper Brown‡‡, Jeffery Chen§§, Ohm Sapa¶¶, Ignacio Lopez-Etchegoyen***, Pratik Janardhanan†††

University of Maryland - Department of Aerospace Engineering, College Park, MD, 20742

This document presents the University of Maryland's 10,000 foot SRAD Motor Category rocket, Honu. It is the fourth time that the team will be attending the Spaceport America Cup in person since 2018, and the team has built on lessons learned over those years. The design process for Honu is centered around a proven design that has undergone rigorous testing over the last two years and aims to refine many of the components involved. An SRAD 98 mm N motor utilizing a custom purple propellant propels the rocket in flight with it being static tested and flown in a test flight prior to the competition. The motor is sized to slightly overshoot the 10,000 foot target in order to allow the rocket's Airbrake system to dial in the altitude. The Airbrake predicts the rocket's trajectory and actively trims its altitude during ascent. It employs a Model Predictive Controller with novel barometric error correction to account for pressure drops due to flap deployment. The CubeSat payload for this rocket deploys a vehicle that recovers under parachute. The vehicle uses a tail rotor and tilted parachute to control the descent path for easier recovery. Student designed avionics will record Kalman filtered flight data while streaming telemetry and live video from the rocket and deployed vehicle back to a ground station. The team tested SRAD systems on four test flights, characterizing motor performance, validating telemetry, and evaluating the Airbrake and payload performance.

*Team Leader, Terrapin Rocket Team.

†Chief Engineer, Terrapin Rocket Team

‡Solids Team Leader, Terrapin Rocket Team

§Payload Team Leader, Terrapin Rocket Team

¶Airbrake Team Co-Leader, Terrapin Rocket Team

||Airbrake Team Co-Leader, Terrapin Rocket Team

**Avionics Team Leader, Terrapin Rocket Team

††Avionics Team Member, Terrapin Rocket Team

‡‡Payload Team Member, Terrapin Rocket Team

§§Payload Team Member, Terrapin Rocket Team

¶¶Payload Team Member, Terrapin Rocket Team

***Aerostructures Team Member, Terrapin Rocket Team

†††Aerostructures Team Member, Terrapin Rocket Team

Contents

I	Introduction	6
I.A	Academic Program	6
I.B	Stakeholders	6
I.C	Team Organization	6
II	System Architecture Overview	8
II.A	Flight Simulations	8
II.B	Propulsion	12
II.B.1	Materials and PV Design	13
II.B.2	Propellant Choice	15
II.B.3	Full Scale Motor Design	16
II.B.4	Motor manufacturing and assembly	18
II.B.5	Test Stand and DAQ	22
II.B.6	Full Scale Motor Testing and Results	22
II.B.7	Post Fire Disassembly	26
II.B.8	Mixing Sessions	27
II.B.9	Igniters	28
II.C	Aerostructures	29
II.C.1	Airframe manufacturing	29
II.C.2	Couplers	30
II.C.3	Nose Cone	31
II.C.4	Fins	31
II.C.5	Thrust Plate	32
II.C.6	Fin Can Construction	32
II.C.7	Airframe Finishing	34
II.D	Recovery	35
II.D.1	Recovery Devices and Shear Pins	35
II.D.2	Recovery Harness	36
II.D.3	Recovery Attachment	37
II.D.4	Deployment System	38
II.D.5	Flame Protection	39
II.E	COTS Recovery Avionics	40
II.E.1	Electronics Bay Introduction	40
II.E.2	SRAD Bulkheads	40
II.E.3	Commercial Electronics	41
II.E.4	Internal Structure	42
II.F	SRAD Avionics	45
II.F.1	Sensor Array	45
II.F.2	Battery	46
II.F.3	Microcontroller	46
II.F.4	Kalman Filter	47
II.F.5	Telemetry	48
II.F.6	Live Video	49
II.F.7	Ground Station	50
II.G	Airbrake	51
II.G.1	Overview	51
II.G.2	Deployment Mechanism	51
II.G.3	Airbrake Structure	52

II.G.4	Avionics	53
II.G.5	State-Estimation	56
II.G.6	Controller Design	63
II.G.7	Parameter Estimation	64
II.G.8	Heat Protection	67
II.G.9	Commanded Angle Validation	67
II.G.10	Controller Analysis	68
II.H	Payload	70
II.H.1	Mission	70
II.H.2	TERP	71
II.H.3	TADPOL	72
II.H.4	Drift control	76
II.H.5	Live video	79
II.I	Flight Tests	80
II.I.1	December 16, 2023	80
II.I.2	February 3, 2024	80
II.I.3	April 7, 2024	81
II.I.4	April 21, 2024	82
III	Mission Concept of Operations Overview	83
IV	Conclusion and Lessons Learned	85
V	Appendix A: System Weights, Measurements, and Performance	86
V..1	Rocket Information	86
V..2	Propulsion System	86
V..3	Predicted Flight Data and Analysis	87
V..4	Recovery System	88
V..5	SRAD Components	89
VI	Appendix B: Project Test Reports	90
VII	Appendix C: Hazard Analysis	143
VIII	Appendix D: Risk Assessment	145
IX	Appendix E: Assembly, Preflight, Launch, Recovery, and Off-Nominal Checklists	147
X	Appendix F: Engineering Drawings	161
XI	Acknowledgements	188
XII	References	189

Nomenclature

ABS	Acrylonitrile Butadiene Styrene
BMP	Barometric Pressure
CAD	Computer-Aided Design
CCW	Counter Clockwise
CFD	Computational Fluid Dynamics
CNC	Computer Numerical Control
CONOPS	Concept of Operations
COTS	Commercial off the Shelf
CP	Center of Pressure
CSV	Comma-separated Values
CW	Clockwise
D	Drag
DAQ	Data Acquisition Device
DOF	Degree of Freedom
FEA	Finite Element Analysis
FPS	Frames Per Second
GNSS	Global Navigation Satellite System
GPS	Global Positioning System
GUI	Graphical User Interface
HTPB	Hydroxyl-terminated polybutadiene
I2C	Inter-Integrated Circuit
IC	Integrated Circuit
ID	Inner Diameter
IMU	Inertial Measurement Unit
L/D	Length to Diameter
KF	Kalman Filter
M	Mach
MDI	Methane Diisocyanate
MDRA	Maryland Delaware Rocketry Association
MEMS	Micro-electro-mechanical Sensors
MEOP	Max Expected Operating Pressure
MPC	Model Predictive Control
NACA	National Advisory Committee for Aeronautics
OD	Outer Diameter
OLED	Organic Light-Emitting Diode
PCB	Printed Circuit Board
PD	Proportional-Derivative
PETG	Polyethylene Terephthalate Glycol
PID	Proportional–Integral–Derivative

PLA	Polylactic Acid
PSRAM	Pseudostatic (Random-Access) Memory
PV	Pressure Vessel
SAC	Spaceport America Cup
SD	Secure Digital
SF	Safety Factor
SPI	Serial Peripheral Interface
SRAD	Student Researched and Developed
SSR	Solid State Relay
T	Thrust
TADPOL	Testbed for Adjusting Drift and Position On Landing
TERP	Testbed for Ejecting Research Payloads
TWR	Thrust-Weight Ratio
UMD	University of Maryland
URRG	Upstate Research Rocketry Group
g	Gravitational Acceleration
C_G	Center of Gravity
C_p	Center of Pressure
P_{max}	Max Operating Pressure
σ	Stress
τ_s	Shear Stress
K_n	Burning Surface Area/Nozzle Throat Area
P_c	Chamber Pressure
C^*	Characteristic Velocity
ρ	Density
T_s	Sampling Time
g_i	Turn Rate Along Axis i
α	Tilt Off Vertical Axis
h	Height
v	Velocity
δ	Flap Deployment Angle
v_∞	Far Field Velocity
τ	Time Constant
Cd_f	Coefficient of Drag of a Flap
Cd_R	Coefficient of Drag of the Rocket Body
A_f	Reference Area of a Flap
A_R	Reference Area of the Rocket Body
Q	Process Covariance Matrix
\mathbf{F}	State Transition Matrix
$\mathcal{P}(h, v, \alpha, \delta)$	Apogee Predict Function
R^2	Coefficient of Determination

I. Introduction

A. Academic Program

The Terrapin Rocket Team (TerpRockets) is a student organization at the University of Maryland, College Park. The team was established with the goal of providing students with hands-on opportunities to learn about rocketry and to gain experience in the engineering design process. The team is made up of over 70 undergraduate students and two graduate students across majors such as Aerospace Engineering, Mechanical Engineering, Computer Science, and Physics. While this team is composed of several different academic backgrounds, the club is sponsored by the A. James Clark School of Engineering - Department of Aerospace Engineering under the advisement of Dr. Christopher Cadou.

B. Stakeholders

There are two primary types of stakeholders for this project: academic and professional. The academic stakeholders are engaged with the development of the team, the members, and the team's reputation. These individuals, with their more complete understanding of rocketry, assist the team through hours of mentorship. They have provided us useful feedback during design reviews and assisted in developing new skills to design a more refined project. One of the most valuable mentors has been the team's Tripoli advisor and prefect of the Maryland Delaware Rocketry Association (MDRA), Dennis Kingsley, who has been working with the team for the last four years and has been monumental in the team's success. Scott Szympruch, the former MDRA prefect, has acted as the Solid Propulsion mentor for the Solids subteam. Bryce Loposky, a systems engineer at Blue Origin and Tripoli L3, has also been an important mentor for many aspects of the team. Additionally, the team's academic advisors, Dr. Christopher Cadou and Dr. Michael Kio, have been instrumental in the team's success.

Professional stakeholders are those who have helped to ensure the team's continued success. ST Engineering has been crucial in the refinement of composite manufacturing processes, a partnership the team hopes to expand. The team's sponsors' support in donations and access to engineering materials and software have allowed it to expand its capabilities. These sponsors include the A. James Clark School of Engineering, The University of Maryland Student Government Association, Maryland Space Grant Consortium, Boeing, Northrop Grumman, Blue Origin, ST Engineering MRAS, VectorNav, Aerojet Rocketdyne, Kratos Space and Missile Defense Systems Inc.

C. Team Organization

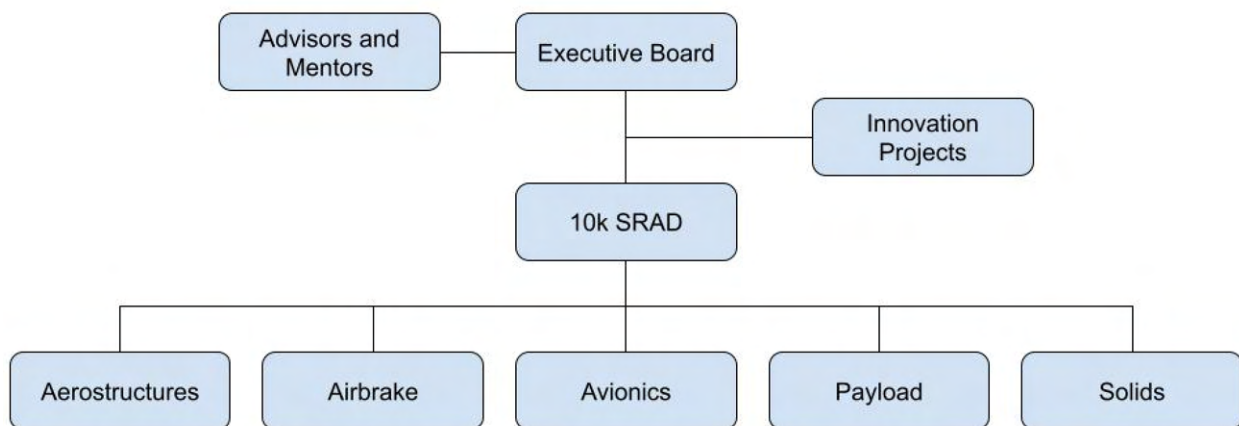


Fig. 1 Team Organization

The Executive Board of TerpRockets oversees all of the team's activities, including direct involvement in the Spaceport America Cup (SAC) team. This SAC team was categorized by subteams: Solids, Aerostructures, Avionics, Airbrake, and Payload. The Solids subteam designed, tested, and fabricated the solid rocket motor for Honu.

Aerostructures was tasked with the design, testing, and fabrication of the rocket's airframe and recovery, including recovery avionics. Recovery fell under the Aerostructures team to ensure one team was responsible for the flight critical components of the rocket. The Avionics subteam developed an SRAD flight computer that logs data and broadcasts telemetry and live video. The Airbrake subteam designed, tested, and fabricated the Airbrake module to trim altitude, as well as the control software. The Payload subteam was tasked with developing the payload system, a released vehicle, for Honu.

This season, the team approached SAC 2024 with the goal of improving on past successes and learning lessons from Karkinos, the team's competition rocket for the 2023 SAC. Honu was built to fly early and often, flying its first test flight in December. The design emphasized previously proven rocketry techniques and incorporated thoroughly tested systems developed over multiple years. To delegate the workload, ensure rapid testing, and increase safety, there existed a separation between flight critical systems and non-critical systems among the subteams. Therefore, the team was able to fly early test flights and have the ability to work on the project's subsystems while minimizing the impact on flight readiness. The full structure of the SAC team is displayed in Fig. 1.

II. System Architecture Overview

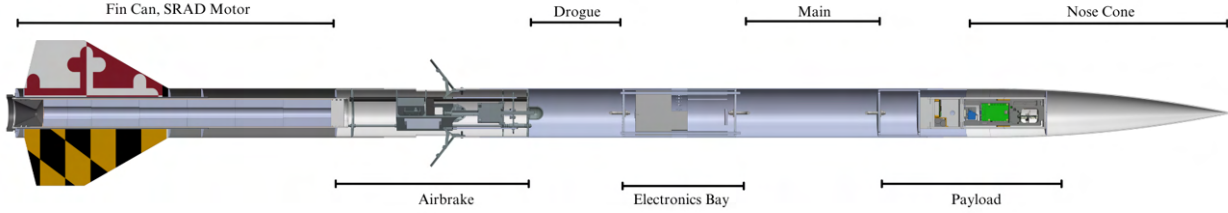


Fig. 2 Honu Cross Section

Honu is composed of six separate subsystems: Propulsion, Aerostructures, Recovery, Avionics, Airbrake, and Payload. The propulsion subsystem is an SRAD solid rocket motor. It is a 98 mm motor with approximately 37" of propellant length and 12,724 Ns of impulse designed to take Honu to over 10,000 feet. The Aerostructures subsystem includes the airframe and structural components of the rocket including the fin can, drogue recovery tube, main recovery tube, and nose cone. All external air frames except for the nose cone were made by students from either carbon fiber or fiberglass. Aerostructures is also responsible for recovery systems, the electronics bay, and all commercial recovery electronics. These include two Altus Metrum EasyMinis and a Featherweight GPS. The Airbrake system sits directly above the fin can and is designed to trim the rocket's flight to a precise altitude. A variety of sensors onboard allow it to deploy flaps into the air stream to induce drag and slow down the rocket. The SRAD Avionics system is contained inside the primary electronics bay and is a custom flight computer collecting data and transmitting telemetry and live video. It does not have deployment capabilities. Honu is a dual break dual deploy rocket with the electronics bay sandwiched between the drogue parachute on the aft side and the main parachute on the forward side. The drogue is deployed at apogee and the main is deployed at 1,000 feet during descent. Directly below the nose cone is a payload bay consisting of a coupler and switchband containing a single EasyMini. This deploys the nose cone at 1,700 feet to allow the payload to release at 1,500 feet. The payload sits on top of nose cone electronics bay bulkhead and is split up into two sections: a vehicle and a vehicle release mechanism. The release mechanism is made of an aluminum frame and holds the vehicle during ascent. Once the nose cone is deployed and the previously covered release mechanism detects light, the vehicle is pushed out and recovers separately. The vehicle will attempt to control its descent using a flat parachute and rotating around slightly biased shroud lines. It will also transmit live video. The vehicle performance parameters for Honu can be found in Table 3. The motor being used for Honu is a SRAD 98 mm seven grain N2900. Details about the performance of the motor are listed in Table 2 and Fig. 3 and further discussed in the Propulsion subsection.

Table 2 TRT N2900 Motor Characteristics

Loaded Weight (lb)	26.6
Propellant Weight (lb)	14
Burnout Weight (lb)	12.6
Total Impuse (N-s)	12,724
Average Thrust (N)	2924
Burn time (s)	4.6

A. Flight Simulations

Honu was primarily simulated using OpenRocket 22.02, with launch conditions at the Spaceport America Cup site. Design and simulation began in OpenRocket before moving to RasAero for more detailed simulations and Solidworks for a more detailed design. This also allowed for mass estimates to assist in designing the solid rocket motor. Honu was

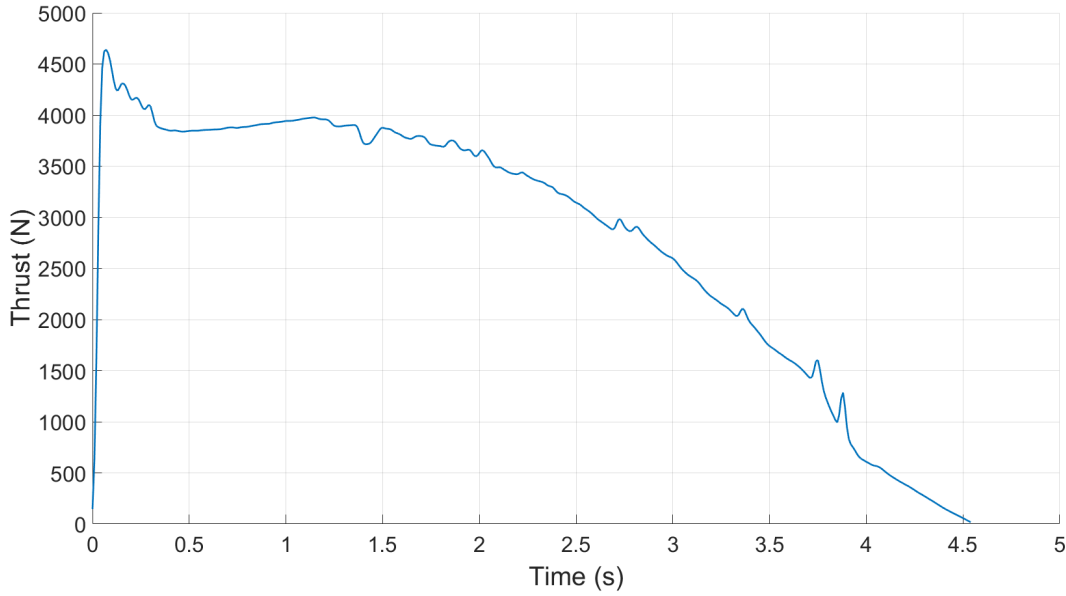


Fig. 3 TRT N2900 motor characteristics

Table 3 Vehicle Parameters

Predicted Apogee (ft)	10,573
Total Impulse (N-s)	12,724
Peak Thrust (N)	4,638
Takeoff Mass (lb)	89
Takeoff TWR	11.7
Rail Velocity (ft/s)	104
Max Velocity (ft/s)	912
Altitude at Max Velocity (ft)	2,100
Max Acceleration (G)	10.7
CG (in, from tip of nose cone)	95.4
CP (in, from tip of nose cone)	120
Stability Margin (cal, %)	4, 16%

designed around concepts that worked over the previous two years, including Terpulence II (SAC 2022) and Karkinos (SAC 2023). The team's student rolled composite tubes are about 50% to 60% lighter than the Wildman Rocketry tubes, which was noted when modeling in OpenRocket. Since the payload release mechanism and the Airbrake module had already been built and flown for Honu, modeling the masses and characteristics for these systems was accurate. The parachute, recovery, epoxy estimates, and avionics masses were then added. Simulation data as displayed in this document, such as predicted apogee, rail velocity, center of pressure, and others, were all provided by the OpenRocket simulation.

Since Honu has a fairly high L/D for a rocket, the standard rules of stability are not consistent. While the rocket may have a stability margin above 1 caliber, since it is fairly long this may not be adequate. A new rule of thumb for stability that has become more popular in recent years has been to calculate stability in terms of percent of body length. The formula for this value is,

$$SM = \frac{C_p - C_g}{L} \quad (1)$$

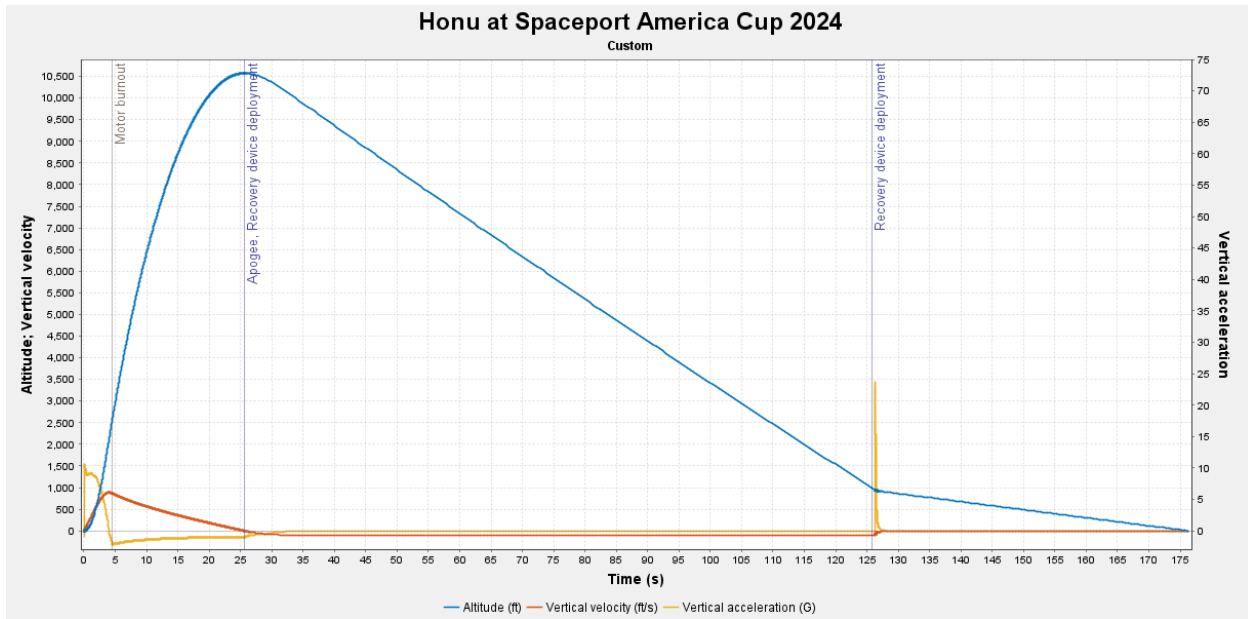


Fig. 4 Honu - OpenRocket Simulation

where C_p is the center of pressure, C_g is the center of mass, and L is the total length of the rocket. For a stable rocket, this safety margin should be between 8%-18%. This means that a long rocket will have a traditional stability margin much larger than one and a very short rocket can have a margin below one. The fins were designed around these restrictions and targeted stability on the far end of this guideline. As seen in Fig. 5, Honu clears the launch rail with a minimum stability margin of 4 calibers, equivalent to 16%. As propellant leaves the rocket, the center of gravity moves forward, and the stability peaks at 5.3 calibers, which is equivalent to 21%.

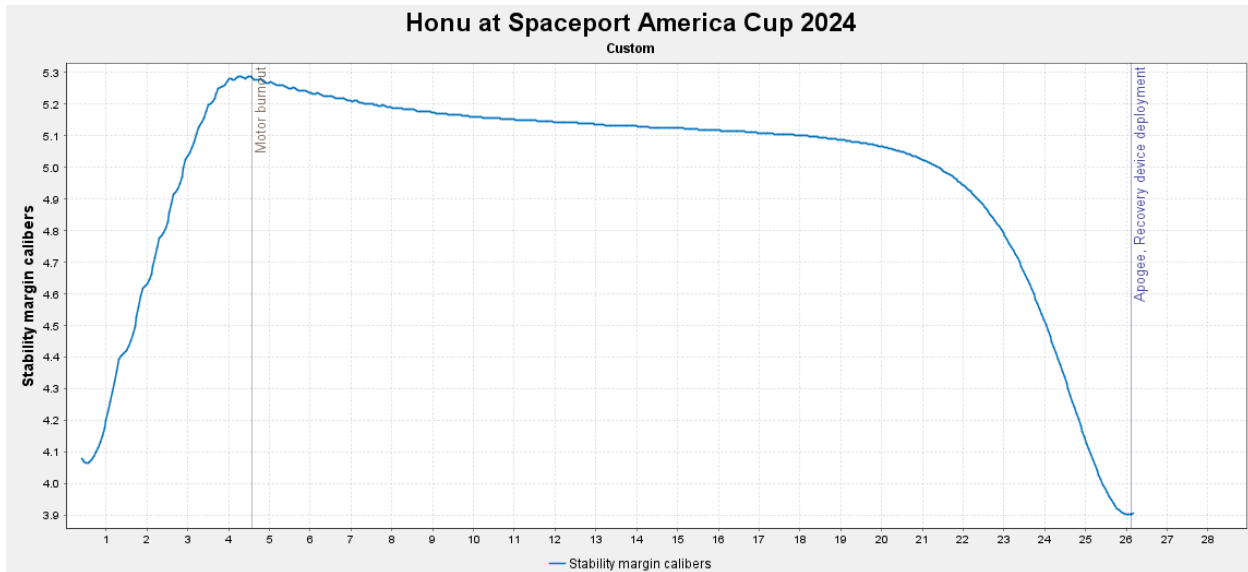


Fig. 5 Honu - OpenRocket Stability

In general, past simulations have overpredicted actual flight results. This is for a variety of reasons, such as extra protrusions like cameras or bolts outside the rocket. This year, the camera was modeled as a pod with the same frontal area and length as the actual camera. As a result, the simulation was made to be conservative. Launch conditions were

set for Spaceport America with an altitude of 4,595 feet and a rail angle of 7° . Since the rail buttons are spaced 3 feet apart, a rail length of 14 feet was used since the buttons can no longer guide the rocket once the first one has left the rail. Since Honu contains an Airbrake module and cannot add any extra thrust, the rocket must overshoot the 10,000 foot target. Theoretically, the Airbrake can decrease a flight's altitude by up to 1,000 feet based on Honu's launch conditions. However, it is much easier and less demanding to correct a smaller altitude difference, so the rocket targets about 10,500 feet.

RasAero was used after the OpenRocket design was completed to verify results and better model the protrusions, especially cameras. After updating the inputs, the RasAero simulation was in strong agreeance with the OpenRocket simulation. The RasAero projected apogee was 10,588 feet.

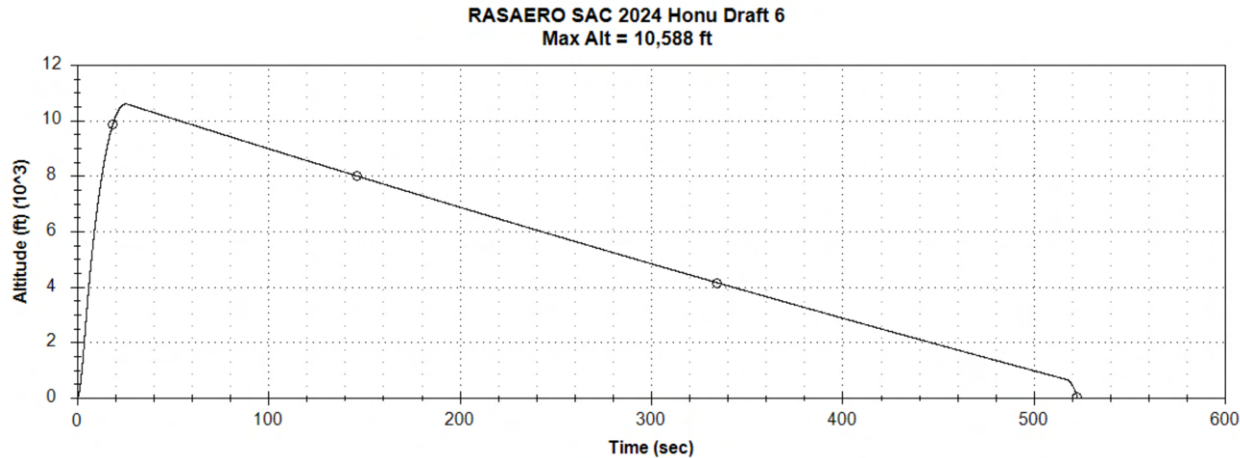


Fig. 6 RasAero Simulation

Once the rocket was built, the center of gravity and total mass were updated in both OpenRocket and RasAero, and following test flights, the surface finish was changed to better match actual flight conditions. In addition, test flights verified that the launch was stable and safe.

B. Propulsion

The motor for Honu is a 98 mm SRAD N motor. It uses a custom purple propellant called Terple Nebula and is designed to launch Honu to 10,000 feet at the Spaceport America Cup. Fig 7 shows a cross-section of the motor geometry. It is made up of an aluminum casing from Fisher Research, an aluminum forward closure, graphite nozzle, and XX phenolic liner. The nozzle and closure are retained on either end with steel snap rings. The motor casing is then slid into the motor mount tube and thrust is transferred from the lip of the case to the thrust plate.

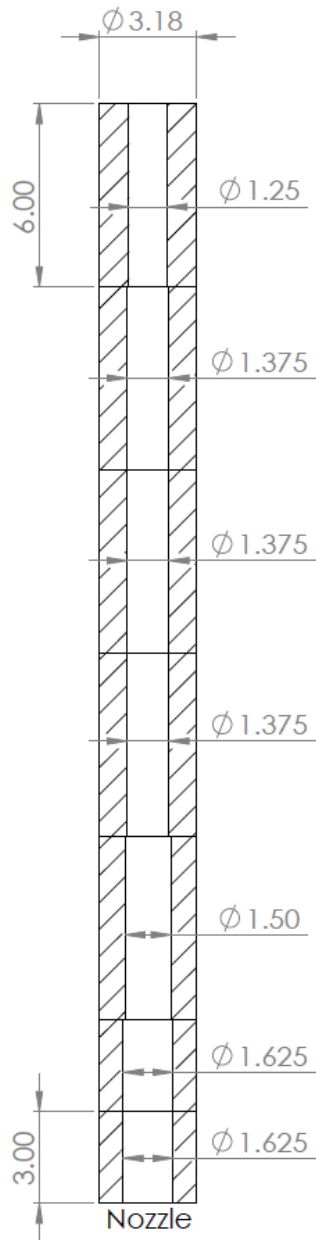


Fig. 7 Grain dimensions (in)

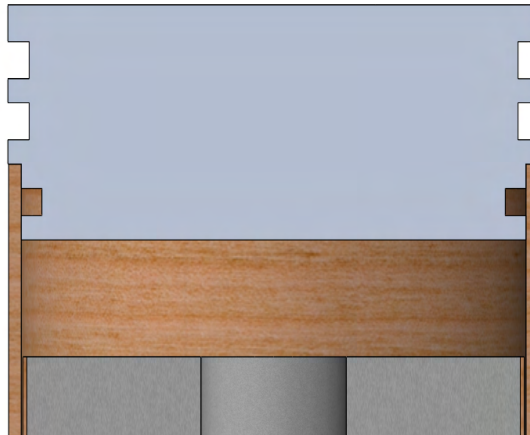


Fig. 8 Example of liner O-ring

1. Materials and PV Design

The primary design for the motor is similar to standard snap ring motors. It is a six grain 98 mm aluminum snap ring case with a full graphite nozzle and aluminum forward closure. The liner is XX grade phenolic from Franklin Fibre with paper casting tubes from Yazoo Mills. The casing, forward closure, and nozzle were all manufactured by Fisher Research. The primary improvement to the motor hardware compared to last year is the addition of a forward liner O-ring as shown in Fig. 8. It accomplishes a very similar purpose to the Forward Seal Disc in many Aerotech reloads. After inspecting the liner and casing after five test firings last year, the top of the liner and case were often very charred. Minor pitting was observed on the casing which got worse with each firing. This decreases the usable life of the casing and is better to prevent. A liner O-ring at the forward closure keeps the gas from leaking around the liner and protects the case at the forward end. Due to the much faster moving gas at the nozzle end, the gas is cooler compared to the hot stagnant gas at the forward end. Sealing both ends of the liner is not an option as that would make the liner a pressure vessel. Since it is a fairly brittle material, if it takes any significant amount of pressure it would crack and cause a burn-through.

While the team is using commercially made hardware for the motor, calculations were done to find the theoretical limits to better inform what pressure range the motor could be operated at safely. First, the necessary dimensions of the casing were measured including the inner and outer diameters as well as snap ring groove depth and distance from the edge. These values can be found in Table 4.

Table 4 Motor Case Dimensions

Inner Diameter (in)	3.5
Outer Diameter (in)	3.88
Wall Thickness (in)	0.19
Length (in)	42
Distance from Edge to Snap Ring Groove (in)	0.3
Snap Ring Groove Depth (in)	0.1

Next, material properties were gathered for Aluminum 6061, the material of the casing. Aluminum 6061 has a yield strength of 40,000 psi and a shear strength of 30,000 psi. However, the aluminum material strength must also be considered at elevated temperatures. This is commonly taken as a 20% reduction in strength. In reality, due to the quick burn, not very hot propellant, and good thermal protection, the casing temperature generally only rises after the burn, not during peak stress. However, evaluating at reduced strength is good practice for an worst case scenario. The

strengths used in analysis can be found in Table 5. The first stress states to evaluate are hoop stress and axial stress.

Table 5 Al 6061 Strength Values

	Ambient Temperature	Elevated Temperature
Yield Strength (psi)	40,000	32,000
Shear Strength (psi)	30,000	24,000

These can be found with equations 2 and 3.

$$\sigma_{hoop} = \frac{P_c D_i}{2t} \quad (2)$$

$$\sigma_{axial} = \frac{P_c D_i}{4t} \quad (3)$$

Where P_c is the Max Expected Operating Pressure or MEOP, D_i is the inner diameter of the casing, and t is wall thickness. The MEOP was taken to be 1000 psi as the magnitude of the erosive spike was unknown and it simplified calculations. Substituting the casing measurements into these equations give stress values of 9210 psi and 4605 psi respectively. To calculate the safety factor to yield, the yield strength is divided by the hoop or axial stress as shown in equation 4.

$$SF = \frac{\sigma_{yield}}{\sigma_{hoop/axial}} \quad (4)$$

This equation yields safety factors of 3.47 and 6.94 respectively. The next stress to evaluate is at the casing wall with the snap ring groove. The groove removes material and introduces a weaker point within the casing. This can be found with equation 5

$$\sigma_{tensile} = \frac{P_c D_i}{D_o^2 - D_g^2} \quad (5)$$

Where D_o is the outer diameter of the casing and D_g is the internal diameter of the snap ring groove. From this equation, a stress of 2314 psi is calculated. The safety factor is then calculated in the same way as the hoop/axial stress and is found to be 13.82 at minimum. The final failure mode is shear stress at the end of the casing. This can be calculated using equation 6.

$$\tau_{casing} = \frac{P_c D_i}{E} \quad (6)$$

Where E is the minimum distance from the edge of the casing to the snap ring groove. This gives a maximum stress of 11,666 psi which yields a minimum safety factor of 2.057. This is the minimum safety factor for the entire system and will be the first to fail. All safety factors are summarized in Table 6.

Table 6 Case Safety Factors

	SF at Ambient	SF at Elevated Temp
σ_{hoop}	4.34	3.47
σ_{axial}	8.68	6.94
$\sigma_{tensile}$	17.26	13.82
τ_{case}	2.57	2.05

In addition to pressure vessel calculations, the casing was also hydro-statically tested to a proof pressure of 1.5x MEOP or 1500 psi for 2 minutes. The casing is assembled with 2 forward closures and filled entirely with water. It is connected to a high pressure flex hose which is then connected to a manual hydraulic pump. Pressure is slowly increased and held at multiple increments to watch for any drops that may occur due to leaks. Once at the proof pressure, it is held for 2 minutes before opening a bleed valve to release the pressure. All pressure testing is done with a 15 feet high

pressure flex hose and all personnel are located around the corner of a building in case of a failure.



Fig. 9 Hydrostatic testing setup



Fig. 10 Motor case at proof pressure

2. Propellant Choice

The propellant chosen for this year's competition motor is called Terple Nebula and is the same propellant used in the motor for the team's entry in the 2023 competition. This propellant was characterized in fall of 2022 using a variety of 38 mm and 54 mm motors. A new propellant was also not necessary as the primary changes required for the motor were more impulse and higher initial thrust, both parameters that could be changed with grain geometry. While the ingredients stayed the same from the previous year, some chemicals were acquired from a new source. First, the Diethyl Adipate (DOA), the plasticizer in the mixture, was changed to a new supplier. This supplier had much cheaper DOA and had good recommendations from others in the experimental solids community. The more major change was the source of Tepanol. The motors last year used Tepanol that was produced multiple decades ago and stored at room temperature. This meant that it became much less reactive and more viscous. Because of this, it could not hold on to the ammonium perchlorate (AP) well and had trouble incorporating with the liquids. The new Tepanol has recently "expired" from an industrial supplier, however it is only a few years old and has been stored in a freezer to minimize degradation. Since the only changes were made to liquids, re-characterization was not deemed necessary. A change in supply of one of the solid components, such as the AP, could change the particle distribution significantly. While it may be sold as a nominal size of 200 micron, it could have a different makeup of finer particles that can still make it through a sieve. All components of Terple Nebula can be found in Table 7.

Terple Nebula was characterized using six subscale motors of similar length/diameter ratios as the competition motor. Three motors were tested in 38 mm and three were tested in 54 mm in a series of rising pressure ranges. Both pressure and thrust were recorded for each firing, however only the pressure data was used during characterization. First, the characteristic velocity (C^*) for each motor was calculated using equation 7.

$$C^* = \frac{A_t}{m_p} \int_0^{t_b} P_c(t) dt \quad (7)$$

where A_t is the nozzle throat area, t_b is burn time, and m_p is the initial propellant mass. Nozzle throats must be measured after firing as slag may accumulate causing abnormally high C^* values to be calculated. The integral can be approximated to the summation 8 which allows it to be used easily with DAQ data.

$$\int_0^{t_b} P_c dt = \sum_i P_c \Delta T \quad (8)$$

After C^* is calculated for each firing, the highest non-erosive pressure is taken along with an approximate Kn value at that moment. Kn is the value of burning surface area divided by the nozzle throat area and is calculated from a

Table 7 Terple Nebula Formula

Ingredient	% of Mixture	Purpose
R45M, HTPB	13	Fuel/Binder
Dioctyl Adipate	2.6	Plasticizer
Castor Oil	0.1	Grain Hardener
Tepanol	0.1	Bonding Agent
Magnesium, 325 mesh	2	Metal Fuel
Strontium Nitrate, 200 μ	15	Secondary Oxidizer
Oxamide	2	Burn Rate Suppressant
Copper Oxide	1	Burn Rate Catalyst
Ammonium Perchlorate, 200 μ	62	Primary Oxidizer
MDI	2.2	Curative

simulation software such as OpenMotor. Density is found using ProPep3. While this density is the theoretical value, accurate density measurements are difficult to make and are often very close to the theoretical value. The burn rate can then be found for each motor using equation 9.

$$R_b = \frac{P_{chamber}}{K_n C^* \rho} \quad (9)$$

Where R_b is the burn rate in in/s . These values can then be plotted against the pressure chosen for each motor and a curve is then fit using a power series of the form of equation 10.

$$R_b = ax^n \quad (10)$$

Here a is the burn rate coefficient and n is the burn rate exponent. The data points as well as curve fit can be seen in Fig. 11. The curve is found to be equation 11. These values along with values such as specific heat ratio, exhaust molar mass, and combustion temperature, which are found using ProPep3 and summarized in Table 8, are inputted into OpenMotor to properly simulate the full motor.

$$R_b = .013x^{.461} \quad (11)$$

Table 8 Outputs from ProPep3

Property	Unit	Value
Density	lb/in ³	0.0632
C^*	ft/s	4,442
Chamber Temperature	K	2,368
Exhaust Molar Mass	g/mol	24.93
Specific Heat Ratio	N/A	1.235

3. Full Scale Motor Design

The primary requirements for the motor for Honu were a total impulse of approximately 12,000 Ns and initial thrust of 4000 N. The impulse target was primarily based off of preliminary OpenRocket simulations and motor impulses from previous years. One of the primary changes made to the motor this year is the higher average thrust. This was done to

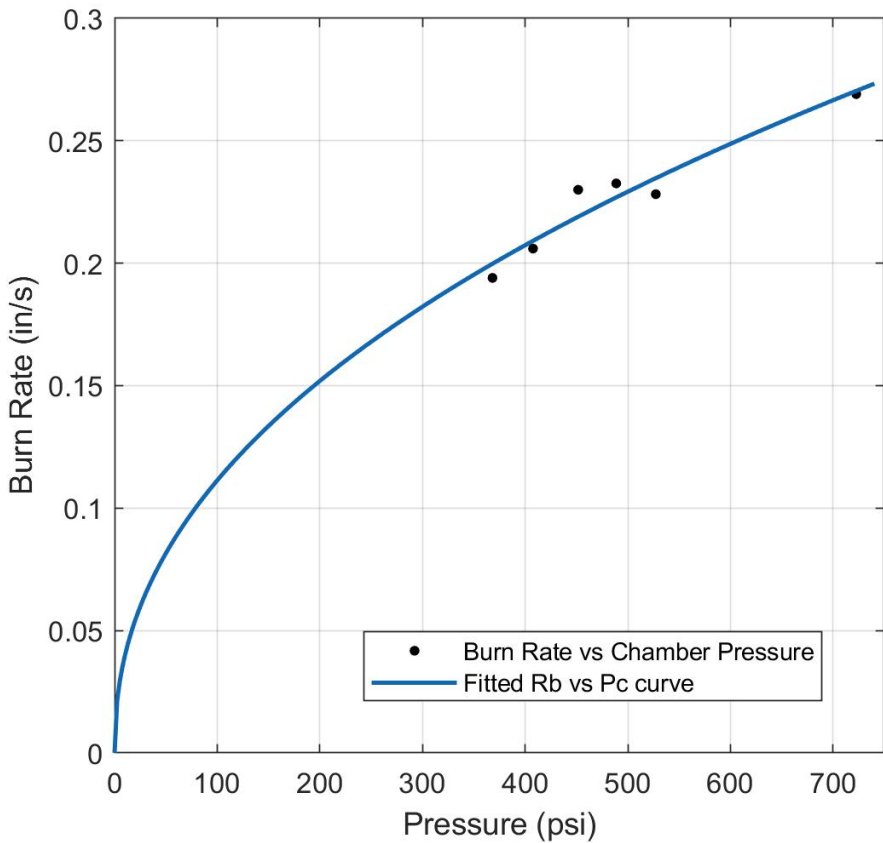


Fig. 11 Burn Rate vs Pressure Curve for Terple Nebula

ensure a fast rail exit velocity and a straight flight. Early estimates placed Honu's mass on the pad at approximately 80 lbs. For a takeoff thrust to weight of 10:1 this meant the motor needed an initial thrust of 800 lbs or approximately 3600 N. The motor was designed to this initial thrust with the knowledge that there would be an erosive spike at startup further increasing the thrust. The motor is designed with grains of four different core diameters. The grains at the forward end of the motor have a core of 1.25" which increases to 1.625" towards the nozzle end. This geometry is made to decrease the peak mass flux in the motor. Mass flux is calculated as the mass flow rate per unit area. The highest mass flow in a motor will be in the aft most grain as all of the gasses from the more forward grains must flow down past it. By widening the grains towards the nozzle, the mass flux can be significantly decreased. OpenMotor calculates the mass flux for each grain throughout the burn and reports it as a value of $\frac{lb}{in^2 \cdot s}$. *Erosive Burning Design Criteria for High Power and Experimental/Amateur Solid Rocket Motors* by Charles Rogers [1] provides some design criteria for erosivity in solid rocket motors which can be found in Table 9. These values are a good starting point when working with a propellant where erosivity is unknown, but erosivity will heavily depend on the propellant makeup, particularly particle sizes. For last year's motor, mass flux was kept conservative to $\sim 1.6 \frac{lb}{in^2 \cdot s}$ at 600 psi. A very minor erosive spike was observed in static testing which gave confidence in running the motor at higher pressures and mass fluxes. A more aggressive target of $\sim 1.9 \frac{lb}{in^2 \cdot s}$ at 800-900 psi was chosen for this years motor. The second consideration when designing with erosivity in mind is the port/throat ratio or the ratio of grain core area to nozzle throat area. If this value is too small, generally less than 2, choked flow can occur within the grain instead of the nozzle. This increases regression locally and causes an erosive spike. Due to the tapered nature of the cores to decrease mass flux, the aft most cores are already large with a port/throat ratio of 2.75. Final design parameters from OpenMotor can be found in Table 10 and predicted mass flux, pressure, and thrust curves in figures 12 , 13 and 14.

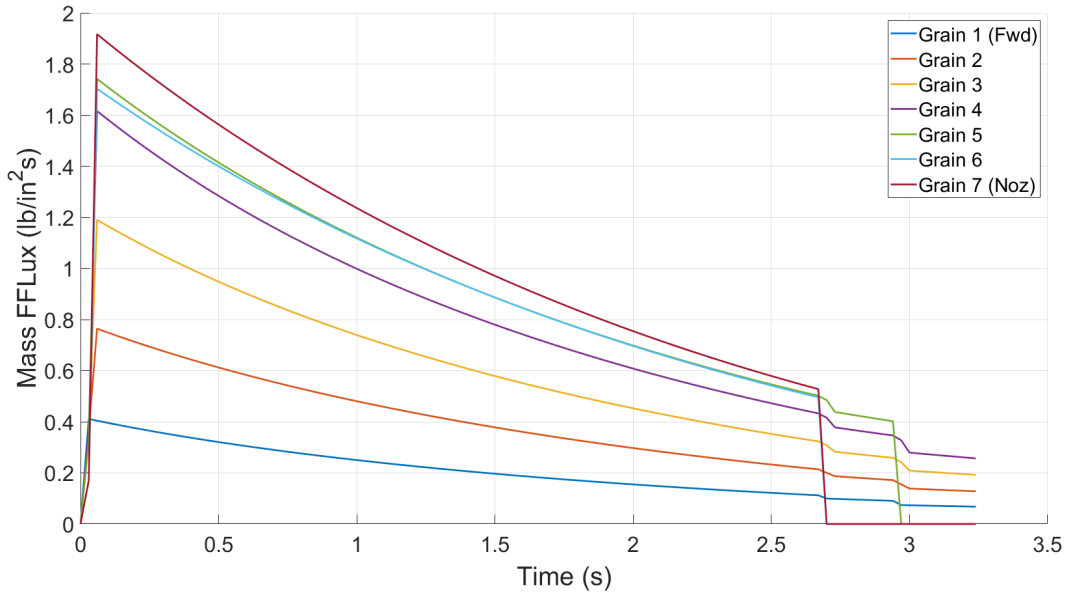


Fig. 12 Mass Flux vs Time

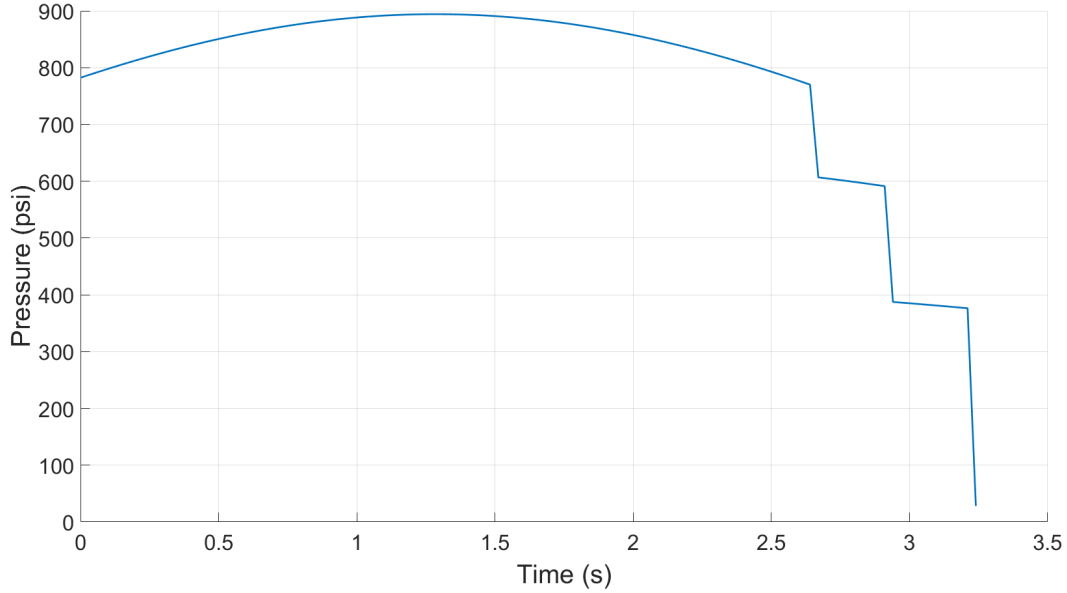


Fig. 13 Simulated Pressure Curve

4. Motor manufacturing and assembly

The team's mixing procedure is fairly standard for a packable propellant. First, all of the liquids are added and incorporated together. This is then put under vacuum for 15 minutes to remove incorporated air. Next, the solids are added one at time into the liquids. They are first incorporated by hand before turning on the mixer to minimize dust. The AP is saved for last as it is the largest component. This too is added slowly and incorporated by hand before turning on the mixer. With all of the chemicals except the curative now in the mixer, it is allowed to mix for at least an hour. The one change to the team's mixing procedure this year is that the mixing process was split up into two days. After mixing all the components for at least an hour, the bowl was removed from the mixer and covered with plastic wrap to

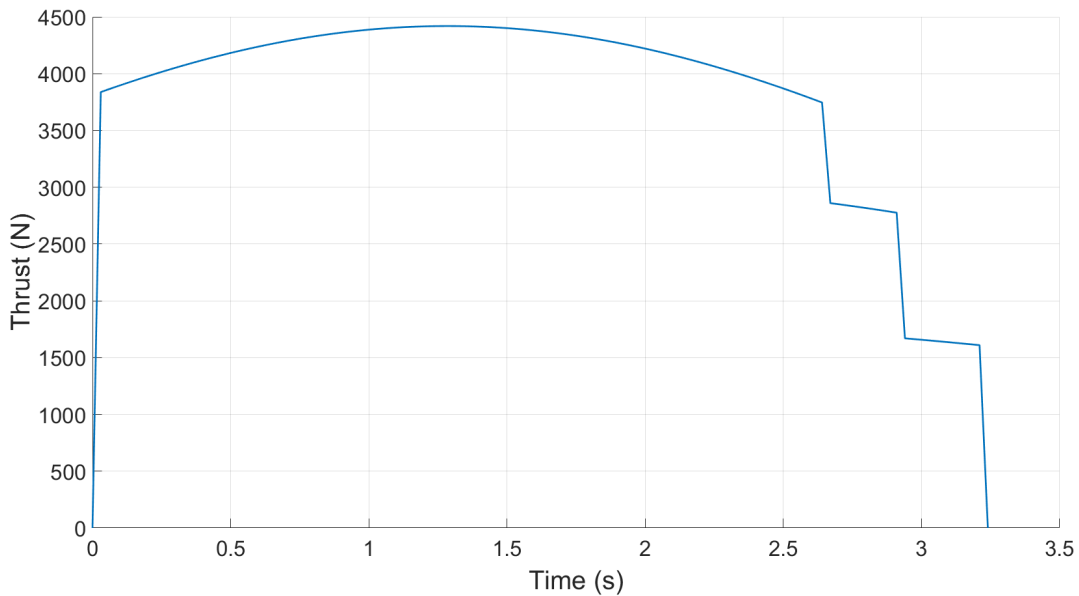


Fig. 14 Simulated Thrust Curve

Table 9 Erosivity Conditions

Non-Erosive:	
Chamber Pressure (psi)	Maximum Mass Flux $\frac{lb}{in^2 \cdot s}$
400-600	1.0
800	1.75
1400	2.0
Erosive:	
400	2.0
600	2.5
800	3.0

sit overnight. This gave the Tepanol much more time to react with the AP so that it would stick to the binder better. The next day, the plastic was removed and the bowl was placed back on the mixer for another hour. This was done to make sure any components that may have settled out overnight were fully incorporated. The bowl is then placed under vacuum to remove air incorporated during mixing. Next the curative is added into the mixture followed by scraping the bowl and paddle every 5 minutes for 15 minutes. This ensures that there are no pockets of unmixed curative sticking to the paddle or bowl and that it's fully distributed. After 15 minutes of mixing, the bowl is removed from the mixer and any remaining propellant is scraped off the paddle. It is then placed under vacuum for a final 15 minutes before packing.

While the propellant is mixing, the casting tubes, mandrels, and bases are all prepared. The mandrels are solid aluminum rods with a tapped 1/4"-20 hole in the bottom. They are first wrapped in a layer of thin plastic wrap along the entire length. Then a spiral of fiberglass reinforced strapping tape is added to the mandrel. The plastic wrap allows the mandrel to easily slide out of the propellant once it is cured and the spiral tape can then be easily pulled out. The mandrel is bolted to a 3D printed base which also has a small piece of plastic wrap to keep propellant from sticking to it. While a sprayable mold release such as Stoner E236 is generally easier to use, the packable nature of this propellant means that the mold release is rubbed off as the propellant is cast, making the mandrel harder to remove. The casting tube is slid onto the base and a hose clamp is tightened at the bottom to keep it from moving. When the propellant is

Table 10 Simulated Motor Parameters

Motor Designation	N3772	Initial Kn	329
Total Impulse (Ns)	12337	Volume Loading (%)	80
Motor Class	20% N	Propellant Mass (lb)	14
Burn Time (s)	3.24	Propellant Length (in)	36
Peak Pressure (psi)	888	Peak Mass Flux $\frac{lb}{in^2 \cdot s}$	1.93
Peak Kn	353	Port Throat Ratio	2.75
Nozzle Diameter (in)	0.98	Peak Thrust (N)	4230



Fig. 15 Bowl of propellant sitting overnight



Fig. 16 Aluminum mandrel wrapped in plastic and tape

ready to pack, a handful is scooped from the mixing bowl and rolled out into a strip. This is then wrapped around the mandrel and dropped down into the casting tube. A wooden dowel is then used to tamp it down. This is continued until the entire casting tube is filled. A 3D printed cap is then added to the top to keep the mandrel centered while the propellant cures. Once solid, the mandrels are easily pushed out and the tape is removed from the core. Grains are then cut to size using a manual miter saw for a straight cut. Faces are then lightly sanded to make them smooth and remove any burrs. Even with straight cuts and no spacer O-rings in the motor, the team has not had any issues with motors coming up to pressure on ignition.



Fig. 17 Casting tubes and mandrels prepared for casting



Fig. 18 2 competition motors (left) curing



Fig. 19 Grains stacked prior to gluing

Once all of the grains are cut to size, the weights and lengths are measured and recorded for density calculations. The liner is then cut precisely so that there is minimal movement with the nozzle and closure when fully assembled. The grains are stacked vertically with a single layer of packing tape at each of the boundaries. This is done to make sure that no glue can seep into the motor and inhibit grain faces. The grain stack is then covered in silicone caulk and the liner is slid down over it. Silicone caulk is very thick and chars well, which makes it great for grain bonding. The nozzle is then inserted into the bottom of the liner to make sure it cures with the proper spacing on either side. A small piece of plastic wrap is placed between the nozzle and liner to prevent the nozzle from being permanently glued in. This plastic remains there until the motor fires as it seals the motor from air and prevents the propellant from absorbing moisture. After the silicone has cured, O-rings are added to the nozzle and forward closure. The inside of the case is cleaned and the snap ring grooves are entirely cleared. The snap ring edges are also inspected and lightly sanded if any burrs are found. This is done to prevent slicing any O-rings during assembly. The liner is then liberally greased and the casing is slid down over it. The aft snap ring and nozzle washer are also greased to prevent oxidation and both snap rings are inserted. Before firing, a hole is poked into the plastic film behind the nozzle to allow igniter insertion.



Fig. 20 Grains glued into liner and curing



Fig. 21 Aft casting tube still adhered after firing

5. Test Stand and DAQ

The test stand for the competition motor is heavily based on the Aerocon style unistrut test stand. It is made of mostly COTS components and assembled with 3/8" steel bolts and spring nuts. The stand has two cross struts that are secured to the stand with custom machined PTFE rail buttons. These buttons allow these cross brackets to slide along the stand and transfer thrust to the load cell while keeping the motor constrained. The motor is held in by two insulated pipe clamps made for unistrut rail.

The Data Acquisition (DAQ) system used for testing the team's experimental motors is the DI-1100 from DATAQ Instruments. In the current setup, the team employs dual redundancy, with each DI-1100 system utilizing two of its four channels. The first channel connects to a load cell amplifier via a pair of wires. Depending on the DAQ system in use and the expected force during static fires, this load cell is either of a 1-ton or 3-ton capacity. The load cell amplifier is INA125BB-BP from Phillips Instruments and amplifies the load cell to a scale of 0-10 V.

The second channel of each DAQ system interfaces with a 1600 psi pressure transducer. For power and data connection to the pressure transducer, the team designed a wiring harness which provides 5 V power over USB and connects to the DAQ. For data recording, the DAQ system interfaces with DATAQ Instruments' WinDaq software, which is operated on a laptop during all static fires. Prior to testing, all sensors were calibrated. A manual hydraulic pump was used to test the pressure transducers, while a sand bucket of known weight was used for the load cells. After confirming accurate voltage readings from each measurement device, the DAQ is configured to convert these readings to Newtons for the load cells and PSI for the pressure transducers.

6. Full Scale Motor Testing and Results

The first full scale motor was fired on February 3rd at the MDRA Higg's Farm. The forward closure of the motor was connected to an NPT tee with two 1600 psi pressure transducers. Force was transferred to the load cell via the tee



Fig. 22 Motor in test stand



Fig. 23 Redundant data acquisition setup

and a combination of oil and grease protected the pressure transducers from the combustion temperature. It was the third in a set of static fires for the team that day and followed two 98 mm tests of a different formula. On the previous two tests, the team encountered multiple issues with the DAQ system. After setting up the first motor and starting the recording, the team left the stand to allow the motor to be fired. With other launches it took some time before the motor was actually fired. After returning to the test stand, the computers connected to both DAQs had fallen asleep and did not record anything. The sleep settings on both computers were changed and the second motor was placed on the stand. After firing the second motor, the computers were still awake but did not record any data. The issue this time was found to be a setting in Windows which turns off USB devices after a set amount of time. For the competition motor, after everything was setup, it was fired as soon as possible to prevent similar DAQ issues. On this final firing, data was recorded from both the load cell and pressure transducer.



Fig. 24 Forward closure with NPT tee and pressure transducers



Fig. 25 Static fire of competition motor

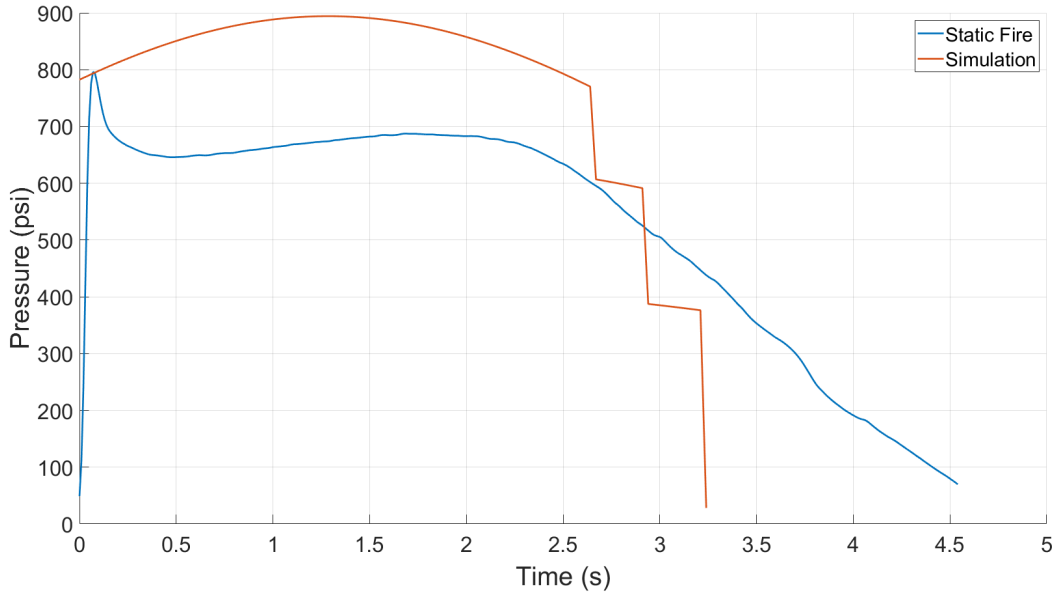


Fig. 26 Recorded Pressure Curve vs Simulated

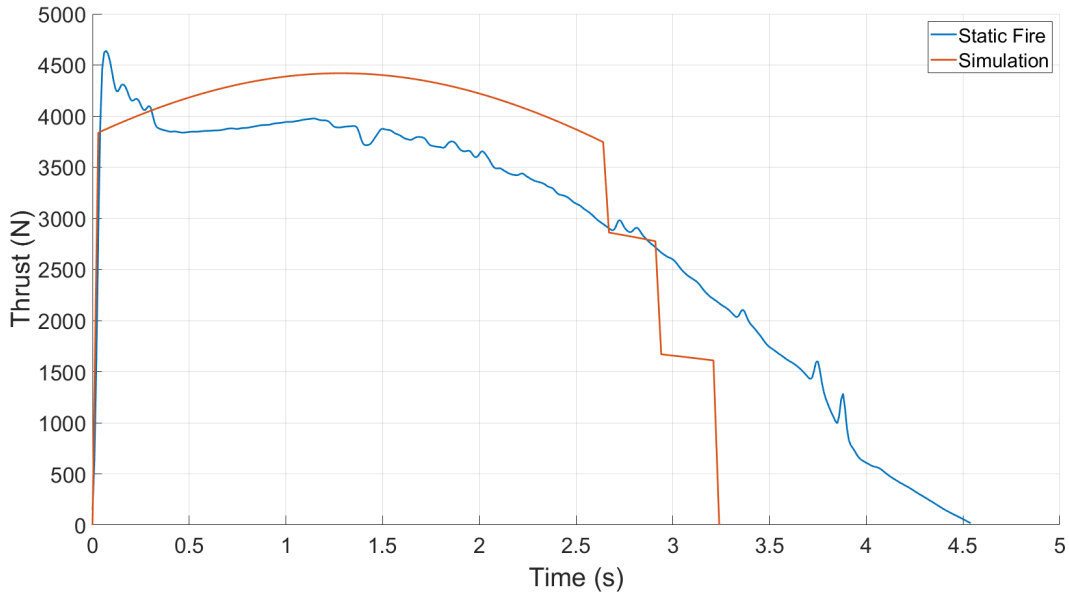


Fig. 27 Recorded Thrust Curve vs Simulated

The second firing of a competition motor occurred on April 21st at URRG in upstate New York. This was the final test flight of the competition rocket and was in complete competition configuration, including motor. A 1600 psi pressure transducer was screwed into the forward closure and packed with oil and grease. An AltusMetrum EasyMotor was connected to the pressure transducer for data recording.

A comparison between the simulated pressure curve and actual pressure curve can be found in Fig. 26. The actual pressure is 100-150 psi lower than expected, however this is consistent with the team's past test fires. While characterizing this propellant, some grains were cut short in order to fit inside the case which led to a minor error in the characterization results. However, even though this is the case, the thrust values from this characterization data are

closer as seen in Fig. 27.

The shapes of the pressure and thrust curves differ fairly significantly between the simulation and static test and this can be attributed to the erosive spike. At the beginning, everything is burning at a higher pressure and the aft most grains are regressing the fastest. Since the web thickness is already the lowest at those grains, after the spike the motor is burning at a lower pressure than simulated, which means lower burn rate and a longer tailoff as can be seen in the plots. This difference in thrust profile does not make a major difference as the overall impulse between the simulation and static test is still very close - 12,337 Ns simulated and 12,668 Ns tested. A comparison of simulated and static test values can be found in Table 11.

Table 11 Comparison of Simulation and Static Test Values

	Simulation	Static Test
Total Impulse (Ns)	12,337	12,668
Peak Thrust (N)	4,419	4,644
Average Thrust (N)	3,772	2,932
Burn Time (s)	3.24	4.56

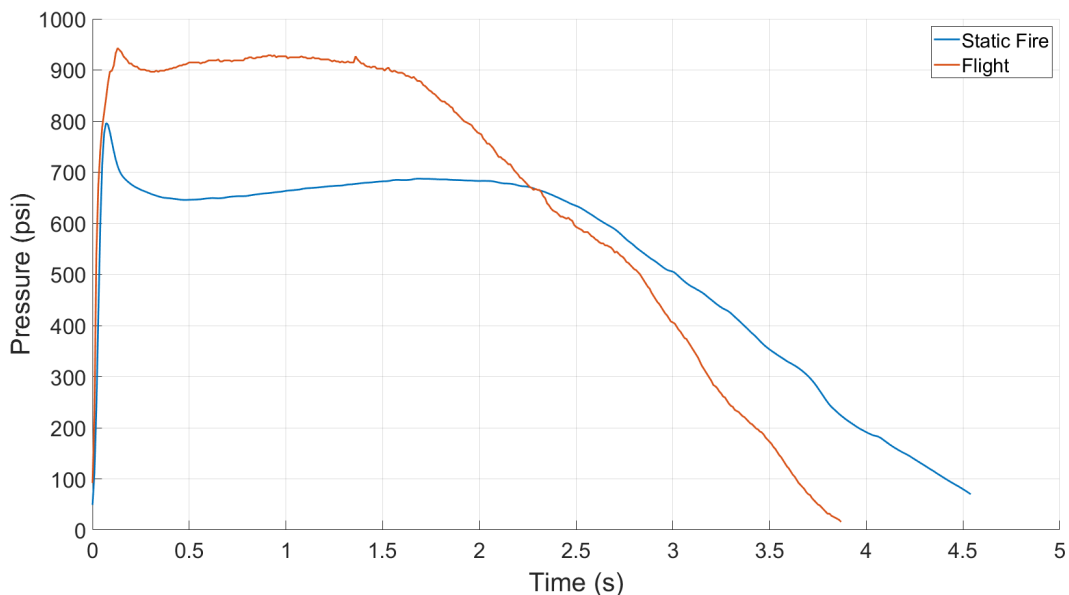


Fig. 28 Static Pressure Curve vs Flight Pressure Curve

During the second motor firing, the motor burned at a significantly higher pressure than in the static test. This can likely be attributed to a few factors. It was under 10-12 Gs of acceleration in flight, which while not extreme, likely causes a small increase in burnrate. The most likely cause of this increased pressure is the presence of slag on the throat of the nozzle from the static firing. This can be observed by plotting the thrust divided by the pressure vs time as shown in Fig. 29. After the initial spike, the plot is relatively level which shows the throat area is staying constant. As the pressure begins to drop during the burn and combustion becomes less efficient, slag collects on the nozzle. This is seen as the value dropping until burnout. Slag is also clearly visible on the nozzle after firing as shown in Fig. 30. For a motor with an eroding throat, such as a single use phenolic nozzle, the plot would increase throughout the burn. Another significant difference between the static test and flight test is the magnitude of the erosive spike. When the static test motor was mixed, the Tepanol was only given a few hours to react before curative was added. For the next two

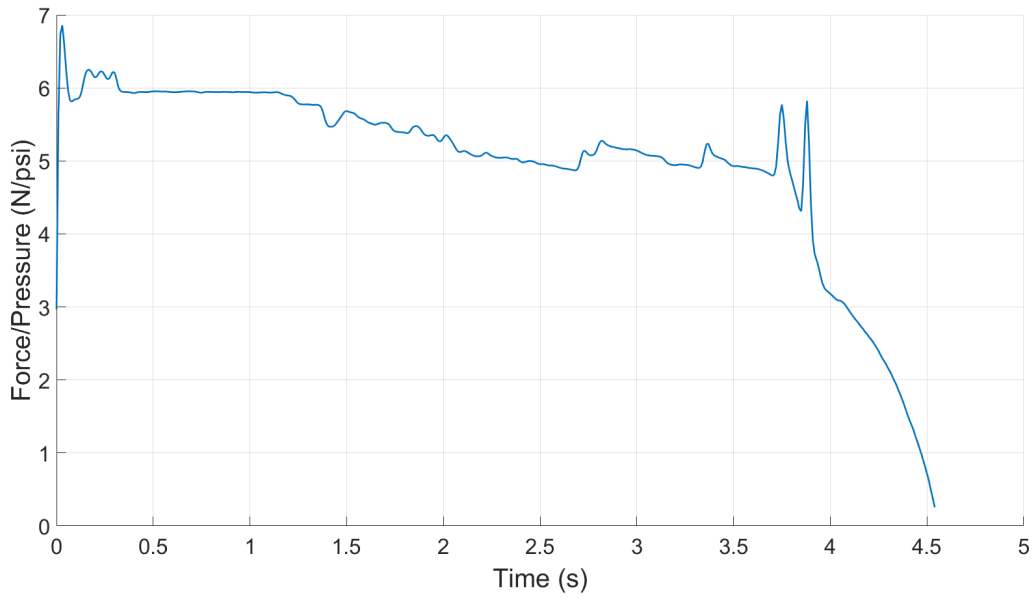


Fig. 29 Thrust/Pressure vs Time

motors, the mixture sat overnight before adding curative to give the Tepanol more time to react. With the much smaller spike, it is clear that this had a significant effect on holding the AP in the binder.

7. Post Fire Disassembly

During disassembly of the first competition motor, a longitudinal crack was discovered along the entire length of the liner as shown in Fig. 31. Compared to previous motors of similar size with the same propellant, this is out of the norm. The casing was cleaned and inspected and did not show any signs of thermal damage. Since this motor is running at a higher pressure than last year's motor, more liner damage was expected but not to this degree. In the middle of the crack it clearly burned through during the firing as there is clear discoloration and bubbling. The rest of the crack is relatively clean which points to it propagating during disassembly. A spare closure is put against the liner and then hit with a mallet to push the liner out which can easily crack a liner like this. After the first firing of the competition motor, the team fired a 6" diameter P motor and experienced a burnthrough at the forward end. During disassembly, the liner was also found to be cracked however with a longer burn and much hotter propellant it was able to burn through the side of the casing. The cause of this failure was traced to both liner tolerances and assembly of the motor. The liner had a 40-50 thousandths gap with the casing, which is similar to the gap between the liner and case for the competition motor. Both motors also have an O-ring on the forward closure that seals into the liner to prevent gas from coming up and over the liner. During assembly, the liner is stood up nozzle end down and coated with grease. The case is then slid



Fig. 30 Slag on nozzle after second firing

over the liner down towards the nozzle. This ends up pooling grease at the nozzle-liner shoulder. When a liner O-ring is utilized, generally only one side is sealed. This is done to prevent the liner from becoming a pressure vessel and pressurising. Because the XX Phenolic is much weaker and more brittle than the aluminum, even a small amount of pressure can lead it to crack, like was seen in the team's first competition motor and the P motor. After learning this, the second motor was assembled differently. The casing was pushed down towards the forward closure to prevent grease pooling at the nozzle. After disassembly of the second motor, the liner was in much better condition. Other than some bubbling at the forward end, which is consistent with past motors, there were no cracks or dark spots on the outside. This was also in spite of this motor running at a higher pressure than the motor in the static test.

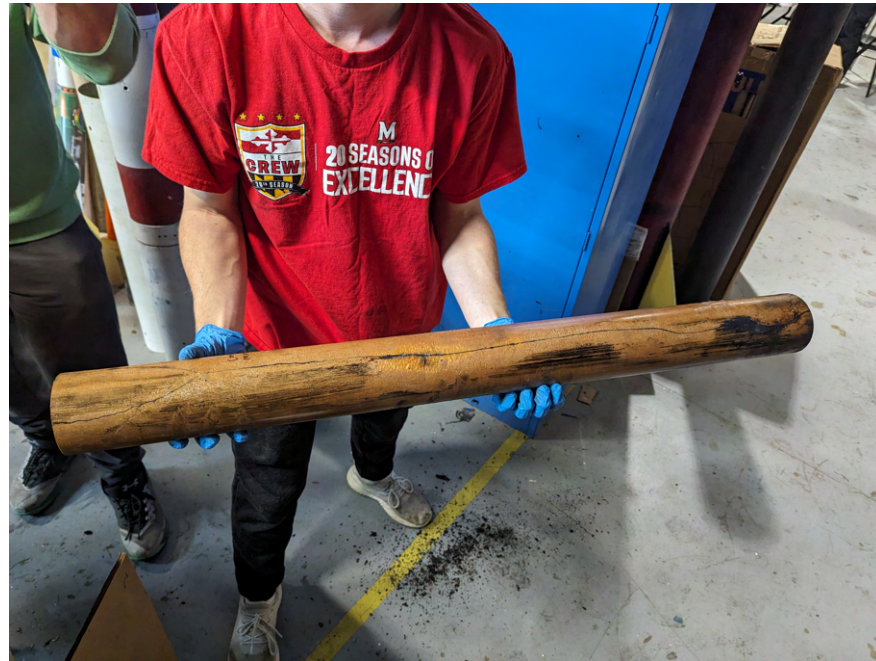


Fig. 31 Liner after static test

8. Mixing Sessions

In the 2023-2024 design cycle, there were two mixing sessions of Terple Nebula. The first mix session consisted of one motor for the static test. Two motors were made in the second mixing session, one for a test flight and one for the competition flight. Total propellant weights for each motor can be found in Table 12. The static test and competition motor are within 2 grams of each other while the flight test is approximately 80 grams lighter. This is only a 1% difference in weight and can be attributed to small differences between grains adding up to cause this error. Due to how the cores are cast, there is some variability in diameter with tape thickness and wrapping technique.

Table 12 Motor Propellant Weights

Static Test Motor	6362 g
Flight Test Motor	6283 g
Competition Motor	6360 g

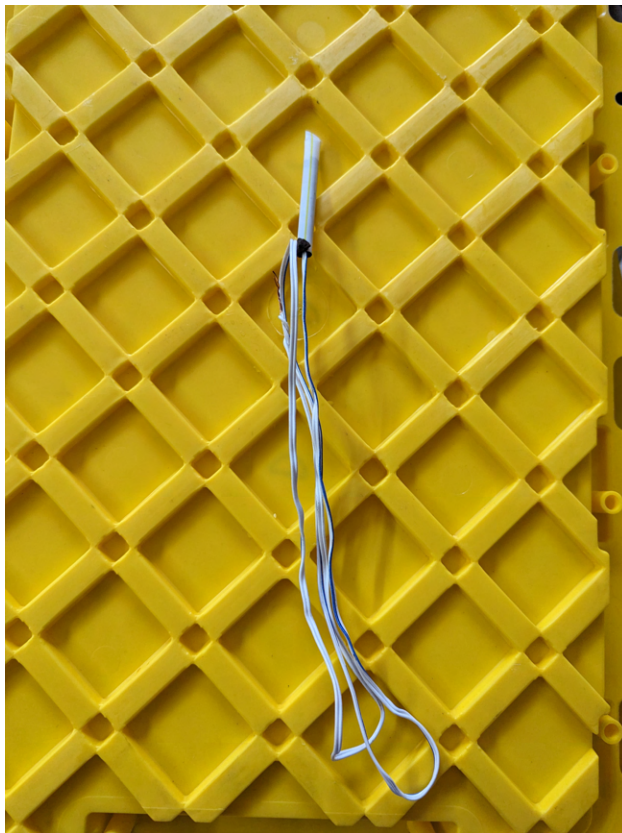


Fig. 32 Example BKnO3 igniter

9. Igniters

The igniters for the motor are made using BKnO3-V from Quickburst. The team has been using this igniter compound for lighting a wide variety of commercial and experimental motors and has had great success. BKnO3 has a small pressure exponent which means it will burn at relatively the same rate even as the motor comes up to pressure, which is helpful for reducing additional pressure during ignition. Igniters are made by putting BKnO3 into a plastic straw then inserting an MJG FireWire ematch. It is then set aside to allow the acetone to fully evaporate and the igniter to harden. The team has found that making these igniters 1.5-2" long allows the competition motor, and other similarly sized motors, to light quickly and reliably. As per the dual igniter requirement, two of these igniters will be wired in parallel. To ensure the igniters are all the at the top of the motor, they are taped to a thin wooden dowel. This is then taped to the base of the nozzle or the launch rail to prevent it from falling out. The dowel is very quickly ejected and burned as the motor starts and the rocket takes off.

C. Aerostructures

The Aerostructures subteam is responsible for the design and fabrication of Honu and its flight-critical components. During design, the team prioritized a proven design and lightweight, cost-efficient systems that were easy to manufacture. Honu has a diameter of 6" and is 12' 7" tall. The COTS nose cone, payload coupler, and electronics bay coupler are made of COTS filament wound fiberglass. The recovery section tubes and Airbrake switchband are made of SRAD fiberglass, while the fin can airframe tube and Airbrake coupler are made of SRAD carbon fiber. The centering rings and fins are made of G10 fiberglass. The recovery section tubes consist of two airframe tubes; the drogue recovery tube houses the drogue parachute and the main recovery tube houses the main parachute. They are connected by an electronics bay. Fiberglass was chosen because it is lightweight, strong, and common in high power rocketry. It is also transparent to radio frequencies, crucial for receiving telemetry from the commercial GPS system and student designed flight computers. For the fin can, carbon fiber was chosen because it is stiff and lightweight, and it did not need to be radio transparent. Its lightness decreases weight at the aft end of the rocket, leading to higher stability, while its strength is useful for touchdown. The rocket is designed to be stable, simple to assemble, and easy to modify.

1. Airframe manufacturing



Fig. 33 Carbon Fiber Layup Process



Fig. 34 6" Diameter, 48" Long Carbon Fiber Tube After Curing

The outer airframes and the motor mount used on Honu are all student-made, except for the nose cone, and are made of fiberglass or carbon fiber. While the team's rockets have used commercial filament wound tubing in the past, they are often fairly heavy, and custom-made tubes can be around 50% to 60% the weight of a commercial tube. Before the team began to make the tubes, a mandrel was selected. Using a 60" Wildman Rocketry coupler tube ensured the tube would fit securely with the purchased couplers from Wildman. Once the mandrel was selected, it went through a preparation process, including repairing small imperfections with Bondo spot putty, cleaning with acetone, and lubricating with fine graphite powder. This powder helped the airframe tube slide off of the mandrel much easier than mold release, which was used last year. Next, one layer of 0.002" thick Mylar plastic with 1" of overlap was wrapped

tightly around the mandrel. The Mylar physically provides a barrier between the part and the mandrel, ensuring it slides off easily. The Mylar was then taped closed on the overlap with two parallel lines of double-sided tape to help ensure that the seam was completely sealed. Then the Mylar was cleaned with acetone and coated with epoxy, which for these tubes was Proset LAM-125 and LAM-226. This epoxy was used due to its availability, ease of use, pot life, and cure cycle. Fiberglass or carbon fiber fabric was wrapped around the tube, using rollers for tension, and epoxy was applied onto it using a brush and plastic squeegee. Six layers of 6 oz fiberglass were used compared to four layers of 3K plain weave carbon fiber based on tubes made in previous years that have flown successfully. An early carbon fiber layup process can be seen in Fig. 33.

The tube was then wrapped in a 1.5 wraps of peel ply, a release fabric, to provide a better surface finish. The tube was left to cure at room temperature for 48 hours, after which the peel ply was taken off. The tubes were then cut to size and their edges sanded square. The surface was sanded and then a thin layer of epoxy was added to the outside to the tubes to create a smooth surface for the tube. The carbon fiber tube at this stage can be seen in Fig. 34. The process concluded with finishing, discussed in the *Airframe Finishing* section.

2. Couplers

Honu contains six separate coupler connections throughout the rocket, creating the need for stiff mates to reduce bending in flight. To ensure a stiff joint, a coupler-airframe overlap of one caliber, or 6", meets the requirements and is sufficient to minimize bending. All coupler connections in the rocket contain 1 caliber of overlap except for the nose cone interface with the nose cone electronics bay. Since the nose cone does not experience major bending loads, this connection uses 0.5 calibers of overlap, which is the maximum amount that can be fit with the nose cone and payload design. This coupler is similar to a normal electronics bay, as it has a 2" switchband and 1 caliber of overlap with the main recovery tube. In addition, a window was cut out of the forward end of the nose cone coupler, shown in Fig. 35, so that the payload vehicle could be deployed through the gap. Over the last two years, the team has flown eight test flights in this configuration and have not noticed any decrease in stiffness.



Fig. 35 Early version of payload with coupler cutout



Fig. 36 Custom coupler curing under heat lamps

The Airbrake module is made up of a 24" long coupler with a 12" long airframe bonded in the middle. After damage during the April low altitude test flight, the Airbrake was determined to be beyond repair to original strength and it was therefore rebuilt. This required producing a new coupler, either by using a Wildman coupler, using a airframe tube with a slot cut out down the length to reduce the diameter, or using a tube built on a new mandrel for couplers. The team chose the latter option to keep the process simple, increase SRAD components, and gain experience making couplers. To produce the coupler, a mandrel was 3D printed in segments and joined together with epoxy. The full mandrel was sanded up to 600 grit, cleaned thoroughly, and prepared with graphite powder similar to airframe tubes. A layer of mylar film was applied, and carbon fiber fabric was rolled onto the mandrel using the LAM-125 and LAM-226

epoxy. The tube is shown curing under heat lamps in Fig. 36 Four total wraps were completed for a stiff fit, and the outer surface was sanded after curing to ensure the coupler went into airframe tubes smoothly. This was the team's first coupler produced in a wet layup and has performed well in flights.

3. Nose Cone

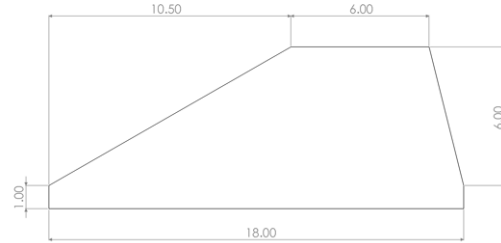
Honu's nose cone is a commercial 5-1 Von Karman filament wound fiberglass nose cone from Wildman Rocketry. This nose cone was chosen because of its compatibility with the couplers. An eyebolt is threaded into the aluminum tip for connection to the payload shock cord that is connected to the top of the payload. Holes are drilled into the sides to allow pressure equalization, which is required for the nose cone EasyMini and payload barometer sensors.

4. Fins

Honu's fins are larger than last year's fins on Karkinos to increase stability, especially when the Airbrake flaps are deployed. The fin shape was designed in OpenRocket to ensure stability throughout the flight. The final design consists of four fins with a swept-delta shape and a semi-span of the same width as the airframe. Additionally, the fins include tabs that extend the entire length of the root chord for maximum through-the-wall attachment length and ease of manufacturing.

Root Chord (in)	18
Tip Chord (in)	6
Sweep (in)	10.5
Semi-Span (in)	6
Thickness (in)	0.25

(a) Fin Dimensions



(b) Fin Shape (in)

Fig. 37 Fin Dimensions

The team used the AeroFinSim program to estimate the flutter velocity of Honu's fins. The shape and input parameters can be found in Fig. 37 and Table 13. The center of gravity of the fin was calculated to be 0.604 from an online calculator, which was then plugged into AeroFinSim. With a flutter velocity of 2,207 ft/s, and a maximum velocity of 912 ft/s, Honu has a safety factor of 2.42 on the competition motor.

Table 13 Fin Sim Inputs

Altitude Input at Max Velocity (ft)	7,000 (ASL)
Center of Gravity (from 0 to 1)	0.604
CN-Alpha	NACA TN 4197
Fin Material	G10 Fiberglass

For manufacturing, the fin shape was cut out on paper templates which were temporarily secured to the G10 Fiberglass plate. To maintain one common edge among the fins, the base and aft edge of the fin tab were placed on the outer corner of the plate. A Dremel was used to cut out the rough shape of the fin and the templates were removed. The fins were stacked, using the base and aft edge of the fin tab as a guide, and temporarily glued together so that they could be sanded together to the same desired shape. Painters tape was applied to the surfaces of the fin and superglue was applied in between so that the painters tape could be peeled off later. A new template was secured to the top of the stack again using the fin tab edges as a guide, and then the fins were sanded to the exact shape using a belt sander. The leading

2-D Flutter Results

Flutter Velocity (UF) = 2206.98 FT/SEC
 Divergence Velocity (UD) = 1986.8 FT/SEC
 Critical Frequency (Fcr) = 168.25904 Hz
 Reduced Frequency (kF) = 0.23951
 Sqr(X) at flutter = 0.93125
 1/k at flutter = 4.17512

Plot Definitions

$$U = \frac{b}{k} \frac{\omega}{\omega_a} \omega_a$$

when, g = 0.0

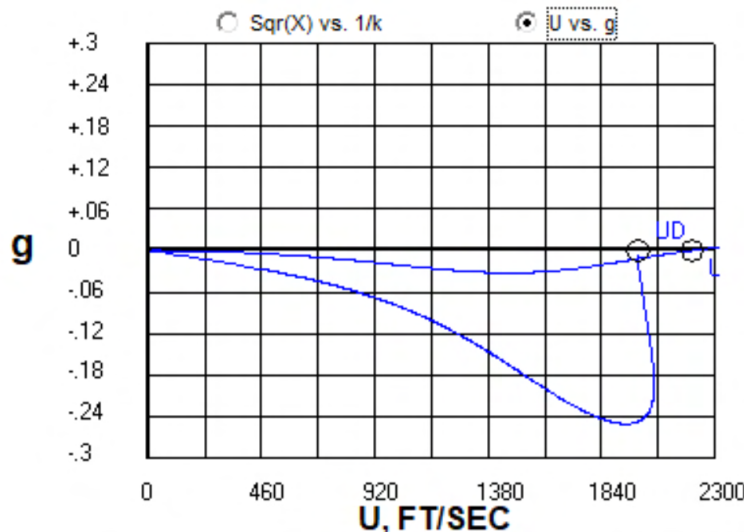


Fig. 38 Fin Sim Flutter Analysis Results

and trailing edges were beveled with a 15° chamfer bit on a router table, then sanded smooth to complete the fins.

5. Thrust Plate

At the aft end of Honu is a thrust plate, made of 6061-T6 Aluminum. Its purpose is to transfer thrust from the motor to the airframe. It is made of two 1/8" thick layers of aluminum plate cut out on a water jet. The aft most plate sits flush with the diameter of the fin can, while the inner layer fits inside the airframe tube. Using two 1/8" plates instead of a single 1/4" plate reduced manufacturing costs because the two plates could simply be cut on a waterjet instead of machined in one piece on a mill. The plates are connected by mounting an Aeropack 98 mm flanged retainer, and the provided bolts and purchased nuts hold all three parts together.



Fig. 39 Thrust Plate Cap Removed



Fig. 40 Thrust Plate Assembled

6. Fin Can Construction

The fin can for Honu serves numerous purposes in terms of the entire build. The fin can must be able to hold the fins rigidly, transfer the thrust of the motor, act as an attachment point for recovery systems, and be light enough to

prevent itself from negatively impacting the rocket's stability margin. The airframe is a student-made carbon fiber tube constructed using the previously mentioned techniques and processes. Inside the fin can is a 24" carbon fiber motor tube that is also student-made with three fiberglass centering rings, two of which are 18" apart to sandwich the fins. Two 1/4"-20 threaded rods run through each centering ring to distribute recovery loads throughout the fin can. There is an eye nut for recovery attachment at the top of these rods and the aft ends extend past the thrust plate. A 98 mm Aeropack screw-on motor retainer is attached to the thrust plate and secured in place via the threaded rods.

Assembly of the fin can begins with the airframe. Using a rotary tool with a cutoff wheel, the fin slots were cut using a paper guide. The slots were cut undersized to help with test fitting the fins. A file was used to gradually widen the fin slots until the fins could be pushed through the airframe. The reasoning behind this was to minimize the amount of epoxy that could leak through gaps while making the external fillets. Next, the motor mount assembly was manufactured. The motor mount consisted of two centering rings placed in the front of the motor tube and one at the aft end. The centering rings were stacked together and drilled to ensure proper alignment of the threaded rods. Centering rings were made slightly larger than the ID of the airframe then sanded down until they were a tight fit. The centering rings were slid onto the motor tube with the threaded rods and nuts to ensure proper spacing. The two forward centering rings along with the bolts were epoxied and set to cure. The aft centering ring was not epoxied as it would need to be removed for internal fillets later on. With the motor tube assembly complete, the airframe was prepared for bonding, as seen in Fig. 41.

Using 180 and working up to 400 grit sandpaper, the inside of the airframe was sanded and cleaned with acetone to prepare the carbon fiber for bonding. This process is used for all other bonding procedures on the rocket, including the motor tube, centering rings, fin tabs, and the fillet surfaces. Epoxy was added just forward of the fin slots (but not the rear) and the motor mount assembly was pushed in. The rocket was set vertically, aft end down, to allow the epoxy to cure and form a fillet around each centering ring. Once fully cured, the aft centering ring was removed and the threaded rods were taped to prevent epoxy from getting on them.

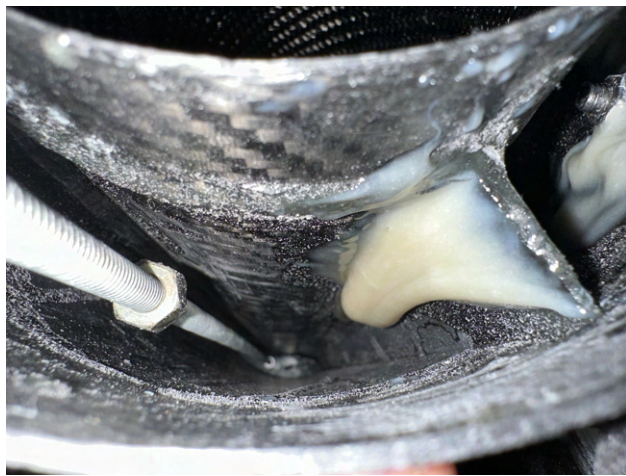


Fig. 42 Starting Internal Fillets

epoxy only runs alongside the root of the fins. External fillets are done using Aeropoxy ES6209, thickened using colloidal silica, and dyed black to match the airframe. The epoxy was poured onto the fillet area and spread evenly using



Fig. 41 Motor Mount Assembly

Next, each of the fins were lined along the bottom of the fin tab with Aeropoxy ES6209 and put into each fin slot. Making sure pressure was applied, all four fins were epoxied into place on the motor mount. Two laser-cut fin jigs aligned with external threaded rods were used to hold the fins in place while the epoxy cured as shown in Fig. 43.

After fully curing, internal fillets were made using more ES6209. The epoxy is mixed and poured into the opening along each fin fillet at the aft end of the rocket, and the rocket is leaned at a 45° angle, aft end up, to allow the epoxy to drip down along each fin. In Fig. 42, more epoxy was added, and the fin can was rested on the bottom fins to ensure an effective, symmetric fillet. Once the fillets are even, the fin can is placed horizontally to allow the internal fillets to cure. After curing, external fillets are completed. Each fin is carefully taped to ensure

a 3D printed fillet tool with a 0.5" radius. A heat gun was run over the fillet to remove air bubbles and smooth the epoxy. It was then set to cure.

The aft centering ring was then secured on the threaded rods with nuts and epoxied into place. Finally, the thrust plate with the retainer assembly was attached using two nuts and thread lock.



Fig. 43 Fin Jig



Fig. 44 Closeup of an External Fillet

7. Airframe Finishing

The tubes were all finished using separate processes for carbon fiber and fiberglass. The fiberglass tubes often had small imperfections even after the thin layer of clear coat epoxy. After sanding the clear coat, the tubes were primed using sandable primer, which exposed the imperfections. These were filled with Bondo spot putty and sanded. The primer, Bondo, and sanding cycle was repeated three to four times until the product was smooth and satisfactory. A final coat of primer was added, followed by the paint, decals, and final clear coat. White was chosen as the main color for the airframe to reflect heat and increase contrast with decals and identifying markings.

For the carbon fiber fin can, clear coats were applied to the tube and sanded numerous times, and then it was wet sanded to 1000 grit. After a thorough cleaning, two coats of primer were applied followed by a few layers of white paint. Fin decorations and decals were applied and a final layer of clear coat was added.



Fig. 45 Wet Sanding the Carbon Fiber Airframe



Fig. 46 Honu's Final Paint Scheme

D. Recovery

Recovery is one of the most important parts of the flight. For this reason, the recovery system is made to be as simple and as reliable as possible. Honu's recovery uses techniques that are proven not only by the high power rocketry community but also from many test flights by the team. Over the last two years, the team has conducted eight successful full scale test flights, and many successful 6" airframe flights with this combination of parachutes, recovery harnesses, and electronics with a very low failure rate. This experience and simplicity allow the recovery system to be integrated quickly, easily, and safely.

1. Recovery Devices and Shear Pins

During flight, Honu has three separation and deployment events. At apogee, the rocket separates in half and deploys the drogue parachute. At 1,700 feet, the nose cone of the rocket is separated, which allows the payload deployed vehicle to exit the rocket at 1,500 feet and begin its independent descent. Finally, at 1,000 feet the main parachute is deployed.

Parachutes for Honu were chosen based on manufacturer-rated descent rates, packing volume, and previous experience by the team. After burnout, Honu weighs approximately 72 lbs. The team has used Recon Recovery and SkyAngle Cert3 parachutes in the past and is very familiar with folding and packing them into 6" airframes. For this burnout weight, the Cert3XXL with a manufacturer reported coefficient of drag of 2.92 was the best fit for a safe descent. This parachute is sized for a rocket weighing between 60 and 130 lbs. With Honu on the low end of this scale, Honu lands at an OpenRocket simulated speed of 19 ft/s which has been confirmed through multiple test flights. This was the same parachute that was used for the competition rocket in 2023 which easily fit in the 6" diameter by 18" space of the main recovery tube. This parachute is also readily available and more economical compared to others in its size class, which is especially important if it needs to be replaced.

For the drogue parachute, the team selected a 24" parachute from Recon Recovery with a coefficient of drag of

roughly 1.16. This parachute has been used as a drogue on multiple large 6" rockets including Karkinos, the competition rocket from last year, as well as three L3s. Previously, the rockets descended around 90 ft/s with this parachute, and that is consistent with this year's test flights. While OpenRocket simulates a higher descent rate, flight tests consistently descend at 90 ft/s under drogue. The airframe induces a considerable amount of drag during descent, which is not simulated by OpenRocket. It is important that the rocket descends quickly under drogue to minimize drift. This makes recovery much easier, especially on the East Coast where trees can be a problem.

Each of these sections are held together with shear pins to prevent premature deployment both during descent and ascent. Between the drogue recovery tube and electronics bay, there are four 4-40 nylon shear pins. Not only could the drag on the fin can cause premature separation at burnout, but the Airbrake system is also producing up to 150 lbs of drag in a worst-case scenario, so it is necessary to retain these sections together. Each 4-40 shear pin provides around 50 lbs of shear force, which means 200 lbs of force is required to separate that section. The nose cone is held together with two 4-40 shear pins. This section does not experience any significant force trying to separate it in flight, so it is held together with the minimum amount of shear pins. Having only one shear pin could cause the coupler to jam in the airframe, so two are used to keep the forces symmetric. The nose cone payload bay coupler is held to the main recovery tube using six 4-40 shear pins, for a required total shear force of around 300 lbs. Because of the heavy 11 lb payload in this section, these shear pins keep inertia from separating the electronics bay when the drogue line snaps taut.

2. Recovery Harness

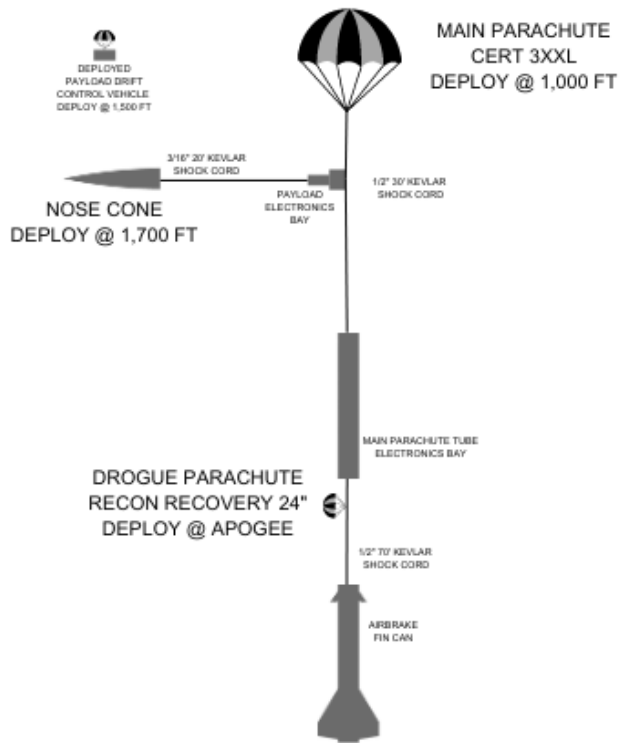


Fig. 47 Recovery harness

Honu has four sets of recovery harnesses throughout the rocket. Starting from the aft end, two 7 feet sections of tubular Kevlar rated for 3,600 lbs are connected to the forward centering ring of the fin can form a Y-harness. These cords are routed through the Airbrake via two carbon tubes and then figure-eight knots are tied at each end. A quick link connects both of these to the primary drogue harness. The drogue harness is made up of two 35 feet sections of 1/2" tubular Kevlar from OneBadHawk, creating a total shock cord length of 70 feet rated for 7,200 lbs. This 70 feet total shock cord for the drogue harness is long for a few reasons. First, since the nose cone with the payload is over 11 lbs, the long drogue shock cord ensures that when it eventually pulls taut, the shear pins in the payload bay coupler to main recovery tube do not break, preventing a premature main deployment at apogee. The longer shock cord lets drag slow down both sections of the rocket, significantly reducing the forces of the shock. A long shock cord also helps keep the sections of the rocket further away from each other during descent which minimizes the chance of sections hitting each other and causing damage. The final reason for a long shock cord is a challenge specific to East Coast flying. While MDRA has a fairly large recovery area, there are multiple large patches of trees surrounding the launch site. Especially if there are high winds, which is common for the Eastern Shore of Maryland, the rocket can end up drifting out of the recovery area and into trees. This occurred for many test flights last year, and two of those times, the long shock cord let team members recover the rocket from the trees. The Kevlar harnesses have three loops, and the drogue parachute is connected to the middle loop on the forward harness.

The main harness is made up of one 30' 1/2" 7200 lb tubular harness from OneBadHawk. This is connected to the forward end of the electronics bay and a knot is tied 6 feet from the payload bulkhead. Both sides are connected to u-bolts with quick links. The main parachute is connected to the end of the cord instead of the middle of the cord , so that all segments of the rocket (other than the nose cone) fall in one line. This configurations helps prevent tangling during deployment and descent.

The final section of the shock cord is between the top of the payload and the nose cone tip. The nose cone needs to separate so that the payload can be deployed, but all sections of the rocket must stay together to avoid tracking too many objects. These two sections are connected by 20 feet of 1/4" tubular Kevlar rated for 3,000 lb. This section does not encounter any major recovery forces and the goal is to get the nose cone away from the rocket so that the payload can deploy cleanly without tangling.

When packing the drogue and main into the rocket, both harnesses are z-folded together. This is accomplished by making multiple bundles throughout the shock cord and using painter's tape to hold them together. This makes packing it into the airframe much cleaner and also helps provide some shock absorption as the tape is ripped during deployment.

3. Recovery Attachment

Recovery mounting for Honu starts in the fin can. There are two 1/4"-20 steel threaded rods running through the three centering rings and out the aft end of the rocket. These threaded rods are tightened with nuts to each centering



Fig. 48 Honu under parachute

ring and then epoxied in place. On the forward most centering ring, two 1/4"-20 steel eye nuts rated for 3750 lbs were then screwed onto the threaded rods and epoxied in place. While these eye nuts are rated for much higher loads than other components, they had a small enough form factor that could fit between the motor mount and airframe without interference. The Y-harness then connects to the eye nuts using 1/4" steel quick links rated for 1,200 lbs. These quick links are connected to the Y-harness with a Figure-8 knot. This knot has been used dozens times over multiple rockets and is resilient. While it has never untied itself, the knot is wrapped a few times in electrical tape to keep it from loosening.



Fig. 49 Y-harness

On the other end, another 1/4" eye bolt is secured to the nose cone tip and kept in place with high strength thread locker.

4. Deployment System

All deployments for Honu are conducted using 4F black powder charges. The team has lots of experience using black powder charges in rockets and they are the simplest solution for parachute deployment. In the past, the team's rockets have used glove finger charges, in which a nitrile glove finger is cut off and filled with the appropriate amount of black powder. An MJG e-match with its leads shunted is then inserted to the bottom of the finger and the entire assembly is wrapped tightly in two layers of electrical tape until it is hard and can't be squeezed or shifted. This year, in an effort to reduce black powder usage and to make the assembly process easier to teach, Honu uses vinyl tube charges. Vinyl tubes with an inner diameter of 3/8" are cut in 5" lengths. The bottom is plugged with hot glue to a depth of 0.5". Once the hot glue is completely cooled, the appropriate amount of black powder is poured into the open end of the tube. An MJG e-match is inserted until the igniter head rests in the top layer of black powder. Dog barf insulation is then packed above the igniter to hold the igniter in place and to pack in the powder. The top is sealed with a layer of electrical tape, and the igniter lead is taped to the body near the bottom. The goal of these charges is to encourage the powder to fully combust so they can be used for higher altitude flights as well as 10,000 foot flights for the competition. The high length to diameter ratio of the tube and lighting the black powder from the top encourages complete combustion rather than just pushing the powder out.

Charge sizes were approximated using a variety of online calculators. For each separation, the shear pins were the main factor in determining charge sizes. Each shear pin takes about 50-75 lbs to break, and the drogue section has



Fig. 50 Example charge

four while the main has six to break through. Initial charge sizing took this into account and started at 3.5 g for the drogue and 4.5 g for the main. In the first ground test of these charges, the sections barely separated and did not pull the parachutes out. Through further testing, the appropriate sizing was determined. Successful charge sizes were finalized in a ground test in Honu and flown successfully. They are shown in Table 14.

Table 14 Charge sizing

Drogue Primary (g)	5.5
Drogue Backup (g)	6
Main Primary (g)	5.5
Main Backup (g)	6.5

5. Flame Protection

Since black powder is being used for deployment events, the parachutes and harnesses need to be protected from the high heat of the charges. All of the harnesses are made from Kevlar, which is naturally flame resistant. It can withstand many ejection charges without weakening like a nylon harness. Since the parachutes are made primarily of nylon, they require extra protection to prevent melting or burning. This is done by wrapping the parachute in a nomex blanket. The drogue parachute uses a 24" x 24" blanket while the main uses a 30" x 30" blanket. Both parachutes are wrapped like a burrito, as shown in Fig. 52, which protects the parachute and shroud lines entirely and allows it to slide easily into the airframe. Once deployed, the blanket easily unravels and lets the parachute inflate. The electronics bay is protected primarily by the bulkheads on either end, but there are pass-through holes for charges. These holes are partially sealed by the e-match wires, and the remaining space is covered with a piece of electrical tape. This prevents the pressurized gas from passing through the ebay, potentially damaging the electronics or venting the pressure leading to a failed deployment. In the nose cone, the payload bay coupler has a bulkhead on the aft side which seals it off with no holes. There is also a bulkhead on the forward side that fits into the nose cone so the interface is sealed. Since there isn't a coupler interface with the top bulkhead, there needs to be an alternative way to seal the payload from the ejection charge. The top bulkhead has a layer of adhesive foam around the outer edge, shown in Fig. 51. When the nose cone is slid over the coupler, the foam is compressed sealing the top of the nose cone from the rest of the compartment. This bulkhead does have a hole for the single charge that deploys the nose cone, which is sealed in the same way as the electronics bay with electrical tape.



Fig. 51 Payload nose cone seal



Fig. 52 Z folded recovery harness and parachute burrito

E. COTS Recovery Avionics

1. Electronics Bay Introduction

The electronics bay sits in between the drogue recovery tube on the aft side and the main recovery tube on the forward side. It is primarily made of a 14" long Wildman Rocketry filament wound fiberglass coupler. A 2" switchband made from student-made rolled fiberglass tube was epoxied in the middle to provide 6" of coupler on either side. To seal the ends of the coupler, two aluminum bulkheads were used, joined by two steel 5/16" threaded rods that formed the mounting points for internal structure.

The internal structure of the electronics bay was a point of major redesign this year. The main goal was to make it modular, so that the student developed avionics sled could easily be separated from the commercial electronics. In addition, the team hoped to mount internal commercial and student cameras, have the capability to add devices and switches, and make it easier to manage cables.

2. SRAD Bulkheads

The bulkheads were designed by the team last year for use in Karkinos and the design was reused this year for Honu. They consist of two 1/8" 6061-T6 aluminum plates joined by a 3/8" u-bolt that is a recovery attachment point. The outer plate has a diameter of 5.998" and sits above the coupler wall, while the inner plate has a diameter of 5.82" and sits inside the coupler wall. In addition to the four total clearance holes for the u-bolt and the threaded rods, two 0.164" holes were included so ematch wires connecting to the charges could pass through the bulkheads. During assembly, the wire is passed through and the gap sealed with electrical tape.

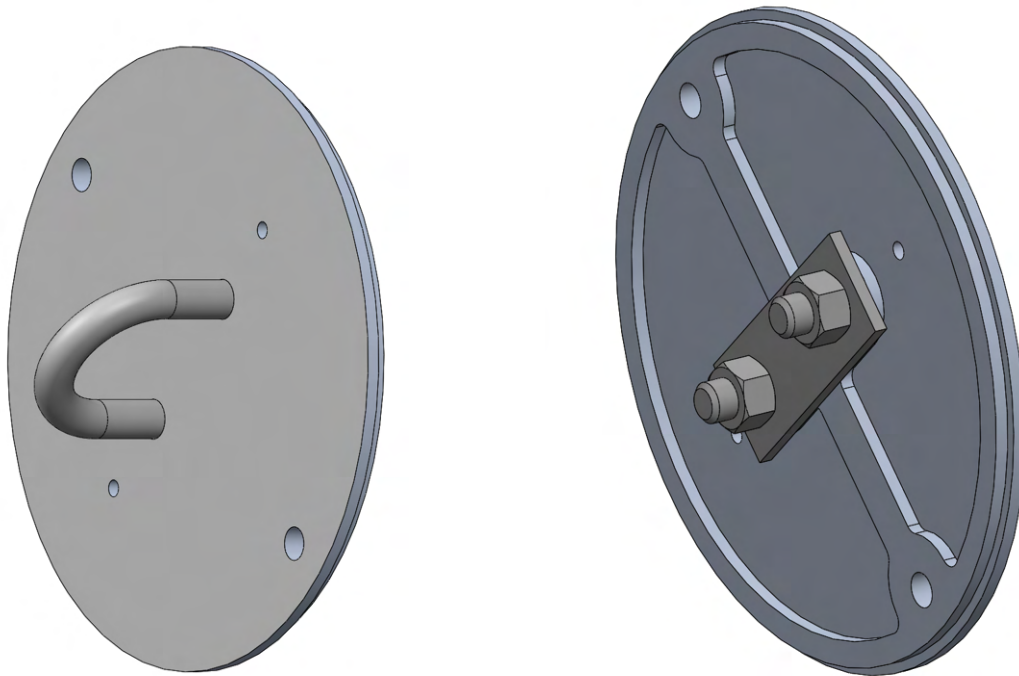


Fig. 53 CAD of Bulkheads

Finite Element Analysis (FEA) was conducted on the bulkheads. They experience the largest loads at two points during the flight: apogee deployment and main deployment. The force at apogee is primarily from the jerking of the recovery harness as it separates. For Honu, this is minimized by having a very long drogue harness and z-folding the

drogue lines, which dissipate the force of the shock. During the main deployment, as the parachute fully inflates, it also induces a jerk on the rocket. The main lines are also z-folded and the way the parachute is packed leads to a more gradual opening to minimize the shock. Based on accelerometer data collected from last year's test flights, the peak loading condition was discovered to be approximately the weight of the rocket from main parachute deployment. Jerk was also considered by measuring change of acceleration over time. Given that the structural design of the rocket underwent few changes this year, it can be reasonably assumed that the maximum force applied is the weight of the rocket which is about 85 lbf. The analysis shown in Fig. 54 progressively increased the element density around high-stress locations. The results show a maximum stress value of approximately 6.7 ksi. Aluminum 6061-T6 has a yield strength 40 ksi and an ultimate strength of 45 ksi. Thus, the bulkheads have a safety factor of 5.97 and will easily handle the peak loading condition. During numerous test flights over the last two years, the bulkheads performed as expected with no deformation or damage visible after the flight.

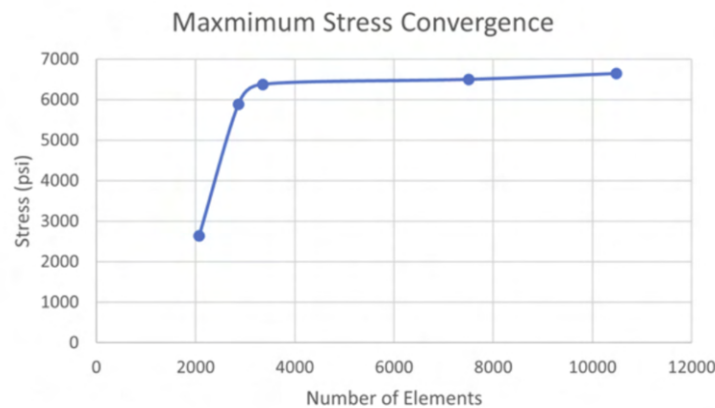


Fig. 54 Convergent Analysis Through Refinement of Mesh Around Concentrated Stress Loads

3. Commercial Electronics

The purpose of the commercial electronics flying on Honu are to provide dual redundant deployment control, tracking, and datalogging.

Altus Metrum EasyMinis are used for all deployments during Honu's flight. They were chosen due to their simplicity, small form factor, and the team's familiarity with the system. Each is completely independent, with its own battery, switch, and set of charges. Both EasyMinis are powered by independent 900 mAh lithium polymer batteries provided by Altus Metrum specifically for their flight computers. In addition, an EasyMini is located in the payload section to deploy the nose cone at 1,700 feet. It uses one charge and a 900 mAh lithium polymer battery.

One disadvantage of the Altus Metrum EasyMini is that it only contains a barometer for data collection. With multiple student developed computers onboard, there was a strong need for their data to be verified by a commercial flight computer. Therefore, the Featherweight Blue Raven was chosen primarily for its simplicity. It easily connects to a mobile app that can monitor health and transfer flight data. It was mounted with an Additive Aerospace Simple Circuit to simplify the wiring of the 400 mAh lithium polymer battery sold by Featherweight and its switch.

Featherweight also produces an easy to use GPS system, the Featherweight GPS. One is located in the electronics bay to track the rocket, while a second is in the deployable payload. These are currently set to the 915 and 917 MHz ranges respectively, but can easily be switched during frequency allocations at the competition. The ebay Featherweight uses a 400 mAh lithium polymer battery provided with the trackers by Featherweight, while the payload Featherweight uses a cylindrical 2.2 Ah lithium ion battery. The tracker has a built-in switch that has to be turned on during assembly. However, from previous experience in test flights and at the competition, the time from assembly to launch can take

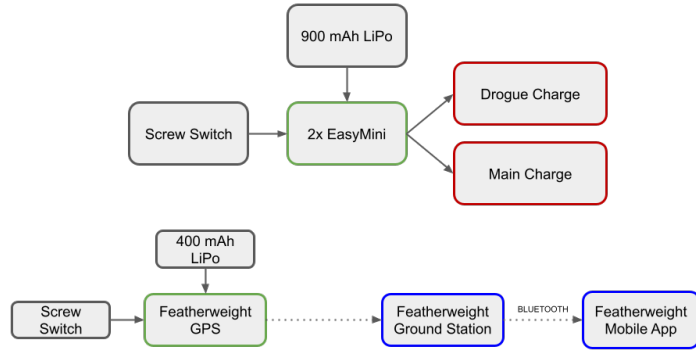


Fig. 55 Recovery Electronics Wiring Diagram

many hours. Therefore, to maximize battery life, an external switch harness was introduced this year. The built-in switch is always powered on, but an external switch is located between the positive terminal for the battery and the positive lead of the battery itself.

All commercial systems and the SRAD avionics system use Missileworks Screw Switches, which have proven reliable through dozens of test flights. Since the Altus Metrum flight computers do not have brownout protection with a capacitor, it is imperative that they do not lose power, and the screw switches have been reliable for the team.

4. Internal Structure

This year, numerous iterations were made on an internal structure to mount the electronics and switches in a compact, modular way. The primary goals were for it to be modular, allowing the team to focus on the student avionics without removing the commercial flight computers. The team also aimed to make it compact with room to add more features later, including two cameras. Cable management was also a concern.

Testing of new structures began in October using a 4" diameter Wildman Extreme testbed. In this launch, the goal was to test the feasibility of a switch ring, a ring that slides onto the threaded rods and mounts screw switches concentrically as shown in Fig. 56. In the past, the switches were directly mounted on slopes on the slide of the sled, which made it difficult to add switches after it was built. It also made drilling access holes difficult to line up perfectly. The switch ring solved both problems by having the capability to expand to more switches and positioning each switch at a known angle. The access holes have the same angle and were drilled using a 3D printed drilling guide. This iteration was easy to use and flew on two test flights. However, the sled portion was very similar to previous years, with little cable management and no specific slot for battery mounting.

In December, the team launched the first 6" diameter rocket test flight, and aboard was a scaled up version of the switch ring and a dual layered sled shown in Fig. 57. The sled aimed to take advantage of 3D space for the first time, mounting the batteries in between the surfaces of the sled, sandwiched between the electronics. However, the placement of the threaded rods made it difficult to access the batteries and the GPS tracker was not in an ideal placement for interference with the rail and rods. It also did not provide a spot for a camera. Despite its shortcomings, it proved that the team could take advantage of 3D space to mount more items in a smaller space.

For the spring semester, a large sled was developed that would integrate all of the flight computers and a GoPro Hero 10 camera. The EasyMinis were mounted on the back to space cables out and ensure that the wires leading from the charges would not interfere with the GPS or Blue Raven or be mistaken for wires from a switch. The Featherweight

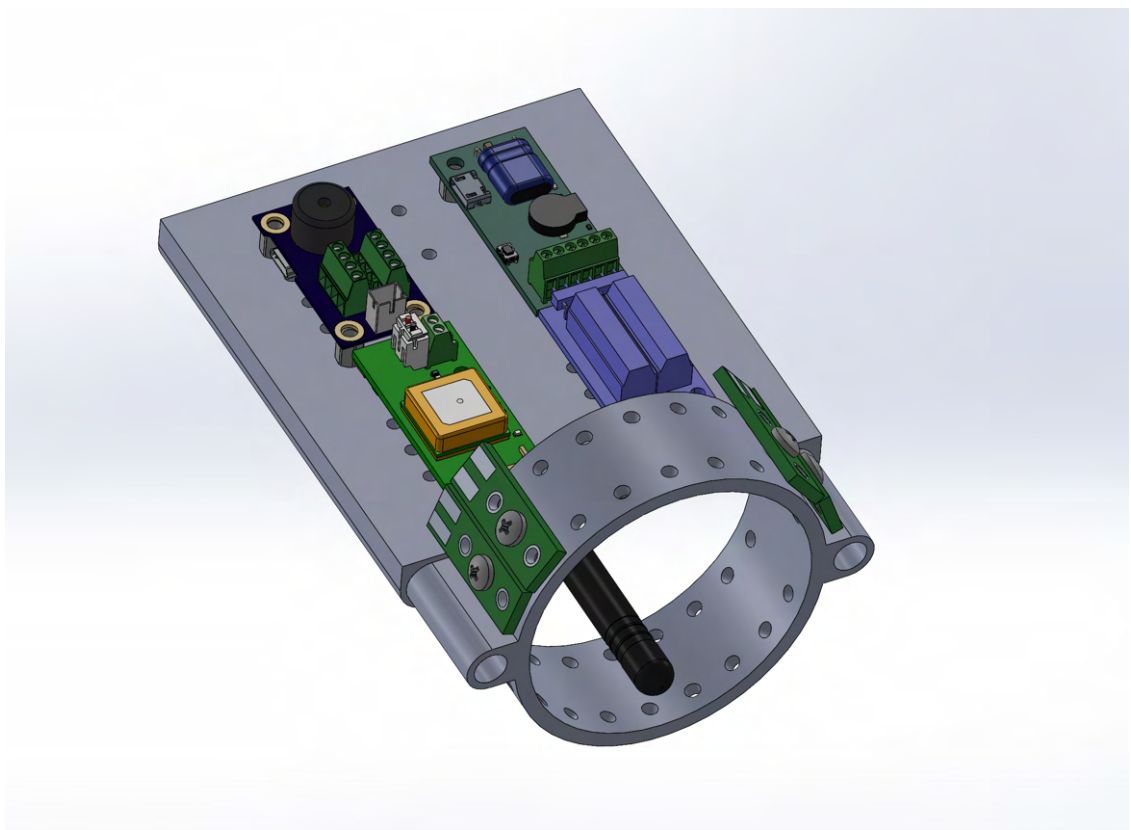


Fig. 56 Initial ebay design

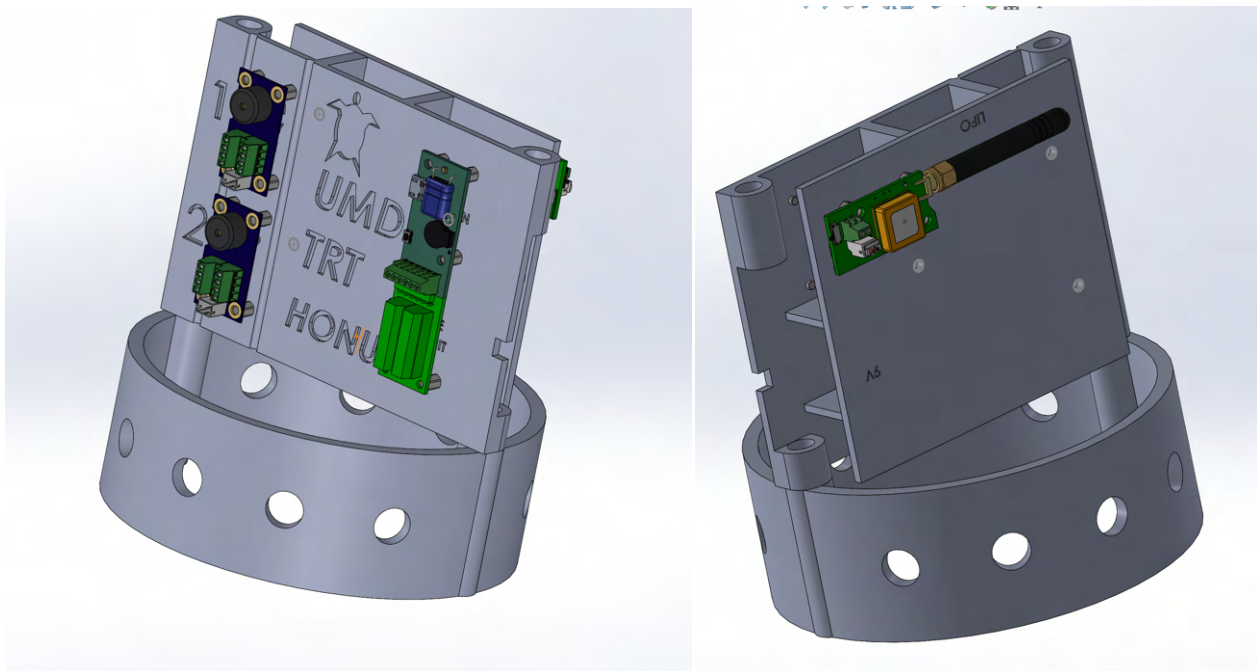


Fig. 57 December Sled Redesign

GPS was placed far from the launch rail, and a Blue Raven was next to it. In addition, the GoPro was mounted at an angle so the lens could be almost tangent to the inside of the coupler. The switch ring was modified with a cutout to allow for the GoPro to fit in the sled. An additional Innomaker camera was secured to the switch ring 180° opposing the GoPro (just above and to the left of the EasyMinis). This would connect to the SRAD Avionics computer, discussed later. Slots were designed into the sled to account for numerous batteries, and these slots were covered securely by panels that screwed into the print. Three batteries were contained in a slot in the center of the sled, under the printed words. The final battery was mounted to the back of the sled for the primary EasyMini. Since weight saving was not a concern in the electronics bay, a small turtle was printed and secured to represent the university and the Honu name. This ebay design can be seen in Figures 58, 59, and 58.



Fig. 58 Ebay front face



Fig. 59 GoPro mounting



Fig. 60 Ebay back face

This design worked well in three test flights. All parts were printed out of PETG filament in order to withstand the heat of the desert during the competition. Its additional strength and heat resistance over PLA made it a good choice to use for this purpose. For future improvements, a panel that secured the GoPro in place would be useful, similar to the battery panels. The design could still be much lighter, since little weight savings measures were taken.



Fig. 61 Flight Ready Electronics Bay Front Face

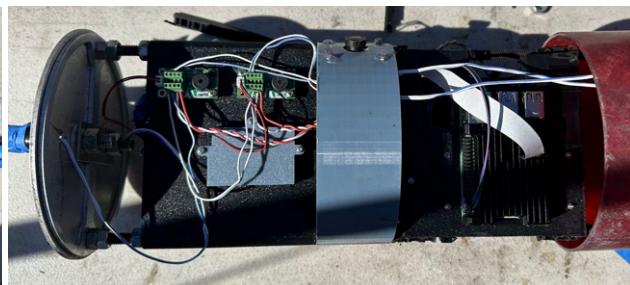


Fig. 62 Flight Ready Electronics Bay Back Face

F. SRAD Avionics

The goal of the SRAD avionics board is to replicate and improve upon the telemetry and data logging capabilities that a COTS flight computer can normally provide. It also includes functionality for live video transmission and data fusion for more accurate readings. A system overview is pictured below in Fig 63.

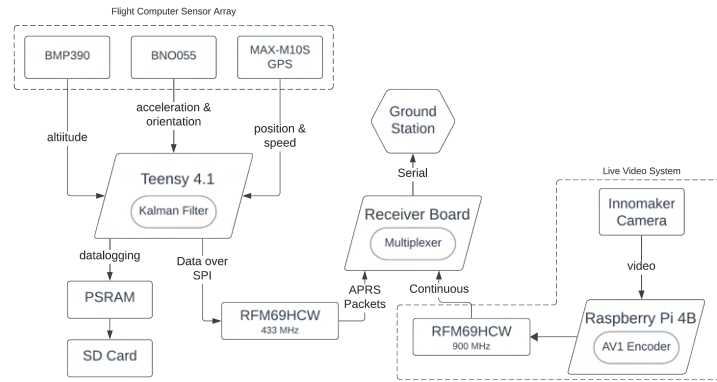


Fig. 63 System overview of the different parts of the SRAD Avionics

1. Sensor Array

A variety of sensors and components are used to collect data for the rocket's flight. These sensors and systems are constructed from scratch at a low level, working directly with the surface-mount device (SMD) chip for each sensor and constructing an auxiliary circuit around it to be able to deliver accurate readings of the environment. Each subcircuit is equipped with 100 nF decoupling capacitors from voltage in lines to ground in order to minimize fluctuations in power. These sensors are all connected to the primary microcontroller via an I2C bus with data being updated at 10 Hz. A custom PCB is used to house and connect all components and sensors, while maintaining a small form factor of about 3" by 3.5". A four-layer PCB is used to break out a voltage and ground plane to minimize signal noise and trace lengths.

A BMP390 chip is used as an altimeter by obtaining barometric pressure readings and converting it to a height reading relative to the start position within an error of about ± 1 foot. Zeroing these readings at a starting ground pressure gives relative altitude, and a resampling of ground pressure while on the pad helps mitigate sensor drift and error due to transient pressure differences. Internally, this sensor incorporates an infinite impulse response (IIR) filter, a form of digital signal processing where previous measurements are recursively fed into the input for the next reading. This filter, enabled with a low weighting coefficient, helps smooth signals while also allowing for minimal raw data to be lost.

A BNO055 chip is used as a 9-DOF inertial measurement unit (IMU) that gives accelerometer, gyroscope, and magnetometer readings. This chip has configurable settings that allow for it to be able to take in a range of accelerations up to ± 8 g and uses data fusion between its orientation and geomagnetic data to generate both absolute and relative orientations. Its subcircuit contains an external 32.768 kHz crystal oscillator to help maintain its internal clock for accurate readings.

A MAX-M10S chip was chosen for GPS readings, due to its ± 5 feet theoretical accuracy and its low-power consumption. Using uBlox library, it's configurable to be in an airborne mode, allowing for >4 g accelerations. This chip is coupled with the Taoglas SGGP12. A patch antenna, which has a low-profile and maximal efficiency at the GPS frequency range of 1575.42/1602 MHz. The subcircuit is designed such that this patch antenna is centered relative to the ground plane, to avoid interference from ground noise, and is paired with a band-pass filter to eliminate noise on the signal line. This was created with a $10\ \Omega$ resistor, a 10 nF capacitor, and a 68 nH ferrite bead in order to match the antenna's desired impedance.

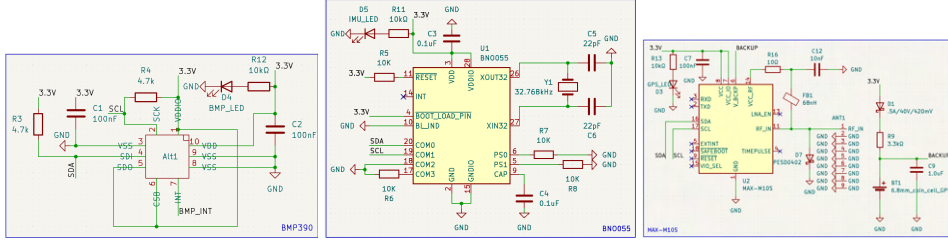


Fig. 64 SRAD Avionics Sensor Subcircuit Schematics

2. Battery

The Tenergy 4.8 V battery pack was selected as the power source for the flight computer due to voltage, runtime, and ease of use. Each of the main components of the flight computer that this battery would power are listed in Table 15. This battery pack runs at 4.8 V, which meets the operational requirements for all of the components, and has 2 Ah of charge, which will provide around 16 hours of runtime on standby and around 6 hours of runtime when at maximum use, which meets the needs of the flight computer.

Table 15 SRAD Avionics Components Current Draw

Components	Idle Operating Current (mA)	Max Operating Current (mA)	Idle Power Consumption (mW)	Max Power Consumption (mW)	Operating Voltage (V)
Teensy 4.1	100	100	500	500	5
BNO055 IMU	0.4	1.23	1.32	4.06	3.3
MAX-M10S GPS	7.6	100	25	330	3.3
BMP390 Barometric Pressure Sensor	0.32	7.20	7.2	7.2	3.3
RFM69HCW Radio Module	16	130	52.8	429	3.3
TOTAL	124.3	338.4	586.32	1270.26	

3. Microcontroller

The Teensy 4.1 was chosen as the SRAD flight computer's primary microcontroller for its ease-of-use, form factor, compatibility with other devices, and processing power. It runs on a 600 MHz clock with 1 MB of onboard RAM which allows it to quickly process and handle data. The software for the flight computer is developed in an object-oriented manner, to help structure and maintain a modular codebase that enables convenient organization and abstractions that help development. By having each sensor or device extend an abstract superclass, the internal state object can operate in an implementation agnostic manner.

In addition to live telemetry provided by the radio, the Avionics system supports local data storage on a Micro SD card. Raw sensor data from each sensor is stored as a CSV, and a log-file-type text file that notes timing of special events such as launch. This is augmented by a Pseudo-Static-RAM (PSRAM) chip that is embedded in the system to extend the Teensy's RAM storage. Every time the sensors are updated, data is written either directly to the SD card or to a buffer on the PSRAM, saving raw sensor data as well as state variables updated by the Kalman filter. Before flight, it simply writes any data directly to the SD card as it processes it. During flight, the team was worried about potential lag issues caused by I/O to the SD card in addition to vibrations causing the SD card to become temporarily disconnected, so the data is written to the PSRAM. Flight computer data and logs are written to two separate buffers on either end of the PSRAM that grow towards each other, and are dumped to the SD card for persistent storage shortly after landing.

4. Kalman Filter

In order to monitor and control the progress of the rocket, it is necessary to know its current state. However, the measurements from onboard sensors are inherently noisy and prone to drift. The goal of the Kalman filter is to combine the individual measurements from these three sensors with a kinematic model of the rocket's flight path to accurately predict the position and velocity of the rocket at any given moment, in a system that is reused by multiple of the rocket's subsystems.

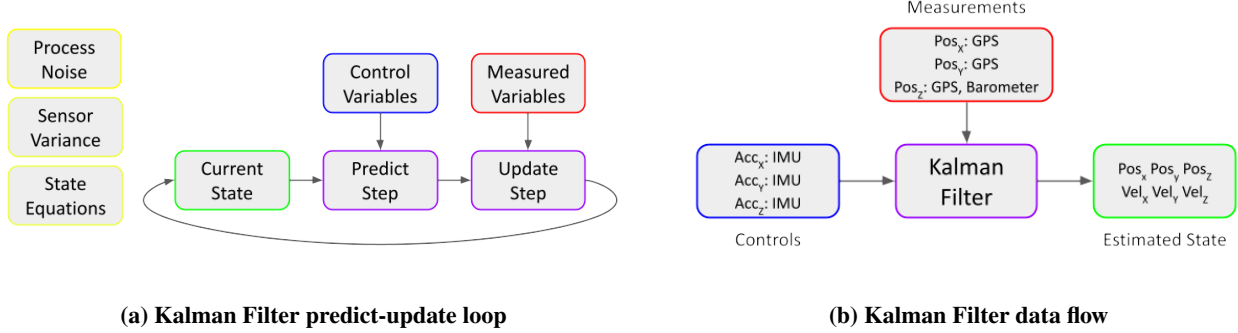


Fig. 65 Kalman Filter System Diagrams

The Kalman filter consists of a predict-update loop, as seen in Fig. 65. At initialization, the process noise, sensor variance, and equations of state are determined. Every loop, a prediction is first made using the control variables, and then an update is made based on the measured variables. A key feature of the filter is the Kalman gain variable, which shifts the weight given to measurements depending on measurement accuracy and the confidence of the model. The variables, matrices, and equations that make up a Kalman filter are described below.

Table 16 Kalman Filter Variable Descriptions

Variable	Description	Size
n_x	Number of State Variables	Scalar
n_u	Number of Inputs	Scalar
n_z	Number of Measurements	Scalar
Δt	Timestep	Scalar
x	State Vector	$[n_x \times 1]$
u	Input Vector	$[n_u \times 1]$
z	Measurement Vector	$[n_z \times 1]$
F	State Transition Matrix	$[n_x \times n_x]$
G	Control Matrix	$[n_x \times n_u]$
H	Observation Matrix	$[n_z \times n_x]$
P	Estimate Covariance	$[n_x \times n_x]$
Q	Process Noise Covariance	$[n_x \times n_x]$
R	Measurement Covariance	$[n_z \times n_z]$
K	Kalman Gain	$[n_x \times n_z]$
I	Identity Matrix	$[n_x \times n_x]$

Predict Step:

$$\text{State Extrapolation: } x = Fx + Gu \quad (12)$$

$$\text{Covariance Extrapolation: } P = FPF^T + Q \quad (13)$$

Update Step:

$$\text{State Update: } x = x + K(z - Hx) \quad (14)$$

$$\text{Covariance Update: } P = (I - KH)P(I - KH)^T + KRK^T \quad (15)$$

$$\text{Kalman Gain: } K = PH^T(HPH^T + R)^{-1} \quad (16)$$

Miscellaneous:

$$\text{Process Noise Covariance: } Q = G * 0.04 * G^T \quad (17)$$

For the purposes of the Avionics and Payload subteams, the most important state information is the X, Y, and Z position and velocity. The Kalman filter uses the X, Y, and Z acceleration as a control input, and the X, Y, and Z position as a measurement, derived from the sensors as detailed in Fig. 65. Matrices G and H in Eq. 18 and Eq. 19 show the kinematics of the systems as well as what entries the various sensors affect.

$$G = \begin{bmatrix} 0.5\Delta t^2 & 0 & 0 \\ 0 & 0.5\Delta t^2 & 0 \\ 0 & 0 & 0.5\Delta t^2 \\ \Delta t & 0 & 0 \\ 0 & \Delta t & 0 \\ 0 & 0 & \Delta t \end{bmatrix} \quad (18)$$

$$H = \begin{bmatrix} \text{gps} & 0 & 0 & 0 & 0 & 0 \\ 0 & \text{gps} & 0 & 0 & 0 & 0 \\ 0 & 0 & \text{baro} & 0 & 0 & 0 \end{bmatrix} \quad (19)$$

The development of the Kalman Filter library began with a MATLAB implementation, utilizing both historical and simulated flight data for validation and tuning. Following validation, the filter was ported to C++ to integrate with the flight control systems running on the microcontroller. All matrices were originally stored as dynamically allocated arrays, but later the created a custom Matrix class.

The final iteration of the Kalman Filter is encapsulated in a custom C++ `KalmanFilter` class, designed to maintain modularity and ensure seamless integration with other onboard systems of the rocket. This class centralizes all state estimation processes, including filter initialization. A dedicated Matrix class handles essential matrix operations, such as multiplication and inversion which employs LU decomposition with partial pivoting to guarantee numerical stability. The `KalmanFilter` class is designed to support state vectors of varying sizes and can be universally applied across different modules, enhancing its utility and adaptability in complex systems. All inputs are verified to be numerical, and any NaN values are simply replaced with 0 and the H matrix is adjusted to remove those values from state updates.

5. Telemetry

For telemetry transmission, the Adafruit RFM69HCW radio module breakout board was selected because it integrates the Semtech SX1231H Integrated Circuit (IC) module into an easy to use breakout board. The SX1231H was selected due to its higher transmit power of +20 dBm (compared to +17 dBm of most other modules), slightly increased sensitivity of -123 dBm, as opposed to -120 dBm, compatibility with the desired frequency band, the 433 MHz amateur band, and availability of breakout modules. Both higher transmit power and increased sensitivity were selected to optimize for reliability at long range, while the 433 MHz band was selected due to familiarity with using the band for radio communication in previous systems. Compared to last year's system, which used a LoRa (Long Range) radio, a Frequency Shift Keying (FSK) radio was selected this year due to limitations noted in the range of LoRa radios when the signal traveled through solid objects like the rocket body. The radio uses a small, omnidirectional monopole antenna tuned to the 433 MHz band due to space constraints within the rocket.

The Teensy 4.1 interfaces directly with the radio module using the Serial Peripheral Interface (SPI) protocol, and

uses the RadioHead library, which abstracts most of the direct interaction with the hardware. However, a custom send and receive method is implemented that allows transmissions of packets of unlimited length, due to the RadioHead library limiting single packets to 60 bytes. These modifications allow increased efficiency and reliability in telemetry transmission. The telemetry radios are configured to transmit at 4.8 kbps, with a frequency deviation of 9.6 kHz. Before being passed to the radio, the packets are encoded in the Amateur Packet Reporting System (APRS) format commonly used in high power rocketry. The encoding method is adapted from third party libraries for better hardware and software compatibility. All radio hardware settings can easily be changed by uploading new firmware in case of a conflict with other teams.

6. Live Video

The primary purpose of the Avionics Live Video System is to capture and transmit a live video stream from the rocket to the ground during flight in order to compete in the Live Video Challenge. The Live Video system is powered on and started by the flight computer due to its high power consumption, after which it operates independently. There is a nearly identical system contained within the payload, that has been modified slightly to fit within tighter space constraints and is discussed in the Payload Live Video section.

The core of the system is built around the Raspberry Pi 4b and an Innomaker camera compatible with the Pi. The camera is connected to the Camera Serial Interface (CSI) port on the Pi, and is based around the OV5647 5 megapixel (MP) sensor. It has a maximum resolution of 1080p at 30 frames per second (fps), which is then downsampled by the libcamera library to 900x720 pixels at 30 fps and transferred to the encoder as raw YUV420 video. To encode the video at a low enough bitrate to be transmitted, while still retaining most of the quality of the video, the AV1 encoding standard is used. The encoding targets a final bitrate of around 280-290 kbps, which is then transferred to the radio for transmission. This process is started by the Teensy 4.1 sending a signal to the Raspberry Pi triggered by launch.

The radios selected for transmitting the video from the rocket to the ground are the same used on the flight computer, but optimized for the 900 MHz amateur radio band rather than 433 MHz to help transmit at higher bit rates with minimal range loss. The live Video radios use a similar modified RadioHead library as used on the flight computer, but adapted to the Pi, to get as close as possible to their 300 kbps limit. Sending them as large packets, about 9.3 kbytes for one frame of video, which means there is very little overhead in the transmission compared to the overall packet size.

The Raspberry Pi, radio, and camera rely on a custom power delivery system to support the high power draw during video encoding and transmission. The recommended power supply for the Raspberry Pi 4b is 5 V at 3 A, and a maximum power draw, with all the electronics together, is likely to draw a maximum of 1.5 A. To support this, two 3.7 V 3000 mAh Samsung button top lithium ion batteries were selected, which support up to a 15 A current draw. To provide 5 V exactly, the batteries are wired in series, producing at minimum 5 V at cutoff voltage, and a buck converter is used to step down the voltage. Assuming 90% efficiency on the buck converter yields 2.66 hours of battery life, at maximum power draw, which is more than enough for the 3 minute long flight, a calculation supported by empirical endurance and flight tests. The buck converter is enabled and starts providing power to the Live Video electronics after 20 minutes from the flight computer. The batteries, radio, and buck converter, as well as connections between the Pi, the radio, power, and the Teensy 4.1 are assembled into the power delivery board shown in Fig 66 and Fig 67.

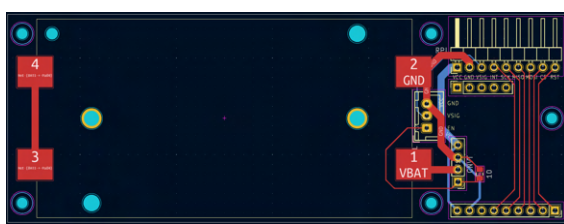


Fig. 66 Live video power deliver schematic

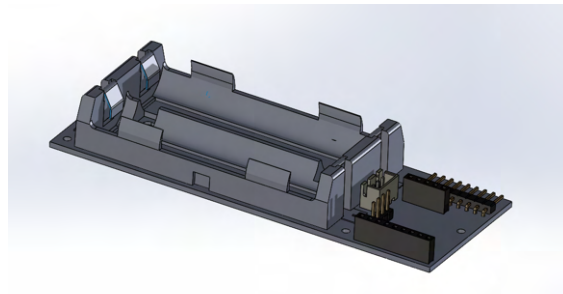


Fig. 67 Live video power circuit CAD

7. Ground Station

On the ground, there are 3 high-gain directional Yagi antennas and 3 RFM69HCW modules configured to act as receivers for the 3 incoming streams - one telemetry stream at 433 MHz, and two video streams in the 900 MHz range, one from SRAD Avionics and another from Payload. A ground receiver PCB facilitates these receivers' connection to a Teensy 4.1 microcontroller, which takes in these streams of data over SPI. The Teensy runs firmware based on the same RFM69HCW class and modified libraries as before to decode the APRS packages and live video streams. A custom Time-Division Multiplexing (TDM) protocol is used to combine these three streams into a single stream that can be sent over Serial and processed by the ground station software. An asynchronous TDM algorithm allows for the up to 600 kbps of combined data to be processed in real-time with differing source frequencies by sending time-driven frames with variable space payloads and indicator bits in the header.

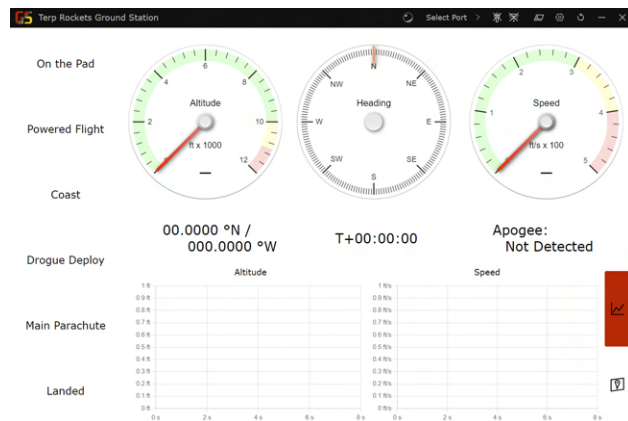


Fig. 68 SRAD Avionics Ground Station Application

The ground station is a custom application developed in Node.js using Electron that incorporates a demultiplexer to split the incoming Serial data into separate streams. It stores telemetry data locally in a Comma Separated Values (CSV) file and displays it using a Graphical User Interface (GUI) shown in Fig. 68. The GUI is designed so that rocket performance can easily be monitored during flight, with a live map that displays GPS coordinates. The application also includes a separate, text based output in the case of issues with the GUI, and error handling has been implemented to avoid errors with one part of the application impacting others. The incoming video streams are decoded to YUV420 using the ffmpeg library running the dav1d AV1 decoder, and then is displayed in a separate application window that is used to display the actual live stream for the Live Video Challenge. This window is locked to 1080p at 30 fps and will be sent to the provided video ingest equipment.

G. Airbrake

The Airbrake team designed a module that minimizes the distance between Honu's actual apogee and desired apogee during the rocket's coasting phase. This system takes into account the various uncertainties within each flight, allowing for repeatable and accurate launches under a broad range of conditions. This project has been in development since 2021 and has undergone several iterations before SAC 2024. Much of the Airbrake's architecture remains identical to last year's and was covered in the Terrapin Rocket Team 2023 Technical Report. This section will be an overview of the system as well as the 2024 team's contributions to the Airbrake unit, with material essential to understanding.

1. Overview

The Airbrake is designed as a separate module in order to minimize the complexity while integrating it with the rest of the rocket. Taking inspiration from traditional ebays the Airbrake's casing is a 12" long 6" airframe tube and a 24" long 6" coupler. This design was chosen over the lighter design of building the Airbrake into the frame of the rocket for two main reasons. First, due to its complexity, there was a significant chance that part or all of the Airbrake would not be certified as flight-ready. In this scenario, it was important to have a contingency plan to allow Honu to still compete at the 2024 SAC without Airbrakes. Since it is designed to be modular a boilerplate with the appropriate fairings would be able to be manufactured rapidly to get Honu to be flight-ready for the competition. Secondly, this multi-year project will outlive the specific competition rocket that it flies on. To reduce the manufacturing time and cost, a modular design allows the team to fly with the Airbrake on a much wider array of rockets. In fact, the current Airbrake has flown on three different rockets in the past two years.

There are two common designs for the control surfaces of Airbrakes: the first are plates that extend out of the rocket body perpendicular to the airflow, and the second are flaps that start parallel to the rocket body and rotate upwards into the flow. Although the first design is usually smaller and less massive, we chose the second design since it is considered to be safer. The aerodynamic forces on the second design will force the flaps into the inert position thereby reducing the chances of undesired external moments on the rocket.



Fig. 69 External CAD of the Airbrake module.



Fig. 70 Internal CAD of the Airbrake module.

2. Deployment Mechanism

The deployment is achieved by a stepper motor. The motor displaces an actuator disk which is connected to four threaded rods. The actuator disk has two channels that restrict the disk to only move in the vertical direction. The rods are connected on their other end to a control horn connected to the flaps. As the disk is displaced down it rotates the flaps into the airflow. The entire assembly is coupled so that the flaps are mechanically locked to each other and are therefore guaranteed to deploy to the same angle; Figs. 71, 72, and 73 show various deployment configurations.



Fig. 71 Flaps fully retracted



Fig. 72 Flaps deployed to 45°



Fig. 73 Flaps fully deployed

3. Airbrake Structure

The structure of the Airbrake module is inspired by standard electronic bays in high-powered model rockets, and it was rebuilt with a few changes after the April low altitude launch due to the damage. The Airbrake frame is, similar to the construction of the main body tube and couplers, a student-made, hand-rolled fiberglass airframe, made by rolling six layers of fiberglass cloth and epoxy resin. Fiberglass was chosen because it is very strong and stiff while being lightweight and inexpensive. To make the Airbrake coupler, a mandrel was 3D printed in segments and joined together. After sanding and graphite powder surface preparation, a layer of Mylar film was applied. This film was coated in epoxy and four layers of carbon fiber cloth were rolled similar to the other student rolled airframes ending with peel ply as seen as Fig. 74. After curing, the lower half of the coupler was reinforced with three layers of carbon fiber sleeve on the inside. This is a new change from last year, when the team sliced an airframe tube to reduce the outer diameter to a coupler size. Two 1/4" steel rods connected to bulkheads placed at the top and bottom of the module provide an anchor for the various systems. The cuts in the switch band which house the flap and screw holes for the upper section of flap assembly were cut using a Dremel and a 3D printed guide. This switch band then acted as a guide for the cutouts on the coupler which were cut using a Dremel. The external and internal bulkheads were cut from 1/8" aluminum stock using a water jet. There are also two carbon fiber tubes that run the length of the Airbrake. These are to allow passage of the recovery shock cords to run from the fincan to the electronics bay. It is desired that the force of the recovery events bypasses the Airbrake, but it is also needed that the shock cords do not tangle with any of the hardware of the Airbrake. Lastly, there are a few 3D-printed bulkheads and tubes to help with cable management. There are a lot of cables that pass close to moving parts so we designed and added barriers to ensure nothing gets tangled.

Last year, the flaps were redesigned because a flap had broken due to the large aerodynamic drag forces right after burnout. The hinge and clevis rod are 3D printed out of stainless steel and the flaps are cutouts of a fiberglass SRAD airframe section. The flaps are then fixed to the clevis rod with a pair of screws. To test the strength of the new design a tensile test was performed. A luggage scale was hooked into a slit in the flap and then the pressure was applied to the luggage scale. We managed to apply 100 lbs of force on the flap and it remained undamaged. This is a minimum factor of safety of three but in reality, it is probably much greater.

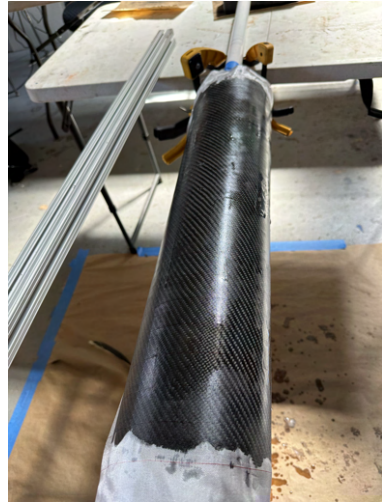


Fig. 74 Carbon Fiber Coupler After Peel Ply Application

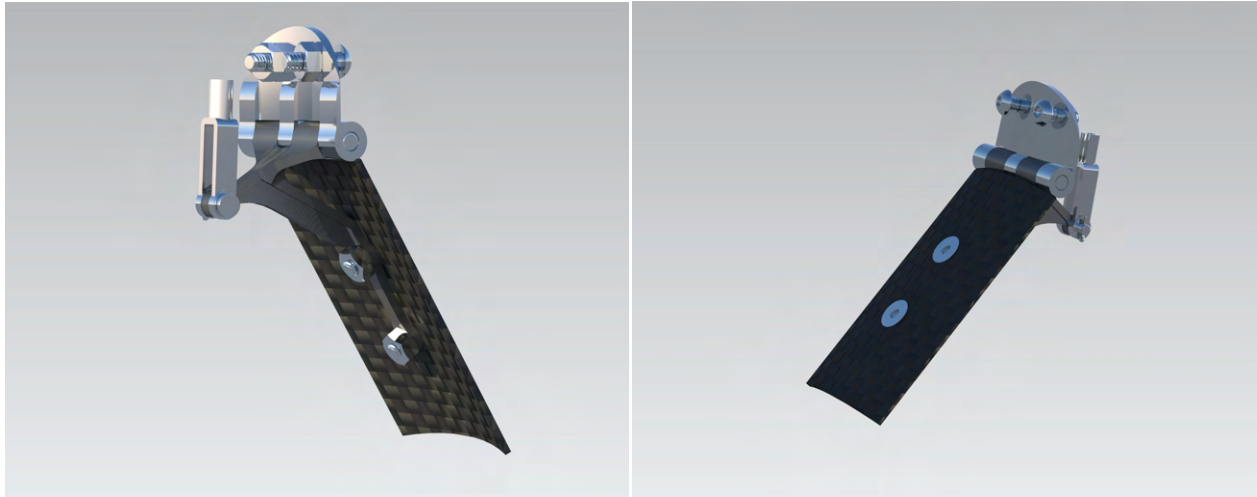


Fig. 75 Back view of flaps

Fig. 76 Front view of flaps

4. Avionics

PCB Overview The Airbrake's printed circuit board measures 3.5" by 2.5", and routes signals between the system's various sensors and computation boards. These components are mounted on one side for easy prototyping, convenience, and because space was not a large concern. Four 0.112" diameter holes interface with the printed ebay via screws. A silk screen outlines the orientation and nameplates for the placement of each component. A local ground and power plane reduce noise and extraneous power from spreading inside the circuit. The PCB uses two Teensy 4.1 microcontrollers. This choice was considered based on ground tests, which saw single microcontroller use as not ideal. Using just one microcontroller substantially strains the processing capabilities since stepper motors constantly require pulsed signals, and we also need computation for vital functions: data collection, state estimation, apogee prediction, and feedback control. By using the primary microcontroller to only process data and send the actuation angle to the secondary Teensy, the Airbrake computer can process data using one microcontroller and actuate continuously through the other.

The main microcontroller collects data from a barometric pressure sensor and IMU. The IMU is oriented along the Y axis of the board, where it will remain near the rocket's axis of symmetry, reducing the measurement of centrifugal forces. While most of the processing components rest on header pins for replacement and convenience, the motor

microcontroller is directly soldered to the board. This compromise is necessary to access the flash and SD ports of each microcontroller. Initial flight tests provided more noise than previous boards, which may have been due to interference between each trace signaling. As a result, all traces are now isolated with a 0.015" tolerance between each other. The PCB went through multiple iterations, each reflective of the change in Airbrake priorities. In the future, the team aims to reduce Airbrake complexity and eventually outline an algorithm that facilitates one microcontroller use.

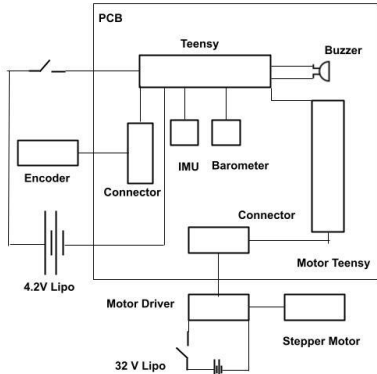


Fig. 77 Schematic of Airbrake computer and actuator

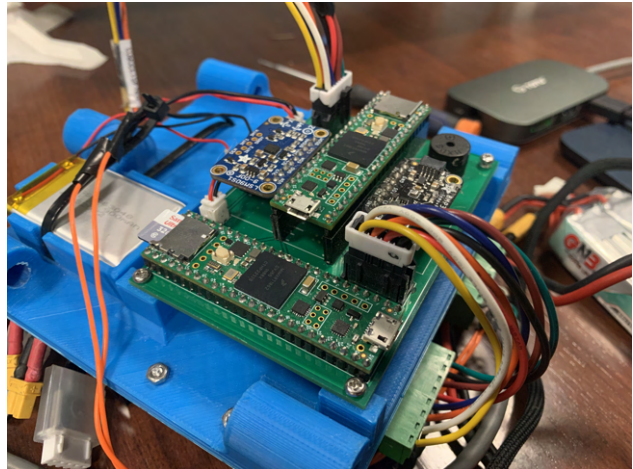


Fig. 78 Circuit board, assembled

Sensor Data Overview

- Data from the LSM9DS1 (IMU) provides acceleration and gyroscopic data
- Data from the BMP388 (Barometric Pressure Sensor) reports height estimates
- Data from the Encoder allows for confirmation that the position of the flaps matches exactly with our expectations. It also allows for error correction after the initial actuation if the flaps are not in the desired position

Data Storage Overview To store data from the sensors along with other diagnostic information, the team utilizes a PSRAM chip for short-term storage and an SD Card for long-term storage. While testing, we noticed that the process of writing to an SD Card is quite slow, but writing to the PSRAM was significantly faster. To take advantage of this finding, the flight data is written to the PSRAM before copying the data to the SD Card after the flight computer determines the recovery event has occurred. The data on the SD Card is in a CSV format for easy importing into MATLAB and Microsoft Excel for analysis.

Offloading of Actuation Along with data collection, the Teensy is tasked with using the sensor measurements to determine how much actuation is required for the Airbrake flaps. While it is possible to actuate from the Teensy directly, the process of stepping the motor causes a critical slowdown in sensor collection. The system therefore, uses a second Teensy 4.1 to step the motor driver. The actuation information is transmitted as the number of motor steps away from the desired actuation and is communicated through a Serial connection.

Main Computer Code Breakdown On the main Teensy, the code consists of a setup process that initializes and calibrates the sensors as well as a control loop that repeatedly polls data that feeds into a state machine. A block diagram of the system is in Fig. 77.

Before launch, sensor data will be written directly to the SD Card until the pre-programmed launch conditions are met. Once the launch condition is met, sensor data will be written to the PSRAM chip instead, and software will calculate the desired actuation angle for transmission to the Teensy actuation controller. The software will also watch for a pre-programmed condition to determine when the first recovery event has occurred. Once triggered, the contents in

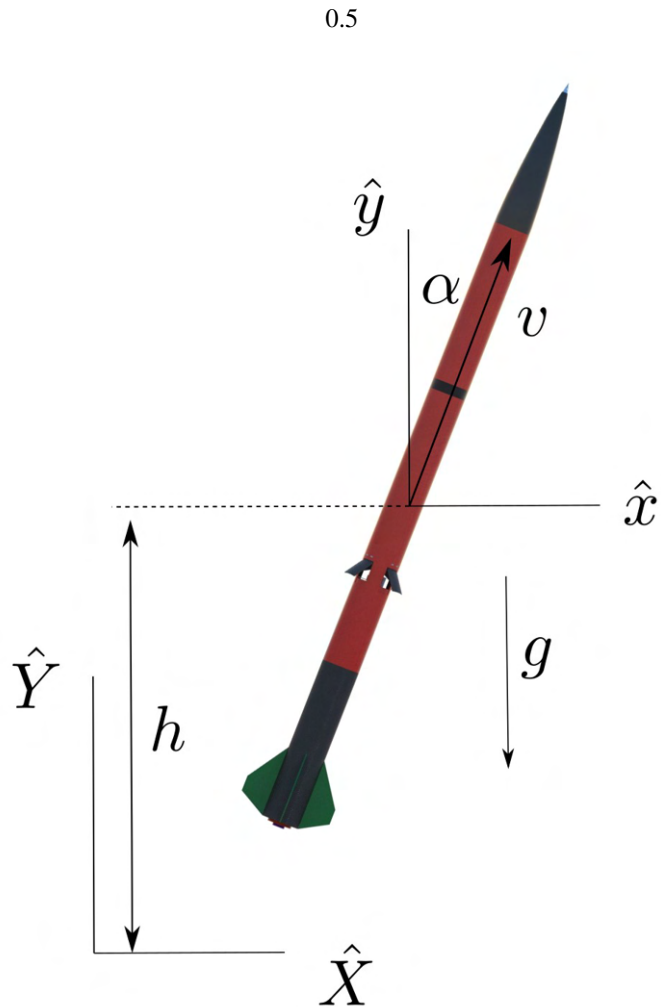


Fig. 79 The relevant states: height, h , velocity along body-axis, v and tilt off the vertical-axis, α of the closed-loop altitude control system and inertial axis

PSRAM will be copied to the SD Card. Sensor data will continue being written to the SD Card until the power is turned off.

Actuation Controller Code Breakdown The Teensy actuation controller operates in a loop of polling for desired actuation angles from the primary Teensy. When the motor Teensy actuation controller receives a number of motor steps away from the desired actuation, it will actuate accordingly. Not all steps are completed in one sequence, so the desired actuation can change mid-sequence and the controller will account for that. The number of steps received from the primary Teensy is based on the desired actuation and encoder values, so the secondary Teensy can be sure that the data received is the exact number of steps from the desired actuation. The value is sent multiple times to prevent issues related to data corruption along the Serial transmission line. If the primary Teensy detects any off-nominal behavior it will command the secondary Teensy to fully retract the flaps and remain closed.

Fig. 80 shows a flow chart of the main parts of the flight computer process.

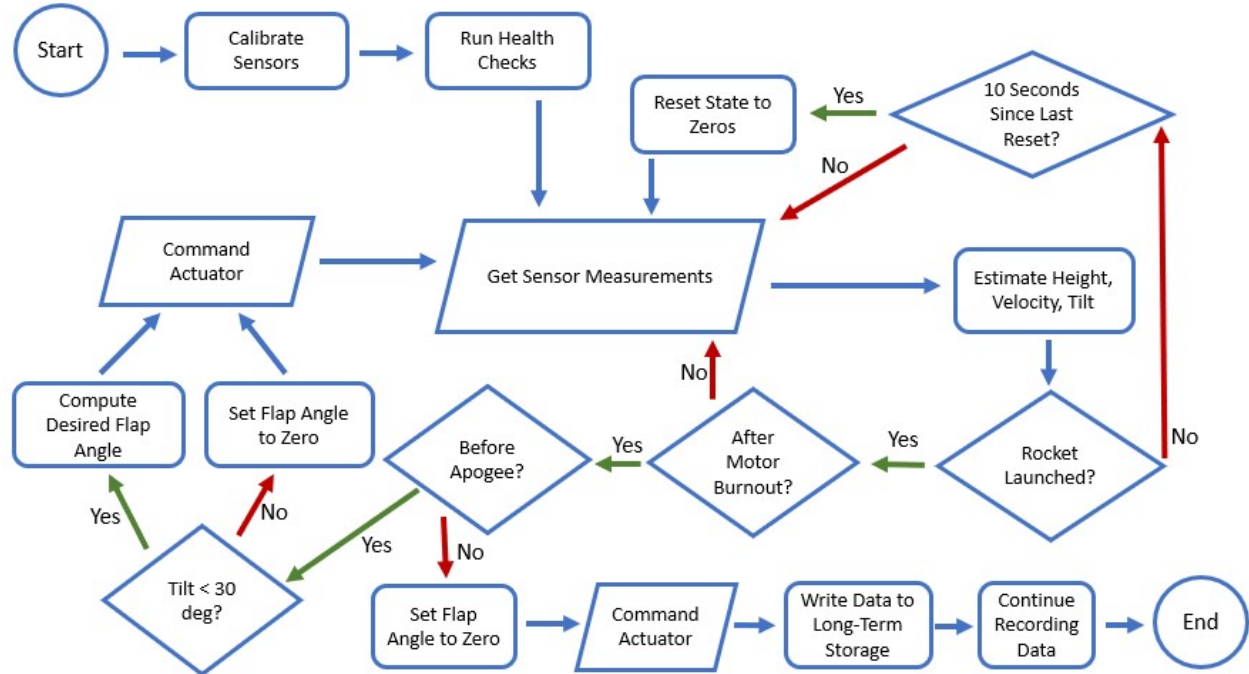


Fig. 80 State machine flow chart of the Airbrake flight computer

5. State-Estimation

Kalman Filter An important aspect of a closed-loop control system is obtaining *state-feedback*. For this case, the state $\mathbf{x} = [h, v]^T$, where h is the height of the rocket and v is its velocity along its longitudinal axis. To this effect, the team uses a Kalman filter (KF) for state estimation. A Kalman filter serves a dual purpose — estimating state feedback and filtering sensor noise.

The Kalman filter comprises of two steps: *predict* and *update*. It uses the system's process model and prior state to *predict*, and sensor measurements to *update* the prediction, obtaining a "filtered" estimate of the state. The filter is a linear, discrete-time, optimal estimator that assumes uni-modal Gaussian noise. In practice, with proper parameter-tuning, Kalman filters are sufficient for most systems with micro-electro-mechanical sensors (MEMS).

Sensor data obtained from the accelerometer (a_m) and barometer (h_m) are used to drive the process model. The tilt of the rocket, α is estimated in a separate process, as described in the subsequent section. The Kalman filter assumes the tilt to be already estimated and uses it as one of the inputs. The state variables are as illustrated in Fig. 79, and the corresponding state equations in discrete time are as follows:

Process model:

$$\begin{bmatrix} h \\ v \end{bmatrix}_{k+1} = \begin{bmatrix} 1 & T_s \cos \alpha_k \\ 0 & 1 \end{bmatrix} \begin{bmatrix} h \\ v \end{bmatrix}_k + \begin{bmatrix} \frac{T_s^2}{2} (a_m \cos \alpha_k - g) \\ T_s (a_m - g \cos \alpha_k) \end{bmatrix} + \omega_k \quad (20)$$

$$\mathbf{x}_{k+1} = \mathbf{F}_k \mathbf{x}_k + \mathbf{u}_k + \boldsymbol{\omega}_k$$

Measurement model:

$$\begin{bmatrix} h_m \end{bmatrix}_k = \begin{bmatrix} 1 & 0 \end{bmatrix} \begin{bmatrix} h \\ v \end{bmatrix}_k + \nu_k \quad (21)$$

$$z_k = \mathbf{H}_k \mathbf{x}_k + \boldsymbol{\nu}_k$$

where, T_s is the sampling time, a_m is the component of the acceleration along the axis of symmetry of the rocket,

measured from the accelerometer, g is the acceleration due to gravity, and k indicates the time-instance. ω and v are normal-distributed Gaussian noise with covariance matrices Q and R respectively. R is a scalar and Q is defined as [2],

$$Q = q^2 \begin{bmatrix} \frac{T_s^2}{2} & \frac{T_s^3}{3} \\ \frac{T_s^3}{3} & \frac{T_s^4}{4} \end{bmatrix} \quad (22)$$

where q is the random noise in the accelerometer. In practice, both R and q were tuned with flight data. The actual Kalman filter algorithm can be found in many common textbooks.

Tilt Estimation Although the rocket's tilt (off the vertical) should ideally be implemented into the aforementioned state estimator, and incorporate all nine measurements from the IMU (three each from gyroscope, accelerometer, and magnetometer), a more simple quaternion-based scheme was tested and shown to work for this specific application.

The orientation of the rocket is described with respect to the earth-fixed frame using quaternions, $\mathbf{q} = [q_1 \ q_2 \ q_3 \ q_4]$. The Airbrake keeps track of the rocket's orientation throughout the flight using the following quaternion dynamics.

$$\dot{\mathbf{q}} = \frac{1}{2} \tilde{\boldsymbol{\Omega}} \mathbf{q} \quad (23)$$

where $\tilde{\boldsymbol{\Omega}}$ is defined as in Eq. (24). The roll, pitch and yaw rates – (p, q, r) are measured from the gyroscope in the IMU.

$$\tilde{\boldsymbol{\Omega}} = \begin{bmatrix} 0 & -p & -q & -r \\ p & 0 & r & -q \\ q & -r & 0 & p \\ r & q & -p & 0 \end{bmatrix} \quad (24)$$

The quaternion at each time instance, k is computed by forward integrating the dynamics in Eq. (23) using a first-order Euler method.

$$\mathbf{q}_{k+1} = \left(I_4 + \frac{1}{2} \tilde{\boldsymbol{\Omega}} T_s \right) \mathbf{q}_k \quad (25)$$

where T_s is the sampling time. Note that the quaternion is normalized at each time instance by dividing by its norm. The initial quaternion is $\mathbf{q}_0 = [1 \ 0 \ 0 \ 0]$ implying that the body frame and earth frame are aligned before lift-off.

To compute tilt, the Airbrake uses a direction cosine matrix (DCM) between the earth and body frame. The elements of a DCM represent the scalar inner product of the axes of the body with the inertial axes. So by definition, the third row and third column of the matrix, DCM_{33} represents the scalar product between \mathbf{z}^B and \mathbf{z}^I , which is in fact $\cos(\alpha)$, α being the tilt. DCM_{33} in terms of the quaternions is as follows,

$$\text{DCM}_{33k} = 2(q_{1k}^2 + q_{4k}^2) - 1 \quad (26)$$

Rocket's tilt (off the vertical) at each time instance is computed from the obtained DCM_{33} using the following equation.

$$\alpha_k = \cos^{-1}(\text{DCM}_{33k}) \quad (27)$$

Calibration The only additional calibration is a *bias-correction* for each of the measurements. After powering up, the software first dumps a few hundred measurements as it waits for the sensors to reach a steady state. The Airbrake then averages the next few hundred measurements and use this quantity for correcting the bias in the subsequent measurements. Due to simplifying assumptions such as zero-mean Gaussian noise, linear process model, etc., and other unmodelled disturbances, the estimated states are expected to drift while on the pad. To counteract this effect, the computer resets the state to zero every ten seconds if it does not detect a launch.

Fig. 81 shows the estimated state as Honu sits on the pad ready for launch. The drifts in the estimated height and velocity are deemed low enough for the system's feedback-loop requirements. The drift in the tilt starts at 0.06 °/s and

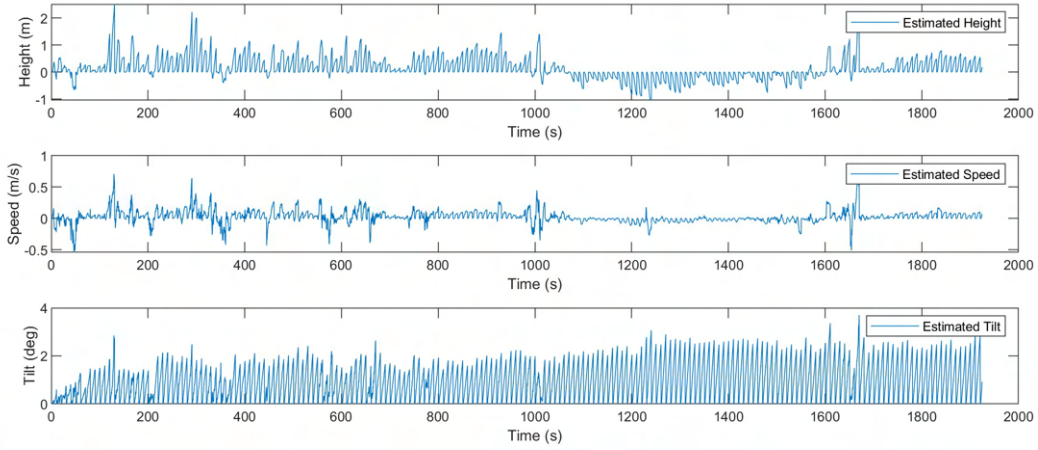


Fig. 81 The estimated state of Honu as it sits on the pad. A small drift is apparent in the state estimator. The estimator resets the state to zero every 10 seconds if it does not detect a launch.

becomes almost $0.3^\circ/\text{s}$ close to motor ignition. This is presumed to be caused by the (small) "random-walk" drift of the gyroscope readings. However, due to the periodic *zeroing-out*, the maximum drift encountered is 3° . In the future, the team plans to explore dynamic calibration to counteract this effect.

Verification And Validation The calibration and estimator were first synthesized and developed in MATLAB using simulated data. Once we were satisfied with the preliminary results, we took raw sensor data from a few flights on small-scale rockets and post-processed them with our MATLAB implementation. Finally, we ran the estimator onboard during the flight and saved the estimated states. Post-launch, we compared these *in-flight* estimates to MATLAB post-processing on the raw data and demonstrated that, within precision bounds, they match.

To validate the estimator design, the team compared the estimated state to those of some commercial flight computers that flew onboard the rocket as well. Fig. 82, Fig. 83, and Fig. 84 show various flight-curves from the Airbrake's estimated states compared against those estimated by commercial flight computers.

Barometric Error Correction One of the many challenges to the feedback-control design of Airbrakes is the fluctuations in barometric pressure around the rocket as the flaps are deployed. Since the altitude measured using the barometer is hugely significant to the Kalman filter, large non-zero-mean noises considerably degrade the estimator's performance. Fig. 86 shows the barometric height from the SRAD flight computer and the commercial flight computer that was housed in the ebay during a flight with flap deployment. It is evident that when the flaps open they cause a decrease in pressure around the Airbrake sensor-suite, and therefore cause an increase in the raw height measurements. The figure also shows that there is a monotonic positive relationship between the flap angle and the "overestimated" height from the barometer.

This behavior was observed in the commercial flight computer too, but to a lesser extent since the commercial flight computer is located much farther away from the flaps. This error is especially concerning since this will cause instability in the controller performance. The flaps will initially deploy if it predicts an overshoot. This will cause the measured height to increase and then the controller will predict an even higher apogee, deploying them farther, thus resulting in a catastrophic positive feedback loop.

Due to the requirement for an expedient, minimum viable solution to this problem, a data-driven model was explored. Though usually an error correction is applied directly to the barometric pressure, we attempt to correct the reported height instead. The team models the measured height at any given time as,

$$h_r = h + f(h, v, \delta), \quad (28)$$

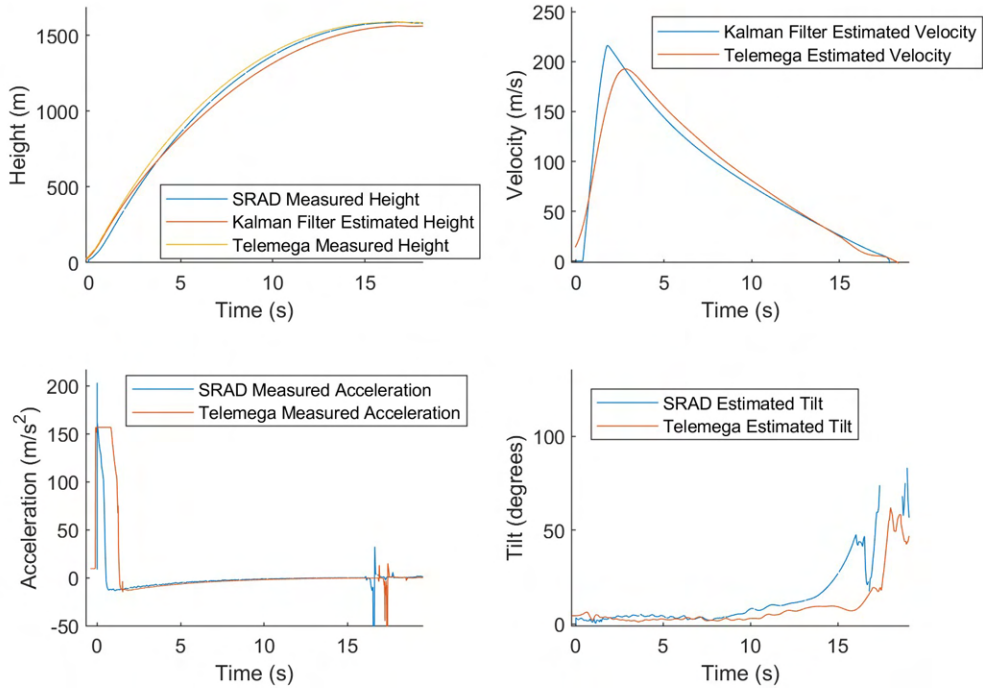


Fig. 82 The estimated states from the flight computer compared to a commercial flight computer (Telemega) for the Blue Rocket. (Launch date: 3/5/23)

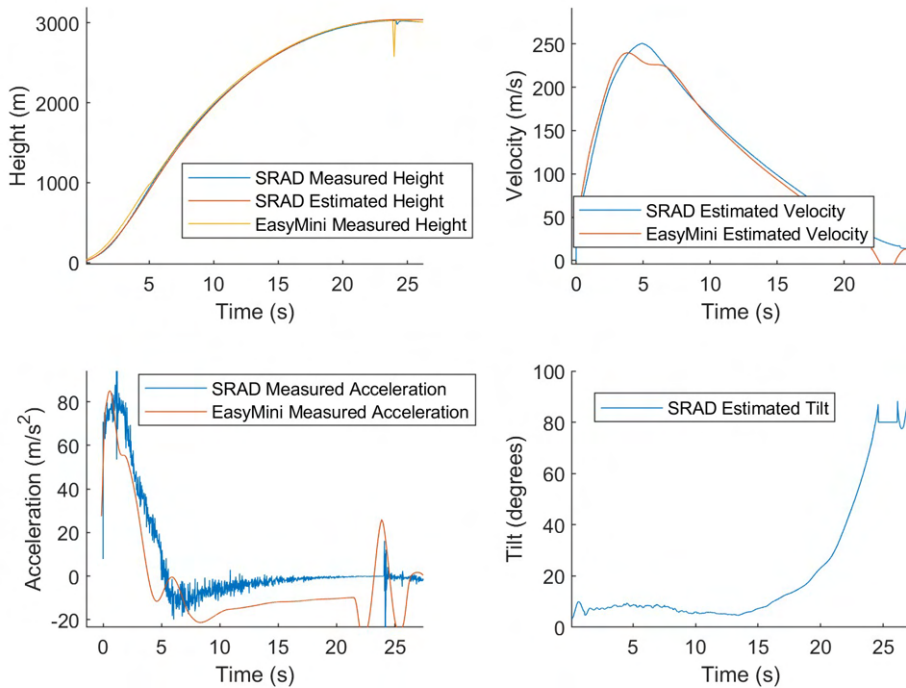


Fig. 83 The estimated states from the flight computer compared to a commercial flight computer (EasyMini) for the Icarus Rocket. (Launch date: 4/2/23)

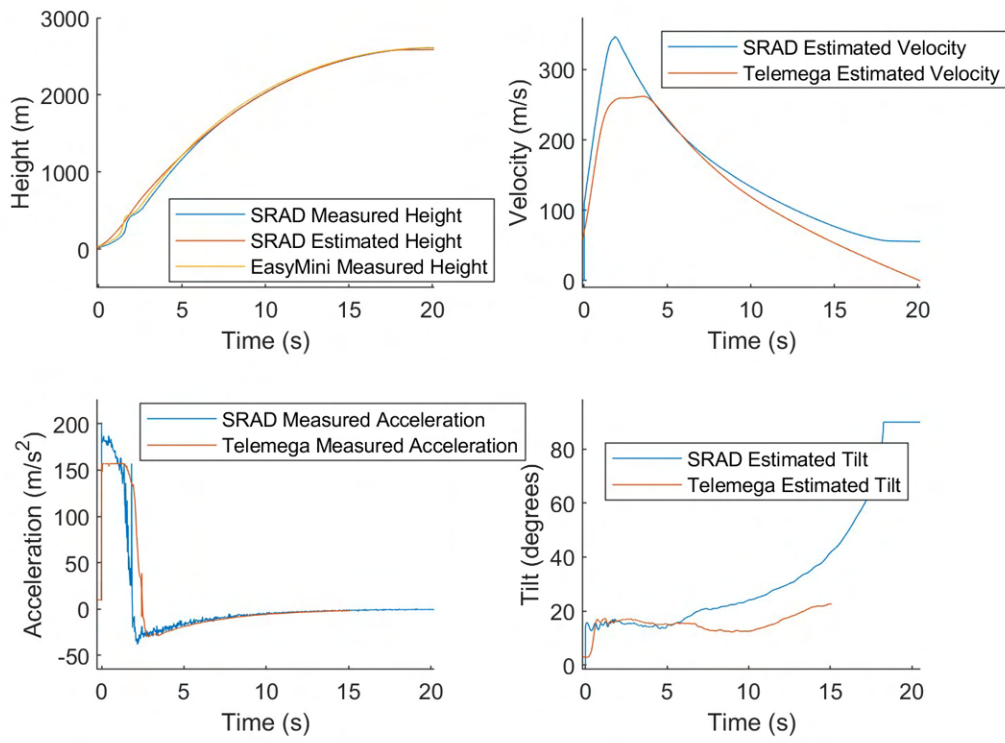


Fig. 84 The estimated states from the flight computer compared to a commercial flight computer (EasyMini, Telemega) for the Blue Rocket. (Launch date: 4/2/23)

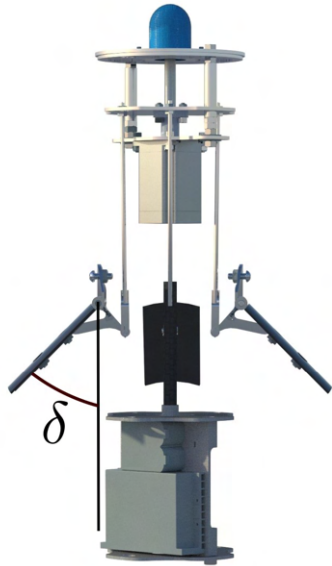


Fig. 85 δ is defined as the flap deployment angle

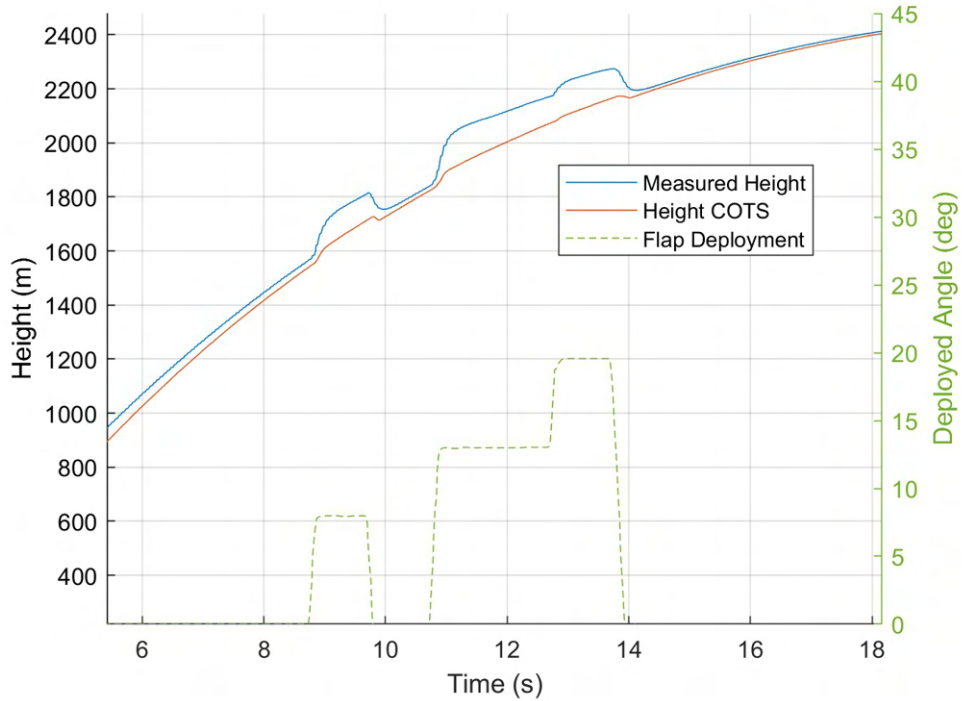


Fig. 86 Barometric sensor reading error while flaps are deployed

where h is the true height, h_r is the height as reported from the barometer, and $f(h, v, \delta)$ is the error in the height measurement and is a function of true height, velocity, and flap deployment angle. Deployment angle δ , is illustrated in Fig. 85.

Fig. 87 shows a *wind-tunnel test* with $v_\infty = 50$ m/s plotting the reported height from the barometer that was housed inside the Airbrake module. The average pressure in the wind tunnel did not change significantly during the test but the local pressure near the barometer was clearly decreasing as the flaps opened. Fig. 88 illustrates all of the wind tunnel tests with the reported error as a function of deployment angle.

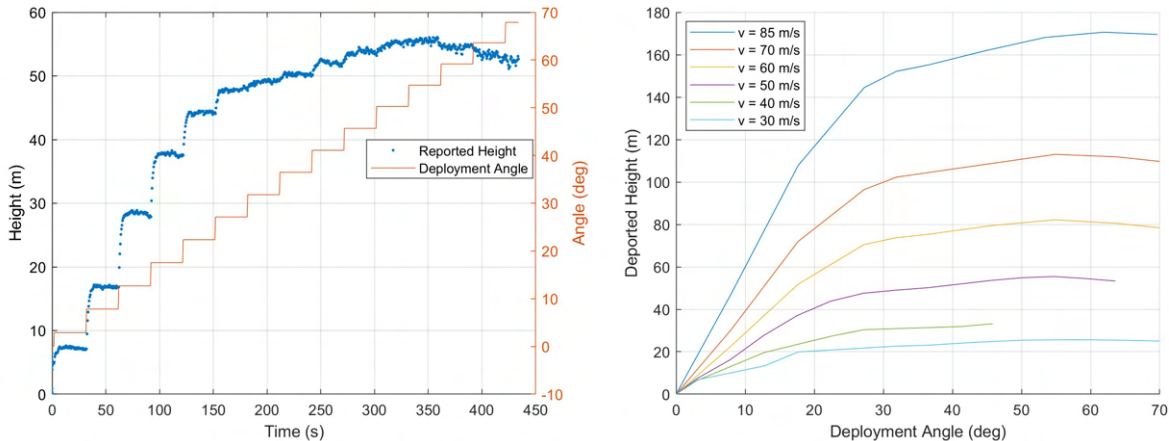


Fig. 87 Barometer height reading while in the wind tunnel with $v_\infty = 50$ m/s

Fig. 88 Height error curves from all wind tunnel tests

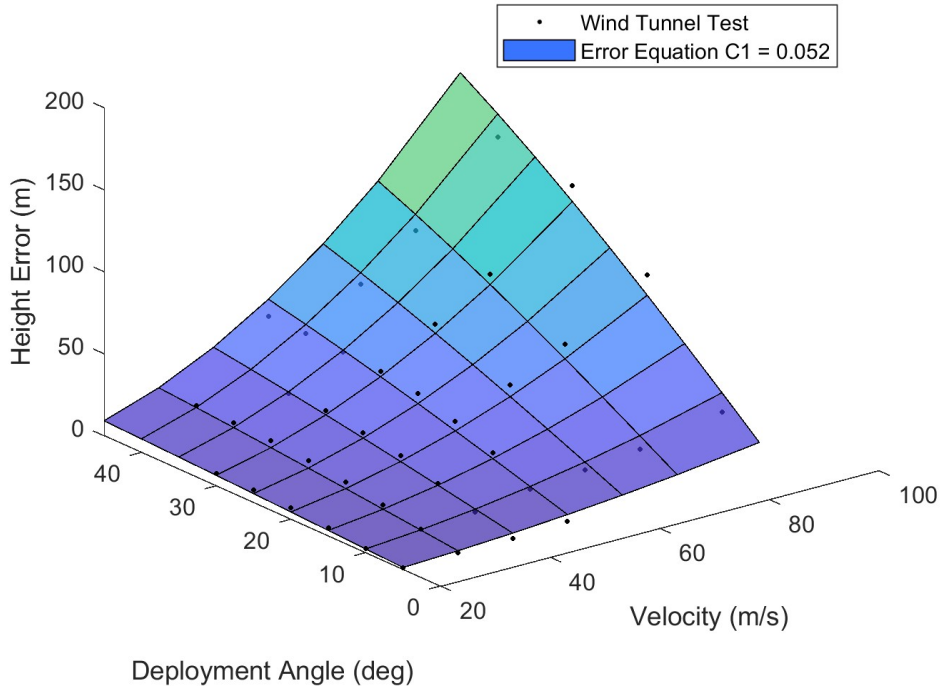


Fig. 89 Surface fit of the Airbrake's error function to the wind tunnel barometer height recordings

Upon careful inspection of the data and trying out a few error models, the following error model produced the best function fit without overfitting,

$$f(h, v, \delta) = \begin{cases} cq \sin \delta & \delta < 45^\circ \\ cq \sin 45^\circ & \delta \geq 45^\circ \end{cases} \quad (29)$$

where $q = \frac{1}{2}\rho v^2$ is the dynamic pressure and δ is the flap deployment angle. We identify the parameter coefficient, c by fitting this error function to data from wind tunnel tests. Using a standard least square method, we estimate $c = 0.052$ with an $R^2 = 0.97$. Fig. 89 shows the wind tunnel data used for fitting and the surface plot using Eq. 29 with $c = 0.052$.

Using this error model, the team first corrects the height error before sending it to the Kalman filter. Fig. 90 shows the reported height as well as the height after the error correction using Eq. 29. It is clear from the plot that although the steady state corrected height is usable there is a transient time that is significant and Eq. 29 does not capture it. The assumption is that there are some complicated aerodynamic effects that take time to settle. A low pass filter was chosen as a candidate to pseudo-capture these effects. The simple time-independent low-pass filter does not work since the bandwidth of the filter is dependent on the sampling time and in this case, it is the underlying physics that we are trying to capture. With this consideration, the team chose a filter defined as,

$$\Delta_{k+1} = (1 - \alpha)\Delta_k + \alpha f(h, v, \delta)_k \quad (30)$$

$$\alpha \equiv \frac{T_s}{T_s + \tau} \quad (31)$$

where Δ_k is the value subtracted from the reported height at time k , T_s is the sample time, and τ is the time constant. τ is then tuned using flight data and a value of $\tau = 0.15$ is chosen. Fig. 91 shows the flight with the corrected error using this low-pass filter. **To reiterate the novelty of this method, the team is able to correct for the complicated aerodynamic effects on a commercial barometer with just two tunable parameters: c and τ .**

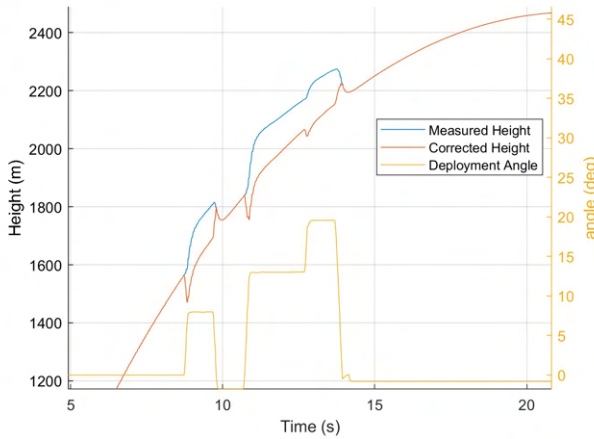


Fig. 90 Height error correction without the low-pass filter

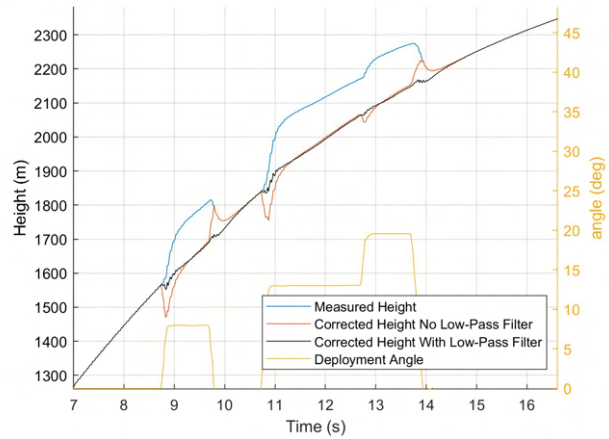


Fig. 91 Height error correction with and without the low-pass filter

This error correction scheme was implemented on the full-scale flight test of Honu. Fig. 92 shows both the height and speed estimated states. The measured height is extremely perturbed due to the change in pressure around the rocket after flap deployment. The blue solid curve is the estimated height if the system did not run any error correction on the reported height and only used the Kalman filter. It is clear that this estimation has a significant error and the controller would most probably have failed and would have saturated very quickly. The increased performance using the low pass filter as defined in Eq. 30 does perform better but the standard Kalman filter is able to mostly correct for the transient period.

6. Controller Design

A few different control schemes were considered but a simple form of Model Predictive Control (MPC) was chosen. Since the Airbrake has a limited control domain, a controller that is able to capture much of the flight dynamics is attractive. Model-free PID controllers were seriously considered but behaved poorly in simulation. Another major benefit of our MPC-based control is that it has few parameters and no gains to be tuned. The Airbrake is expensive to full-scale test so getting sufficient flight data sets to properly tune gains is not feasible.

The planning horizon of the MPC is chosen in the velocity space instead of the standard time domain. The MPC plans until velocity goes negative, indicating apogee. To simplify the planning optimization, a static control angle constraint is applied to the planning algorithm. At each controller iteration, the MPC predicts the apogee for various sample flap angles assuming that the Airbrake will hold that sampled flap angle for the rest of the flight, and chooses the best flap angle that will get the rocket closest to the desired apogee.

There are three main assumptions about the dynamics of the rocket. First, the angle of attack is always zero; second, the rocket's flight is constrained to a plane; and third, the drag of the rocket body and flaps are decoupled. The second assumption is valid from rocketry experience and the third from wind tunnel tests. With these assumptions, the equation of motion during the rocket's coast phase is,

$$m\ddot{\mathbf{r}} = -\frac{1}{2}\rho(4Cd_fA_f(\delta) + Cd_R A_R)\dot{\mathbf{r}}^2\hat{\mathbf{r}} - mg\hat{\mathbf{y}}, \quad (32)$$

where m is the mass of the rocket, \mathbf{r} is the position vector, ρ is the local air density, Cd_f is the coefficient of drag of the flaps, $A_f(\delta)$ is the effective surface area of the flaps and is a function of the flap angle, Cd_R is the coefficient of drag of the rocket body, A_R is the reference area of the entire rocket, and g is the acceleration due to gravity. The constant '4' appears in the equation since there are four flaps on the Airbrake.

Note that $\dot{\mathbf{r}}^2 = \dot{\mathbf{x}}^2 + \dot{\mathbf{y}}^2$. Using the three assumptions mentioned before and further assuming that ρ is locally

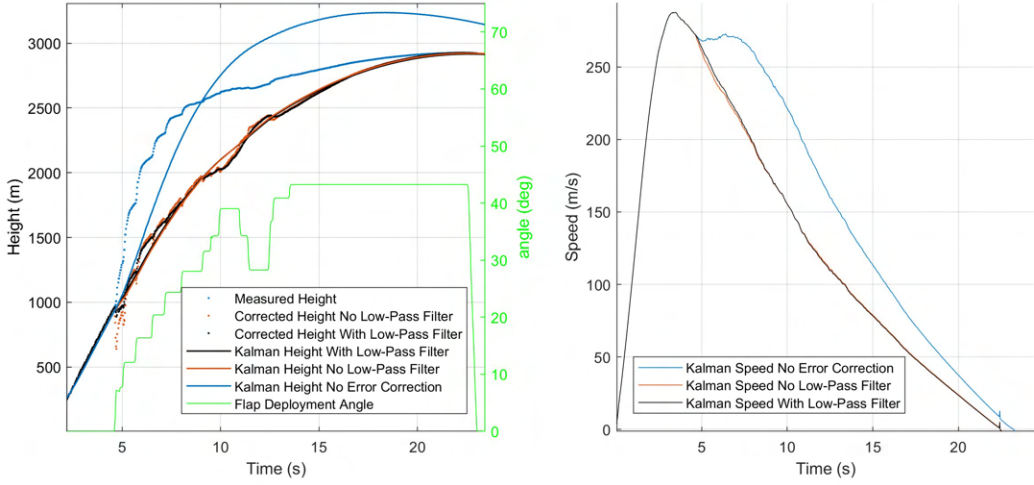


Fig. 92 Estimated states from the Kalman filter with various type of measured height inputs — uncorrected/corrected, with/without low-pass filter

constant, the equations of motion can be written as,

$$\ddot{\mathbf{y}} = -\frac{1}{2m}\rho(4Cd_f A_f(\delta) + Cd_R A_R)\dot{\mathbf{y}}\sqrt{\dot{\mathbf{x}}^2 + \dot{\mathbf{y}}^2} - g, \quad (33)$$

$$\ddot{\mathbf{x}} = -\frac{1}{2m}\rho(4Cd_f A_f(\delta) + Cd_R A_R)\dot{\mathbf{x}}\sqrt{\dot{\mathbf{x}}^2 + \dot{\mathbf{y}}^2}. \quad (34)$$

At any point in the flight, the Airbrake can forward integrate Eq. 33 and 34 with the initial conditions being the current state to obtain apogee-predictions. The initial conditions are computed from the state estimates obtained using Kalman filter,

$$\begin{bmatrix} \mathbf{x} \\ \dot{\mathbf{x}} \\ \mathbf{y} \\ \dot{\mathbf{y}} \end{bmatrix}_0 = \begin{bmatrix} 0 \\ v \sin \alpha \\ h \\ v \cos \alpha \end{bmatrix} \quad (35)$$

where h , v and α are the estimated height, velocity, and tilt of the rocket at the current time. Using this formulation the team can define an apogee predict function \mathcal{P} ,

$$h_{max} = \mathcal{P}(h, v, \alpha, \delta) \quad (36)$$

The function takes in height, velocity, tilt, and a flap deployment angle and integrates Eq. 33 and 34 until $\dot{\mathbf{y}} \leq 0$ (descent-phase). Recall that \mathcal{P} assumes a constant δ . It returns \mathbf{y} (h_{max}) at the time instance when $\dot{\mathbf{y}}$ first becomes negative as the predicted apogee. Equation 36 was implemented with a second-order Runge-Kutta integrator since it gave a sub-meter precision compared to the more standard fourth-order but runs a bit faster on the resource-limited flight computer. Using $\mathcal{P}(h, v, \alpha, \delta)$, the MPC-based planner determines the *optimal* flap-angle, δ that will result in h_{max} being close to the desired apogee. The software uses a binary search method with a 5° resolution to search over the space of control inputs (flap-angles).

7. Parameter Estimation

The predict function, \mathcal{P} , requires the estimation of constants: m , C_{df} , $A_f(\delta)$, C_{dR} and A_R – the mass and drag characteristics of the rocket and the flaps. m is simply the empty mass of the rocket. It is calculated as the measured

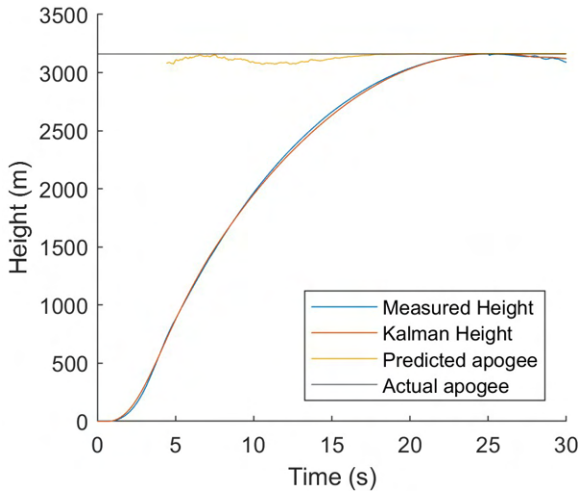


Fig. 93 Estimated height and predicted apogee in time on the Honu flight of March 5th

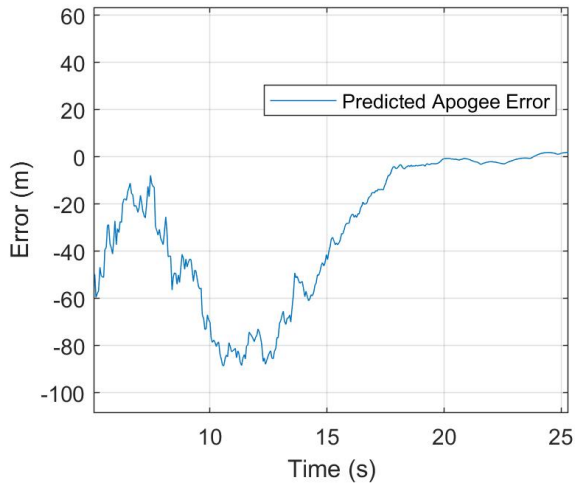


Fig. 94 Error in the predict apogee function of the controller

wet mass minus the expected propellant mass. Next, consider C_{dR} and A_R . The team can obtain estimates of these values from the OpenRocket model but OpenRocket does not have all of the details of the rocket such as surface finish and various exposed hardware. Another option is using a CFD tool to estimate C_{dR} but this has the same downside as OpenRocket with the additional issue that this usage of the simulation software is not validated. Lastly, the team can use the wind tunnel tests to estimate C_{dR} . There are two problems with using the wind tunnel tests: the measured drag includes the model mount and the team was unsure how to accurately subtract it out and second, wind tunnel tests are expensive and logically complicated. So it was determined to not be a long-term solution as rockets designs can change much more rapidly than the team's ability to run wind tunnel tests. The solution was to estimate these constants *in-flight* using onboard sensors. The acceleration due to drag without flap deployment is considered. It can be written as,

$$a_D = \frac{1}{2m} \rho C_{dR} A_R v^2. \quad (37)$$

a_D is precisely what the IMU measures while the rocket is in the coast phase. Given the fact that C_{dR} and A_R only ever appear as a product in the controller equations, it can be readily estimated from Eq. 37 as,

$$C_{dR} A_R = \frac{2ma_D}{\rho v^2}. \quad (38)$$

In practice, a_D is generally noisy, so the Airbrake takes the mean of $C_{dR} A_R$ over one second of measurements after motor burnout and before any flap deployment. This method was found to be within 15% of the value obtained from OpenRocket.

Table 17 Coefficient of drag of the rocket assuming a 29.9 in² reference area

	Wind Tunnel	OpenRocket	In flight sensors	CFD
C_{dR}	0.71	0.51	0.58	0.66
Drawback(s)	Includes mount	Missing rocket features	Noisy measurements	Low fidelity model and simulation tool complexities

The drag characteristics of the flaps: C_{df} and $A_f(\delta)$, were determined from wind tunnel tests with the assumption

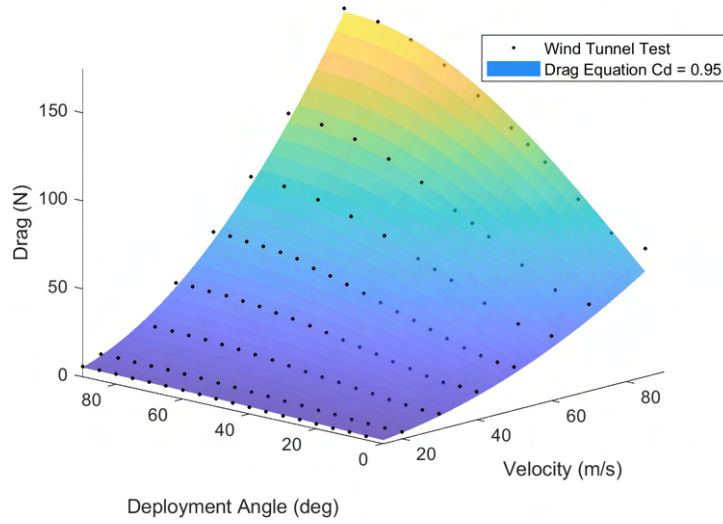


Fig. 95 Wind tunnel test and resultant fit of the drag equation

that,

$$A_f(\delta) = A_0 \sin \delta, \quad (39)$$

where $A_0 = 10 \text{ in}^2$ is the approximate surface area of each flap, and δ is flap-deflection angle. Using the standard drag equation and assuming the drag of the rocket and flaps are decoupled, the equation for the total drag is,

$$D = \frac{1}{2} \rho (4C_{d_f} A_0 \sin \delta + C_{d_R} A_R) v^2. \quad (40)$$

This equation was fit using a linear least square method to the data from wind tunnel tests. This method resulted in estimated $C_{d_f} = 0.95$ with a $R^2 = 0.996$. Fig. 95 shows the data points as well as the contour fit of Eq. 40 using $C_{d_f} = 0.95$.



Fig. 96 Testing configuration of the Airbrake with the mylar

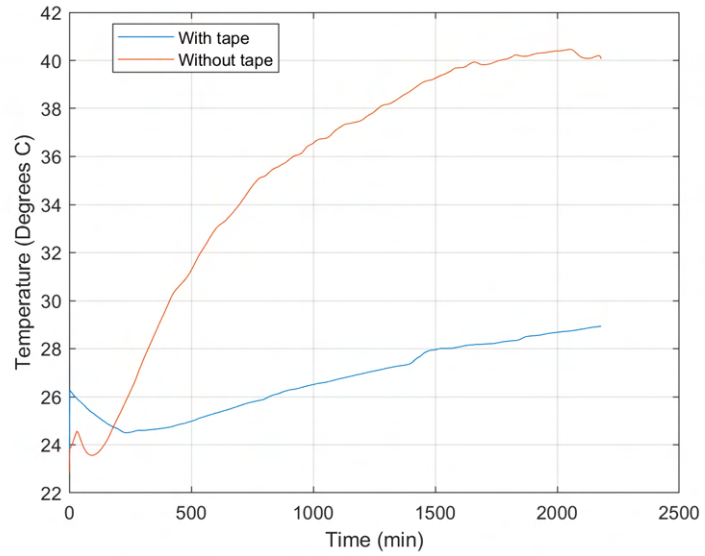


Fig. 97 Difference in temperature over time with and without mylar tape

8. Heat Protection

At the 2023 Spaceport America Cup, the Airbrake did not deploy due to an overheating issue with our motor driver. To counter this issue, mylar tape was applied to the outside of the Airbrake, specifically where the motor driver is. The mylar tape reflects light from the sun, keeping the motor driver cool enough to operate. To test the mylar tape, a heating lamp was used to mimic the heat of the sun. The Airbrake is shown in Fig. 96 in this testing configuration with the mylar tape. The Airbrake was also tested without the mylar tape in the same configuration. Fig. 97 shows the difference between the temperature over time in the Airbrake frame with and without the mylar tape. It shows there is a significant decrease in the change of temperature over time with the tape when compared to without the tape.

9. Commanded Angle Validation

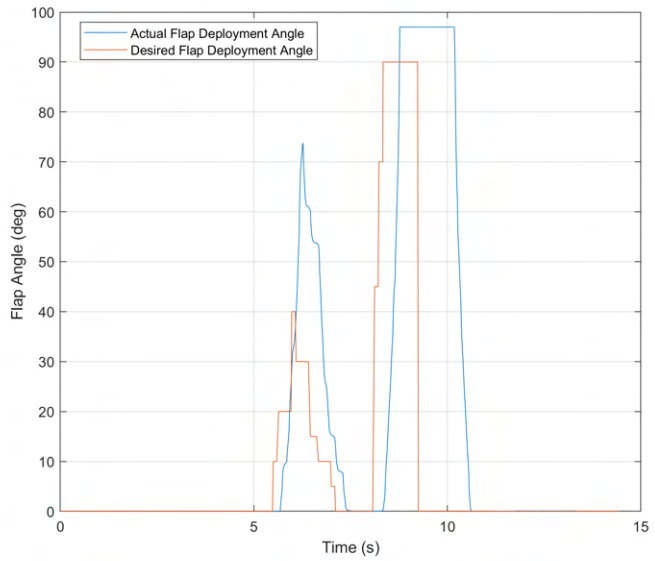
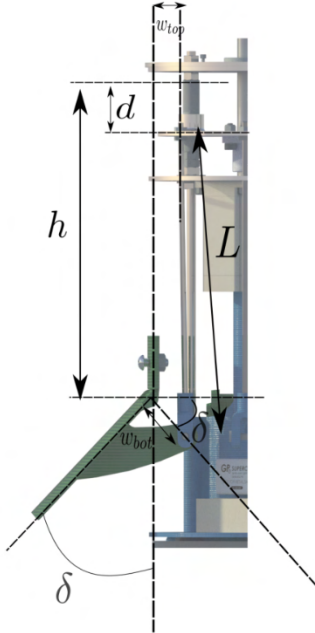


Fig. 99 Estimated Actual vs Desired Flap Deployment Angle on a Flight Test on 4/7/2024

Fig. 98 Airbrake Dimensions

Within the controller, we command the Airbrake to actuate to certain flap deployment angles. There is an encoder on the motor that outputs steps taken by the motor. We need a function to convert angle into number of steps for the stepper motor. Fig. 98 shows the geometry of the problem. Here the constraint is that the length of the actuator rod is constant. The length of the rod for any angular displacement can be written as,

$$L = \sqrt{(h - d + w_{bot} \sin \delta)^2 + (w_{bot} \cos \delta - w_{top})^2} \quad (41)$$

where h is the vertical distance from the actuator rod in the fully retracted position to the flap hinge, d is the displacement of the actuator plate, w_{bot} is the width of the control horn to the hinge, w_{top} is the width from the place the actuator rod is fixed to the actuator disk to the vertical line passing through the hinge, and θ is the flap deployment angle. This equation simplifies if a small angle is assumed but since the range of deployment angle is $[0, \pi]$ this approximation is not valid. Since at $\theta = 0 \rightarrow \delta = 0$,

$$L = \sqrt{h^2 + (w_{bot} - w_{top})^2} \quad (42)$$

Setting Eq. 41 equal to Eq. 42 and solving for δ results in,

$$d = h + w_{bot} \sin \delta - \sqrt{h^2 + (w_{bot} - w_{top})^2 - (w_{bot} \cos \delta - w_{top})^2} \quad (43)$$

According to the manufacturer there are 200 steps per 0.24" of vertical displacement of the stepper motor, so the final form of the steps as a function of angle is,

$$steps = 847(h + w_{bot} \sin \theta - \sqrt{h^2 + (w_{bot} - w_{top})^2 - (w_{bot} \cos \theta - w_{top})^2}) \quad (44)$$

To validate that the Airbrake deployed to the commanded flap angle, the steps from the encoder can be converted to flap deployment angle in degrees using Eq. 44. Given encoder steps, θ can be solved numerically in MATLAB. Fig. 99 shows the estimated flap deployment angle based on the actual encoder steps the motor took and the desired flap deployment angle commanded by the controller. The two values differ slightly because the estimated flap deployment angle based on encoder steps is an estimate by iteratively solving for θ using Eq. 44 until convergence. This estimation method inherently produces a slight error in its approximation.

10. Controller Analysis

To determine the optimal controller type to be used in the Airbrake, a closed-loop feedback system was developed in Simulink to model the rocket's dynamics and the Airbrake's system. It consists of four submodels: the nominal (rocket) model, sensor model, state estimation model, and controller model. The nominal model outputs idealized values of the rocket's state derived from two-dimensional kinematics. It was validated with test-flight data from the full-scale competition rocket. The sensor model adds noise to the true state values given by the nominal model. The state estimation model contains a Kalman filter using the noisy state values from the sensor model. The controller model takes in the estimated state values from the state estimation model and outputs a desired flap angle. The input to the nominal model is flap angle deployment, and it is used in the dynamics of the rocket.

Within the controller model, various controller types were implemented and tested, including a Model Predictive Control (MPC), Proportional-Integral-Derivative (PID) controllers, and Linear-Quadratic Regulator (LQR) controllers. The MPC is similar to the MPC used in the Airbrake. However, tilt is not taken into account within the MPC, more generally the entire controller model, to reflect the reduced order dynamics within the controller seen in the real rocket.

Four variations of PID controllers were implemented. For some implementations of the PID controllers, some of the gains were set to zero. Additionally, two types of errors were used in the various PID controllers. The error first type was the difference between the current height of the rocket and the desired apogee. The second error type was the difference between the current predicted apogee and desired apogee. A Proportional-Integral (PI) and Integral (I) controller were used with the former error type. A PI and PID controller were used with the latter error type.

Similar to the PID controllers, two versions of the LQR controller were constructed: one with the error value as difference between current height and desired apogee and one with the error value as difference between predicted apogee and desired apogee.

Table 18 Assessment criteria each controller was tested on

Performance with Uncertainty Robustness	Performance with Varying Rocket Conditions	Actuator Conservation with Baseline Conditions
Coefficient of Drag of the Rocket	Ground Altitude	Maximum Force on a Flap
Coefficient of Drag of the Flaps	Desired Apogee	Maximum Moment on a Flap
Dry Mass		

Each controller implemented was tuned to the same baseline conditions and assessed for its apogee error and actuator conservation under varying conditions and robustness to uncertainties in its vehicle characteristics. The assessment categories and the criteria in them are shown in Table 18.

Table 19 Weighting scheme for the values tested in each category

Coefficient of Drag of Rocket	Coefficient of Drag of a Flap	Dry Mass	Ground Altitude	Desired Apogee	Maximum Force on a Flap	Maximum Moment on a Flap
0.4 1	0.25 1	22 kg 1	250 meters 1	2900 meters 1	1	1
0.5 3	0.35 3	25 kg 3	750 meters 3	2950 meters 1		
0.65 3	0.55 3	31 kg 3	1200 meters 3	3100 meters 1		
0.75 3	0.65 3	35 kg 3				

The criteria selected are uncertainties and concerns that have arisen during test flights and post-flight data processing. An iterative process was used to test these criteria in the Simulink model. For each piece of criterion, excluding those that fall under actuator conservation, the error between each of the controller's apogee and desired apogee is computed. A weighting system, similar to a trade study, was used to evaluate the performance of each controller, and the weight used for each criterion in this system was determined by how relevant the value is to the Spaceport America Cup. The weighting for the different values tested for each criterion is shown in Table 19.

Table 20 Cumulative weighted errors for each controller, with MPC having the lowest score

	MPC	PI Height Error	I Height Error	PI Apogee Error	PID Apogee Error	LQR Height Error	LQR Apogee Error
Score	300.18	616.2	621.47	1086.1	918.56	920.2	748.01

For each controller, their weighted errors and actuator conservation values are summed to compute the total score. The lower the score, the better the controller performed. The cumulative weighted errors for each controller are shown in Table 20.

H. Payload

1. Mission



Fig. 100 TADPOL integrated into TERP



Fig. 101 TADPOL (unpainted)

The Terrapin Rocket Team payload is a 10.5 lb, 4U system that is made up of 2 primary subsystems. The first is a vehicle release mechanism, referred to as the TERP (Testbed for Ejecting Research Payloads, Fig. 100). This system was originally developed for the 2022-23 SAC competition and has been updated for this year. The TERP mechanism remains in the rocket and is responsible for powering on and releasing the vehicle. The second subsystem is the deployed vehicle, TADPOL (Testbed for Adjusting Drift and Position On Landing, Fig. 101). The TADPOL houses a live video system for streaming to the ground and an experimental drift control mechanism. A CONOPS diagram of the TERP-TADPOL system can be found in Fig. 117.

Table 21 Payload CONOPS Table

Stage	Start condition	Events
0: Integration	Payload assembly	TADPOL Featherweight power on: Immediately
1: Pre-launch	Payload power on	Manual TERP power on: Immediately
2: Launch	Launch acceleration detected	Automatic TADPOL power on: Immediately Data logging begins: Immediately
3: Drogue descent	Apogee	Live video transmission begins: Immediately Nose cone separation: 1700 feet altitude
4: Vehicle descent	1500 feet altitude	TADPOL deployment: Immediately Drift control begins: 3-second delay
5: Vehicle touchdown	Vehicle landing	Drift control ends: Immediately Data transferred to SD card: Immediately

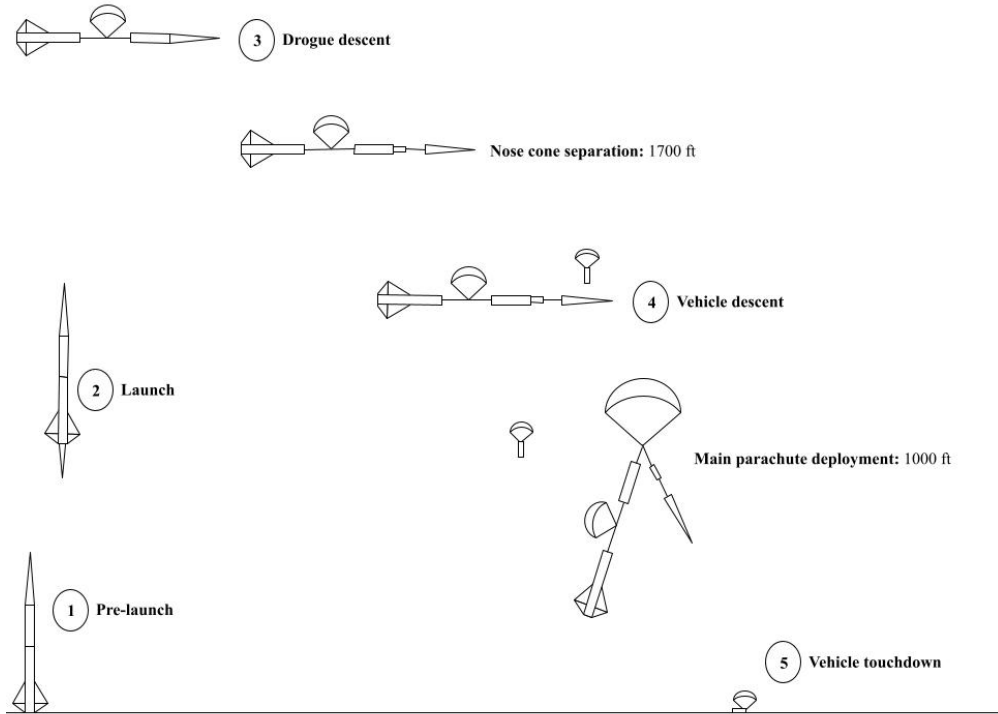


Fig. 102 Payload CONOPS Diagram

2. TERP

Functionality overview The TERP system was developed for the 2023 SAC as a universal vehicle deployment system. Vehicles are constrained in the TERP's vehicle bay using two monofilament lines and a series of shims. At deployment, these lines are released, allowing a set of torsion springs to push the vehicle out of the TERP.

Similar to last year, the TERP fills the 4U cubesat factor and weighs 8.6 lbs. This mass is divided between a 2.5U vehicle bay, 1U avionics bay, and 0.5U ballast section. The size and weight were selected to reduce the required weight of the vehicle; as the TERP remains in the launch vehicle for the duration of the flight, mass offloaded to the TERP reduces recovery loads on the deployed vehicle, allowing the use of 3D printing of vehicle structures and reducing the danger posed by vehicle recovery. The extra mass budget also allows recovery loads from the launch vehicle to pass through the TERP, saving weight by removing the need for additional integration hardware. In addition to housing and deploying the vehicle, TERP sends signals to power on the vehicle once the rocket is on the pad, removing the need to power the vehicle on before integration or attempt to reach a switch through the nose cone wall, and records an additional dataset for comparison with the vehicle and other subsystems.

The TERP PCB uses a Teensy 4.1 microcontroller, barometer (BMP280), 9 DOF IMU (BNO055), and light sensor (BH1750), the same as last year. The team has built experience with these sensors and uses them on several other systems, including the TADPOL. The light sensor and barometer are used in TADPOL deployment, to ensure the nose cone of HONU has popped off and trigger deployment at 1,500 feet. Both the TERP and the TADPOL use the I2C bus to communicate to sensors and employs open-source Arduino-based C++ code to read data from the breakout boards and communicate with the TADPOL board.

Payload Integration As the TERP system remains very similar to last year, the integration hardware has not changed. TERP connects to two bulkheads using four 1/4" bolts; the first connects to the bottom of the TERP frame, and forms the top of the nose cone's electronics bay (ebay). This ebay holds the EasyMini used to fire the 1 g charge that triggers nose cone separation, as well as rotary switches for the TERP/TADPOL and EasyMini. The second bulkhead connects to the top of the TERP frame, and seals against the nose cone wall. The charge for separating the nose cone runs from the nose

cone ebay below the TERP through the two aforementioned bulkheads into the cavity above the TERP. A shock cord connects the tip of the nose cone to the top-most bulkhead, while another connects the bottom of the nose cone ebay to the rest of the rocket. As a result, the vehicle deployed from the TERP is the only object that recovers independently from the launch vehicle, while the rest remain intact.

Updates While the TERP performed well during development and the 2023 competition, the team identified a number of areas for improvement, both with respect to performance, and ease of use. As a result, this year's TERP has a few notable changes from its previous iteration.

The primary change was to the TERP PCB, the addition of two connectors for a custom nichrome cutter PCB (Fig. 103) used to release the TADPOL from the TERP. These PCB's replace the previous servo-actuated system with a more reliable, solid-state alternative. The previous servo mechanism was difficult to set and tended to jam if not properly adjusted. The nichrome PCB instead uses a strand of nichrome wire in contact with the monofilament retention lines that hold the TADPOL in place. When a substantial current is passed through this nichrome wire, it heats up, melts the line, and the TADPOL is released. The nichrome is held against two contact pads using a set of screws, allowing for easy replacement of the nichrome without the need for soldering equipment. Control of current passing through the nichrome is accomplished with a solid state relay (SSR). As the teensy microcontroller is not tolerant to voltages over 5 V, the disconnect between the signal and switching lines present in an SSR made it a more desirable choice compared to a mosfet.

Another substantial change was to TERP's power bank. As we switched the TADPOL to lithium-ion batteries, the TERP transitioned to the same battery type, using two 3.7 V 2200 mAh cylindrical lithium-ion cells. These cells are wired in parallel to provide 7.4 V, which is dropped to 5 V for use by the Teensy and actuators via a linear 5 V regulator. These cells were primarily selected using factors influencing the design of the TADPOL vehicle and were also used in the TERP for compatibility. For more information on the selection of the battery cells, see the TADPOL Avionics section.

The final change was to the spring panels. Previously, the free end of the torsion spring arms was clamped in place using a 3D-printed bracket that connected to the TERP frame. However, these brackets had to be removed while loading the vehicle, which increased assembly time. To streamline this process, the clamps have been replaced with a Z-shaped bracket. This bracket allows the spring arms to be pushed sideways out of the bracket, releasing spring tension without needing to remove the clamp, considerably speeding up the loading process. To ensure the springs can only be released with considerable force, a small lip is present on the edge of the clip. While not large enough to cause issues when manually loading the springs, when combined with the force of the springs, the lip keeps the spring arm in place throughout the flight.

3. TADPOL

Overview The TADPOL vehicle is a new system developed for this year's competition that builds on previous vehicle systems. As previously mentioned, TADPOL implements two primary functionalities. The first system is a new live video system in conjunction with the ALVS implemented in the rocket itself to provide video to the ground. The second

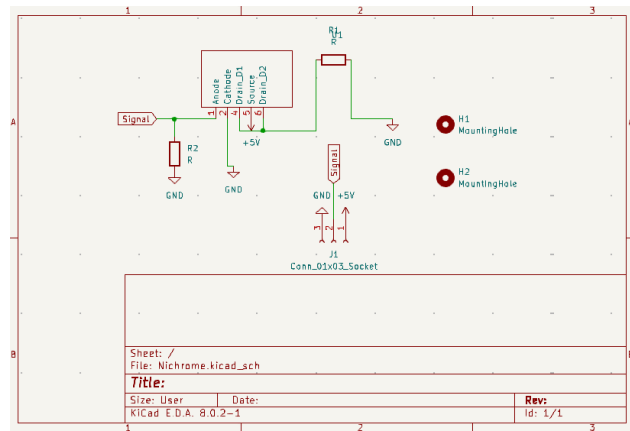


Fig. 103 Nichrome line cutter PCB wiring diagram

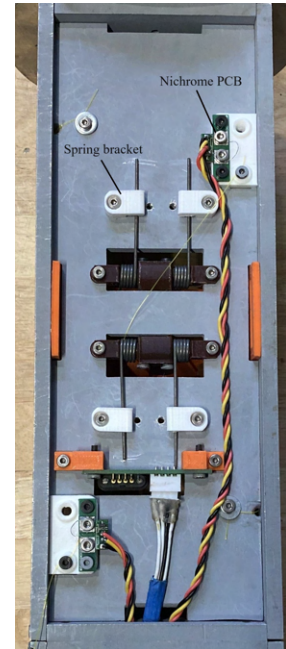


Fig. 104 TERP release mechanism updates

system is an improved drift control mechanism that builds on functionality originally developed for the 2023 competition. This system uses a tilted circular parachute and tail rotor setup to control TADPOL's descent trajectory. Tracking of the vehicle as it descends is accomplished using a Featherweight GPS tracker. Due to the section of the weight budget accounted for by TERP, TADPOL weighs 1.9 lbs, reducing recovery loads and improving safety.

Structure The TADPOL's structure is primarily composed of a single 3D print, with various additional 3D printed component covers and mounted brackets. 3D printing is favored for vehicle structures due to the tighter space constraints from the TERP vehicle section. The tight fits required between components, in addition to channels for routing wire harness, create complicated geometries that would be difficult and expensive to produce through other methods. Quick part production times also allow the team to rapidly prototype vehicle mechanisms between test flights. As a result, structural issues encountered in one test flight can be addressed by the next, allowing the team to continually gather relevant performance data.

While the recovery loads experienced by the vehicle are relatively small, the team takes several steps to ensure vehicle structural integrity. First, all 3D printed parts use PETG for its balance of improved impact and temperature resistance when compared to PLA and ease of printing when compared to ABS. To further reduce the softening of 3D prints, parts flying at Spaceport are either printed in or painted white to reduce their steady state temperature. Furthermore, all parts are printed with 15% gyroid infill and 5-6 wall layers. When oriented so that force is distributed along the slicing plane, the continuous filament lines that form the walls effectively transmit force through the vehicle. This allows the infill percentage to be reduced to save weight, while the gyroid pattern provides support. These settings have produced reliable parts evaluated through 8 drop tests and 11 test flights over the past 2 years, including parts flown at previous Spaceport America Cups.

Electrical covers, PCB mounting brackets, and other parts that connect to the primary vehicle structure are bolted in place using M3 hardware. Bolts are used whenever possible to aid in testing and replacement of parts as needed. The M3 sizing was selected for interchangeability with the TERP. These bolts thread directly into the 3D printed plastic, reducing the complexity of assembling. The threads formed in this manner have held up to repeated testing and demonstrated resilience to applied loads. To allow for easy integration and removal, the PCB is mounted between two grooves, and held in place with a 3D printed bracket.



Fig. 105 Parachute riser connection

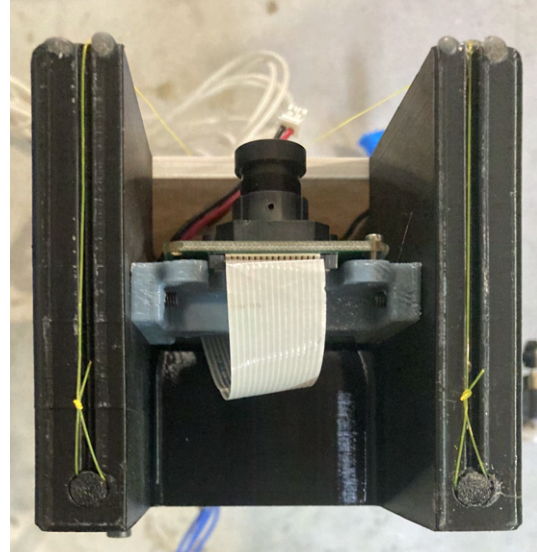


Fig. 106 Parachute retention line connection

Recovery The TADPOL uses a 36" parachute, providing an 18 ft/s descent rate. As with last year, the parachute for the TADPOL is constrained using the same retention lines that hold the vehicle in place. As a result, the TADPOL deploys immediately to its main parachute, removing the complexity of dual deploy systems and allowing the drift control system to work immediately. The parachute is connected to the top of the vehicle using washers and M3 screws, as seen in Fig. 106. Each individual riser line is passed through a hole in the vehicle frame to transfer recovery loads to the structure. The end of each riser is then held in place using a bolt and washer. To further reduce loads on the threads, two risers are connected to each screw from opposite directions, preventing the risers from pulling the screws out of the threads.

As the parachute is connected to the top of the TADPOL, the opening of the parachute causes a moment that has the potential to cause a jam. The spring mechanism is designed to prevent this jam from occurring, by pushing the vehicle free before the parachute can cause an issue. However, the TADPOL is also testing a deployment mechanism that fully relies on the parachute for separation from the TERP. To prevent a jam, force from the parachute needs to be transferred to the bottom of the TADPOL, which is accomplished using a monofilament line connected to two half circles at the ends. When in the TERP, these half circles are held in cutouts in the TADPOL by the wall of the vehicle bay, as seen in Fig 105. The parachute risers are passed through the loop formed by this line so that when the parachute inflates the risers pull on both ends of the TADPOL. Once the vehicle has cleared the vehicle bay, the half circles are no longer held against the TADPOL and release, allowing the vehicle structure to swing down.

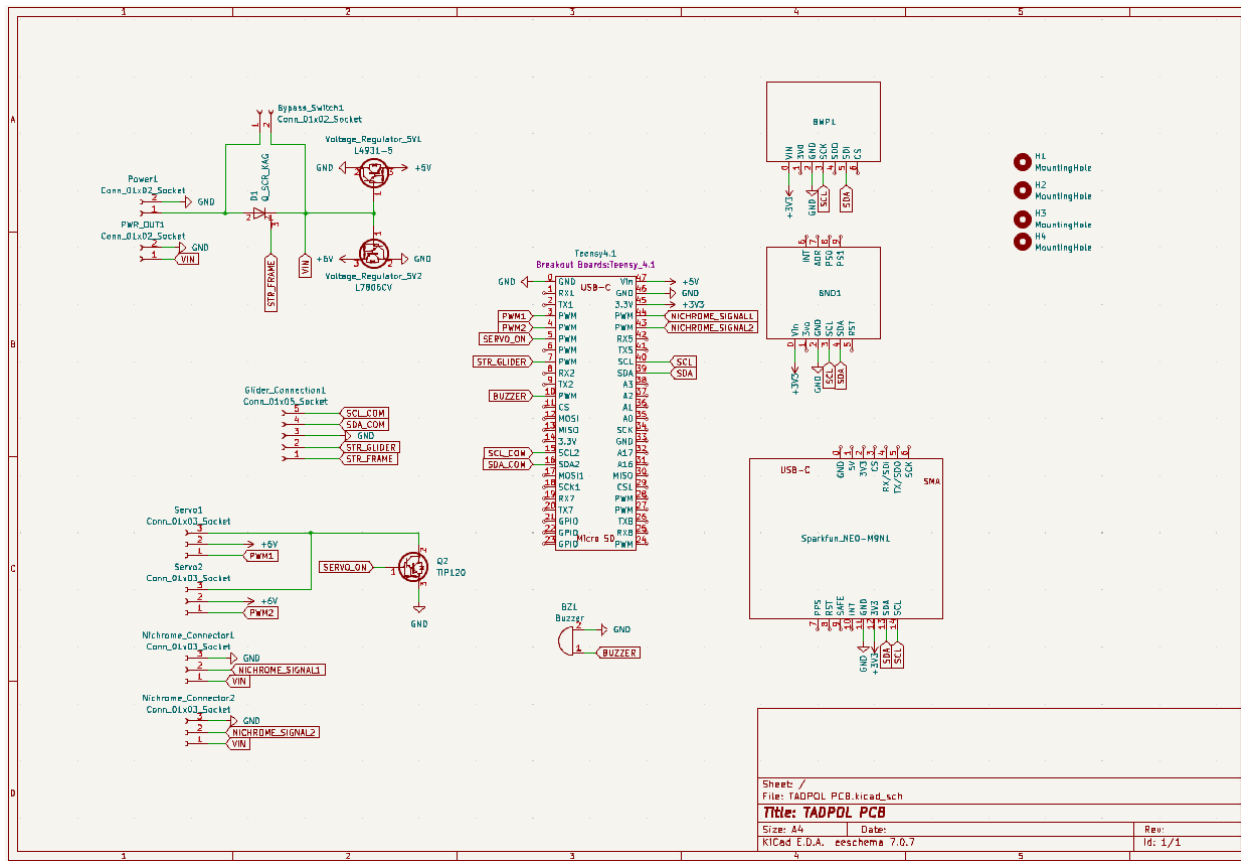


Fig. 107 TADPOL PCB wiring diagram

TADPOL Avionics The TADPOL SRAD avionics system (Fig. 107) has two primary purposes. First, to log telemetry of the TADPOL's descent after deployment, and second, control the TADPOL actuators to operate the drift control and live video systems.

The board is based off of the TERP PCB with a few modifications. The basic sensor package is controlled by a Teensy 4.1 microcontroller and has the same barometer (BMP280) and 9 DOF IMU (BNO055) as the TERP. However, unlike the TERP, the TADPOL doesn't need a light sensor to detect nose cone separation and instead adds a GPS (NEO-M9N Sparkfun Breakout Board) to gain a set of longitude and latitude (X, Y position) measurements. All of these boards are wired on an I2C bus and employ open-source Arduino based C++ code to read data from the breakout boards. This data is then run through a 3 axis (6 dimension) linear Kalman filter as discussed in section II.F.4. Data is recorded to pseudo static RAM (8 MB PSRAM) during flight and once the rocket is landed it is dumped to an SD card.

As previously mentioned, the TADPOL uses the same 18650 Lithium ion cells as TERP. The primary concern when selecting batteries for the TADPOL system was to balance current capacity with size. As servo motors use 5 V, a input voltage of greater than 5 V was required, resulting in the use of two 3.7 V lithium ion cells. As the teensy board is only tolerant up to 5 V, a linear 5 V regulator drops the voltage to an acceptable level. This meant two cells were required for the TADPOL PCB, bringing the total number to 5 cells (two for TADPOL, two for live video, and 1 for the Featherweight GPS). As volume constraints on the TADPOL system from the TERP vehicle bay are tight, cells had to be as small as possible. To reduce the size slightly, batteries with a prewired 2 mm JST harness were selected. The integrated harness removed the need for external battery connectors, saving on space. Furthermore the length of the harness allowed cells to be placed further from the board they were powering, improving space efficiency. The expected current draw for the TADPOL system during flight is around 0.42 A, maxing out at 1.3 A. While the TERP is able to activate the TADPOL at launch, a current capacity capable of powering the TADPOL at idle for a few hours on the pad was desired to account for potential issues with booting up at launch, primarily with respect to sensor calibration and gaining a GPS lock. With these constraints in mind, the 3.7 V 2200 mAh cylindrical lithium-ion cells were selected, providing roughly 5.2 hours of power.

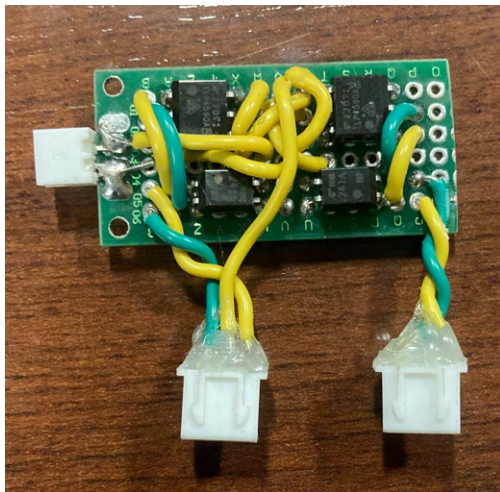


Fig. 108 SSR H-bridge circuit

motor speed, the H-bridge circuit is passed a PWM signal. This allows for easy adjustment of thrust from the motor using standard teensy functionality.

Finally, in an effort to reduce the number of external switches on the nose cone, the TADPOL was given the ability to be switched on by the TERP. Additionally, this opened the door for saving battery life by switching on the TADPOL only once the TERP determined Honu had launched. This was accomplished with a silicon control rectifier (SCR), specifically the TYN1012RG. This IC is nominally closed until a signal is sent to the gate pin, at which point it stays open even if the signal is removed. This is necessary for the TADPOL as it will lose the signal from the TERP once ejected from the rocket.

4. Drift control

Operating principle The drift control system implemented on TADPOL is an iteration of a system originally implemented on the payload developed for last year's competition. In both cases, the system controls the descent trajectory of a vehicle under a circular parachute by tilting the parachute in the desired direction. The tilt of the parachute allows high-pressure air captured in the parachute to escape in the opposite direction, causing the vehicle to move forward.

The previous iteration used continuous rotation servo motors to pull in or release the riser lines. To aid in developing the drift control mechanism and software, this mechanism was implemented on a small test rocket, as seen in Fig. 109. Flying the test rocket to 3,000 feet allowed for longer flight time compared to a drop test without having to fly the TERP on a 6" rocket. These flight tests demonstrated considerable issues with line slip and jams. Furthermore, the motors struggled to adjust the lines fast enough to keep the parachute pointed in the same direction as the system turned. However, these flights did demonstrate the parachutes ability to move the system in the direction of tilt. Fig. 110 shows a plot of the test rockets orientation (i.e. "forward" direction, taken from the systems magnetometer) and the direction of the systems velocity (taken from the change in GPS position updates) over the course of a test. The parachute riser system jammed early in this flight, resulting in the parachute staying at a constant tilt relative to the system. As a result, as the system turned due to outside forces, the orientation of the parachute turned as well, resulting in the rocket steering itself randomly as it descended.



Fig. 109 Drift control test rocket with nose cone and parachute removed

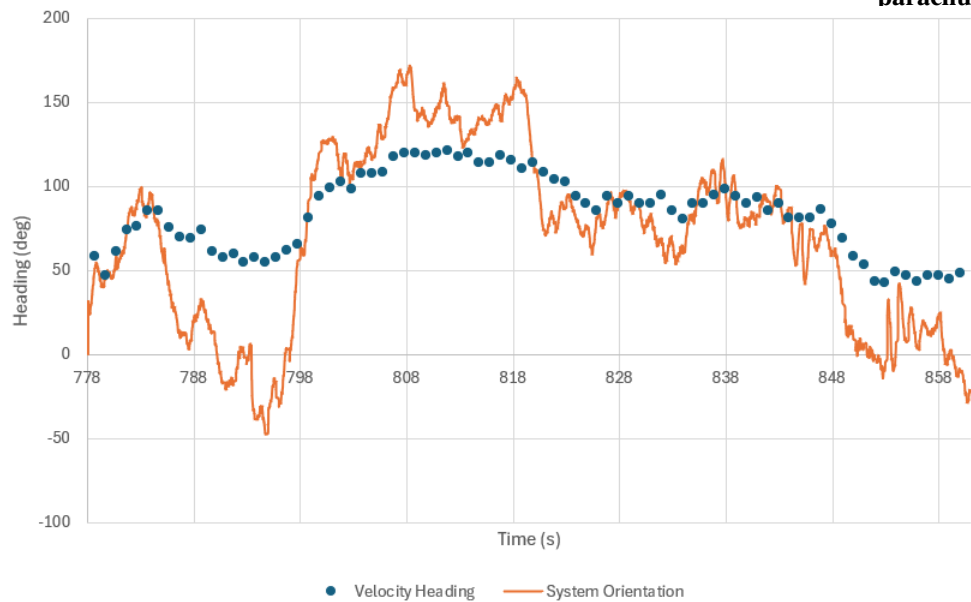


Fig. 110 System orientation and velocity heading over time

While the servo design had several issues, these drop tests did demonstrate the feasibility of the system, and suggested that should it be possible to control the heading of the parachute by controlling the heading of the vehicle. As a result, this year's system uses a static, deformed parachute and a DC motor tail-rotor to control system heading. Static tilt is accomplished by tying knots at the end of two neighboring risers, moving the end of the riser closer to the parachute. The tail rotor configuration was selected due to its lightweight and compact structure (when folded into the vehicle) and small circuit footprint.

The parachute is connected to 4 points at the corners of the top of the vehicle. These connection points are at a slight distance from the center of rotation to allow torques applied to the vehicle from the tail rotor to transfer to

the parachute. The connection points on the test rocket were considerably closer to each other, which allowed greater variation between the parachute and system headings. The two sets of risers that connect to the front of the vehicle are shortened slightly to cause the required parachute tilt. As previously mentioned, the tail rotor is mounted on a spring-powered folding arm for storage in the TERP. When the vehicle is ejected this arm is released and folds out automatically. Once deployed, the vehicle uses a PD controller to drive the motor via a variable voltage h-bridge. This allows for control over system heading, so the system is guided very similarly to a parafoil, albeit with a lower glide ratio.

Recovery point selection The goal of the recovery point selection system is to eliminate circumstances where the payload gets stuck on top of obstacles like trees (making it difficult or impossible to retrieve) or travels over a populated area. As the team conducts flight tests in areas with nearby forested regions, avoiding such obstacles is a necessity. To remove the complexity of determining if the system has sufficient altitude to clear a line of trees, this is accomplished by creating a flight path where the vehicle travels to recovery points without crossing over any obstacles.

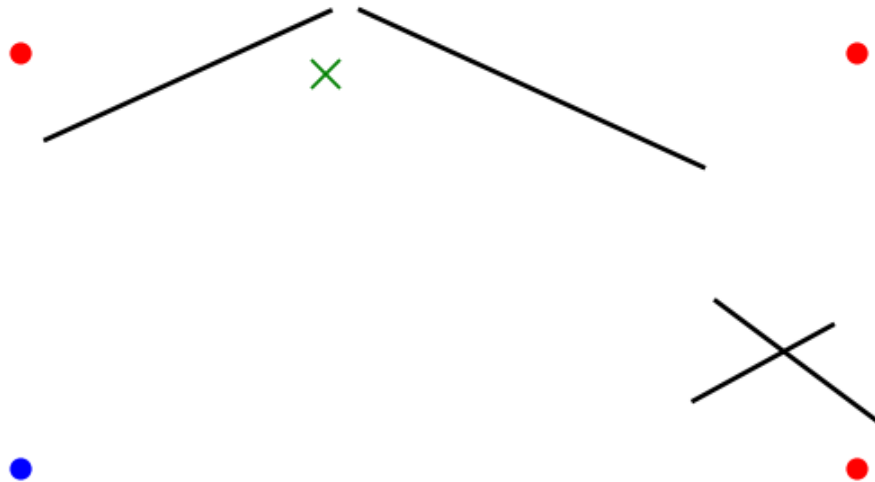


Fig. 111 Example recovery point selection case study. Obstacles pictured in black, invalid recovery points in red, valid recovery points in blue, starting point in green

Obstacles in this logic are represented with line segments, as seen in Fig. 111. When viewed from above, 1D-like obstacles (such as a line of trees) are represented with a single line segment. 2D-like obstacles (such as a building or parking lot) are represented by two, crossed line segments, where the endpoints define 4 corners of a bounding box around the obstacle. This accounts for cases where a payload ejects within the boundaries of an obstacle and is effectively “stuck”, with no valid recovery points. There is also a slight performance increase, as any given obstacle is defined using half as many lines, reducing the number of calculations required. Using these obstacle representations, navigation logic relies on determining if two line segments (one segment representing an obstacle and the other representing the path the vehicle takes from its current position to any given recovery position) intersect each other. There are three states for a recovery point in this logic: invalid, within an error margin of intersection, or clear.

The intersection logic is as follows: Suppose the first line segment has endpoints A and B, and the second line segment has endpoints C and D. The intersection of two line segments can be determined by tracing the direction of rotation through 3 different endpoints. The two line segments intersect if and only if: A→B→C has an opposite rotation to A→B→D and C→D→A has an opposite rotation to C→D→B (i.e. one set rotates CW and the other rotates CCW).

A recovery point is completely invalid if the line segment produced by connecting the vehicle's current position with the recovery point intersects any obstacle defined on the map.

When determining if a recovery point is within the margin of error of an intersection, two lines are created on either side of the line segment connecting the payload to the recovery point. These lines are rotated a predetermined number of degrees clockwise and counterclockwise each, creating a “cone” of error around the original payload-recovery point line segment. Therefore, if either of these two new line segments intersect any obstacle, but the original line segment does not, then the recovery point is not invalid, but within the margin of error for an intersection.

If several recovery points are not invalid, the vehicle won't automatically choose the closest one, but instead look for recovery points that have a lower likelihood of an intersection with an obstacle. As avoiding the defined obstacles is more important than reaching any given recovery point, a recovery point being out of range is inconsequential.

When the vehicle is within 20 feet of a recovery point, the recovery point selection code is no longer used. Instead, the system maintains its current heading until the 20 feet condition is no longer met and recovery point selection resumes. This causes the vehicle to circle the recovery point while still adjusting for drift due to wind.

Accounting for drift due to wind Once the vehicle has selected the desired heading, the system determines the heading offset required to account for drift due to wind. As the magnitude and direction of this drift are both hard to predict and will vary over time, the system continually updates an estimate for the change in velocity due to wind, allowing for a dynamic response. The wind estimate vector (\vec{w}) is broken into head/tailwind (\vec{w}_h) and cross-wind components (\vec{w}_c) using the heading calculated from the recovery point selection program (\vec{h}). Any drift due to wind parallel to the heading direction will simply change the speed of the vehicle, and so does not need to be actively accounted for. To account for cross-winds, the system needs to add an offset angle to the desired heading. The actual heading vector is then defined by components of $-\vec{w}_c$ and \vec{h}' , where \vec{h}' is a velocity of unknown magnitude in the direction of the original heading. $-\vec{w}_c$ and \vec{h}' form a vector \vec{g} , where $|\vec{g}|$ is equal to the standard vehicle speed v_s , a value measured from low wind drop tests to be roughly $1.6 \frac{m}{s}$. $|\vec{h}'|$ can then be computed using $\sqrt{v_s^2 - |\vec{w}_c|^2}$, and the required offset angle using $\arctan \frac{|\vec{w}_c|}{|\vec{h}'|}$. At the next time step, the system determines the average system velocity (\vec{v}) over the time step using \vec{p}/t for change in position \vec{p} and loop time t . By subtracting \vec{g} from \vec{v} , the system can update its wind estimate for the next time step. This new wind estimate is averaged with the previous estimate to prevent small gusts from further impacting the vehicle trajectory.

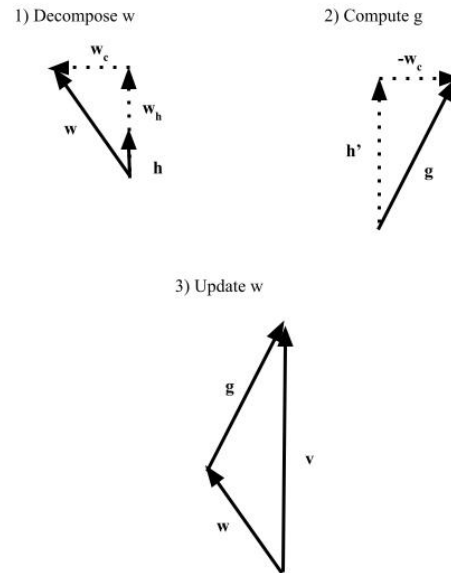


Fig. 112 Vectors used in wind prediction

Controller design As previously mentioned, a PD controller is used for attitude control. As the IMU gyroscope provides angular rate measurements, the system has access to derivative error measurements. This allows the use of the PID family of controllers, simplifying the design process. The integral control term was removed due to the slow turn rate requirement to prevent issues with the parachute lines getting tangled up. This slow turn rate requirement means the system may spend a long time facing away from the ideal direction, causing an I-term build-up that creates errors further down the line.

A PD controller uses proportional and derivative error terms multiplied by a respective gain value to determine the required output to the actuators. Proportional error is the difference between the current and required heading, as measured using a magnetometer present in the IMU. Derivative error is the rate of change of error, which describes how fast the system is approaching zero error. For a constant heading, this term will be equivalent to the vehicle's angular rate, measured from the gyro. While the actual heading will vary, it is likely to remain roughly constant, except when

moving very close to a recovery point (at which point the system switches to using a constant heading). As a result, angular rate values are used to take advantage of the BNO's internal noise filtering.

The proportional and derivative gain values (K_p and K_d respectively) are constants multiplied by the error terms to produce the final output signal. To form an initial measurement for these values, the system dynamics are for a range of different voltage inputs to the fan. From this data a relation between the PWM signal sent to the motor and the resulting angular acceleration can be determined. For simplicity, this relation is modeled as a constant K . This value is then used to tune a PD controller in MATLAB for a plant $\frac{K}{s^2}$, corresponding to a mass with no drag or spring forces. The tuned constants were further refined manually through testing to improve response time and reduce oscillations.

5. Live video

The live video system onboard the TADPOL is a modified version of the Avionics Live Video system discussed in the SRAD Avionics Live Video section. Similar to that system, the purpose of the live video system on the TADPOL is to capture and transmit a live video stream to the ground as part of the Live Video Challenge. While functionally the same, the system needed to be modified so it would fit in the space constraints of the TADPOL, which are much tighter compared to the electronics bay that houses the SRAD avionics.

The primary modification made to the Avionics Live Video system in the TADPOL is the power delivery system. The power delivery board used for the Avionics system was shortened, allowing the battery cells and power regulation systems to be stored more efficiently. The previous battery connectors were replaced with a wire harness for connecting two 3.7 V 2200 mAh lithium-ion batteries (the same used for other TADPOL and TERP systems) in series. Based on the same buck converter efficiency of 90%, and estimated maximum system power draw of 5 V at 1.5 A, the battery life of the live video system on the TADPOL is 1.95 hours. While this is significantly shorter than the Avionics Live Video system, other modifications were made to reduce the required battery life. The live video system in the TADPOL is powered on by the TERP at launch using the same SCR-based power latching circuit present on the TADPOL, resulting in no power usage while idle on the pad. As the live video system camera will not be able to see out of the nose cone until vehicle deployment, the system will not need to begin transmissions until that time. Once the TADPOL avionics detect apogee, they signal the Raspberry Pi to begin transmitting video, filling the role of the SRAD flight computer. Aside from these modifications, the live video system on the TADPOL functions the same way as the Avionics Live Video system.

The camera is mounted on a servo motor mount. When stored in the TERP, this mount faces backwards, such that the system will record the TERP during separation. After TADPOL deploys, the servo motor rotates the camera so it faces in the forward direction. Aside from providing a better visual of the TADPOL flight path, the rotation also moves the camera away from structural elements of the TADPOL, providing a better field of view. At 100 feet altitude the camera is rotated back into its initial, back-facing orientation for protection on landing.

I. Flight Tests

Honu flew four flight tests in a few different configurations in preparation for the Spaceport America Cup. Since the high altitude field, Higgs Farm, was only open December through March, it was vitally important to launch early and often. This allowed the team to make changes early in the year, improve designs and implement new solutions at a reasonable pace. They also offered opportunities to increase the efficiency of the assembly process and to give experience to younger members, building the overall experience of the team.

1. December 16, 2023

The first test flight of the season occurred on December 16, 2023. Although the payload and Airbrake PCBs had flown on a previous flight to collect data, this was the first 6" rocket flight of the year. The rocket consisted of last year's fin can, Airbrake, and nose cone assembly, but featured new fiberglass airframe tubing and a new electronics bay. Due to its mix of parts from last year and this year, it was titled Karkonu, a combination of Karkinos and Honu. It flew on an Aerotech M1780 to 6,000 feet. It was a test flight to ensure the recovery systems worked as planned, and the flight flew successfully without recovery problems.



Fig. 113 Karkonu's First Flight

2. February 3, 2024

While a January flight was planned, it was scrubbed due to weather. The second flight occurred on February 3, 2024 on an Aerotech M1939, flying to 8,400 feet. The goal was to provide a high altitude opportunity to test the Airbrake and to test another iteration of the electronics bay. The payload would not deploy the vehicle, but the system would still collect data for the flight. However, due to the rocket underperforming because of added weight, the Airbrake did not deploy, but the rocket recovered nominally without damage. Additionally, a static fire of the N2900 was completed.



Fig. 114 Combined Image of Karkonu and the EX N2900 Static Fire

3. April 7, 2024

A March test flight on the team's SRAD N2900 was planned, but was canceled due to a broken launch controller. Therefore, the next test flight was on April 7, 2024 on a low altitude Aerotech M1500 flight at the MDRA Sod Farm. The goal was to deploy the payload vehicle and test the Airbrake, as well as test the functionality of the final electronics bay structure iteration. This was also the first flight of the new 2024 fin can, 2024 nose cone assembly, and vinyl tube deployment charges, which functioned as intended. The Airbrake deployed, as did the payload vehicle. However, recovery was not successful. Due to winds that day, the rocket flew drogueless, which caused the rocket to tumble during drogue descent. The drogue shock cord caught the main parachute as it was unfolding, and the rocket hit the ground much faster than expected as a result. In addition, the shock cord connecting the nose cone shell to the TERP snapped due to a knot in the line. As a result, checking shock cords for knots has been added to the teams checklist. The rocket had damage in the Airbrake, payload, and electronics bay, and these sections were repaired and rebuilt. Further information on the failure can be found in the test reports in the Appendix.



Fig. 115 Honu on an Aerotech M1500

4. April 21, 2024

Honu flew its SRAD motor test flight on April 21, 2024. Previously, the motor had been static fired in February, but had not flown aboard the rocket. It featured a rebuilt airbrake, so one goal was to verify it worked and its strength. Other major goals included recovering the rocket safely and acquiring more data about the motor. Based on static fire data, the rocket on the SRAD motor was simulated to reach 9,800 feet if the Airbrake did not deploy. The ascent and descent were nominal, and recovery went as planned. There were two Featherweight GPS trackers aboard the rocket, one in electronics bay and one in the payload vehicle, but for this flight, the payload would not deploy. Therefore, there would be two redundant trackers on the ascent. This was useful because contact was lost with the primary electronics bay Featherweight GPS due to an error in using the new Blue Raven app. The payload tracker functioned nominally. After recovery, it was found that the rocket flew to about 11,100 feet. The motor overperformed, mostly due to slag buildup in the nozzle and higher pressures.



Fig. 116 Honu's Flight on the SRAD N2900

III. Mission Concept of Operations Overview

Honu's mission profile will be that of a standard two-break dual deploy high power rocket. The use of a smaller drogue and a larger main minimizes drift from the launch site and makes recovery easier. The concept of operations for Honu can be found below along with the phases on a simulation plot.

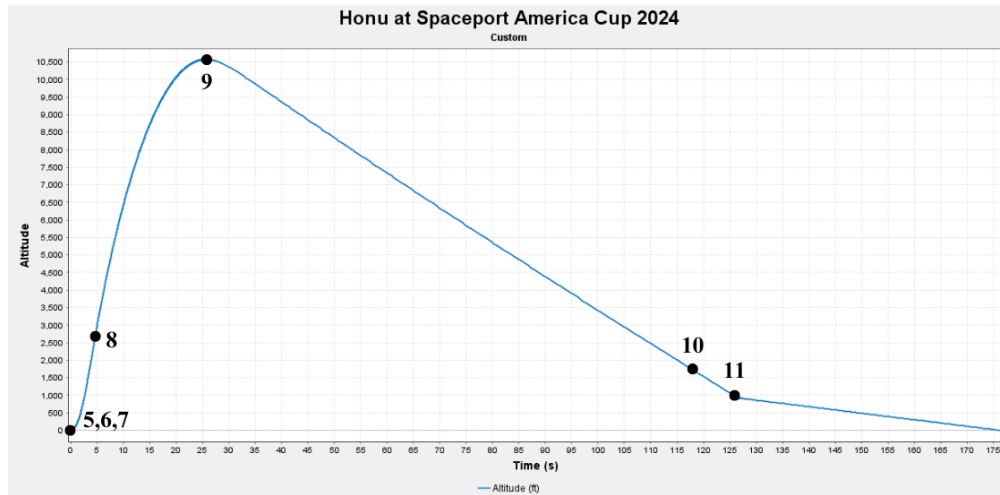


Fig. 117 Honu Concept of Operations

- 1) Phase 1: Preflight Preparation
 - During the week leading up to the flight, the motor is assembled, the electronics are mounted in the electronics bay, and the Airbrake, avionics, and payload modules are prepped for flight.
- 2) Phase 2: Preflight Assembly
 - The motor is integrated, charges are connected to the electronics, and the rocket is assembled. Recovery parachutes and shock cord are packed into the recovery tubes. Shear pins and bolts are used to connect the tubes together.
- 3) Phase 3: Launchpad Integration
 - The rocket is slid onto the rail and the payload SRAD avionics switch is turned on. The rail is raised vertical and locked.
- 4) Phase 4: Arming
 - Airbrake computer is powered on. SRAD Avionics are powered on. Cameras are powered on. Featherweight GPS and Blue Raven are powered on. EasyMinis are powered on. Continuity on all E-matches is confirmed via auditory cues from computers. Telemetry is checked for GPS lock. Unnecessary personnel are cleared from the area and the motor igniter is installed.
- 5) Phase 5: Ignition ($t = 0.00$ s)
 - Current is sent through the igniter and the motor is lit. Smoke is seen coming out the aft end of the motor.
- 6) Phase 6: Lift Off ($t = 0.01$ s)
 - The motor begins to produce thrust and vertical motion is visible.
- 7) Phase 7: Launch Rail Clearance ($t = 0.35$ s)
 - The rocket accelerates upward under motor power and clears the rail. The boost phase lasts approximately 4.6 seconds, at which point the rocket is 2,700 feet above the ground.
- 8) Phase 8: Motor Burnout ($t = 4.6$ s)
 - Motor burnout occurs and the rocket coasts to apogee. One second after motor burnout, the Airbrakes deploy as needed in order to reach 10,000 feet accurately. This occurs from 4.6 seconds into flight and continues until apogee.
- 9) Phase 9: Apogee, Drogue Deployment, and Descent ($t = 26$ s)

- At apogee, the primary EasyMini fires its drogue charge, followed by the backup EasyMini on a one second delay. The booster separates from the electronics bay and the four shear pins break. The two halves of the rocket separate, the drogue parachute inflates, and the rocket falls at a rate of 90 ft/s.
- 10) Phase 10: Nose Cone and Payload Deployment (t = 118 s)
- Once the nose cone EasyMini detects an altitude of 1,700 feet during descent, the nose cone charge fires and separates the nose cone. The payload detects an increase in light and deploys the payload at 1,500 feet.
- 11) Phase 11: Main Deployment and Descent (t = 126 s)
- When the primary EasyMini detects an altitude of 1,000 feet, the main charge fires. This is followed by the backup EasyMini which is set to deploy its charge at 900 feet. The nose cone electronics bay is separated from the rocket and the main parachute inflates, slowing it to a safe descent velocity of 19 ft/s.
- 12) Phase 12: Ground Recovery (t > 178 s)
- The rocket has hit the ground and the flight has ended. A recovery team will be sent to locate the rocket using GPS data received from the Featherweight GPS. Once recovered, electronics are powered off and the rocket is taken back to the judges for post-flight evaluation. Flight computer, payload, avionics, and Airbrake data is then downloaded and analyzed.

IV. Conclusion and Lessons Learned

This year will be the team's fourth time attending SAC. TerpRockets has previously completed in the 10,000 foot COTS Solids Division in 2018 and 2022 and most recently in the 10,000 foot SRAD Solids Division in 2023. At SAC 2023, the team had its most successful year to date coming in 2nd place in the 10,000 foot SRAD Solids Division.

Prior to SAC 2022 and 2023, the competition rocket was launched four times each year, a trend continued with Honu. This is in stark contrast to many of the other teams at SAC who might only fly their rocket once before the competition. This quick launch cadence allows the team to hone operations skills and be able to launch quickly and efficiently. To make the most of this opportunity, the team focuses on simple yet effective designs that allow for rapid testing and iteration.

TerpRockets enters the competition this year, again in the 10,000 foot SRAD Solids Division, with the hope to refine the skills learned last year improve on previous successes. Having another year and more test flights allows the team to be confident in Honu's design and experience launching it reliably. MDRA provides a local launch site that the team has flown at for many years. They host launch events once a month and have been a great support to the team. Whether launching the competition rocket or personal rockets, the team makes it a habit to attend each launch and develop a close relationship with MDRA and its members.

One of the biggest improvements this year has been manufacturing our tubes. The team's mentors at ST Engineering MRAS offered their time and advice to help improve the process. After making eight airframe tubes and meeting with MRAS, the team learned a couple lessons and refined the process. This year, the biggest hurdle was removing the finished tube from the mandrel. Through consulting and experimentation, three main solutions were developed. First, the mandrel would be repaired each use to increase the smoothness of the surface. Second, the wrap of Mylar was decreased from 1.5 wraps to 1 wrap with an inch of overlap, which helped prevent it from bunching together and jamming when pulling off the tube. During this process, mold release on the Mylar was omitted so that the film adhered to the part better, ensuring a smooth slide off the mandrel. Finally, instead of sealing the seam with a layer of packing tape over the top, which caused wrinkles, the team switched to two thin parallel lines of double sided tape, greatly minimizing wrinkles and improving the surface finish. These lessons greatly helped the team towards the end of the year, when manufacturing a new set of fiberglass airframes and a carbon fiber coupler for the Airbrake was much easier and faster. The team is excited to continue our work with MRAS and improve the quality and production rate of SRAD tubing.

Some of the largest challenges for any collegiate rocket team are a lack of knowledge transfer, lack of high-power rocket experience, or falling victim to design paralysis by making overly complicated designs. The team has witnessed the impact of members earning their certifications and took note of the positive difference in work production. The motivation to have members earn their certifications is to further build our knowledge of dual-deployment, recovery, solid rocket motors, and general launch operations and manufacturing techniques. As of recent records, the team has added 35 L1s, 2 L2s and 1 L3 this year bringing the team's certification total to 55 L1s, 5 L2s, and 2 L3s. These are the most certifications in the team's history. The ability to understand the fundamentals of rocketry will push our team to further heights with more technical projects in the future.

In addition, the team has learned that offering multiple projects outside of SAC has kept members engaged and curious about the field of rocketry. These projects include a 2-stage high-power rocket, a minimum diameter rocket, a liquid-powered rocket, and hybrid-powered engine testing. There are a variety of skills and interests that university students have. By offering projects that meet their interests, the team has been able to recruit and retain members at a higher rate.

V. Appendix A: System Weights, Measurements, and Performance

1. Rocket Information

Table 22 Overall Rocket Parameters

Stages	1
Vehicle Length (in)	153
Airframe Diameter (in)	6
Number of Fins	4
Fin Semi Span (in)	6
Fin Tip Chord (in)	6
Fin Root Chord (in)	18
Fin Thickness (in)	0.25
Vehicle Weight (lbs)	50.5
Propellant Weight (lbs)	14
Empty Motor Casing Weight (lbs)	12.6
Payload Weight (lbs)	10.5
Liftoff Weight (lbs)	89
Center of Pressure from Tip of Nose (in)	120
Center of Gravity from Tip of Nose (in)	95

2. Propulsion System

Table 23 Propulsion System

Motor Type	Solid
COTS, SRAD	SRAD
Manufacturer	Terrapin Rocket Team
Designation	N2900
Motor Classification	N
Average Thrust (N)	2,924
Total Impulse (Ns)	12,724
Burn Time (s)	4.6

3. Predicted Flight Data and Analysis

Table 24 Flight Predictions

Launch Rail Length (ft)	17
Effective Launch Rail Length (ft)	14
Liftoff Thrust to Weight Ratio	11.7:1
Rail Departure Velocity (ft/s)	104
Minimum Static Margin (at Launch Rail Clearance)	4 cal, 16%
Maximum Acceleration (G)	10.7
Maximum Velocity (ft/s)	912
Fin Flutter Velocity (ft/s)	2,207
Target (ft)	10,000
Predicted Apogee (ft)	10,573

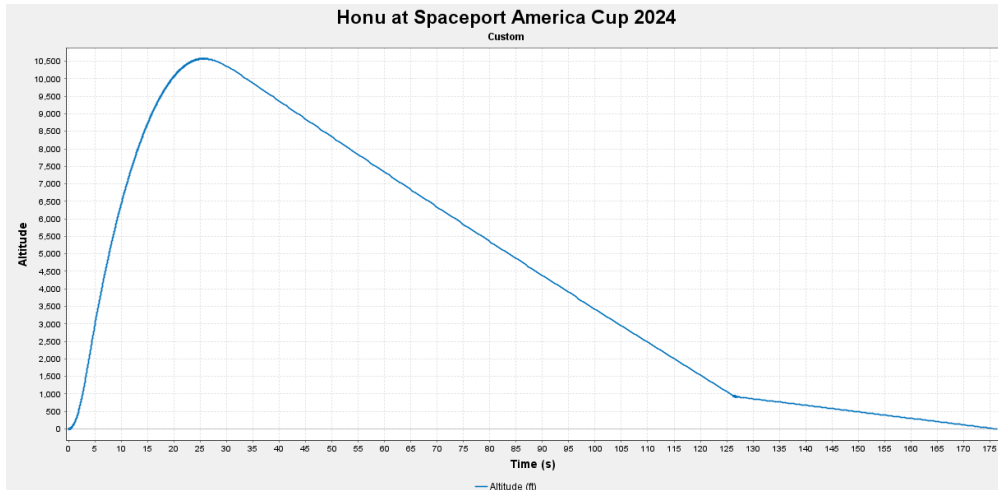


Fig. 118 Honu Flight Profile Graph

4. Recovery System

Table 25 Recovery System

Primary Deployment System	COTS Altus Metrum EasyMini
Backup Deployment System	COTS Altus Metrum EasyMini
Drogue Primary Black Powder Charge	0.012 lbs, 5.5 g
Drogue Backup Black Powder Charge	0.013 lbs, 6 g
Drogue Deployment Altitude	Apogee
Drogue Descent Rate (ft/s)	90
Drogue Shock Cord Length (ft)	70
Nose Cone Black Powder Charge	0.001 lbs, 1.5 g
Nose Cone Deployment Altitude (ft)	1,500
Nose Cone Shock Cord Length (ft)	20
Main Primary Black Powder Charge	0.012 lbs, 5.5 g
Main Backup Black Powder Charge	0.014 lbs, 6.5 g
Main Deployment Altitude (ft)	1,000
Main Descent Rate (ft/s)	19
Main Shock Cord Length (ft)	30
Bulkhead Mechanical Links	Steel Quicklinks (1/4", 5/16")
Fin Can Mechanical Links	Steel Eyenuts (1/4"-20)
Shock Cord Connection Mechanical Links	Steel U-Bolts (3/8")

5. SRAD Components

Table 26 SRAD Components

Retainer	COTS	Aluminum (Aeropack)
Thrust Plate	SRAD	Aluminum
Motor Mount Tube	SRAD	Carbon Fiber
Fin Can Tube	SRAD	Carbon Fiber
Fins	SRAD	G10 Fiberglass
Centering Rings	COTS	G10 Fiberglass (Wildman)
Airbrake Airframe	SRAD	Fiberglass
Airbrake Coupler	SRAD	Carbon Fiber
Airbrake Bulkheads	SRAD	G10 Fiberglass, Aluminum
Drogue Recovery Tube	SRAD	Fiberglass
Electronics Bay Coupler	COTS	Fiberglass (Wildman)
Switch Band	SRAD	Fiberglass
Electronics Bay Bulkheads	SRAD	Aluminum
Main Recovery Tube	SRAD	Fiberglass
Nose Cone Electronics Bay Coupler	COTS	Fiberglass (Wildman)
Nose Cone Electronics Bay Bulkheads	SRAD	Aluminum
Payload	SRAD	Primarily Aluminum and PETG
Nose Cone	COTS	Fiberglass (Wildman)

VI. Appendix B: Project Test Reports

(As seen on next page)

Date	Subteam	System	Type	Goal	Status
9/17/2023	Airbrake	Flight Computer	Flight	Verify tilt and predicted apogee for vertical orientation	Successful
10/20/2023	Payload	TADPOL	Drop Test	Verify parachute tilt causes drift	Successful
10/20/2023	Payload	TADPOL	Drop Test	Analyse riser tilt mechanism	Failure
11/12/2023	General	Blue Raven	Flight	Build familiarity with Blue Raven	Successful
11/17/2023	Payload	Payload TADPOL	Drop test	Analyse riser tilt mechanism when subject to yaw	Failure
12/17/2024	General	Recovery	Ground	Ensure glove finger ejection charge sizes separate the airframe sections	Success
12/17/2023	General	Karkonu	Flight	Overall Flight Test	Successful
12/17/2023	Payload	TERP, TADPOL	Flight	Data logging	Failure
2/3/2024	General	Karkonu	Flight	Overall Flight Test	Successful
2/3/2024	Payload	Terp, TADPOL	Flight	Data logging	Successful
2/3/2024	Solids	Motor	Static Test	Successful static fire of motor, record pressure and thrust data	Successful
2/3/2024	Payload	Drift Control Test Rocket	Flight	Analyse riser tilt mechanism from higher altitude	Failure
2/3/2024	Avionics	SRAD Master Board	Flight	Collect flight data and verify that sensors and data logging work	Failure
2/3/2024	Airbrake	Flight Computer	Flight	Verify tilt, check on state estimation, test new flaps	Successful
2/24/2024	Payload	TADPOL	Bench Test	Determine pwm-angular acceleration relation	Successful
3/3/2024	General	Recovery	Ground	Determine vinyl tube ejection charge sizes	Partial Success
3/17/2024	Avionics	Flight Computer	Ground	Test ability to record and store sensor and GPS data	Success
3/30/2024	Payload	TADPOL	Drop Test	Measure passive system dynamics	Successful
3/30/2024	Payload	TADPOL	Drop Test	Analyse effect of PD controller on system heading	Failure
4/7/24	General	Honu Flight Test	Flight	Determine quality of fin can, test new camera setup, test new ebay	Partial Success
4/7/24	Payload	TERP,TADPOL	Flight	Deploy payload without nichrome and evaluate drift control system	Partial Success
4/7/24	Avionics	Flight Computer	Flight	Record and store data, receive and display telemetry data, record video	Partial Success
4/15/2024	Solids	Motor	Ground	Proof test motor casing to 1.5x MEOP	Successful
4/21/24	Payload	TERP,TADPOL	Flight	Data logging	Successful
4/21/2024	Solids	Motor	Flight	Record pressure data in Flight	Successful
4/29/24	General	COTS Electronics	Ground	Determine battery life under high heat conditions for COTS Electronics (EasyMini, Featherweight GPS)	Successful

Passive TADPOL Analysis Drop Test

Michael Mallamaci, Nathan Roy, Payload
October 20th, 2023

Test Objective:

Drop the drift control system with risers statically deformed. Analyze the resulting vehicle dynamics to determine the effectiveness of a tilted parachute for locomotion.

Test Procedure:

1. Bias the 2 riser loops in forward roughly 1" from the starting position
2. In low winds, drop the system 6 times from a height and record the path.
3. Analyze the resulting motion to determine the effectiveness of the parachute

Test Results:

While impacted by yaw, drift in the direction of displacement is clearly present. During the descent, the front face of the parachute is pulled flat, while the back end is extended. As this deformation continually lines up with the direction of motion, it is clear the resulting drift was the result of the parachute's tilt.

As the parachute yawed, the direction of travel changed to match the parachute heading. For drops 4 and 5 yaw was more pronounced, and the system followed a spiral path. In both cases, the parachute begins to turn before the vehicle (the result of the vehicle's momentum carrying it forward while the parachute turns much faster), causing the system to swing wide as it circles around. While this does not seem to affect the motion in any noticeable way, further testing from higher altitude is required.



Event and Success Criteria		
Validate that the system moved in the direction of tilt	PASS	10/20/23
Validate that risers do not slide against the drive wheels	PASS	10/20/23
System Analysis	SUCCESS	10/20/23

Active TADPOL Yaw Analysis Drop Test 1

Michael Mallamaci, Nathan Roy, Payload
October 20th, 2023

Test Objective:

Drop the drive wheel drift control system with active riser deformation to determine its ability to account for system yaw.

Test Procedure:

1. Set servo motors to turn in the direction of magnetic North.
2. In low winds, turn the system on, let the motors start turning, and then drop the system
3. Analyze the results to determine how well the system accounts for yaw

Test Results:

The first drop was effectively a moot test, as the drop altitude was too low to see any real motion. It should be noted, however, that once the chute opens, it does deform in the correct direction.

The second failed due to excessive riser displacement. When combined with the spiral of the system, it caused the parachute to momentarily collapse, preventing any movement.

The third was the best of the 3; the system moved in the expected direction without much issue. It should be noted that the system demonstrated little yaw during this test, so the effectiveness of the system during yaw has not been fully validated.

There are a few notes for these tests, the first being that the motor were unable to spin at full speed due to the current draw limitations of 9v batteries. As a result, testing stopped here. The second is that the max riser displacement was set larger than needed (over 2"), resulting in the parachute coming close to collapsing. The passive tests were done at closer to 1.5" and had no issues with the parachute collapsing. Finally, IMU data was not recorded, and so analysis depended solely on observed dynamics.

Moving forward this test should be repeated with more powerful batteries, increased riser spread, and data recording.

Event and Success Criteria		
Validate that the system moves in a single direction regardless of yaw	FAILURE	October 20, 2023
System Analysis	FAILURE	October 20, 2023

Blue Raven Datalogging Flight Test

Sunjun Mehta, Chief Engineer

November 12, 2023

Test Objectives:

1. Build familiarity with the Blue Raven Altimeter by using it on a test flight as a datalogging altimeter. The deployment altimeters will be Altus Metrum EasyMinis which the team has significant experience with.

Test Procedure:

1. Gain familiarity with basic functions by connecting the Blue Raven to the app through Bluetooth and learn functions.
2. Mount Blue Raven inside an electronics bay and wire it with the Additive Aerospace Simple Circuit.
3. Fly the rocket with the Blue Raven as payload.
4. After the flight, ensure Blue Raven recorded flight data and functioned nominally. Export data to shared Drive.

Test Results:

The Blue Raven functioned as intended and the team built familiarity with the device.

Event and Success Criteria		
Fire both drogue and main charges	SUCCESS	11/12/2023
Collect flight data	SUCCESS	11/12/2023
System Analysis	SUCCESS	11/12/2023

Active TADPOL Yaw Analysis Drop Test 2

Michael Mallamaci, Max Weinstock, Nathan Roy, Payload

November 17th, 2023

Test Objectives:

Analyze the affects of yaw on the tadpol system

Test Procedure:

1. Load the drop test code onto the system with the test PCB
2. Turn the system on, let the motors start turning, and then drop the system
 - a. Dont try to remove any yaw pre drop
3. Determine if the parachute lags behind the structure during yaw
4. Determine if the parachute deformation can keep up with system yaw

Test Results:

Evaluation of the system compared to the previous drop test was complicated by 2 factors. The first was wind, which was stronger than before and likely exaggerated the system's oscillation under the chute. The oscillations also create drift by tilting the chute, which makes evaluating the cause of drift harder. The second was the riser bias was still too large, resulting in the chute coming close to collapsing a few times. It's also believed the system's recent rate was faster, which might be explained by these factors.



Parachute lag was noticed in a few tests. For two drops the system rotates $\sim 90^\circ$ with respect to the chute over a few seconds. The chute generally catches up to the system just before it touches the ground, and had the tests occurred from a higher altitude, the system likely would have continued to damp out the oscillations. In one test, however, the system spun in a full circle under the chute. The oscillations here were much larger and would have taken much longer to damp out. This criterion was defined as a partial success, as it is possible to further damp the yaw rate.

Due to the outside complications, we are unable to determine with any certainty if the system is capable of keeping up with the yaw rate. That said, the previous criterion means the yaw rates from this test will be outside the allowable scope for the time being, which invalidates this test anyway.

Between this and the previous drop test, we have some confidence that at low yaw rates the system can move as expected. There are 2 immediately apparent paths forward. The first is to improve the yaw rates at which the system and chute rotate together, which can be accomplished

by moving the riser path exits outward on the tadpol, increasing the damping between the 2 systems. The second is to implement a yaw damping system (either passive or active) on the tadpol to limit yaw in the first place.

Event and Success Criteria		
Parachute and tadpol yaw together	PARTIAL SUCCESS	Nov. 17, 2023
Parachute deforms to meet yaw	FAILURE	Nov. 17, 2023
System Analysis	FAILURE	Nov. 17 2023

December Ejection Ground Test

Sunjun Mehta, Chief Engineer

December 17, 2023

Test Objectives:

1. Airframe volumes and shear pin quantities are the same as last year's Karkinos rocket. Therefore, the charge sizes for testing remained the same. Each was made of the appropriate amount of black powder inside a nitrile glove finger. An igniter was inserted to the bottom of the finger and the assembly was tightly wrapped in electrical tape.
 - a. Main Primary: 6 g
 - b. Drogue Primary: 6 g

Test Procedure:

1. Assemble the rocket as if for launch, including connecting and folding shock cords, packing parachutes, and inserting shear pins. The ejection charges themselves would be routed through the electronics bay coupler and out through the holes in the switchband.
2. Set up the rocket parallel to the A-rack, and prop the rocket up near the Airbrake using a box.
3. Connect the ejection charge ematch leads to the launch system, Main on Pad 7 and Drogue on Pad 8.
4. The LCO then will ignite the charges.

Test Results:

Both primary charges easily separated and allowed clearance for the parachutes to come out without excessive force. The following charge sizes were chosen and were the same as the charges on Karkinos.

- c. Main Primary: 6 g
- d. Main Backup: 7 g
- e. Drogue Primary: 6 g
- f. Drogue Backup: 8 g

Event and Success Criteria		
Main Separation	SUCCESS	12/17/2023
Drogue Separation	SUCCESS	12/17/2023
Overall	SUCCESS	12/17/2023

Karkonu Flight Test 1

Sunjun Mehta, Chief Engineer

December 17, 2023

Test Objectives:

1. Test the integrity of new airframe components
 - a. Karkonu is a combination of parts from Karkinos in 2023 and Honu in 2024.
Karkonu used the 2023 fin can and nose cone, but used the 2024 fiberglass body tubes and electronics bay.
2. Test functionality and practicality of the new electronics bay design
3. Flight test on M1780
4. Safe recovery - flight test of the recovery system
5. Data collection on the Blue Raven, maintain tracking throughout the flight

Test Procedure:

1. Assemble Karkonu as per the assembly and launch procedures.
2. Verify 3 beeps on both EasyMinis and connection to the Featherweight GPS.
3. Insert igniter, clear the pad.
4. Post launch:
 - a. Turn off all recovery electronics
 - b. Check that the recovery system worked as intended, with no major tangles
 - c. Check that all four deployment charges were fired.
 - d. Check for damage

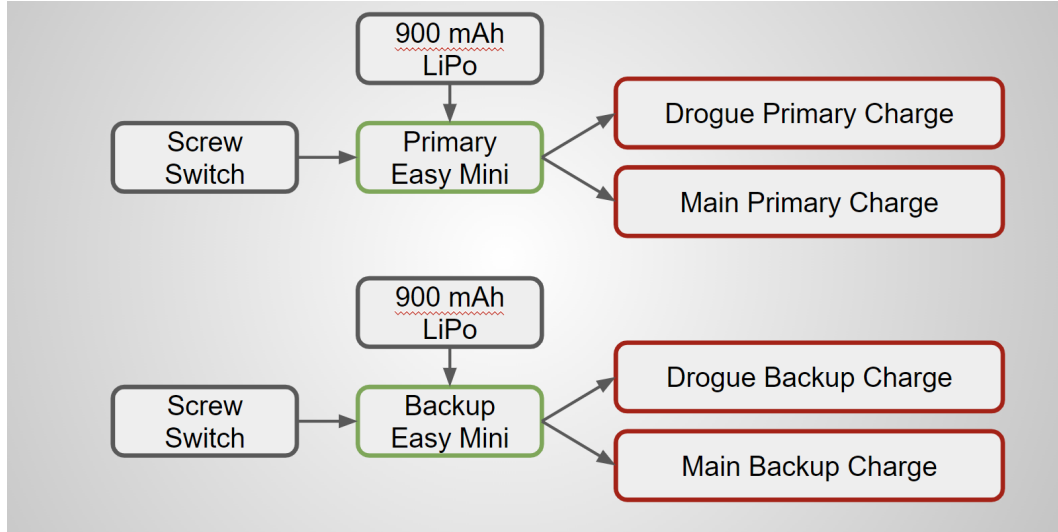
Test Results:

1. Karkonu flew very straight and similar to simulations.
2. There were no problems with the new airframe components.
3. The new electronics bay design had problems with fit, placement of batteries, and these were noted.

Event and Success Criteria		
Fly a stable, safe flight	SUCCESS	12/17/2023
Safe Recovery	SUCCESS	12/17/2023
Maintain Tracking	SUCCESS	12/17/2023
Blue Raven Data Collection	SUCCESS	12/17/2023
Ebay Functionality	PARTIAL SUCCESS	12/17/2023

Overall	SUCCESS	12/17/2023
---------	---------	------------

Test Images:



Each flight computer has its own switch, battery, and set of charges, leading to dual redundancy. The backup fires drogue one second after apogee. The primary deploys main at 1,000 ft, while the backup fires at 900 ft.

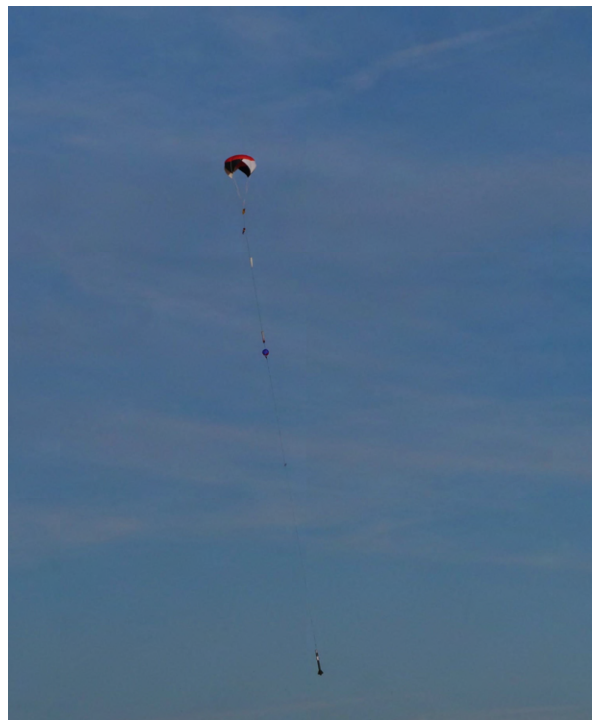


The December version of the electronics bay, showing two independent EasyMinis and a Blue Raven with a Simple Circuit on the front. The Featherweight GPS was included on the back of this assembly.

Terrapin Rocket Team



Karkonu lifts off on an Aerotech M1780 for the first full flight test of the season.



The recovery system worked as planned, and no major tangles or damage was found. The parachutes easily unfolded and the rocket descended as intended.

Payload Data Collection

Michael Mallamaci and Nathan Roy, Payload

December 17, 2023

Test Objectives:

Collect flight data from a competition-like flight profile using the TERP and TADPOL

Test Procedure:

1. Load the TADPOL into the TERP
2. Power the TADPOL on through the TERP
3. During the flight collect data from all sensors and share it over I2C
4. Separate the nose cone
5. Save data to an SD card

Test Results:

There were several issues with the SCR, which prevented the use of the camera system trigger. These can be summarized as the SCR outputting voltage from the input, and only functioning with the I2C bus attached. While the circuit used can power on the TADPOL by some miracle, it needs to be updated for the future.

Furthermore, the I2C program requires replacing the wire library, which complicates sensor communication. This needs to be fixed, and so I2C was not used.

The TERP did not identify the SD card and as a result did not record data. The buzzer error for this was missed (in part due to the easy mini being activated before the payload), and so a restart was not attempted. A clearer error system should be developed to make this as fool proof as possible (and the easy mini should be turned on second).

While the TADPOL did identify the SD card, due to the launch g trigger being set higher than the saturation of the IMU, both systems remained in the prelaunch state throughout the flight. As a result, data collection was intermittently interrupted by dumping to the SD card. Furthermore, the GPS failed to get a lock given its placement deeper in the TERP than usual. Testing should be conducted to determine if the GPS can get a lock at the appropriate height.

Event and Success Criteria		
TADPOL remote power on	PARTIAL SUCCESS	December 17, 2023
TADPOL data collection	PARTIAL SUCCESS	December 17, 2023
TERP data collection	FAILURE	December 17, 2023
System Analysis	FAILURE	Dec 17, 2023

Karkonu Flight Test 2

Sunjun Mehta, Chief Engineer

February 3, 2024

Test Objectives:

1. Overall Karkonu Flight Test
 - a. Airbrake flight test
 - b. Payload integration to collect data (no drift control vehicle deployment)
 - c. Avionics board integration to collect data
2. Flight on an Aerotech M1939
3. Safe Recovery

Test Procedure:

1. Assemble Karkonu as per the assembly and launch procedures.
2. Verify 3 beeps on both EasyMinis and connection to the Featherweight GPS.
3. Insert igniter, clear the pad.
4. Post launch:
 - a. Turn off all recovery electronics
 - b. Check that the recovery system worked as intended, with no major tangles
 - c. Check that all four deployment charges were fired.
 - d. Check for damage

Test Results:

1. Safe recovery, no damage
2. The rocket was initially projected to fly to 9,600 ft. However, due to added weight from integrating other systems, the final weight was 5 lbs over the expected weights. Additionally, a large camera system was added to the airframe which contributed to a higher drag coefficient. A communication error prevented the team from resetting the parameters of the Airbrake. While the Airbrake computer worked as intended, flaps were not deployed because the rocket greatly underperformed.

Event and Success Criteria		
Stable Flight Test	SUCCESS	2/3/2024
Safe Recovery	SUCCESS	2/3/2024
Airbrake Deployment	FAILURE	2/3/2024

Payload, Avionics Data Collection	SUCCESS	2/3/2024
System Analysis	PARTIAL SUCCESS	2/3/2024

Test Images:



The images above show the camera system fixed to the outside of the rocket with the goal of capturing Airbrake footage. It transmitted live video and the antenna can be seen near the bottom of the left image. The camera itself is on the right image. The camera system, antenna, and battery were very securely fixed to the airframe using electrical tape, which contributed significantly to drag. However, the thorough taping job was desired to ensure the camera stayed connected to the rocket and did not separate, or even fall and hit a fin.

Terrapin Rocket Team



Karkonu lifts off the pad on an Aerotech M1939

Payload Data Collection 2

Michael Mallamaci, Cooper Brown, and Nathan Roy, Payload

Feb 3, 2024

Test Objectives:

Collect flight data from a competition-like flight profile using the TERP and TADPOL. In addition, fly the avionics camera system to record video from the nose cone (results not covered here) and run live kalman filtering on TERP data.

Test Procedure:

1. Load the TADPOL into the TERP
2. Power the TADPOL and avionics camera system on through an external switch
3. Launch the TADPOL and TERP
4. During the flight collect data from all sensors and share it over I2C
 - a. Collect IMU, barometer, light sensor, and gps
5. Separate the nose cone
6. Save data to an SD card

Test Results:

The TADPOL remote power-on circuit ran into issues that resulted in it failing to maintain power and the TERP teensy frying. As a result, the TADPOL was powered on using a wire switch that ran out through the nose cone vent holes. The TADPOL and TERP systems both collected data sets, with the TADPOL achieving a GPS lock. While the Kalman filter ran, it predicted a landing position of over 20,000 m, so more tuning is needed.

Event and Success Criteria		
TADPOL remote power on	FAILURE	Feb 3, 2024
TADPOL data collection	SUCCESS	Feb 3, 2024
TERP data collection	SUCCESS	Feb 3, 2024
TERP kalman filter	FAILURE	Feb 3, 2024
System Analysis	PARTIAL SUCCESS	Feb 3, 2024

Drift Control Test L1

Cooper Brown, Michael Mallamaci, and Nathan Roy, Payload
Feb 3, 2024

Test Objectives:

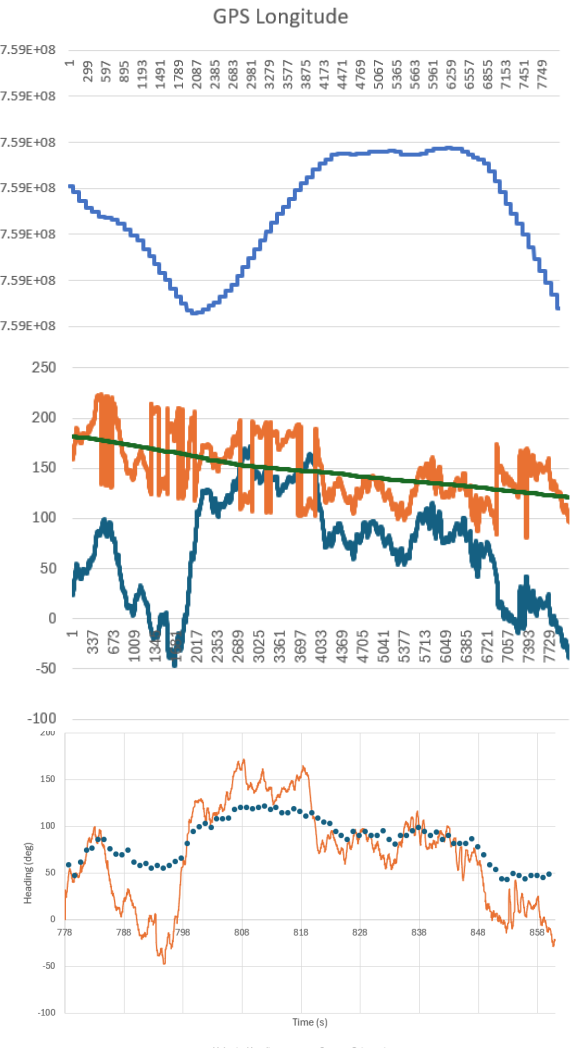
Evaluate drift control performance in navigating to a point using obstacle avoidance

Test Procedure:

1. Launch the L1
2. Record featherweight, easy mini, and srad avionics data (including drift control logic)
3. A few seconds after apogee, begin drift control using obstacle avoidance
4. Stop drift control after touchdown

Test Results:

The L1 successfully launched, deployed the chute, and landed. Due to an issue with the Featherweight app changing the transmitter frequency, featherweight GPS was lost halfway down. The vehicle did move in a manner suggesting some form of influence over motion, as seen in the latitude plot, and the video (see folder in the drive), where the rocket outpaces the smoke produced by the motor (assumed to be at wind speed). However, this control seems to be the result of the vehicle moving forward while subject to a few distinct yaw events. The second graph shows the yaw angle (blue), heading of attempted motion (orange), and goal direction with a 90° offset (green) (the reason for this offset is unknown). The servos change direction as yaw changes to keep the orange line close to the goal. However, as seen in the first plot, the system's movement is primarily influenced by yaw and the servo motors fail to have any noticeable effect. This is believed to be the result of a jam or slip in the lines. However, as seen in the 3rd plot, the system heading (blue, measured from GPS) generally lines up with the system orientation (orange, measured from magnetometer). This suggests that the parachute generally turned with the system as it rotated, demonstrating improved relative yaw damping.



Event and Success Criteria		
Record SRAD and COTS data	PARTIAL SUCCESS	Feb 3, 2024
Attempt to move to a valid landing point	PARTIAL SUCCESS	Feb 3, 2024
Move towards a valid landing point	FAILURE	Feb 3, 2024
System Analysis	FAILURE	Feb 3, 2024

SRAD Avionics Board 1st Flight

Joseph Hauerstein, Varun Unnithan, Avionics

Feb 3, 2024

Test Objectives:

Test the data recordance capability of the flight computer and test the sensors' ability to record accurate data

Test Procedure:

1. Assemble the Master Board to combine subcircuits into a working unit
2. Integrate the Master Board into rocket eBay
3. Launch the Karkonu rocket
4. Record sensor data from the BNO, BMP, as well as internals of the computer
5. Evaluate sensor data in post to assess accuracy

Test Results:

The computer successfully turned on and recorded data, however, only the IMU recorded reliable data, with the altimeter giving garbage values (-10 to 20 ft) for during the rocket's flight. The MAX-M10S subcircuit didn't connect over I2C properly.

Event and Success Criteria		
Computer turns on and operates normally	SUCCESS	Feb 3, 2024
SD Card records data properly	SUCCESS	Feb 3, 2024
Dynamic stage detection works properly	PARTIAL SUCCESS	Feb 3, 2024
BMP390 gives reliable data	FAILURE	Feb 3, 2024
MAX-M10S gives reliable data	FAILURE	Feb 3, 2024
BNO055 gives reliable data	SUCCESS	Feb 3, 2024
System Analysis	FAILURE	Feb 3, 2024

Airbrake Data Collection and Mechanical Update Test

Sophie Jack, Airbrake

February 3, 2024

Test Objectives:

The primary objectives of this flight were to validate the airbrake's tilt estimation, ensure state estimation is still working properly, and test the new flaps and hinges that were recently installed. The data will be compared against COTS and avionics data from the same flight.

Test Procedure:

1. Updated airbrake code with correct vehicle definitions and desired apogee to ensure flap deployment
2. Install new flaps and hinges on airbrake
3. Launch on Karkonu, save data to SD card

Test Results:

The airbrake flight computer worked properly, but the flaps did not deploy. The anticipated apogee without flap deployment was 9600 feet, so the airbrake desired apogee was set to 9000 feet. However, the rocket's actual apogee for this flight was 8100 feet, meaning the airbrake flaps did not need to deploy. The difference in apogee could have been from the rocket being heavier than expected or added drag from a camera mounted on the rocket.

Event and Success Criteria		
Flight computer and state estimation worked	SUCCESS	February 3, 2024
Flaps deployed	FAILURE	February 3, 2024
System Analysis	SUCCESS/FAILURE	DATE

Full Scale Static Fire

Andrew Bean, Solids
February 3rd, 2024

Test Objectives:

Static fire the full scale motor in competition configuration. Must record thrust and chamber pressure during firing. Must also include a video of the entire static fire duration.

Test Procedure:

1. Assemble forward closure with elbow/tee and pressure transducers. Use 3-4 wraps of teflon tape on all NPT connections and tighten with a wrench.
2. Pack pressure transducers starting with a liquid oil such as way oil and cap off with a grease such as super lube. There should be no air trapped in the system.
3. Place the test stand upright in a flat, open location and place stakes in the ground around the base of the test stand. Hook four ratchet straps from the top of the test stand and run them radially outward, hooking the other end of the straps to stakes in the ground about 5-10ft from the base of the stand
 - a. Verify safe distance for size of motor with RSO and standoff tables (https://www.tripoli.org/content.aspx?page_id=22&club_id=795696&module_id=520420)
4. Tighten ratchet straps and keep the stand upright
5. Place load cell on the base of the test stand concentrically with the motor casing brackets
6. Slide motor clamps onto motor casing and connect to the cross beams on the stand
7. Ensure the 90 degree fitting is directly on top of the load cell
8. Wire pressure transducer and load cell to the necessary amplifier and data acquisition devices
9. Feed igniter into the top end of the motor casing. Verify it is at the “top” (in this case closest to the ground) of the motor
10. Set up the necessary data acquisition software on laptop and get ready to begin data collection
11. Begin data collection and ignite motor
12. Record a video of the burn as a backup to find burn rate
13. The pressure transducer and the load cell will record the output force v time and pressure v time data

Test Results:

Event and Success Criteria		
Static fire without any CATO	SUCCESS	2/3/2024
Record Thrust Data	SUCCESS	2/3/2024
Record Pressure Data	SUCCESS	2/3/2024
Record Video	SUCCESS	2/3/2024
System Analysis	SUCCESS	2/3/2024

Test Images:



Torque Motor K Analysis

Ohm Sapa, Nathan Roy, Payload

Feb 24, 2024

Test Objectives:

This test measures the angular acceleration that results from a given pwm value passed to the torque motor on the drift control mechanism. These results are then analyzed to determine a value of k such that $\text{pwm} \cdot k = \text{angular acceleration}$.

Test Procedure:

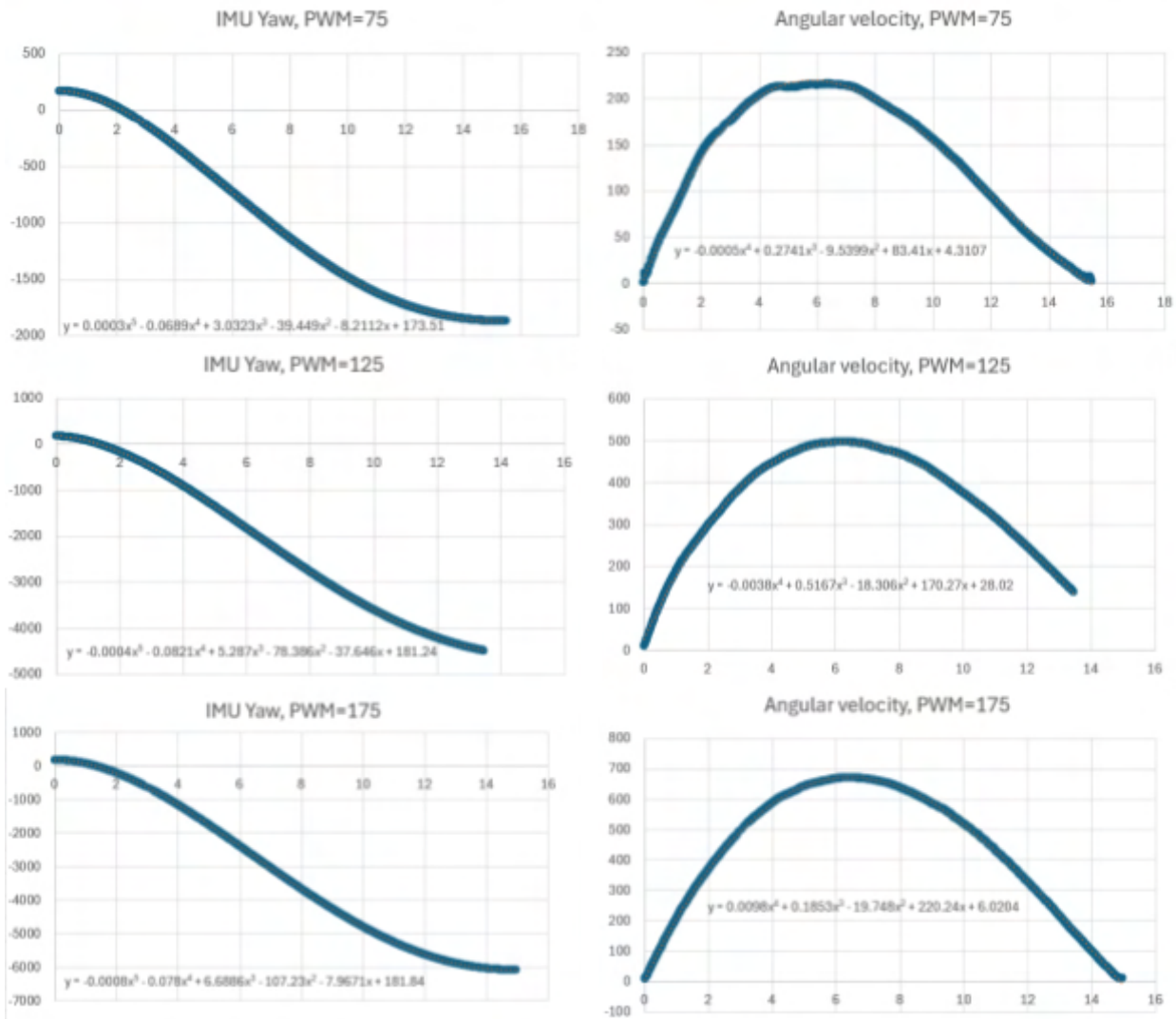
1. Run each of the following pwm profiles in turn:
 - a. Hold at 75
 - b. Hold at 125
 - c. Hold at 175
2. Record angular rates
3. Reset the system to 0 angle
4. Plot angular velocity vs time and extract k values

Test Results:

The plots used to calculate K can be found below. K varied from 1.1 to 1.4 over the pwm range tested, with the maximum value occurring at a PWM of 125. Given the system is expected to spend more time at lower PWM values (closer to zero error, smaller corrections), K was averaged to 1.2, suggesting a K_p of 15 and a K_d of 27. To increase the gain slightly, these values were increased to 17 and 30 respectively.

Event and Success Criteria		
Measure k	SUCCESS	Feb 24, 2024
System Analysis	SUCCESS	Feb 24, 2024

Test Images:



Vinyl Tube Ejection Ground Test

Sunjun Mehta, Chief Engineer

March 3, 2023

Test Objectives:

1. In order to conserve black powder and make it easier to teach the assembly of an ejection charge, the team switched to vinyl tube style charges in March. This involved using a 6 in section of $\frac{3}{8}$ " inner diameter vinyl tubing. The bottom of the tube was plugged with a half inch of hot glue and the appropriate amount of black powder was poured inside. An ematch was inserted to rest on the top of the black powder to ensure it burns completely. Dog barf insulation was stuffed inside to secure the ematch in place and the assembly was wrapped in electrical tape. Since these charges used less black powder than the glove fingers, these sizes were chosen through online calculators but knowing the forces desired on the bulkheads:
 - a. Main Primary: 4.5 g
 - b. Drogue Primary: 3.5 g

Test Procedure:

1. Assemble the rocket as if for launch, including connecting and folding shock cords, packing parachutes, and inserting shear pins. The ejection charges themselves would be routed through the electronics bay coupler and out through the holes in the switchband.
2. Set up the rocket parallel to the A-rack, and prop the rocket up near the Airbrake using a box.
3. Connect the ejection charge ematch leads to the launch system, Main on Pad 7 and Drogue on Pad 8.
4. The LCO then will ignite the charges.

Test Results:

1. The main separated but did not fully pull out the parachute, so the charge size was bumped up.
2. The same problem happened with the drogue, so this charge size was also increased.

Final Vinyl Charge Sizes:

- c. Main Primary: 5.5 g
- d. Main Backup: 6 g
- e. Drogue Primary: 5.5 g
- f. Drogue Backup: 6.5 g

Event and Success Criteria

Terrapin Rocket Team

Main Separation	PARTIAL SUCCESS	12/17/2023
Drogue Separation	PARTIAL SUCCESS	12/17/2023
Overall	PARTIAL SUCCESS	12/17/2023

Test Results:



Ejection Charge without any electrical tape



Main separation



Drogue separation

SRAD GPS and Sensor On-The-Ground Test

Varun Unnithan, Andrew Brandt, Avionics

March 17, 2024

Test Objectives:

Test the sensor's ability to record accurate data and the flight computer's persistent storage capabilities. Measure the accuracy of Kalman Filter controlled state variables, and have these be smooth and filtered. Measure the GPS' ability to track location.

Test Procedure:

1. Assemble the Unified Board with all sensors and components
2. Integrate Unified Board, Live Video Power Board (LVPD), and Raspberry Pi into rocket electronics bay
3. Turn on the Ground Station and confirm packets are being received
4. Move around locally on the ground
5. Monitor Ground Station for telemetry
6. Record sensor data from the BNO055, BMP390, and MAX-M10S
7. Artificially simulate launch conditions with on-the-ground equivalent thresholds
8. Evaluate sensor data in post to assess accuracy

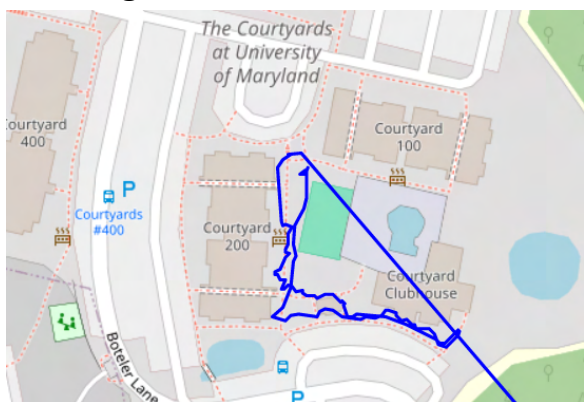
Test Results:

The flight computer turned on, and all systems reported nominal behavior. The board correctly identified launch via lowered conditions, and was able to actively transmit and report accurate data from the barometer and GPS. The Kalman Filter generated readings for velocity and other state variables, albeit with a little noise.

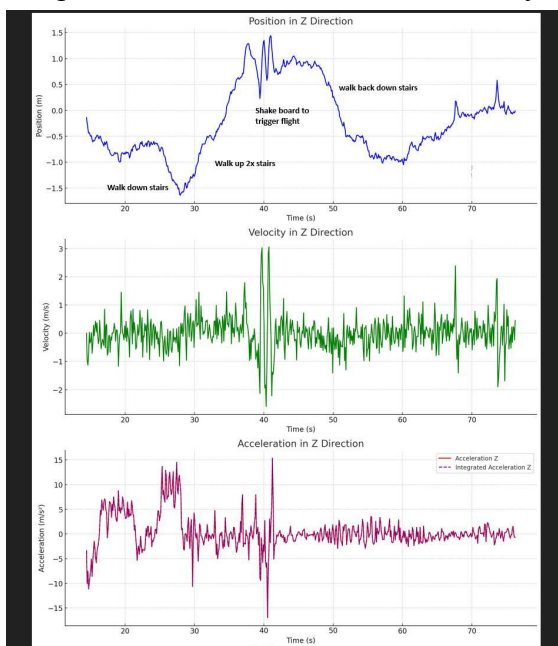
Event and Success Criteria		
Computer turns on and operates normally	SUCCESS	March 17, 2024
Onboard radios transmit	SUCCESS	March 17, 2024
Ground Station receives and decodes packets, properly displaying data	SUCCESS	March 17, 2024
BMP390 gives reliable data	SUCCESS	March 17, 2024
MAX-M10S (GPS) gives reliable data	SUCCESS	March 17, 2024

BNO055 gives reliable data	SUCCESS	March 17, 2024
Kalman Filter works properly	SUCCESS	March 17, 2024
Kalman Filter gives smoothed data	PARTIAL SUCCESS	March 17, 2024
SD Card storage system works	SUCCESS	March 17, 2024
System Analysis	SUCCESS	March 17, 2024

Test Images:



The above image shows the ground tracks as reported by the MAX-M10S GPS sensor the computer has. These tracks follow closely the route walked while testing.



The above plots show the Kalman Filter's reported data over the course of the simulated launch, which are accurate to the events that are expected, however, come with some added noise and slight inaccuracies.

Passive TADPOL Drop Test

Michael Mallamaci, Nathan Roy, Payload

March 30th, 2024

Test Objectives:

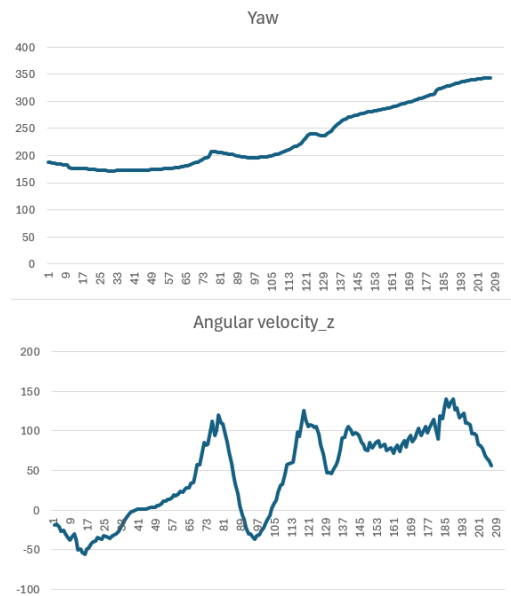
Compare the natural movement modes of the TADPOL system during a drop test to those measured through bench testing.

Test Procedure:

1. Record data for system heading and position during a drop with no motor input
2. Determine angular drag, noise, and speed values

Test Results:

The system demonstrated disturbances that significantly outweighed any drag forces. The vehicle speed is believed to be around 1.6m/s (calculated from acceleration values). While the calculated values approach 6m/s, this is believed to be due to acceleration measured while the system turned. As the system settled at 1.6 before the turn, this is assumed to be the maximum velocity.



Event and Success Criteria		
Determine angular drag value	SUCCESS	March 30th, 2024
Determine effect of disturbances	SUCCESS	March 30th, 2024
Determine vehicle speed	SUCCESS	March 30th, 2024
System Analysis	SUCCESS	March 30th, 2024

Torque Arm TADPOL Actuation Drop Test, $K_p = 0.17$, $K_d = 0.3$

Michael Mallamaci, Nathan Roy, Payload

March 30th, 2024

Test Objectives:

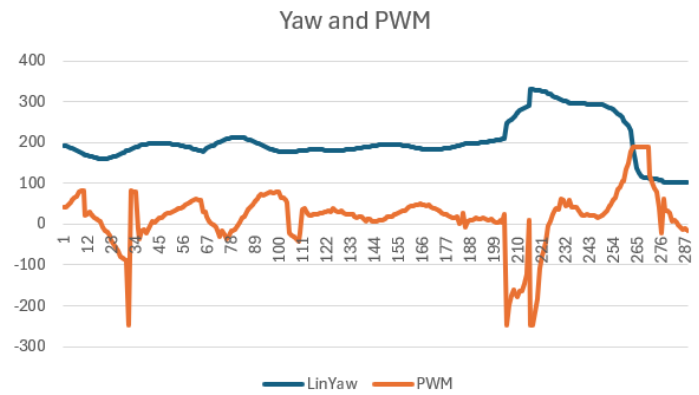
Determine the effectiveness of a PD controller in controlling vehicle heading

Test Procedure:

1. Drop the system with a k_p of 0.17 and a k_d of 0.3
2. Determine the steady-state error and settling time

Test Results:

The system succeeded in maintaining its heading for some of the drop (effectively no oscillations), but due to the low gain was unable to account for disturbances that forced the system off from its steady state. However, the maintained heading was 180 degrees offset from the desired. As other systems with higher gain values also demonstrated steady state offset issues, this may not be a gain issue but an issue regarding the K_p/K_d ratio, or a bug elsewhere. Further testing is necessary to determine the cause.



Event and Success Criteria		
Demonstrate low settling time	FAILURE	March 30th, 2024
Demonstrate low steady state error	FAILURE	March 30th, 2024
System Analysis	FAILURE	March 30th, 2024

Torque Arm TADPOL Actuation Drop Test, $K_p = 17$, $K_d = 30$

Michael Mallamaci, Nathan Roy, Payload

March 30th, 2024

Test Objectives:

Determine the effectiveness of a PD controller in controlling vehicle heading

Test Procedure:

3. Drop the system with a K_p of 17 and a K_d of 30
4. Determine the steady-state error and settling time

Test Results:

This system demonstrated larger oscillations at steady state, but was also unable to account for disturbances pushing it off from the desired heading. This system demonstrated a roughly 90° offset, although it drifted farther from this offset than the 0.17, 0.3 controller.

The K_d gain for this system is likely too high, as the system is primarily focused on stopping velocity even when the system is far away from the desired heading. However, the controller also struggled to overcome disturbances, even when running at full speed the motor was unable to quickly stop the system from rotating away from the desired heading. As a result, the maximum force the system can exert needs to be increased. This suggests that the oscillation issue may be the result of a delay in response time due to sensor filtering, as system inputs are arriving later than desired.



Event and Success Criteria		
Demonstrate low settling time	FAILURE	March 30th, 2024
Demonstrate low steady state error	FAILURE	March 30th, 2024
System Analysis	FAILURE	March 30th, 2024

Torque Arm TADPOL Actuation Drop Test, $K_p = 30$, $K_d = 30$

Michael Mallamaci, Nathan Roy, Payload

March 30th, 2024

Test Objectives:

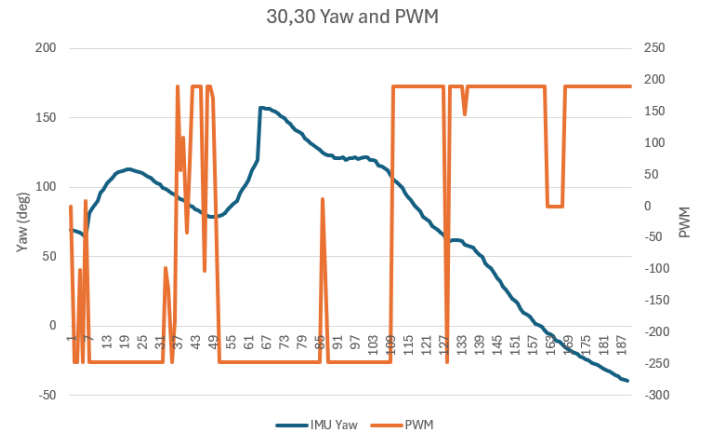
Determine the effectiveness of a PD controller in controlling vehicle heading

Test Procedure:

1. Drop the system with a k_p of 30 and a k_d of 3
2. Determine the steady-state error and settling time

Test Results:

This system demonstrated the same issues as the previous; primarily larger oscillations, an inability to account for disturbances, and a dominating k_d . Increasing the K_p/K_d ratio did not impact the oscillations, further suggesting the issue lies with response time. Further testing with a faster response time is required to determine if this is the case.



Event and Success Criteria		
Demonstrate low settling time	FAILURE	March 30th, 2024
Demonstrate low steady state error	FAILURE	March 30th, 2024
System Analysis	FAILURE	March 30th, 2024

SRAD Pressure Vessel Hydrostatic Testing

Andrew Bean, Solids

April 5th, 2024

Test Objectives:

Proof test competition motor casing to 1.5x MEOP (1500psi) for 2 minutes minimum.

Test Procedure:

1. Hook up all testing components
 - a. Hydraulic Pump
 - b. Long High Pressure Line
 - c. Pressure Gauge
 - d. Check valve (prevents backflow)
 - e. Bleed valve
 - f. Cross Fitting
2. Connect hose to female $\frac{1}{4}$ " NPT on one of the forward closures
3. Connect other end of hose to check valve on cross fitting
4. Fill casing and hose with water from open end of the casing
 - a. Make sure to move the casing around to allow as much air as possible to come out
 - b. Slightly open bleed valve to allow air to come out of casing/hose assembly
 - c. Once water begins to come out of bleed valve and casing/hose assembly is full of water, close bleed valve fully
5. Close open end of casing with second closure and snap ring
6. Make sure to set up casing away from any people. Around the corner of a building or with a blast shield in between.
7. Turn on the camera to watch both the pressure gauge and casing.
8. Begin pumping until pressure begins to rise.
 - a. Each pump afterwards should raise the pressure in the system. If it does not, the case might be yielding.
 - b. If this is happening at a not super high pressure, there are two possible options
 - i. Check for leaks at the connections. Make sure there are no leaks anywhere
 - ii. Some air is compressing in the system
 - iii. There is not enough pressure difference across the check valve for it to crack.
9. Pump incrementally up to 1.5x Max Expected Operating Pressure (MEOP) (1000 psi x 1.5)
10. Wait twice the expected motor burn time at 1.5x MEOP
11. Use bleed valve to relieve pressure slowly
12. Dump water and clean out any residual hydraulic oil. .

Test Results:

The casing passed hydrostatic test with no sign of failure or yielding.

Event and Success Criteria		
Reach 1.5x MEOP (1500psi)	SUCCESS	4/5/2024
Hold at proof pressure for at least 2x burn time	SUCCESS	4/5/2024
System Analysis	SUCCESS	4/5/2024

Test Images:



Casing Connected to Hydraulic Pump



Casing at Proof Pressure

Honu Flight Test 3

Sunjun Mehta, Chief Engineer

April 7, 2024

Test Objectives:

The primary objectives for this flight were to fly all of the new components manufactured this year for the first time. This would be the first flight of the new fin can, nose cone assembly, and the updated iteration of the electronics bay. It would be a low altitude flight test on an M1500 to 3000 ft in order to test the full vehicle with low accelerations. It was important to make sure that the fin can was built strongly, that the flight was stable, and that the parts did not come back with damage.

1. Test integrity of new systems described above
2. Safe Recovery
3. Airbrake Deployent
4. Payload Deployment
5. Avionics Data Collection and Live Video

Test Procedure:

1. This was a standard flight test, so it involved all assembly and range procedures, including assembly, connecting charges, final assembly, weight measurements, and loading onto the pad.
2. Due to the higher winds and location of trees and properties at the MDRA Sod Farm, the decision was made to fly drogueless to minimize some drift.

Test Results:

The ascent of the rocket performed nominally and flew mostly straight, though it did weathercock into the wind that had an average speed of 15 mph. Apogee deployment was nominal, but the halves of the rocket more violently tumbled over each other during the descent. At main deployment, the ejection and deployment was initially successful, but the tumbling caused the main parachute to become constricted and the rocket landed hard, damaging the Airbrake module, the electronics bay, and the payload. In addition, the nose cone was separated after it deployed at 1,500 ft and it landed separately.

Event and Success Criteria		
Stable Ascent	SUCCESS	April 7, 2024
Integrity of New Components	SUCCESS	April 7, 2024
Electronics Bay Functionality	SUCCESS	April 7, 2024

Airbrake Deployment	SUCCESS	April 7, 2024
Onboard Cameras - Capture Footage	FAILURE	April 7, 2024
Payload Deployment	SUCCESS	April 7, 2024
Avionics Data Collection	SUCCESS	April 7, 2024
Avionics Live Video	FAILURE	April 7, 2024
Safe Recovery	FAILURE	April 7, 2024
System Analysis	PARTIAL SUCCESS	April 7, 2024

Notes:

1. Due to the higher winds at the launch and the proximity of trees at the MDRA Sod Farm, many rockets had drifted into neighboring properties and trees that could not be accessed. Therefore, Honu did not fly with a drogue parachute, instead going drogueless. On descent, instead of being in a flat spin upon drogue descent, the halves of the rocket tumbled over each other. This was still occurring during main ejection, which was successful. However, at this moment, the fin can was higher in altitude relative to the main parachute and the drogue shock cord formed a loop a few feet above the unfurling main parachute. As the main expanded and the fin can continued to fall, the drogue shock cord collapsed the main parachute, and the rocket then hit the ground at a speed of at least 30 ft/s. The parachute situation can be seen in the images below.



2. Upon inspection of the landing site, it was found that two Airbrake flaps and hinge mechanisms had broken off, the electronics bay internal structure was damaged, and the payload structure was damaged.
 - a. The fin can was the first to touch down, and it landed in such a way that the bulkhead resting on top of the Airbrake coupler had been forced into the Airbrake tube, forcing the flaps to overextend outwards and snap a moment later when the Airbrake itself hit the ground. This caused damage to the coupler, flaps, hinges,

- actuation mechanism, and aluminum bulkheads. The 3D printed electronics sled was shattered, but most of the electronics remained intact, including the SD card.
- b. The electronics bay coupler and bulkheads themselves had no damage. However, the 3D printed structure that held the COTS and SRAD avionics in place were shattered. Some parts of the SRAD avionics were damaged and data could not be recovered from the broken SD card. The two Easy Mini deployment computers were damaged as the buzzer on one had broken and the screw terminals on both had been broken. The Featherweight GPS and the Blue Raven remained intact, though they will be replaced on future flights. During data collection, data was easily recovered from the Featherweight GPS and Blue Raven. For the Easy Minis, the boards themselves were intact, so the pads for the switch terminals were soldered over to form a connection, a battery was connected, and the board was plugged into a computer. Data was successfully collected from the Easy Minis.
 - c. The payload coupler landed on the top bulkhead first, which caused it to shear off. Some 3D printed parts were damaged but the payload was in overall good shape.
 - d. The fin can was also inspected and no damage was found. All fins were still in alignment, the recovery attachment points had not moved and were still strong, there were no cracks, and there was nothing shaking around inside the rocket.
3. Another issue during recovery was the deployment of the nose cone at 1,500 ft. This was controlled by an Easy Mini, which worked as intended. The charge was a 1.5 g black powder charge in a vinyl tube, which was an unnecessarily high amount of black powder. In addition, a knot was found at the breaking point in the payload shock cord, which can significantly reduce the strength of the cord. The excessively large charge and the knot combined likely led to the accidental separation of the nose cone. It landed about 20 yards away from the rest of the rocket. The images below show the nose cone snapping off after deployment and the knot in the broken shock cord.

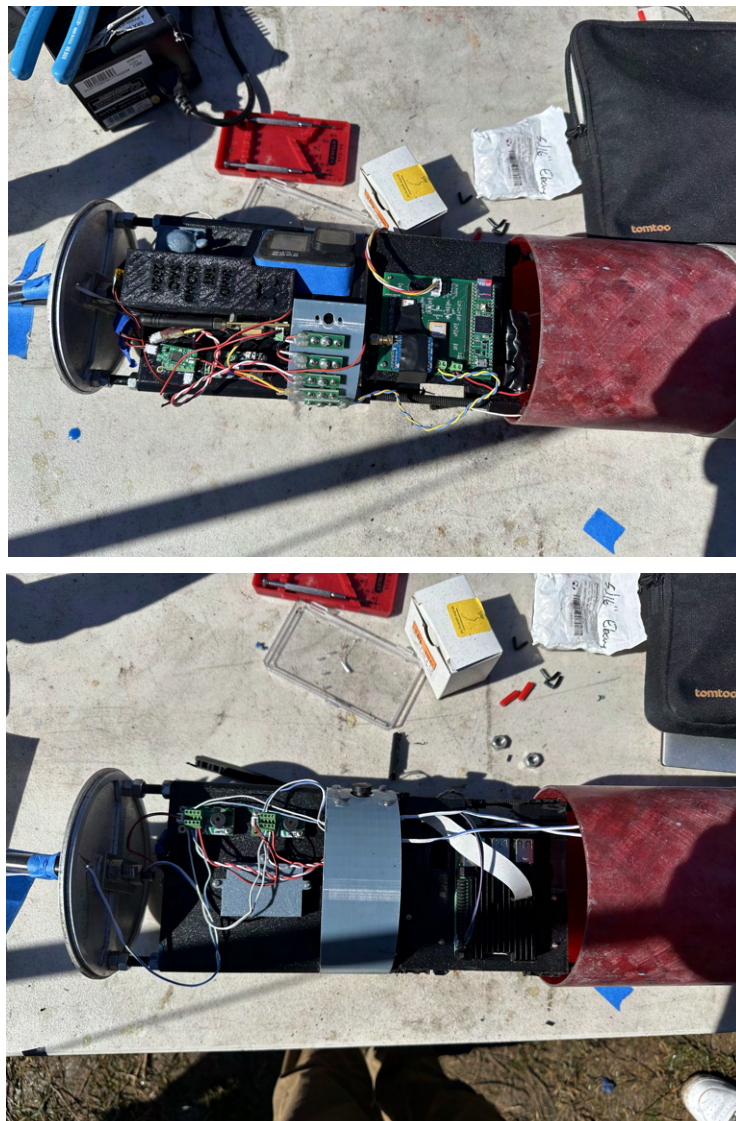


4. Two major improvements were noted for future flights. First, in addition to the standard assembly inspection, all shock cords and connections will be inspected for fraying or

Terrapin Rocket Team

knots or other issues prior to the assembly. Second, an alternative to the 24 in Recon Recovery drogue parachute will be determined. This would be used on windy days at the Sod Farm to reduce drift but ensure a nominal drogue descent to prevent lines from tangling the main parachute.

Electronics Bay Notes:



A new electronics bay was flown that contained SRAD Avionics, a GoPro, a Featherweight GPS tracker, a Blue Raven, and the two EasyMinis for deployment. It functioned well and was easy to assemble.

Airbrake Battery Test and Data Collection

Sophie Jack, Airbrake

April 7, 2024

Test Objectives:

The primary objectives of this flight were to test the new lithium ion batteries that replaced the lithium polymer batteries. Another goal was to have a new set of data to validate the tilt estimation in the air brake and post-processing code to validate commanded flap actuation angle.

Test Procedure:

1. Updated airbrake code with correct vehicle definitions and desired apogee to ensure flap deployment
2. Install new batteries on eBay
3. Turn on air brake on upright rocket on pad

Test Results:

The airbrake flight computer worked properly, and the flaps did deploy, meaning the battery transition was successful. However, video was not captured of them like expected. With an 865 meter target apogee, the rocket had an apogee of 915 meter. The apogee with no flap deployment was predicted to be about 975 meters.

Event and Success Criteria		
Flight computer and state estimation worked	SUCCESS	April 7, 2024
Battery transition was successful	SUCCESS	April 7, 2024
Flaps deployed	SUCCESS	April 7, 2024
Apogee was close to desired apogee	PARTIAL SUCCESS	April 7, 2024
System Analysis	SUCCESS/FAILURE	DATE

Payload Full Deploy Test

Michael Mallamaci, Payload

April 7, 2024

Test Objectives:

Collect data from both TERP and TADPOL. Release TADPOL and have it perform drift control.

Test Procedure:

1. Load TADPOL into TERP
2. Data collection begins at launch
3. TERP deploys TADPOL at 1,500 ft
4. TADPOL begins drift control 3 seconds after deployment

Test Results:

Due to a power draw issue with the nichrome cord cutter, the TADPOL flew without retention lines. Because of the snug fit between the top of the TERP frame and the nose cone, and the snug fit between the TADPOL and TERP shims, if the cord cutters fire too early, TADPOL is retained in the TERP by the nose cone wall, sticking out roughly 1 cm. As the spring system provides pressure against the wall, the TADPOL will stay in place throughout launch. Furthermore, as this is a low-altitude flight (apogee ~3,000 ft), the forces acting on the TADPOL were comparatively low, and so the retention lines were not needed.

Due to concerns over winds, the rocket flew drogue-less. As a result, TADPOL deployed but under relatively extreme dynamic conditions. While this did not impair TADPOL recovery, it induced a lateral spin that the drift control system was unable to overcome.

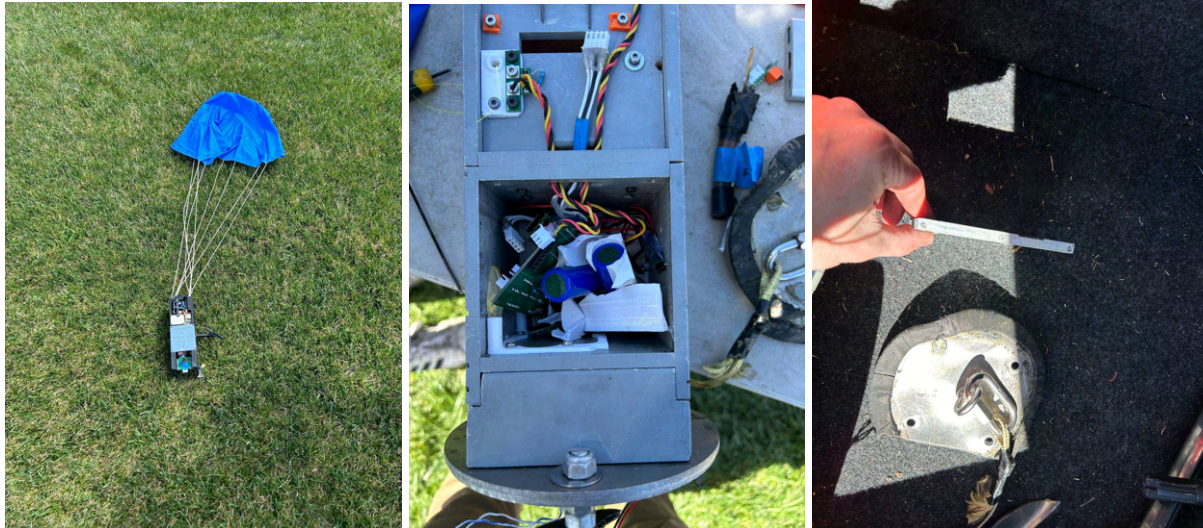
The Kalman filter on the TERP performed well, however due to a nan value from the GPS, the TADPOL Kalman filter was unable to provide accurate data.

The rocket's main parachute got tangled, resulting in a hard impact that damaged several structural components on the TERP. No TADPOL components were damaged.

Event and Success Criteria		
Record Terp Data	SUCCESS	April 7, 2024
Run Terp Kalman Filter	SUCCESS	April 7, 2024
Record TADPOL Data	SUCCESS	April 7, 2024
Run TADPOL Kalman Filter	FAILURE	April 7, 2024
Release TADPOL	SUCCESS	April 7, 2024

TADPOL Drift Control	FAILURE	April 7, 2024
System Analysis	Partial Success	April 7, 2024

Test Images:



SRAD Avionics Board Test Flight

Joseph Hauerstein, Varun Unnithan, Avionics

April 7, 2024

Test Objectives:

Test the sensor's ability to record accurate data and the flight computer's persistent storage capabilities. Measure the accuracy of Kalman Filter controlled state variables. Receive telemetry and display data on the Ground Station. Test local video recording using H264 hardware encoding on the Raspberry Pi.

Test Procedure:

1. Assemble the Unified Board with all sensors and components
2. Set up Live Video systems
3. Integrate Unified Board, Live Video Power Board (LVPD), and Raspberry Pi into rocket electronics bay
4. Turn on the Ground Station and confirm packets are being received
5. Launch the Honu rocket
6. Monitor Ground Station for telemetry
7. Record sensor data from the BNO055, BMP390, and MAX-M10S
8. Recover the rocket
9. Evaluate sensor data in post to assess accuracy

Test Results:

The flight computer turned on, and all systems reported nominal behavior, except for the Live Video subsystem. The buck converter that steps down the voltage for the Raspberry Pi had burned out onsite, and stopped working, meaning that the video recording system was inoperable. The Ground Station received transmissions throughout the launch, and displayed correct information, except for the stage detection, which was incorrect. However, the rocket didn't deploy its parachute correctly and was damaged on landing, breaking the SD card and making it impossible to retrieve the local data.

Event and Success Criteria		
Computer turns on and operates normally	SUCCESS	April 7, 2024
Live Video system turns on correctly	FAILURE	April 7, 2024
Live Video system properly	UNKNOWN	April 7, 2024

encodes and records video		
Onboard radios transmit packets	SUCCESS	April 7, 2024
Ground Station receives and decodes packets, properly displaying data	PARTIAL SUCCESS	April 7, 2024
BMP390 gives reliable data	SUCCESS	April 7, 2024
MAX-M10S gives reliable data	SUCCESS	April 7, 2024
BNO055 gives reliable data	SUCCESS	April 7, 2024
Kalman Filter works properly	UNKNOWN	April 7, 2024
SD Card storage system works	UNKNOWN	April 7, 2024
System Analysis	PARTIAL SUCCESS	April 7, 2024

Honu (SRAD Motor) Flight Test 4

Sunjun Mehta, Chief Engineer

April 21, 2024

Test Objectives:

1. Recover the rocket safely.
2. Fly the new airbrake module and verify its flight worthiness by assessing bending and fit.
3. Fly the rocket using the SRAD N2900 motor to be used at the Spaceport America Cup.
Compare motor data to the simulation data to better predict the motor's performance.
4. The payload would not deploy.
5. Avionics would attempt to transmit telemetry and live video.

Test Procedure:

1. Assemble Honu as usual, inspect the fit and tightness of the new Airbrake.
2. Assemble the solid rocket motor, including a pressure transducer with an Altus Metrum EasyMotor connected to the forward closure. This EasyMotor will have it's own battery and switch located in the fin can above the motor.

Test Results:

1. The rocket flew nominally and had a successful, normal recovery. It flew with a drogue and recovered without incident.
2. The Airbrake fit snugly and had 1 caliber of overlap on both sides of the module. It was stiff and did not produce noticeable bending or fractures during the flight.
3. The motor overperformed, flying to about 11,100 ft. Pressure and accelerometer data was recorded and a thrust curve was assembled, details of which can be found below.

Event and Success Criteria		
Safe Recovery	SUCCESS	4/21/2024
Maintain Tracking	PARTIAL SUCCESS	4/21/2024
Verify Flight Worthiness of Airbrake	SUCCESS	4/21/2024
Deploy Airbrake	FAILURE	4/21/2024
Assess SRAD Motor Performance	PARTIAL SUCCESS	4/21/2024
Telemetry and Live Video	FAILURE	4/21/2024

System Analysis	SUCCESS	4/21/2024
-----------------	---------	-----------

Test Images:



The above images depict Honu's launch and successful recovery.

Notes:

1. Attempts were made to develop another thrust curve to improve motor data using accelerometers in the EasyMotor during the flight test. Data was collected from $t=0$ until the acceleration went negative, indicating burnout.
 - a. Mass was estimated using simulation data from OpenRocket.
 - b. Drag was estimated using the second of flight directly after motor burnout.
 - $ma = -mg - D$, with a being the experimental accelerometer data from the EasyMotor. Therefore, $D = ma - mg$.

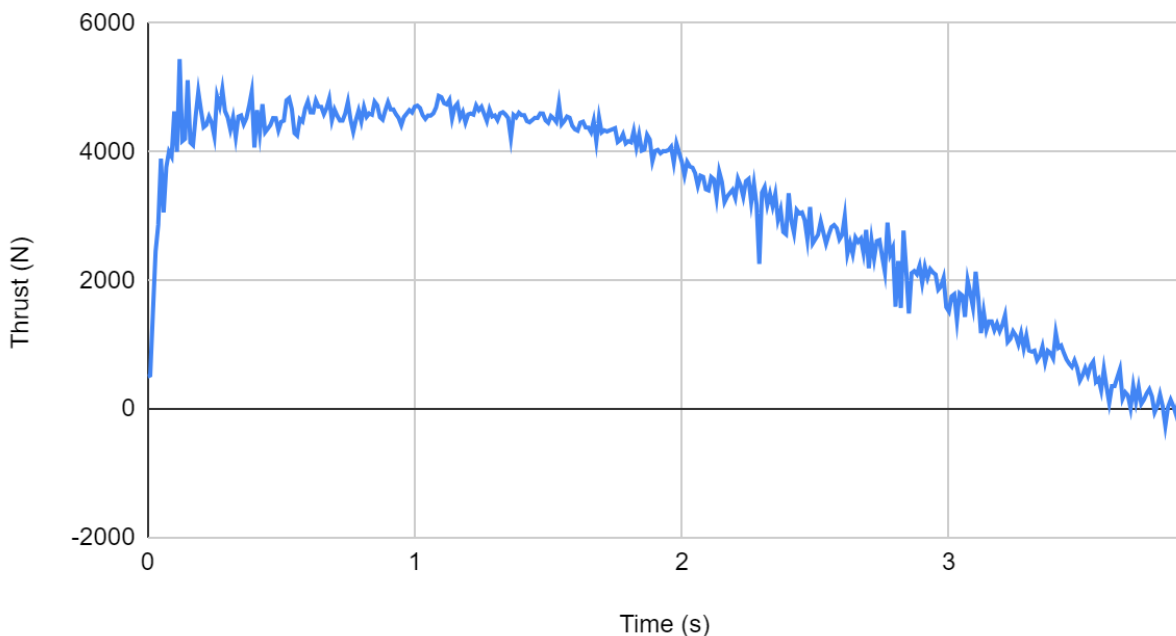
$$D = \frac{1}{2} \rho v^2 (Cd) A$$

$\rho = 1.247 \text{ kg/m}^3$ at the launch altitude, v came from the velocity provided by the EasyMotor

After solving for average CdA one second after burnout, a new equation was used to solve for thrust during the burn.

$$ma = T - mg - \frac{1}{2}\rho v^2(Cd)A$$

Thrust Curve for 4/21/24 Flight



Average Thrust: 3178 N

The higher average thrust was traced to two problems.

1. The throat area was slightly smaller due to slag buildup. This would increase pressure.
2. The pressure was also higher than expected after factoring the throat area.
 - a. Due to the higher temperatures at SAC, the motor pressure would likely increase further.

Solutions to the overall overperformance:

1. Better simulations of the motor and of the drag of the rocket
2. Added weight to bring down apogee based on simulation results

Honu Air Brake Flight Test

Sophie Jack
April 21, 2024

Test Objectives:

1. Rebuild air brake after damage on 4/7/24.
2. Successfully deploy flaps in-flight.
3. Achieve an apogee within 5% of desired apogee

Test Procedure:

1. Remake air brake frame and fully assemble
2. Upload relevant rocket parameters
3. Turn air brake on on launch pad

Test Results:

1. The air brake deployed, but not exactly how it was commanded to deploy
2. The air brake did not achieve an apogee within 5% of desired apogee

Event and Success Criteria		
Rebuild Air Brake	SUCCESS	4/20/2024
Successfully Deploy Flaps	SUCCESS	4/20/2024
Achieve Apogee within 5% of Desired Apogee	FAILURE	4/20/2024
System Analysis	SUCCESS	4/20/2024

Payload Data Collection 3

Michael Mallamaci and Nathan Roy, Payload

April 21, 2024

Test Objectives:

Collect flight data from a competition-like flight profile using the TERP and TADPOL. In addition, fly the avionics camera system to record video from the nose cone (results not covered here) and run live kalman filtering on TERP data.

Test Procedure:

1. Load the TADPOL into the TERP
2. Power the TADPOL and avionics camera system on through an external switch
3. Launch the TADPOL and TERP
4. During the flight collect data from all sensors and share it over I2C
 - a. Collect IMU, barometer, light sensor, and gps
5. Separate the nose cone
6. Save data to an SD card

Test Results:

Due to damage sustained during the previous flight, the sealing bulkhead had not been replaced, and so the nose cone did not separate and the TADPOL remained in the rocket for the entire flight. The TADPOL and live video power triggers worked as expected and all systems recorded data (including GPS for TADPOL). The kalman filter also worked as expected on both systems.

Event and Success Criteria		
Power on all systems without issue	SUCCESS	April 21, 2024
Data Collection	SUCCESS	April 21, 2024
Kalman filter	SUCCESS	April 21, 2024
System Analysis	SUCCESS	April 21, 2024

Competition Motor Test Flight

Andrew Bean, Solids

April 21st, 2024

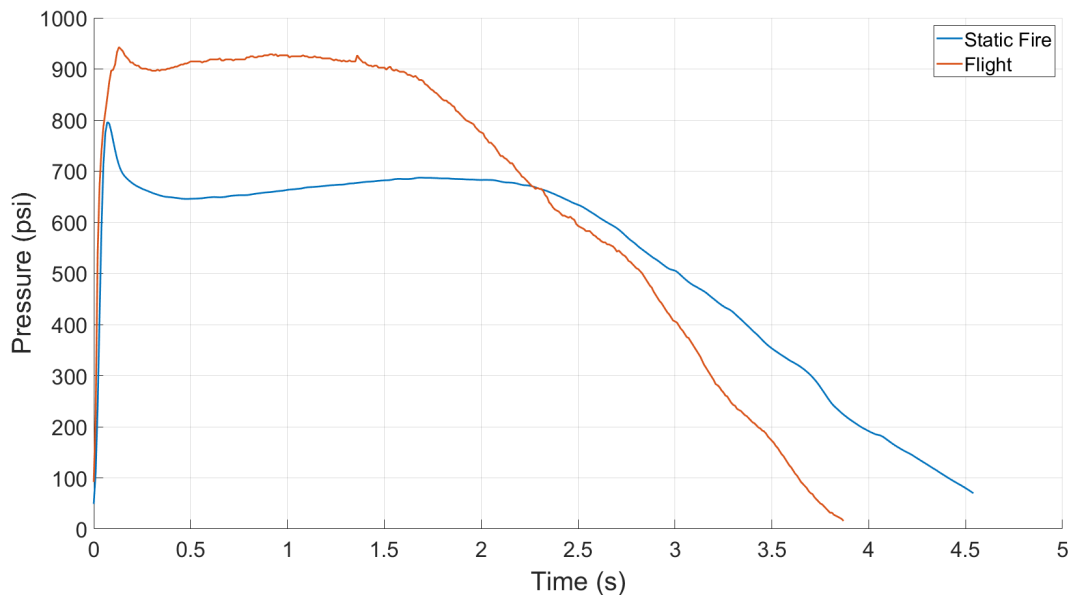
Test Objectives:

Fly the competition motor in Honu and record pressure data during flight.

Test Procedure:

1. Screw in Pressure transducer to forward closure
2. Pack pressure transducer with oil and grease to protect from high temperature
3. Tape EasyMotor and battery to pressure transducer and verify pressure transducer lines are wired correctly
4. Power on EasyMotor before liftoff
5. After recovery, power off EasyMotor and download data

Test Results:



Event and Success Criteria		
Motor does not CATO	SUCCESS	4/21/2024
Pressure is recorded in flight	PARTIAL SUCCESS	4/21/2024
System Analysis	SUCCESS	4/21/2024

Results:

The EasyMotor successfully recorded pressure data in flight, however the pressure was higher than expected. This is likely due to the slag that had accumulated on the nozzle during the static test. The smaller nozzle throat caused the motor to burn at a higher pressure than normal. This is not very significant as the total impulse will stay close to the value obtained during the static test.

Battery Drain Test

Sunjun Mehta, Chief Engineer

April 29, 2024

Test Objectives:

1. Determine the battery life of the two deployment Altus Metrum EasyMinis and the Featherweight GPS.

Test Procedure:

1. Assemble the electronics bay, with the appropriate batteries connected to the flight computers.
2. Turn on EasyMini (850 mAh), connect to the Featherweight GPS (400 mAh) on a phone.
3. Set the electronics bay under a heat lamp to simulate the temperatures at Spaceport.
 - a. Outer tube temperature: 120°F
 - b. Electronics Temperature = Inside Tube = 90°F
4. Let the batteries drain, record how long they last, and periodically monitor voltage.

Test Results:

Time	Tracker Voltage (V)	EasyMini Voltage (V)
0 (9:45 AM)	4.20	4.20
2:13:32 (11:58 AM)	3.83	4.12
2:57:30 (12:42 PM)	3.74	4.11
5:15:00 (3 PM)	3.58	4.09
6:15:00 (4 PM)	3.54	4.09

Event and Success Criteria		
EasyMini - Battery Drain	SUCCESS	4/29/2024
FW GPS- Battery Drain	SUCCESS	4/29/2024
System Analysis	SUCCESS	4/29/2024

Notes:

1. The initial plan was to record voltage data directly from the EasyMini and the tracker. However, they only recorded data between launch and landing detections, so this was ruled out for the simple bench test. The plan pivoted to using multimeters and recording the displayed voltages over time, but the multimeters displays shut off automatically after 15 minutes. There were no settings on the multimeters to turn off this feature. Therefore, a Zoom meeting was set up which would monitor the tracker LED light that flashed and the sound from the EasyMini. The meeting was recorded in case a computer shut off or an anomaly occurred for future review or while the test was running and the student was in class. Periodically between classes, the voltages were checked and recorded.
2. The test ended after 6 hours and 15 minutes because the electronics were needed for safety reviews. The EasyMini would have lasted much longer, and from past experiences of tracker life, the Featherweight GPS was almost on its last legs.
3. The main priority was ensuring the tracker functioned well with its battery under hot conditions. The expected run time was 4.5 hours from the user manual, but the tracker performed well in this scenario. To mitigate battery drain at Spaceport, an external switch harness was connected in between the battery and the tracker so that it could be turned on at the pad instead of during assembly. This saves precious hours of battery life, and mitigates the concern over tracker lifespan.

VII. Appendix C: Hazard Analysis
(As found on the following page)

Hazard Analysis						
Hazardous Material	Storage	Handling	Transportation	Risk of Mishap	Mitigation (Process/Design)	Risk of Injury after Mitigation
Black Powder	Stored in a dry cabinet away from any flammable substances	When used, avoid any heat and ignition sources. Use Black Powder vials to measure and load. Do not touch directly. Wear safety glasses.	Kept in original packaging until used.	Low	Restricted access to individuals who are experienced and familiar with the material and handling procedures.	Very Low
Fuel Grains	Ensure fuel grains remain in plastic bags. Keep stored in a flame locker.	Keep fuel grains in sealed plastic bags until ready to be loaded into casing. Loading should only be done by certified individuals. Once in the casing, the motor is handled carefully to prevent fracturing the grains or nozzle.	Keep in original packaging out of the sun and somewhere cool and dry.	Low	Only individuals whom hold certifications for given rocket motor (or are in the process of obtaining) are authorized to handle fuel grains.	Very Low
Lipo Batteries	Keep in cool dry places. Ensure in a flame retardant battery case. Stored at "storage voltage".	LiPo batteries should be stored in safe places until ready for use. Avoid sharp objects and high temperature areas.	Batteries should only be transported in the authorized LiPo battery transportation bags per safety instructions.	Low	Ensure battery charging is done correctly with multi-cell battery charger. Charging only prior to launch/test events. Inspect batteries before/after use for punctures or any other signs of damage.	Very Low
E-Matches Igniters	Stored in a dry flame locker. Keep away from any ignition sources or energetics.	Careful when handling to ensure circuitry doesn't prematurely activate. Leads are twisted or shunted when not connected to flight computer.	Transport in a separate container from energetics and ignition sources.	Low	Circuit switches will be switched off and flight computers will only be powered on once the vehicle is on the pad ready for the flight to prevent premature ignition.	Very Low

VIII. Appendix D: Risk Assessment

(As found on the following page)

Risk Assessment					
Risk	Possible Causes	Risk of Mishap and Rationale	Mitigation Approach	Risk After Mitigation	Overseeing Division
Explosion of solid-propellant rocket motor during launch with blast or flying debris causing injury	Cracks in propellant grains, incorrect assembly of motor	Low	Grains will be inspected before assembly and the motor will be assembled only by those certified following the proper procedure.	Low	Propulsion
Rocket deviates from nominal flight path, comes in contact with personnel at high speed	Rocket has low rail exit velocity, is unstable, or fins have broken off	Low	Simulate rocket in Open Rocket to calculate stability caliber, calculate fin flutter for expected speeds. Rocket has been test flown multiple times to verify simulation results.	Low	Aerostructures
Recovery system fails to deploy, rocket or payload comes in contact with personnel	Flight computers fail to fire charges, charges are undersized	Low	Redundant independent flight computers, batteries, and charges. Ground and flight testing of ejection and separation systems.	Low	Recovery
Recovery system partially deploys, rocket or payload comes in contact with personnel	Parachutes become tangled, main does not deploy	Medium	Parachutes carefully packed to ensure clean exit from body tube and easy inflation. Test flights to check for correct packing of recovery system and charge sizing.	Low	Recovery
Recovery system deploys during assembly or prelaunch, causing injury	Flight computers are turned on while loading and packing the rocket. E-matches are accidentally shorted	Low	Flight computers are powered off while connected to igniters and charges. Computers are only powered on once on the pad and ready for launch. Igniters are twisted or shunted until connected to flight computers. Personnel handling energetics are minimized and wearing proper safety equipment	Low	Recovery
Main parachute deploys at or near apogee, rocket or payload drifts to highway(s)	Incorrect wiring to flight computers, heavy nosecone separates due to drogue ejection forces	Medium	Flight computer connections are checked by multiple team members to verify correctness. Long drogue lines and extra shear pins in nosecone are in place to prevent early separation	Low	Recovery
Rocket ignites prematurely while on launch pad.	Igniter ignites unexpectedly when connected to launch system. Igniter is installed prematurely into motor.	Low	Igniter leads are shunted until connected to launch system. Igniter is only installed in motor once rocket is vertical, recovery computers have been turned on, and non-essential personnel have cleared the area. Launch control system is verified to be off and alligator clips are touched together to check for sparking. Personnel move away from rocket while checking for continuity.	Low	Propulsion
Rocket does not ignite when command is given ("hang fire"), but does ignite when team approaches to troubleshoot	Igniter incorrectly inserted, not following proper procedure	Low	Make sure igniter is inserted all the way into the motor. Tape dowel to launch tower to prevent it from falling out. Adequate time is given before approaching rocket.	Low	Propulsion
Rocket falls from launch rail during prelaunch preparations, causing injury	Rail buttons fall off	Low, Rail buttons tightly secured	Rail buttons are tightened into nuts in airframe. Rocket is raised by the rail buttons to make sure they are on properly before flight. Rocket is test flown to show rail button rigidity.	Low	Aerostructures
Power loss	Batteries not charged, wired disconnected during flight, flight causes a switch to flip	Low	Batteries are charged/replaced prior to flight. Only switches used are those that will not turn off during flight	Low	Recovery
Fail to deploy at decoupling event altitude	Power loss due to severed wires or flipped switch. Insufficient ejection force to break shear pins. Bad e-match.	Medium	Redundant independent flight computers, batteries, and switches. Ground testing of ejection and separation. Switches used cannot be turned off by flight forces. E-matches are checked with multimeter to check continuity before connecting to computers.	Low	Recovery

IX. Appendix E: Assembly, Preflight, Launch, Recovery, and Off-Nominal Checklists
(As found on the following page)

Assembly, Preflight, Launch, Recovery, and Off-Nominal Checklists

Honu			June 2024
Step	Division	Task	Completed?
ASSEMBLE MAIN RECOVERY SECTION			
1.0 Recovery		Fold main tightly and burrito wrap in nomex blanket	<input type="checkbox"/>
1.1 Recovery		Verify nose cone is connected to second loop from the top and the main parachute to the top loop	<input type="checkbox"/>
1.2 Recovery		Verify all quick links are connected to shock cords and tightened fully	<input type="checkbox"/>
1.3 Recovery		Insert packed main parachute into recovery airframe	<input type="checkbox"/>
1.4 Recovery		Carefully z fold shock cord with blue tape and insert behind main parachute	<input type="checkbox"/>
1.5 Recovery		Slide nosecone into main airframe and align marks for shear pins (make sure payload is ready first)	<input type="checkbox"/>
1.6 Recovery		Stand section vertically and insert 6 4-40 shear pins into nosecone	<input type="checkbox"/>
ASSEMBLE PAYLOAD SECTION			
2 Payload		Bolt the payload to the middle bulkhead, aligning the black stripe	<input type="checkbox"/>
2.1 Payload		Run the payload switch wire through the middle bulkhead and seal the hole with tape	<input type="checkbox"/>
2.2 Payload		Run a 1.5 g black powder charge through the top and middle bulkheads, and seal the top hole with electrical tape	<input type="checkbox"/>
2.3 Payload		Place the payload in the coupler, aligning the release hole with the cutout	<input type="checkbox"/>
2.4 Payload		Connect the payload switch, easy mini switch, and black powder charge to their respective points on the nose cone sled	<input type="checkbox"/>
2.5 Payload		Load the nose cone sled into the coupler	<input type="checkbox"/>
2.6 Payload		Bolt the sled down	<input type="checkbox"/>
2.7 Payload		Bolt the bottom bulkhead to the coupler (ensure the bulkheads sit flush against the inner coupler)	<input type="checkbox"/>
2.8 Payload		Bolt the payload to the upper bulkhead (use nuts as spacers)	<input type="checkbox"/>
2.9 Payload		Connect the shock cord from the nose cone tip to the eye bolt on the top bulkhead	<input type="checkbox"/>
2.1 Payload		Turn on the vehicle Featherweight GPS and verify connection to groundstation	<input type="checkbox"/>
2.11 Payload		Turn on the vehicle	<input type="checkbox"/>
2.12 Paylaod		Connect the nose cone to the coupler with 2 shear pins, ensuring the top bulkhead seals correctly	<input type="checkbox"/>
ASSEMBLE DROGUE RECOVERY SECTION			
3 Recovery		Fold drogue tightly and burrito wrap in nomex blanket	<input type="checkbox"/>
3.1 Recovery		Verify all knots and quick links are tightened	<input type="checkbox"/>
3.2 Recovery		Assemble air brake module (see section 6)	<input type="checkbox"/>
3.3 Recovery		Feed Y harness lines through airbrake module	<input type="checkbox"/>
3.4 Recovery		Connect Y harness to drogue harness and slide drogue tube onto airbrake	<input type="checkbox"/>
3.5 Recovery		Secure airbrake module using 2 1/4"-20 screws on each foward and aft ends	<input type="checkbox"/>
3.6 Recovery		Carefully z fold shock cord lines with painters tape	<input type="checkbox"/>
3.7 Recovery		Push drogue harness and folded drogue parachute into airframe. Push it all the way in.	<input type="checkbox"/>

ASSEMBLE AVIONICS BAY		<input type="checkbox"/>
4.0 Recovery	Make sure main power switches are turned off and batteries are disconnected	<input type="checkbox"/>
4.1 Recovery	Locate four 3ft ematches and verify continuity with multimeter. Twist leads to shunt	<input type="checkbox"/>
4.2 Recovery	Pack charges using 4F black powder to the following amounts: main 5.5 g / 6.5 g, drogue 5.5 g / 6 g	<input type="checkbox"/>
4.3 Recovery	feed charges through bulkheads and secure into proper terminals	<input type="checkbox"/>
4.4 Recovery	Lightly tug each wire to make sure it is secure in the screw terminal	<input type="checkbox"/>
4.5 Recovery	Use electrical tape to seal wire holes on both bulkheads	<input type="checkbox"/>
4.6 Recovery	Plug in batteries	<input type="checkbox"/>
4.7	Plug in batteries for GPS units. Turn on switch if necessary. Verify lock and telemetry	<input type="checkbox"/>
4.8 Avionics	Press the small button near the usb port on the SRAD TTGO radio transmitter and release - light should turn on	<input type="checkbox"/>
4.9 Recovery	Slide aft bulkhead onto threaded rods and align sled with screw switch holes	<input type="checkbox"/>
4.10 Recovery	On each threaded rod add a washer and two 5/16" nuts. Tighten each with a wrench.	<input type="checkbox"/>
4.11 Recovery	Verify quick links have been connected to U-bolts and tightened	<input type="checkbox"/>
4.12 Recovery	Align electronics bay with marks on main recovery airframe. Secure with two 1/4" 20 screws	<input type="checkbox"/>
4.13 Recovery	Align electronics bay on booster section, stand rocket vertically	<input type="checkbox"/>
4.14 Recovery	Insert four 4-40 shear pins into booster - electronics bay connection. Wrap completely with tape	<input type="checkbox"/>

ASSEMBLE MOTOR SECTION		
5.0 Propulsion	Glue grains to liner at least 24 hrs before launch	<input type="checkbox"/>
	Run nail along snap rings to find any burrs. Use sandpaper to remove and sharp edges. Clean snap ring grooves and o ring grooves of any debris.	<input type="checkbox"/>
5.1 Propulsion	Verify both the forward closure and nozzle each have two greased orings	<input type="checkbox"/>
	Stand liner on top of nozzle and grease thouroughly. Slide casing over liner.	<input type="checkbox"/>
	Insert forward closure and nozzle washer. Insert snap rings and verify that they are fully seated.	<input type="checkbox"/>
5.2 Propulsion	Insert motor into motor tube and secure with aeropack retainer	<input type="checkbox"/>
5.3 Propulsion	Tape igniter to thin dowel rod. Tape multiple dowels together if necessary.	<input type="checkbox"/>
5.4 Propulsion	Do not insert igniter until on pad and electronics have been turned on	<input type="checkbox"/>
Assemble Air Brake Module		
6.0 Air Brake	Charge Batteries	<input type="checkbox"/>
6.1 Air Brake	Install air brake electronics bay into module	<input type="checkbox"/>
6.2 Air Brake	Flash ardiuno test code and test configuration	<input type="checkbox"/>
6.3 Air Brake	Turn off arduino	<input type="checkbox"/>
6.4 Air Brake	Turn linear screw until flaps are fully retracted	<input type="checkbox"/>
6.5 Air Brake	Install linear screw guard	<input type="checkbox"/>
PREFLIGHT CHECKLIST		
Nominal Procedure		
7.0 N/A	Carry rocket out to launch pad	<input type="checkbox"/>
7.1 N/A	Install rocket on rail	<input type="checkbox"/>
7.2 Avionics	Turn on nose cone non-deployment electronics	<input type="checkbox"/>
7.3 N/A	Lift launch rail vertically	<input type="checkbox"/>
7.4 Air Brake	Turn on Airbrake flight computer	<input type="checkbox"/>
7.5 Avionics	Turn on nose cone easy mini via wifi switch	<input type="checkbox"/>
7.6 Avionics	Turn on SRAD avionics	<input type="checkbox"/>
7.7 Avionics	Turn on Featherweight Blue Raven and Featherweight GPS, verify connecti	<input type="checkbox"/>
7.8 Avionics	Turn on Primary EasyMini switch and verify continuity on both charges	<input type="checkbox"/>
7.9 Avionics	Turn on Backup EasyMini and verify continuity on both charges	<input type="checkbox"/>
7.10 Avionics	Verify GPS systems are still transmitting	<input type="checkbox"/>
7.11 N/A	Clear area of personnel and insert motor igniter. Tape to Launch rail.	<input type="checkbox"/>
Off-nominal Procedure		
7.0A Safety Officer	Remove igniter	<input type="checkbox"/>
	Turn off recovery electronics followed by cameras, airbrakes, SRAD	<input type="checkbox"/>
7.1A Safety Officer	avionics, and payload.	<input type="checkbox"/>
N/A	Remove rocket from rail	<input type="checkbox"/>
LAUNCH CHECKLIST		
Nominal Procedure		
8.0 Propulsion	Ignite motor	<input type="checkbox"/>
8.1 All	Track rocket visually and via telemetry	<input type="checkbox"/>
Off-nominal Procedure		
8.0A All	Take cover until given all clear to approach rocket or rocket wreckage	<input type="checkbox"/>

8.1A Safety Officer Turn off flight computers if necessary	<input type="checkbox"/>
8.0A Safety Officer Disconnect charges from flight computers	<input type="checkbox"/>
8.1A Safety Officer Remove any LiPo batteries that may be damaged	<input checked="" type="checkbox"/>

RECOVERY CHECKLIST

9.0 Avionics	Turn off flight computers, payload, airbrake, and avionics	<input type="checkbox"/>
9.1 Avionics	Turn off cameras	<input type="checkbox"/>
9.2 Avionics	Verify all charge have fired. If not cut wires and remove powder from charge	<input type="checkbox"/>
9.3 Avionics	Turn off both GPS units after opening electronics bay	<input type="checkbox"/>
9.4 All	Verify all sections of the rocket have been accounted for	<input type="checkbox"/>

Full Motor Procedure: Mix to Firing

Pouring the Motor:

1. Weigh all mixing bowls and record weight on mix sheet
2. Measure out liquids directly into mixing bowl **Wear Gloves**
 - a. R45M, HTPB (Rubber, Fuel/Binder)
 - b. Diethyl Adipate, DOA (Plasticizer)
 - c. Castor Oil (Cross-Linker, Binder)
 - d. Tepanol, HX-878 (Binding-Agent)
 - e. Add two liquids **not on the Propellant Formula Spreadsheet**
 - i. Silicone oil 2 drops per 500g
 - ii. Triton X 4 drops per 500g
3. Mix all liquid components in stand mixer until thoroughly incorporated and homogenous milky yellow mixture (about 20 to 30 minutes)
 - a. Make sure the Tepanol has fully incorporated. You may need to use a popsicle stick to pull it off the bottom of the beater.
4. Remove from stand mixer
5. Vacuum the liquids in the mixing bowl until the majority of the bubbles have stopped.
6. Return the mixing bowl to the stand mixer
7. Measure metals individually, in separate bowls. Add to the liquid mixture one at a time in the following order with the mixer off (follow the order on the mix sheet):
 - a. Magnesium -325 mesh atomized (Metal Fuel)
 - b. Strontium Nitrate (Oxidizer)
 - i. If it is old, you will have to force it through a sieve. Large chunks that don't make it through can be broken up with a mortar and pestle.
 - c. Oxamide (Burn Rate Suppressant)
 - d. Copper Oxide (Accelerates Burn Rate)
8. Mix until incorporated completely (5-10 minutes) each, repeat for each metal leaving out the Ammonium Perchlorate
 - a. DO NOT mix dry solids. Make sure each solid is completely incorporated before adding the next one.
9. Let mix for about 15 min after last metal added
10. Vacuum for another 10 minutes and bubbles have mostly stopped.
11. Add Ammonium Perchlorate (Oxidizer) **RESPIRATOR OR MASK REQUIRED WHILE HANDLING Ammonium Perchlorate**
12. Let everything mix for 2 hours
 - a. Cut casting tubes
 - b. Prepare mandrels (wrap loosely with cellophane, wrap again with fiber-reinforced tape). The mandrel should still be able to slide
 - c. Screw mandrel into base and hose clamp casting tube on.
 - d. Make sure that all surfaces other than the casting tube that contacts propellant have cellophane on them
13. After 2 hours pull vacuum the mix again
 - a. When it begins to bubble up, twist the bowl and shake it and tilt it all around to prevent it from bubbling into the valve

- b. Keep pulling the vacuum for about 15 minutes
14. Take the bowl off the mixer and scrape as much propellant as possible off the paddle.
 Cover bowl with plastic wrap and let sit overnight to allow Tepanol to react.
- a. If a vacuum lid is available, the bowl can also be kept under vacuum over night.
15. The next day, put the bowl back on the mixer and start to mix again.
- a. This incorporates and components that may have settled out
 - b. This also warms up the propellant and makes it easier to mix
16. Add curative (**measure 10 grams over the total amount as curative will stick to the side of the cup**)
- a. MDI (Curative)
17. Return the mixing bowl to the stand mixer
18. Every 5 minutes **TURN OFF THE MIXER** and scrape the sides of the bowl and paddle to recombine the mixture, repeat 3 times
19. Scrape everything off of the paddle into the mixing bowl
20. Cast the motor
- a. Wear Gloves
 - b. Grab a ball of the mixture, press into a long oval shape in your hand
 - c. **Evenly** wrap the mixture around the mandrel
 - d. Let the mixture slip down into the casting tube
 - e. Press down, inside the casting tube, with a dowel (long pole) that fits between the mandrel and the casting tube until even, trying to work all of the voids out
 - f. Repeat a-e until your mixture fills the casting tube
 - g. To create a motor with a flat top, once the mixture has reached the top overfill it slightly and press down using the flat side of a ruler around the casting tube
 - h. **Check that mandrel is centered** with measurements or jig, adjust as necessary
21. Leave to cure for at least 4 hours

Cutting the Motor:

22. Push mandrels out of grains and remove any remaining tape and cellophane
- a. It helps to twist and pull the tape. If some still remains, it will be easier to remove once the grains are cut. If not, it will burn away easily.
23. Cut grains
- a. Use a box knife to trim away the excess casting tube
 - b. Measure out grain length
 - c. Use the hand miter saw to cut the first grain
 - i. It helps to clamp a 2x4 or similar to the back so that each grain has a consistent length.
 - d. Repeat a-g until all grains are cut to the correct size
 - e. Sand grain faces by hand so that they are flat and to remove burrs

Gluing the Grains:

24. Make sure liner is cut to correct size - test fit into casing without grains
- a. Make sure there is good overlap with the shoulders on both the nozzle and forward closure

- b. Make sure the snap rings can be fully seated with the nozzle and closures on. Ensure there is just enough play that you can still get the pliers into the snap ring for removal.
 - c. Square ends are very helpful. Using the same jig to cut grains to cut the liner works well. If you have one end that's less square, use that as the nozzle end.
25. Insert grains into the liner and make sure closures can still fit, if not cut the top grain. Make sure to record the new length and weight.
26. Remove grains and stack them up vertically. The nozzle end should be on the table.
27. Using wide packing tape, carefully wrap the seam once with a little overlap. Try to minimize wrinkles as this will make it harder to get the liner on.
- a. Have a second person push down on the top grain while it is being taped.
28. Once the full stack has been taped together, do another dry fit of the motor and make sure everything still fits. If not, remove the appropriate amount from the top grain and record the change.
29. Put the nozzle on the table and cover with a piece of cellophane. Make sure it is large enough to cover the entire shoulder with the liner on
30. Using a paper towel, make sure the inside of the liner is free of any dust.
31. With the grain stack standing upright, begin to apply adhesive
- a. 100% silicone caulk works very well and was recommended by Scott Kormier at Loki.
 - i. Make sure you are doing this in a well ventilated area and use respirators with organic cartridges. You do not want to breathe in the fumes.
 - ii. You will have a short working time with this. It is useful to have an extra person on hand to start a timer and call out every fifteen seconds. Try to get the entire thing coated in 1-2 minutes. Any longer and you risk not being able to get the liner on.
 - b. If you choose to use something else, make sure it is NON FOAMING or MINIMAL FOAMING. Elmers Glue All Max is recommended for Aerotech motors, but we have spit casting tubes in our EX motors with it.
32. Apply glue evenly over the entire grain stack. Make sure not to get any glue on the exposed grain faces.
33. Once fully covered, slide the liner down the grain stack. Use a paper towel to wipe up extra glue that collects at the bottom. Wipe off any glue on the sides of the liner as well so that it can still fit into the casing.
34. Lay the stack horizontally and push the nozzle into the aft end. Make sure the cellophane is covering the nozzle.
35. Stand it back up and let it cure vertically at least overnight. Make sure the grains are fully pushed down and inspect for any foaming that may push the grains outwards (foaming is not an issue with silicone)
36. Once cured, you can leave the cellophane on the nozzle as this will help seal the grains from humidity. If there is too much, cut away the cellophane so that it cannot touch the o-rings.

Final Motor Assembly:

37. Prepare 4 -338 and 1 -234 silicone O-rings. Lightly grease (Super Lube) your fingers and pull the O-Rings through your fingers to lubricate them.
38. Once greased, put the O-rings onto both the nozzle and forward closure (2 each). The liner O-ring goes onto the lowest groove on the forward closure.
39. Place the liner vertically and grease it liberally. Add some grease to the inside of the forward end of the liner and insert the forward closure into the liner.
40. Grease nozzle washer and nozzle snap ring
41. Make sure snap ring grooves are clean and free of any grime or debris. Run your fingernail across the snap ring grooves to check for burrs. These can cut your orings and are important to check for. Use a small piece of sandpaper to remove these.
42. Slide casing down over the liner towards the forward closure, wipe away excess grease at the bottom.
 - a. This prevents pooling of grease at the nozzle end which can seal both ends of the liner, leading to a burnthrough.
43. Lay casing horizontally and push the nozzle past the snap ring groove. Insert the greased washer and snap ring.
44. Insert the forward snap ring.
45. Make sure to verify that both snap rings are FULLY seated. This can be done by squeezing them slightly and rotating them within the groove.

Post Firing Disassembly:

46. After firing, try to disassemble the motor while it is still warm (not hot). The grease will seize if allowed to cool, making disassembly much more difficult.
47. Remove snap rings and washer. Be careful as the graphite will retain heat much longer than other parts of the motor.
48. Using a wooden dowel (or similar) push on the forward closure until the liner slides out (this may take a decent amount of effort).
 - a. If the motor has fully cooled, take a spare closure and rubber mallet and hit the forward end of the motor. Once it is deep enough, you can use a thick dowel to transfer the force.
49. Remove orings from nozzle and forward closure. Make sure to clean O-ring and snap ring grooves.
50. Inspect casing for any bulging or discoloration. If there is any, the casing can no longer be used.
51. Clean motor casing as best as possible. Once dry, a light coat of oil or grease can help prevent corrosion. There is a decent chance you will not be able to clean everything off, a dirty casing still works fine.

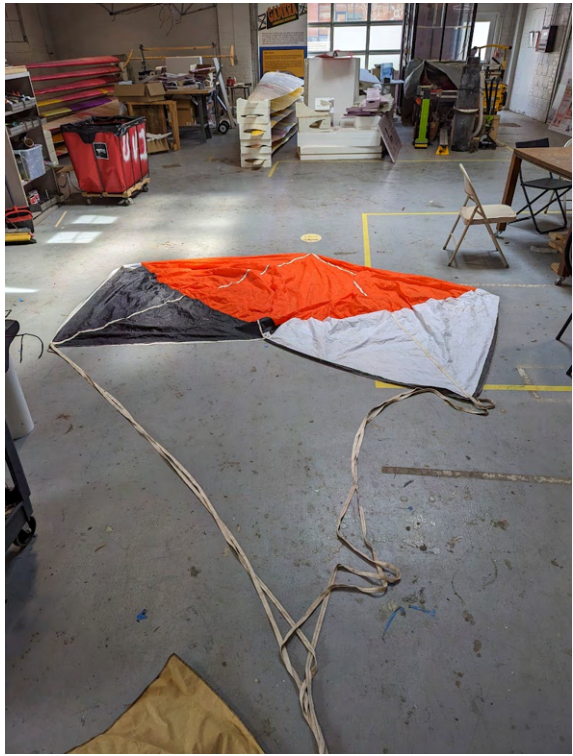
Parachute Packing Procedure

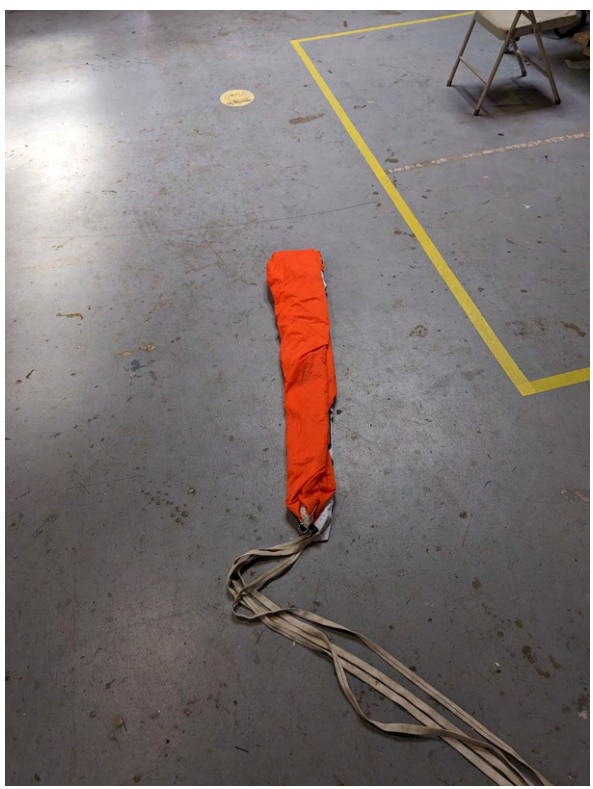
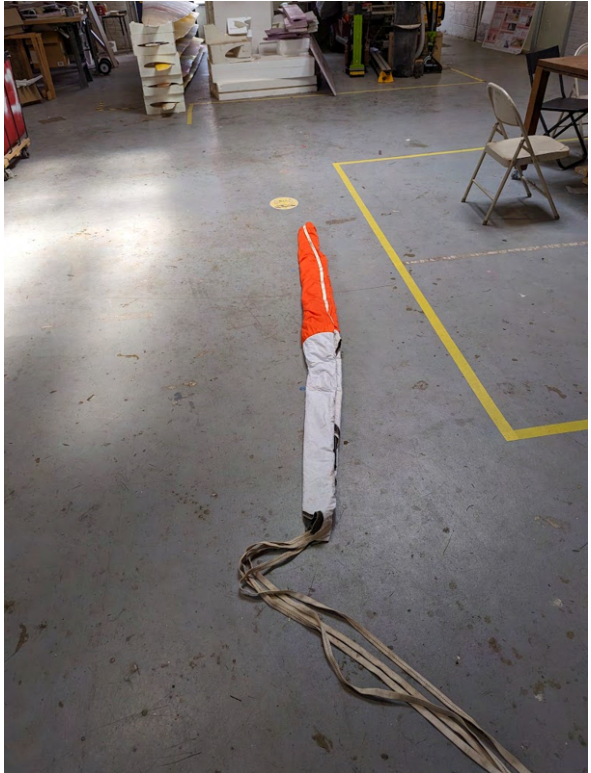
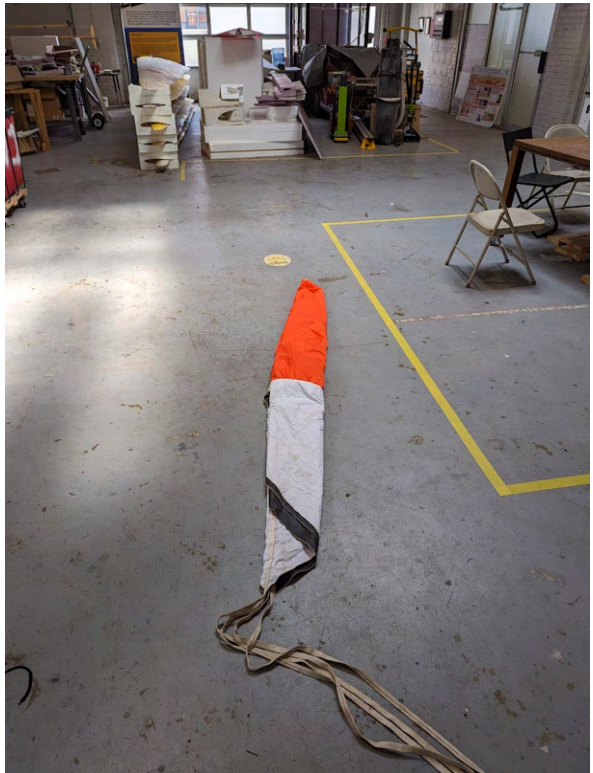
Andrew Bean

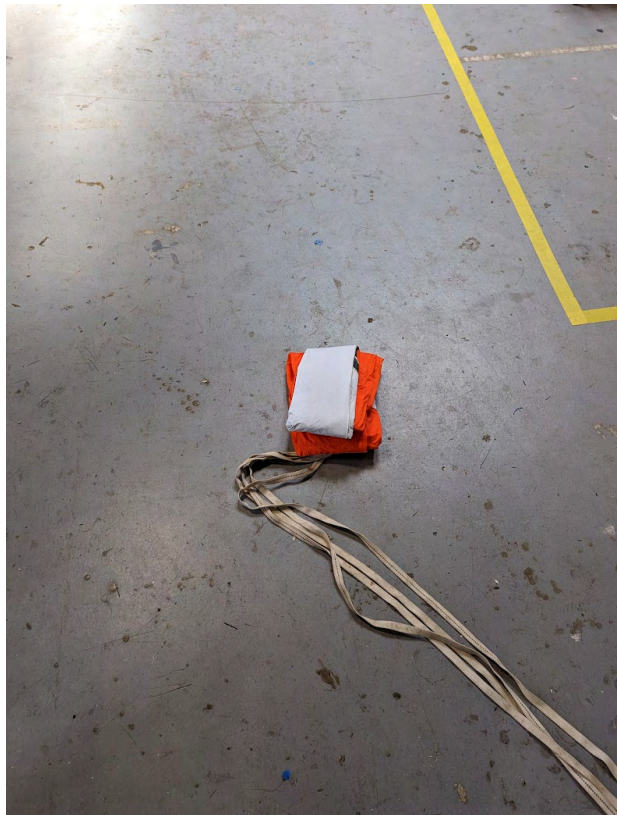
This procedure is made for packing parachutes and harnesses for the Terrapin Rocket Team competition rocket, but is applicable to many other rockets. These pictures are using a Skyangle Cert3XXL parachute with a 30"x30" nomex blanket, but works for smaller and larger parachutes.

1. Lay the parachute out on the ground and align the corners.
Make sure it is flat and completely spread out. Begin to fold it in half lengthwise, for this parachute it is done 4 times.
Make sure to push as much air out of the parachute as possible in between each fold.
2. Begin to fold the parachute widthwise. For this parachute, it is done three times. Just like the initial folds, make sure to push out the air for each fold. Once in the final folded position, it is helpful to push your knee on top to push air out and keep it folded.
3. Place the folded parachute on the corner of the nomex connected with the quicklink.
4. Lightly place the shroud lines in front of the parachute on the nomex.
5. Begin to roll the nomex over the blanket. Make sure to keep it tight and try not to let extra air into the parachute.
6. Once you are slightly less than halfway up the nomex, fold the sides into the middle, like a burrito. Make sure the sides of the nomex are angled slightly inwards or straight, not outwards.
7. Continue rolling until the end, keeping the wrap tight. It should be able to fit in the airframe. If not, repeat the process.









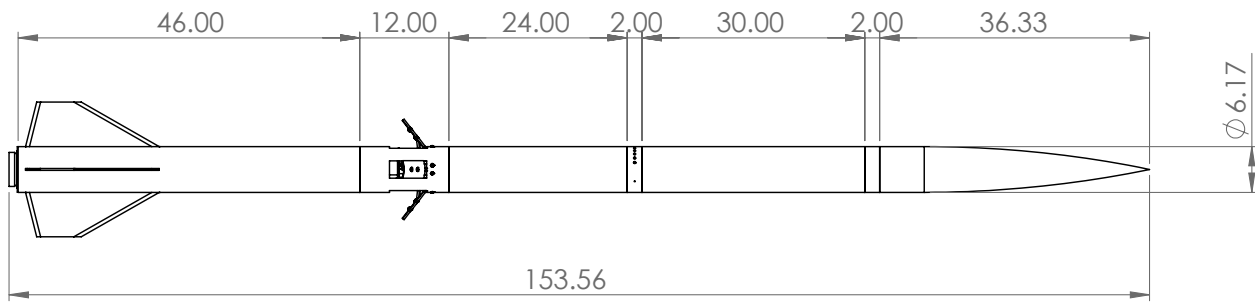


X. Appendix F: Engineering Drawings

(As found on the following page)

2

1



B

B

A

A



TERRAPIN ROCKET TEAM UNIVERSITY OF MARYLAND, COLLEGE PARK

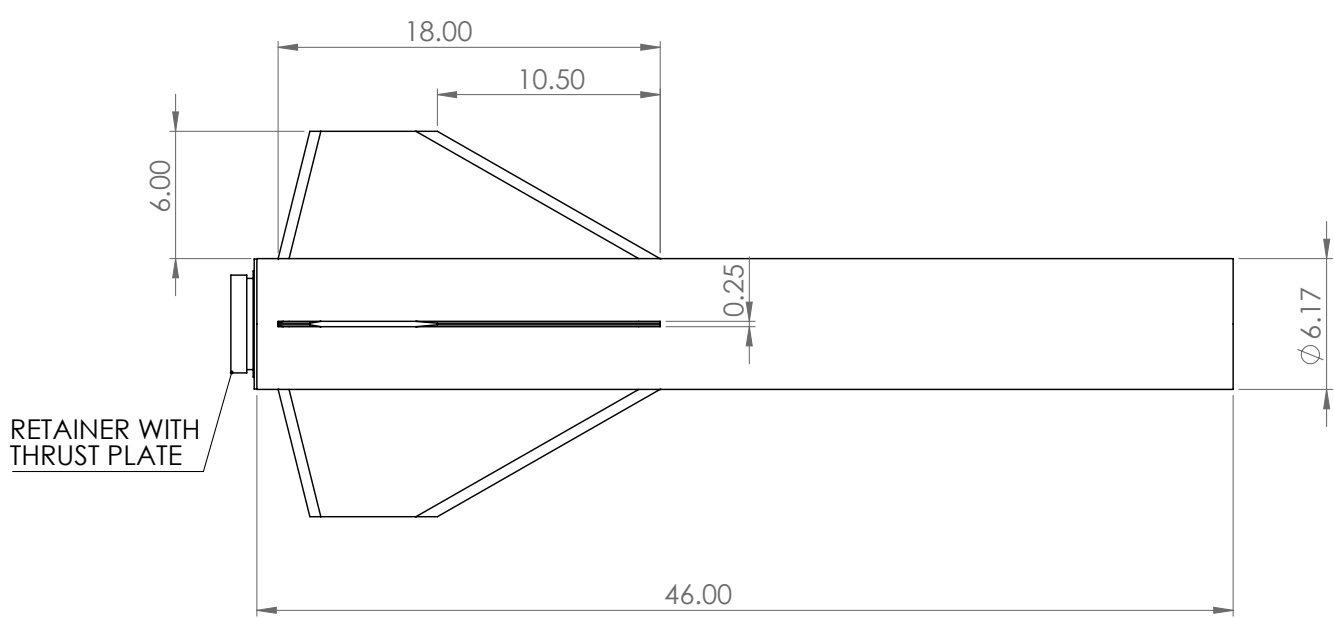
TITLE: HONU	DATE: 04/30/2024	DRAWN BY: S. MEHTA
ALL UNITS IN INCHES UNLESS STATED OTHERWISE		MATERIAL:
SCALE: 1:20		PRIMARILY CARBON FIBER, FIBERGLASS

2

1

B

B



TERRAPIN ROCKET TEAM UNIVERSITY OF MARYLAND, COLLEGE PARK

TITLE: FIN CAN

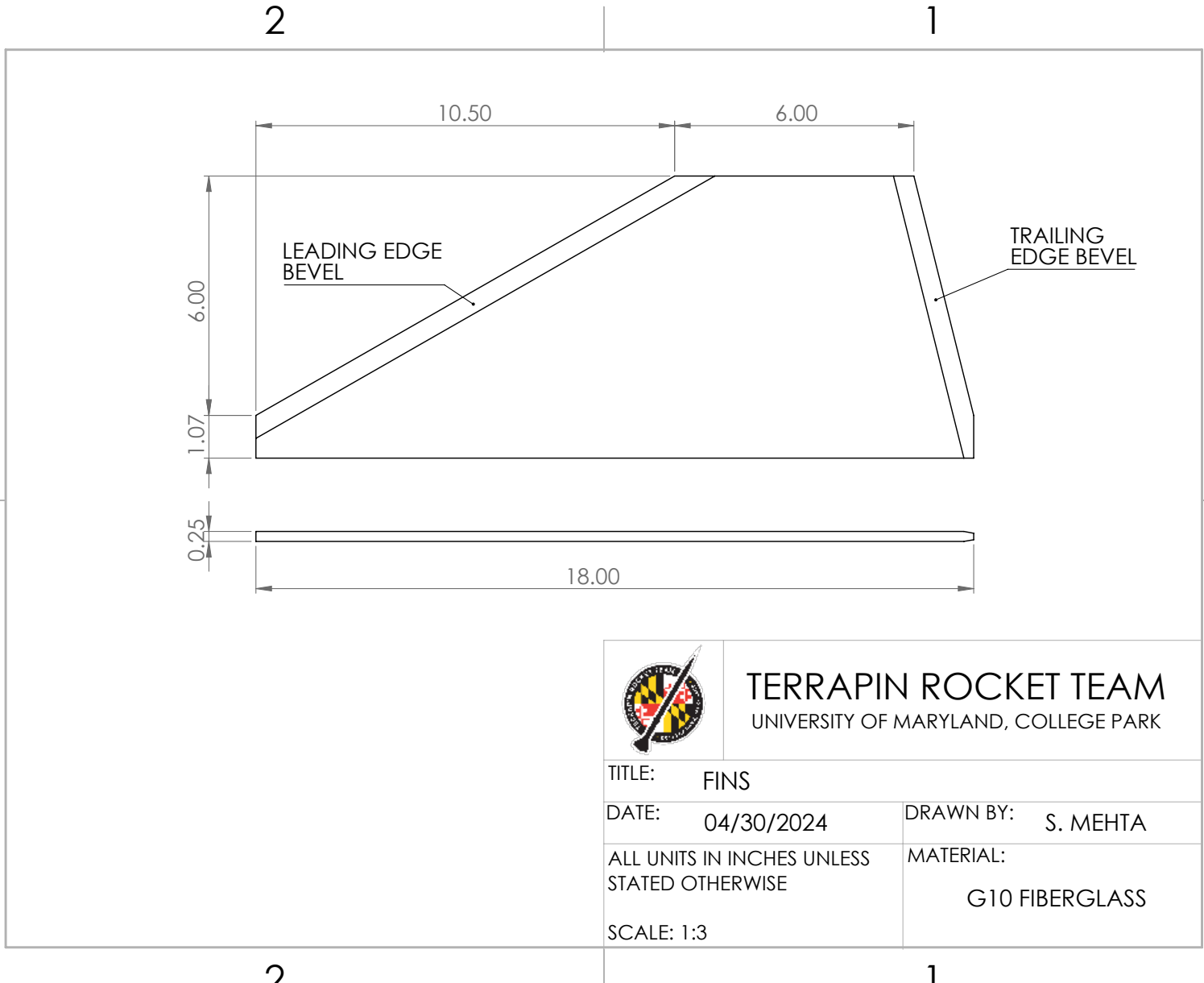
DATE: 04/30/2024

DRAWN BY: S. MEHTA

ALL UNITS IN INCHES UNLESS
STATED OTHERWISE

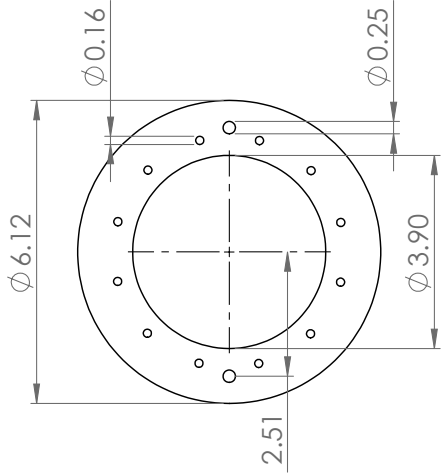
MATERIAL:
PRIMARILY CARBON FIBER,
FIBERGLASS

SCALE: 1:7

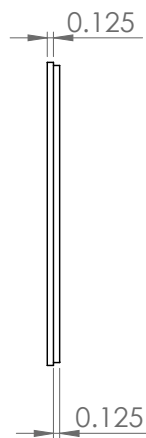


2

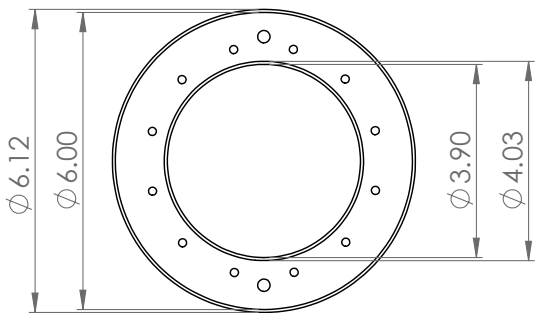
1



Bottom View



Side View



Top View



TERRAPIN ROCKET TEAM UNIVERSITY OF MARYLAND, COLLEGE PARK

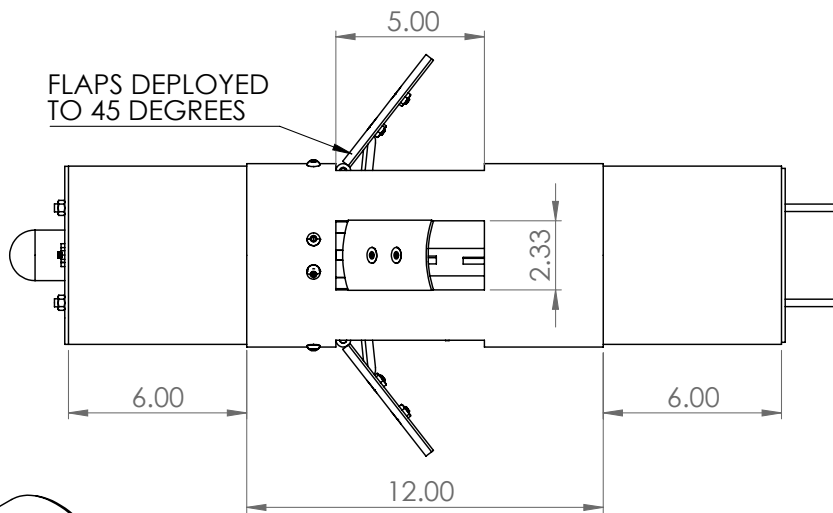
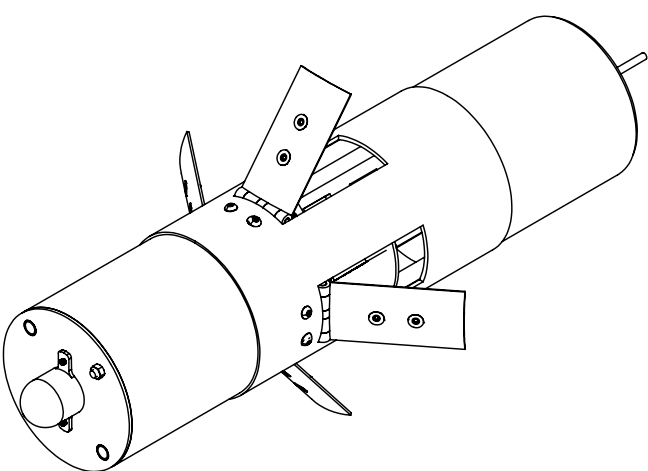
TITLE: THRUST PLATE	DATE: 04/30/2024	DRAWN BY: S. MEHTA
ALL UNITS IN INCHES UNLESS STATED OTHERWISE		MATERIAL:
SCALE: 1:3		ALUMINUM

2

1

B

B



A

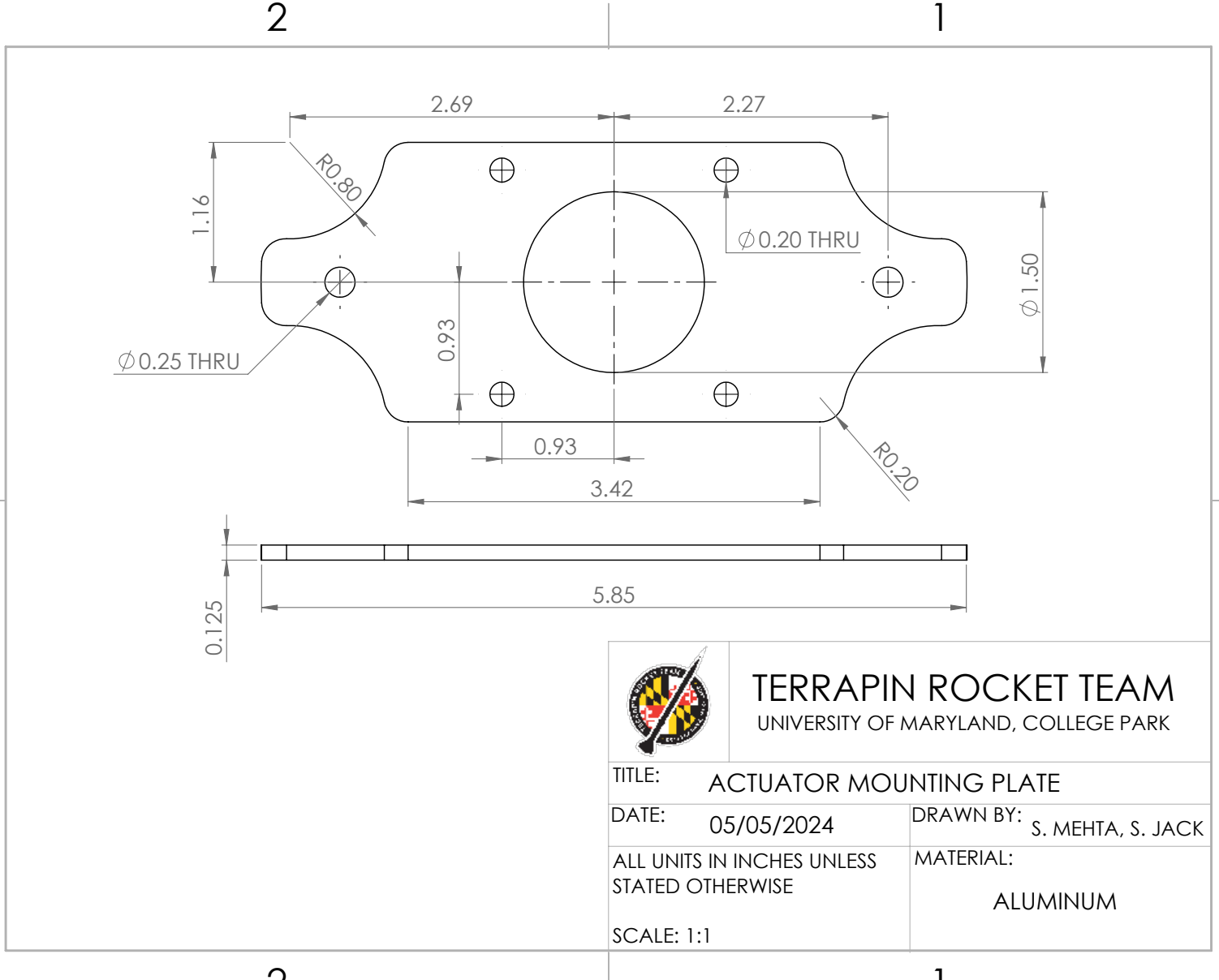
A



TERRAPIN ROCKET TEAM

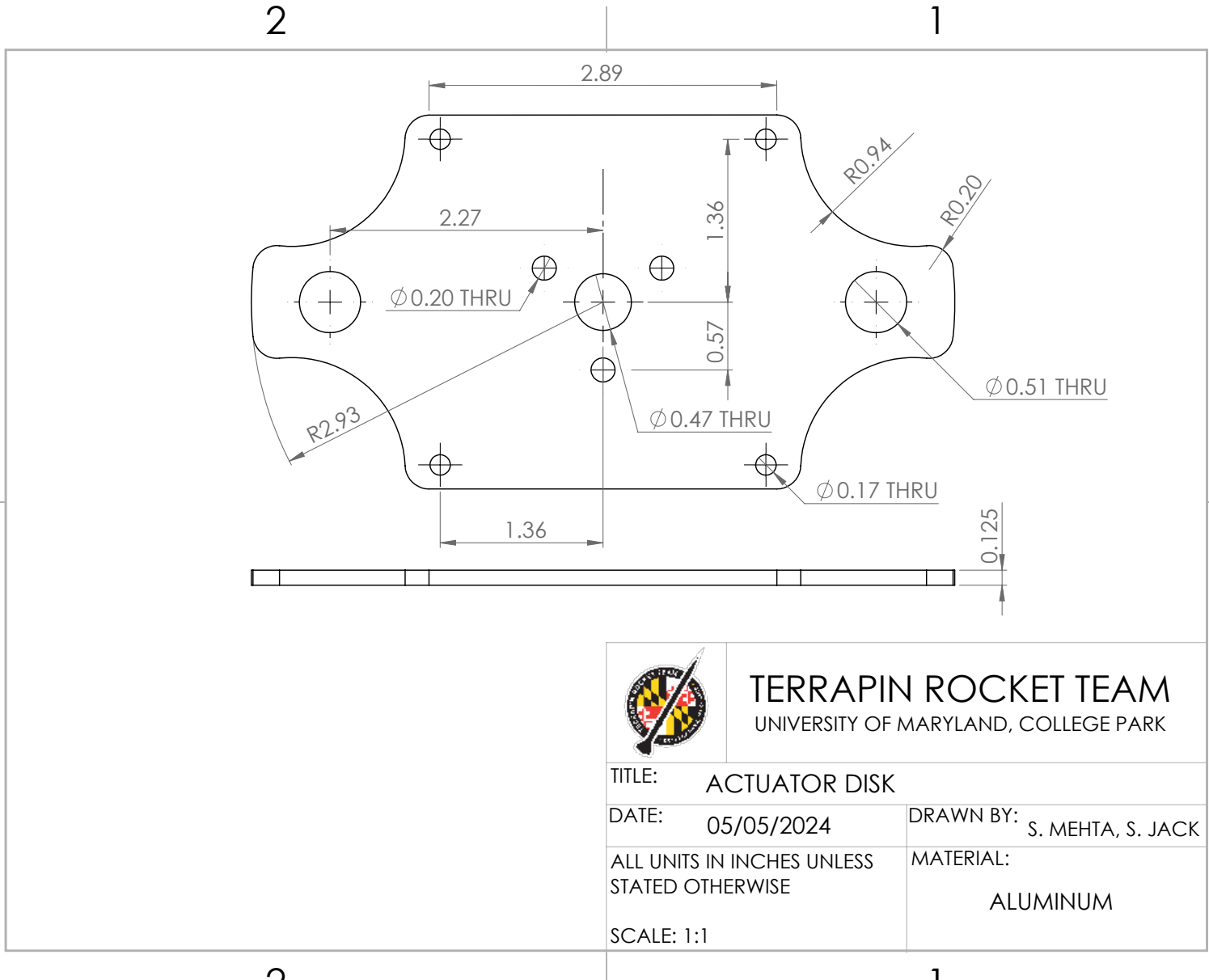
UNIVERSITY OF MARYLAND, COLLEGE PARK

TITLE: AIRBRAKE	DRAWN BY: S. MEHTA
DATE: 04/30/2024	
ALL UNITS IN INCHES UNLESS STATED OTHERWISE	MATERIAL:
SCALE: 1:5	PRIMARILY CARBON FIBER, FIBERGLASS, ALUMINUM



SOLIDWORKS Educational Product. For Instructional Use Only.

1



SOLIDWORKS Educational Product. For Instructional Use Only.

2

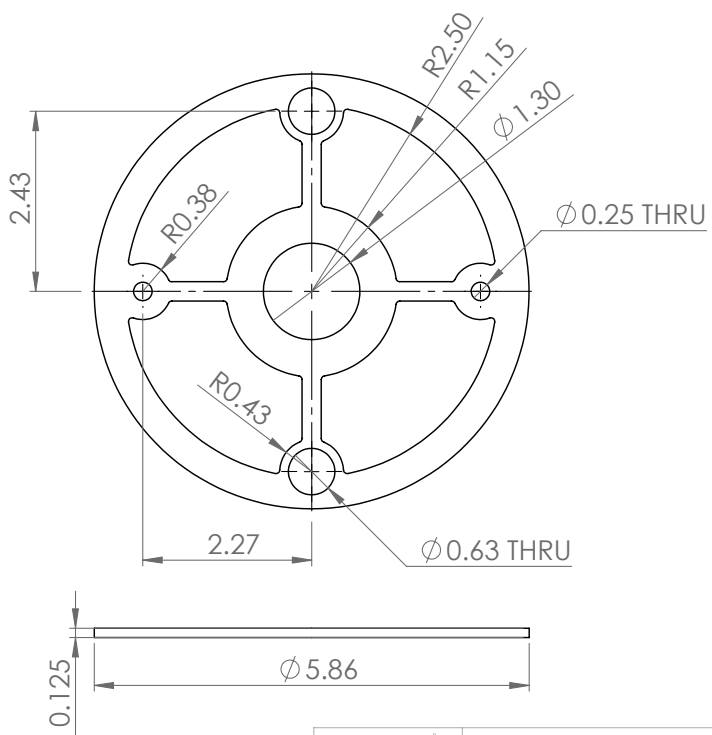
1

B

B

A

A



TERRAPIN ROCKET TEAM UNIVERSITY OF MARYLAND, COLLEGE PARK

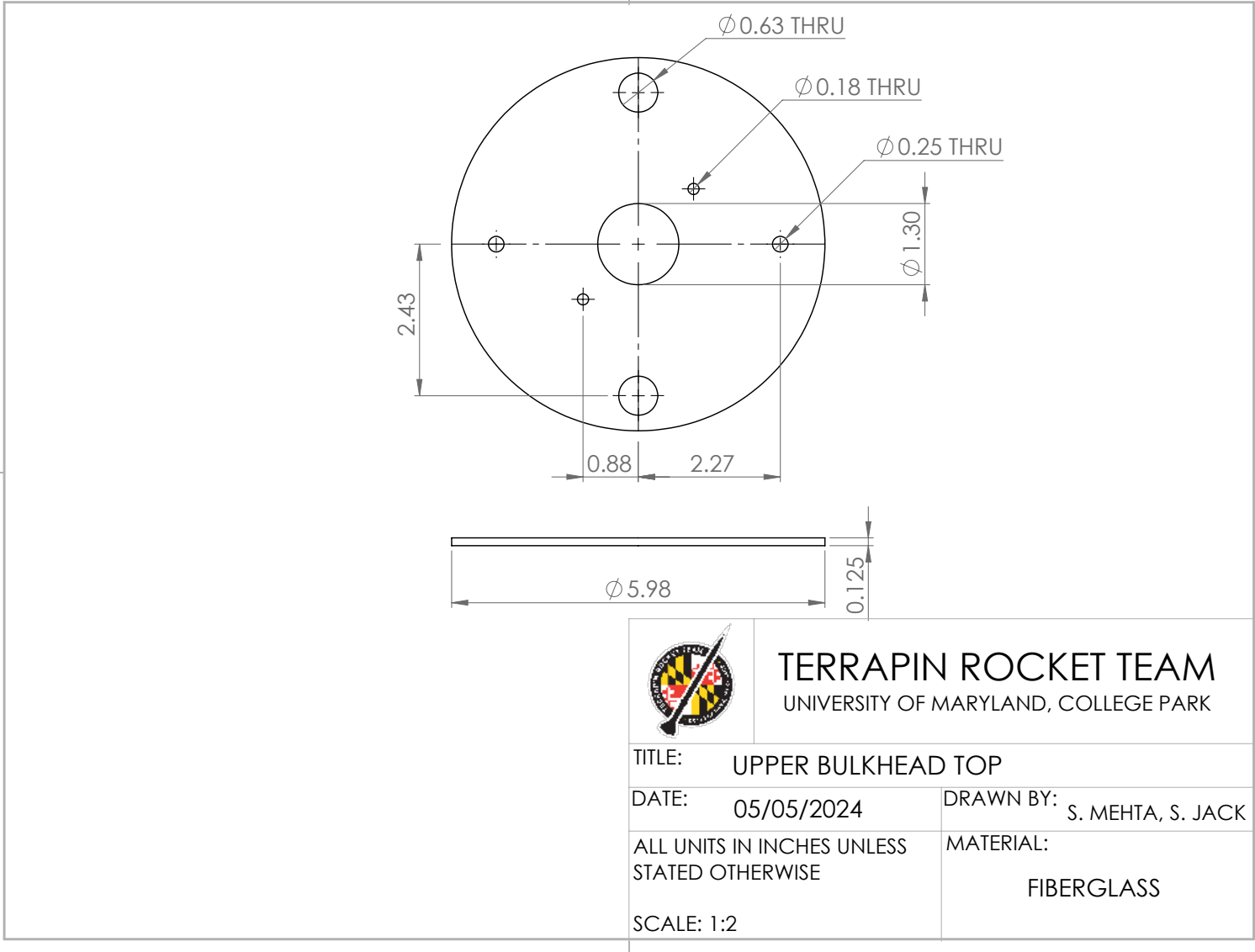
TITLE:	UPPER BULKHEAD BOTTOM	
DATE:	05/05/2024	DRAWN BY: S. MEHTA, S. JACK
ALL UNITS IN INCHES UNLESS STATED OTHERWISE		MATERIAL: FIBERGLASS
SCALE: 1:2		

2

1

B

B

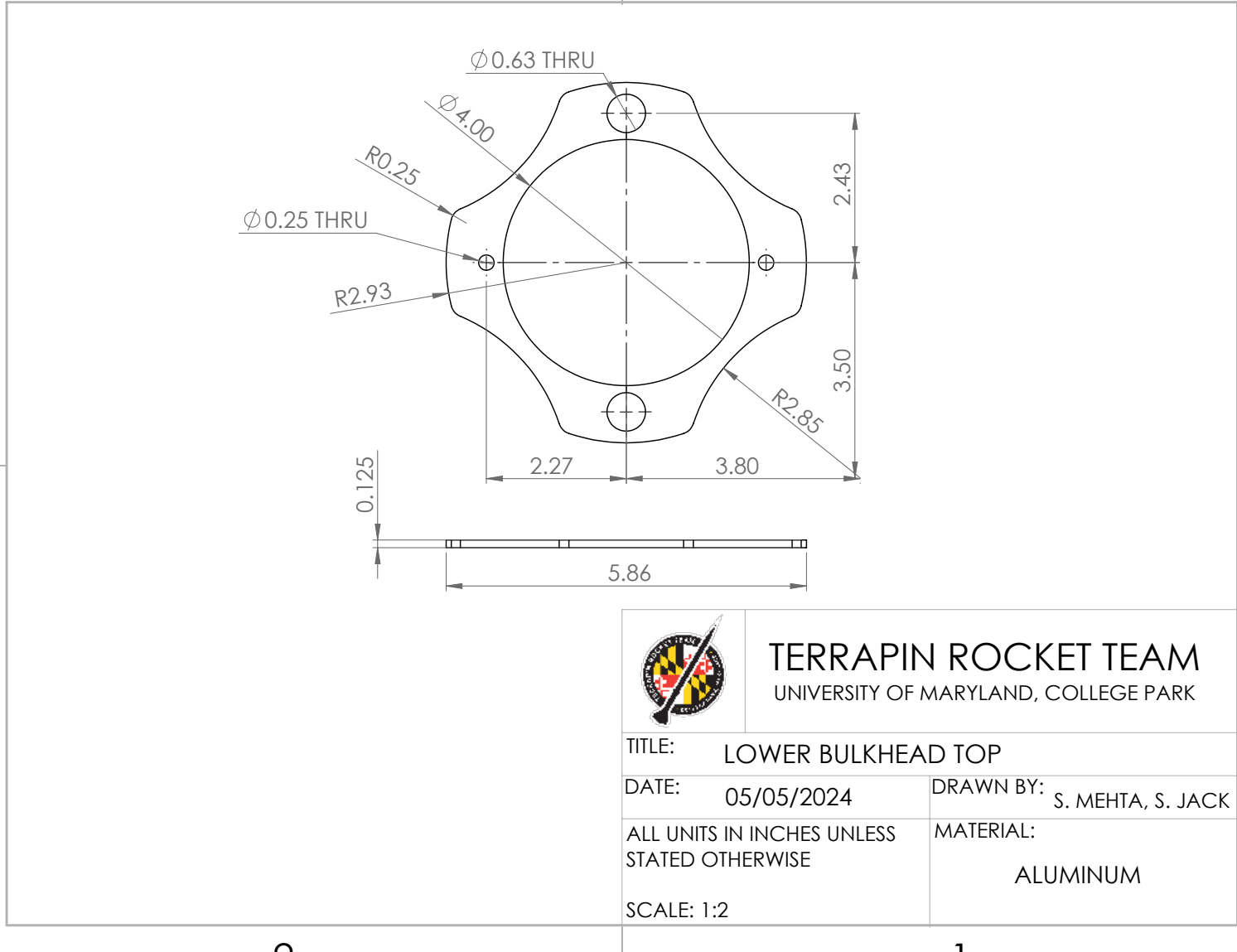


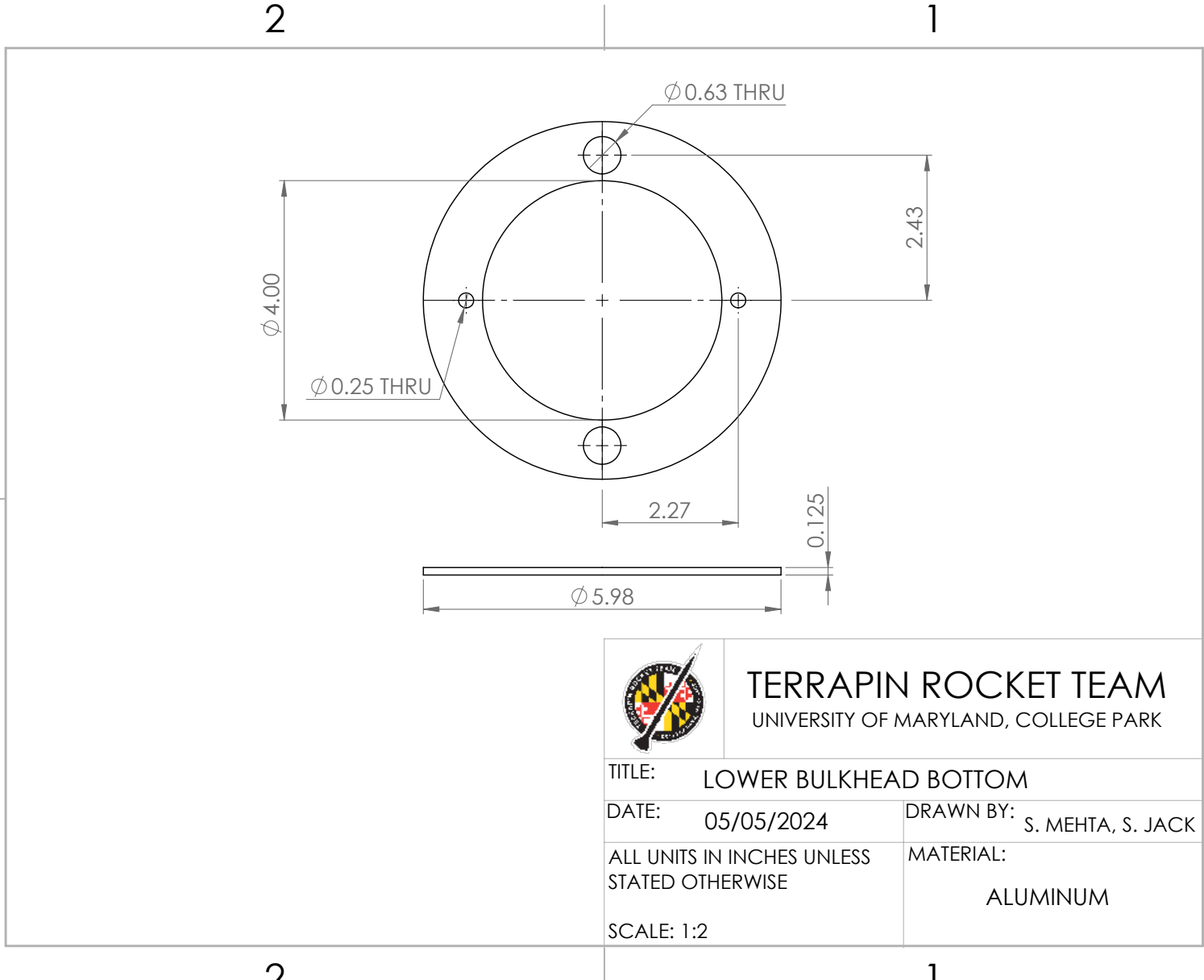
2

1

B

B



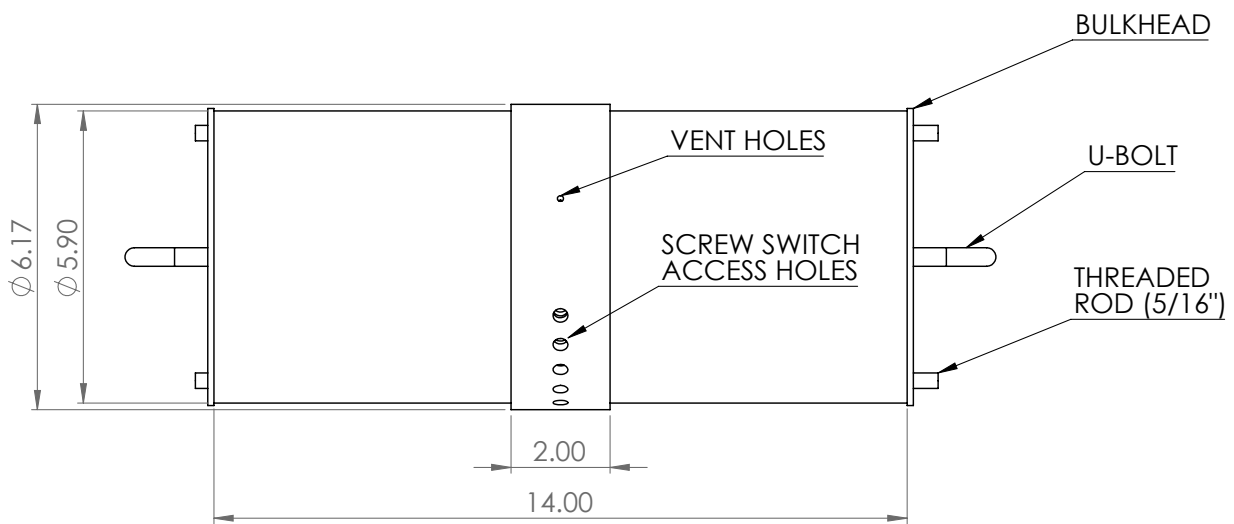


2

1

B

B

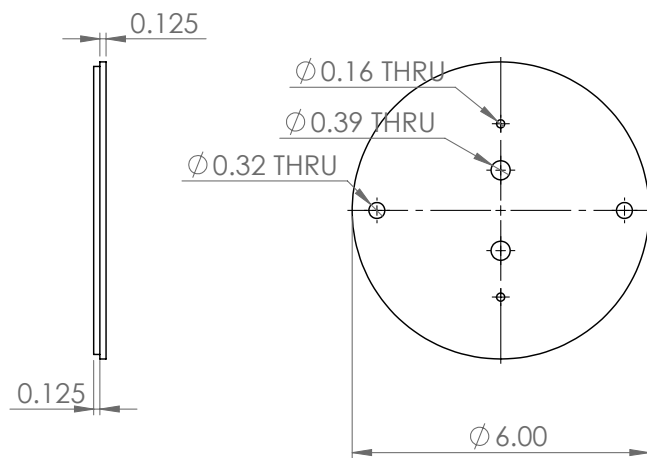
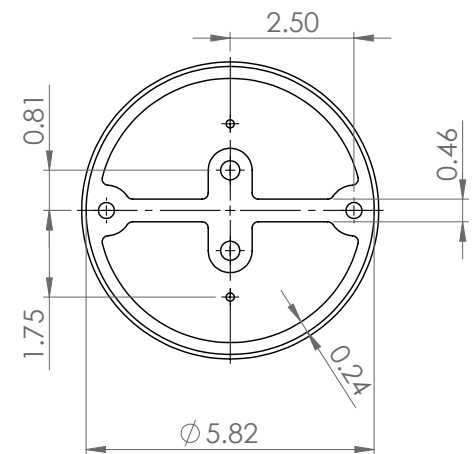


TERRAPIN ROCKET TEAM
UNIVERSITY OF MARYLAND, COLLEGE PARK

TITLE: ELECTRONICS BAY	DATE: 04/30/2024	DRAWN BY: S. MEHTA
ALL UNITS IN INCHES UNLESS STATED OTHERWISE		MATERIAL:
SCALE: 1:3		FIBERGLASS COUPLER ALUMINUM BULKHEADS

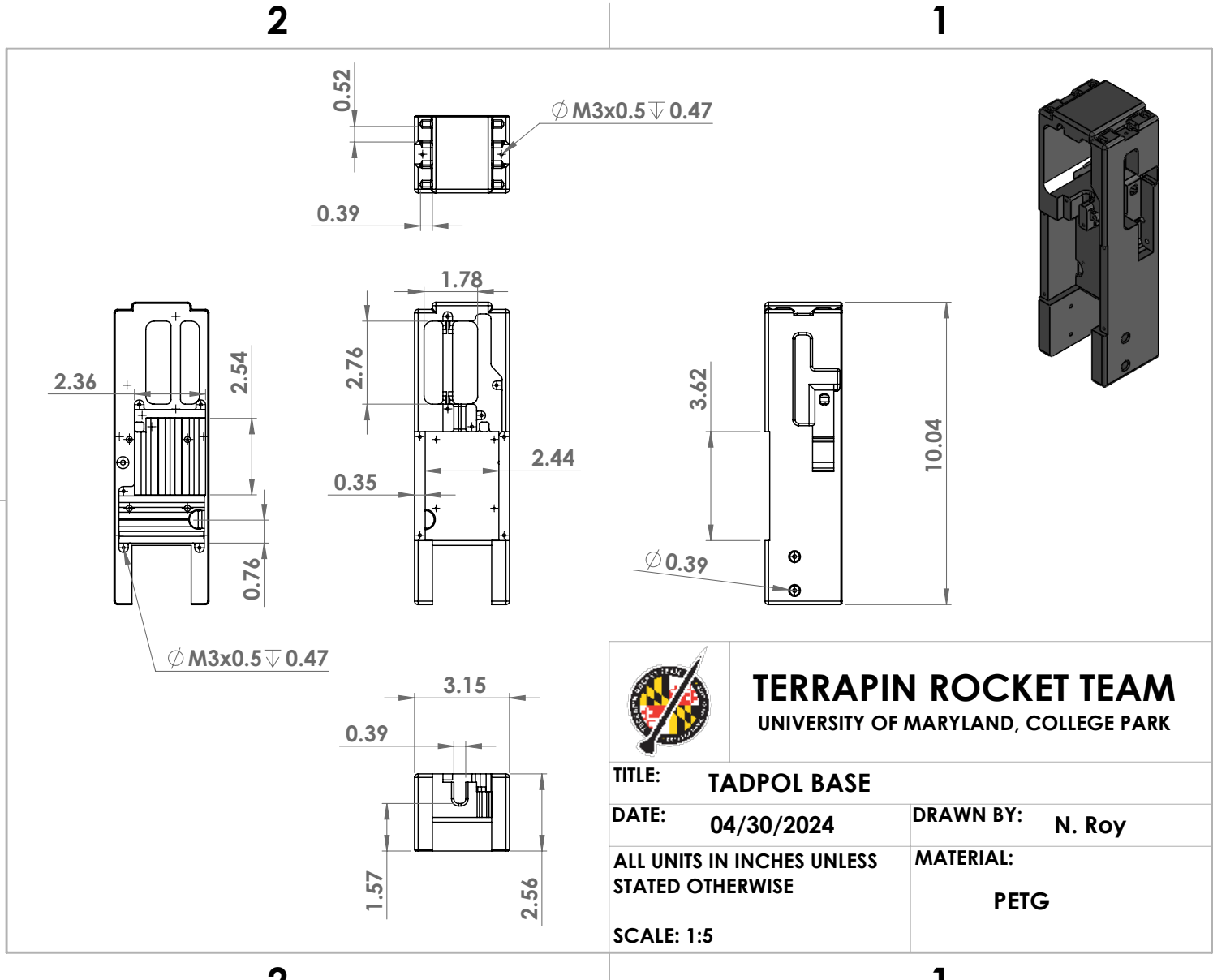
2

1



TERRAPIN ROCKET TEAM UNIVERSITY OF MARYLAND, COLLEGE PARK

TITLE: ELECTRONICS BAY BULKHEADS	
DATE: 04/30/2024	DRAWN BY: S. MEHTA
ALL UNITS IN INCHES UNLESS STATED OTHERWISE	MATERIAL: ALUMINUM
SCALE: 1:3	



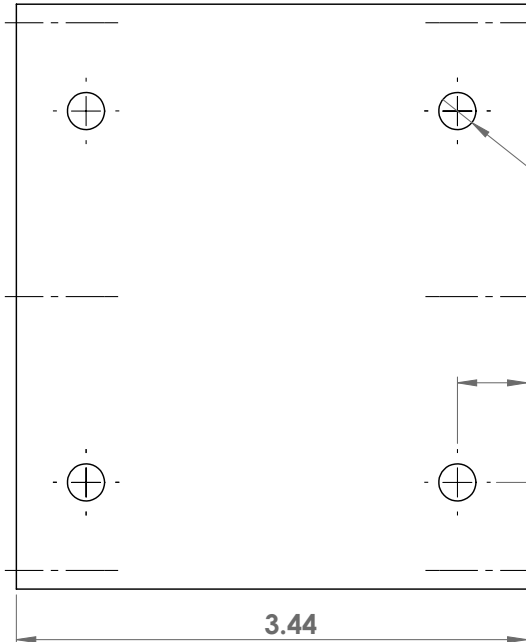
SOLIDWORKS Educational Product. For Instructional Use Only.

2

1

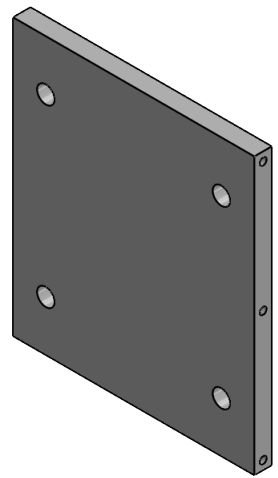
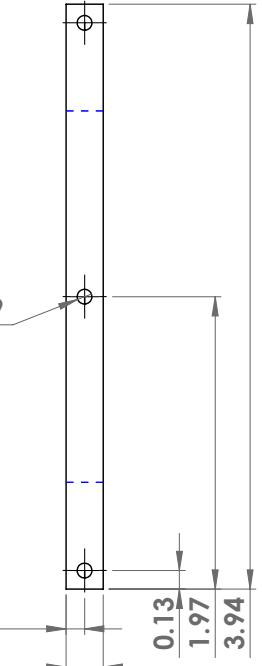
B

A

2**1****B****B***4x Ø 0.25x28 THRU**6x Ø M3x0.5 ↓ 0.59*

0.47

0.72

0.13
0.25**TERRAPIN ROCKET TEAM**
UNIVERSITY OF MARYLAND, COLLEGE PARK

TITLE: TERP TOP PLATE

DATE: 04/30/2024

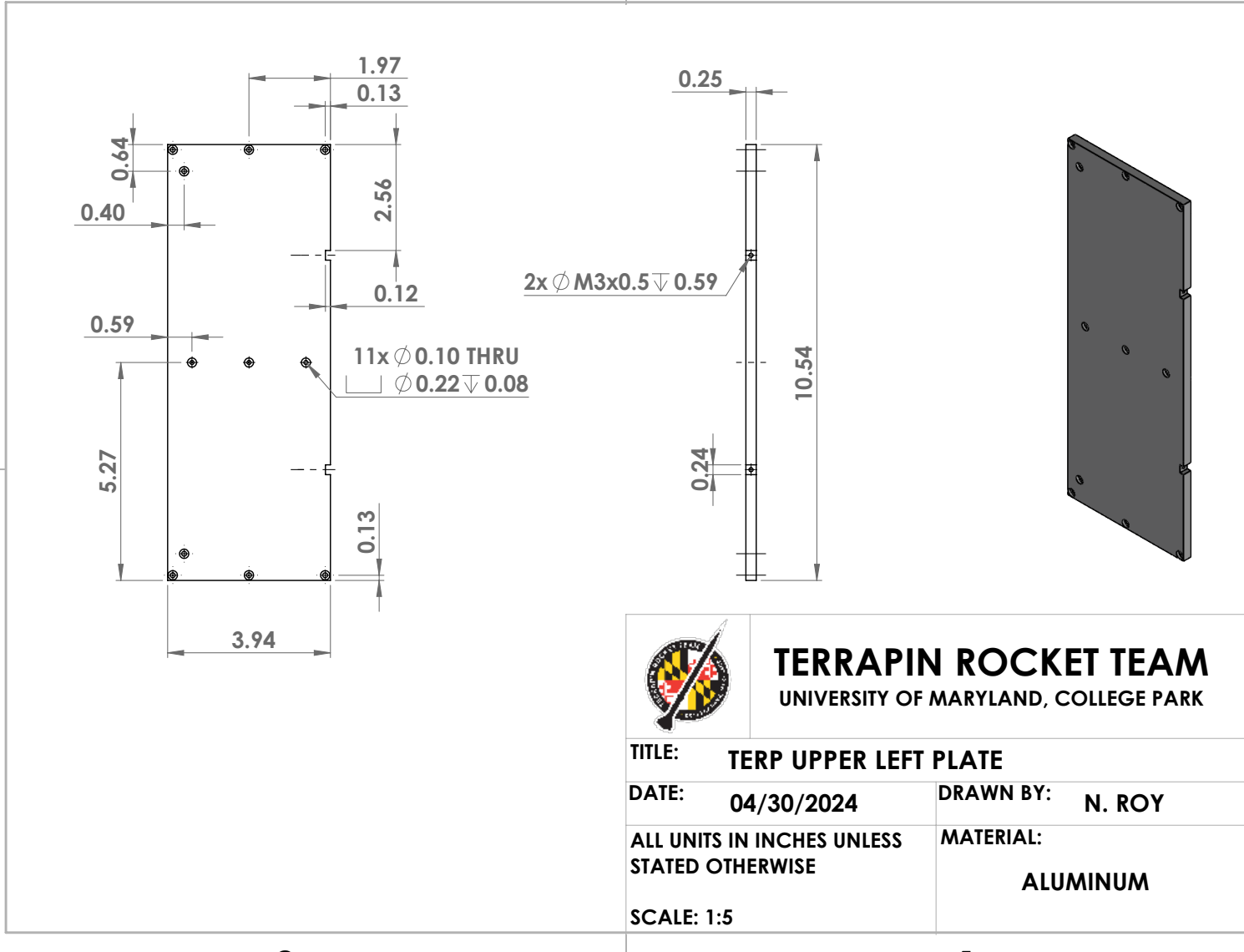
DRAWN BY: N. ROY

ALL UNITS IN INCHES UNLESS
STATED OTHERWISE

MATERIAL:

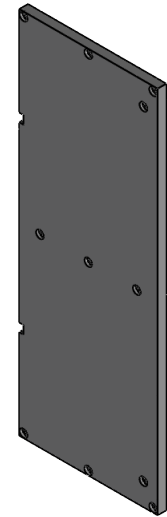
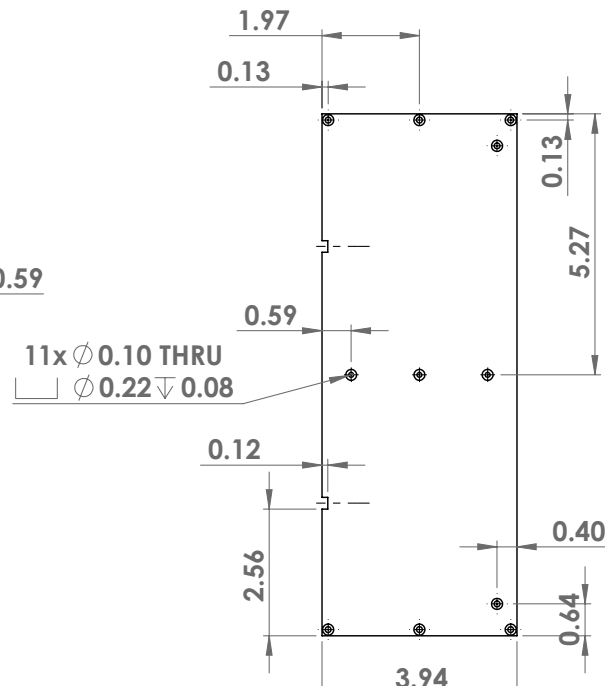
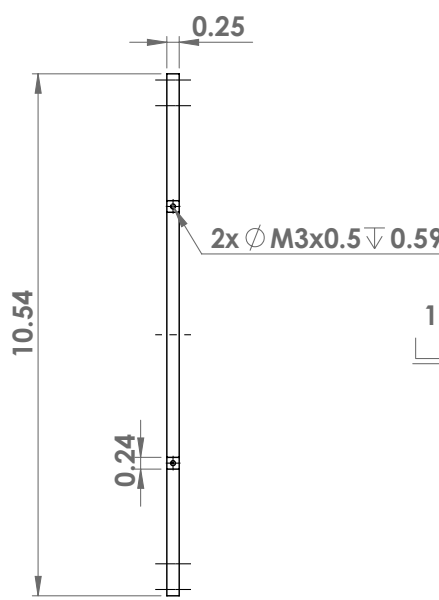
ALUMINUM

SCALE: 1:5

2**1****B****B**

SOLIDWORKS Educational Product. For Instructional Use Only.

2**1****A**

2**1****B****B**

TERRAPIN ROCKET TEAM UNIVERSITY OF MARYLAND, COLLEGE PARK

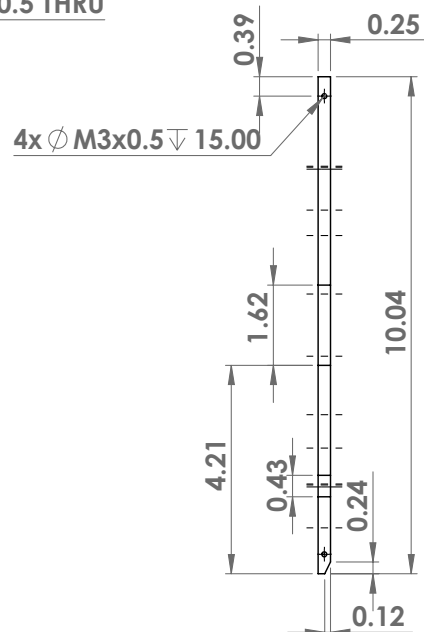
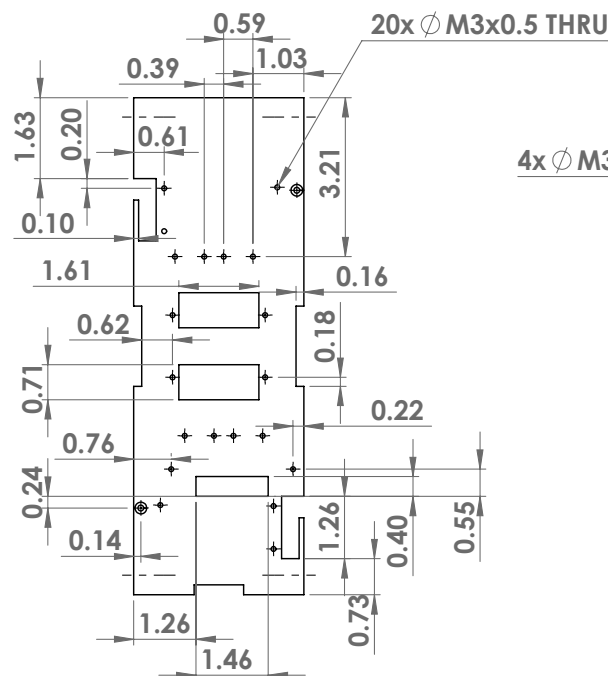
TITLE:	TERP UPPER RIGHT PLATE	
DATE:	04/30/2024	DRAWN BY: N. Roy
ALL UNITS IN INCHES UNLESS STATED OTHERWISE		MATERIAL:
SCALE: 1:5		ALUMINUM

2

1

B

B



TERRAPIN ROCKET TEAM

UNIVERSITY OF MARYLAND, COLLEGE PARK

TITLE: TERP UPPER BACK PLATE

DATE: 04/30/2024 DRAWN BY: N ROY

**ALL UNITS IN INCHES UNLESS
STATED OTHERWISE**

MATERIAL:

SCALE 1:5

SOLIDWORKS Educational Product. For Instructional Use Only.

2

1

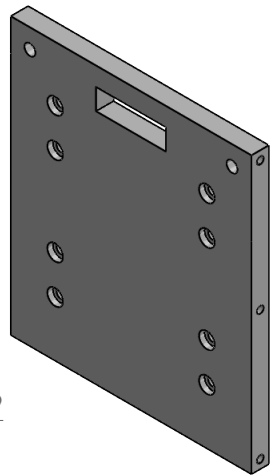
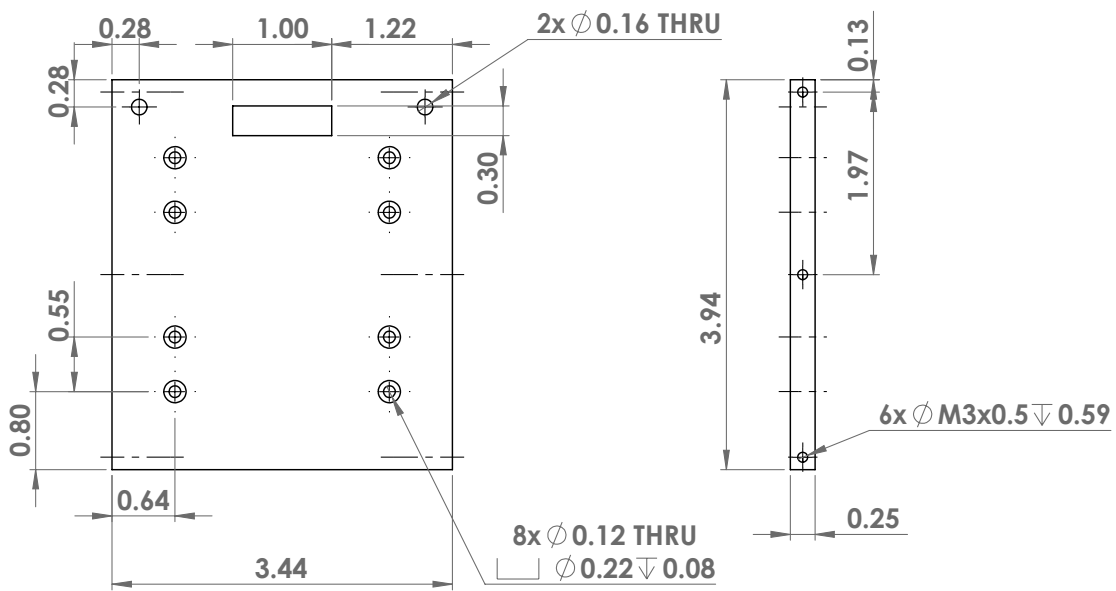


2

1

B

B



TERRAPIN ROCKET TEAM UNIVERSITY OF MARYLAND, COLLEGE PARK

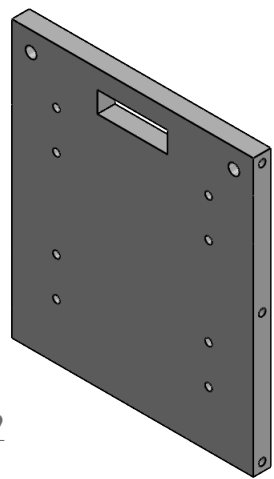
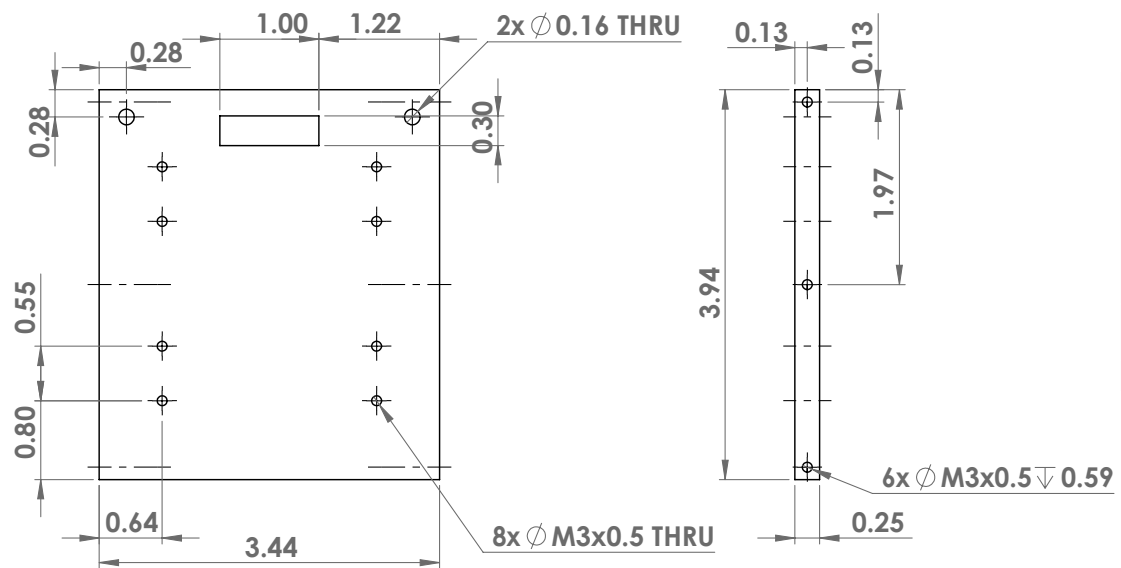
TITLE: TERP MIDDLE UPPER PLATE	DATE: 04/30/2024	DRAWN BY: N. ROY
ALL UNITS IN INCHES UNLESS STATED OTHERWISE		MATERIAL:
SCALE: 1:5		ALUMINUM

2

1

SOLIDWORKS Educational Product. For Instructional Use Only.

A

2**1****B****B**

TERRAPIN ROCKET TEAM UNIVERSITY OF MARYLAND, COLLEGE PARK

TITLE: TERP MIDDLE LOWER PLATE	DATE: 04/30/2024	DRAWN BY: N. ROY
ALL UNITS IN INCHES UNLESS STATED OTHERWISE		MATERIAL:
SCALE: 1:5		ALUMINUM

2**1**

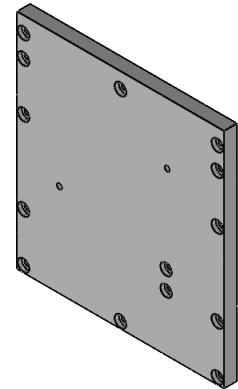
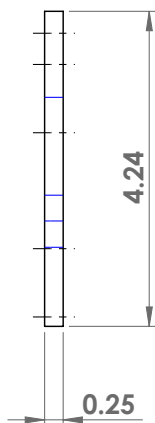
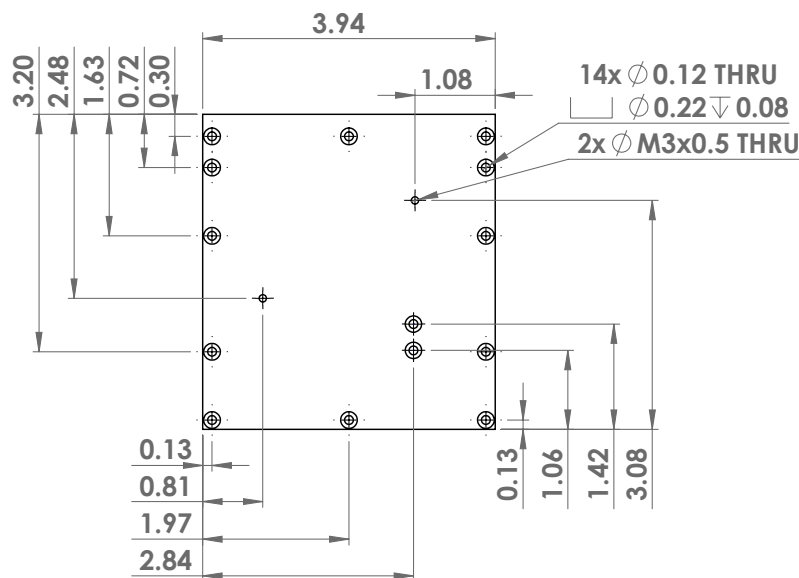
SOLIDWORKS Educational Product. For Instructional Use Only.

A**A**

2

1

B



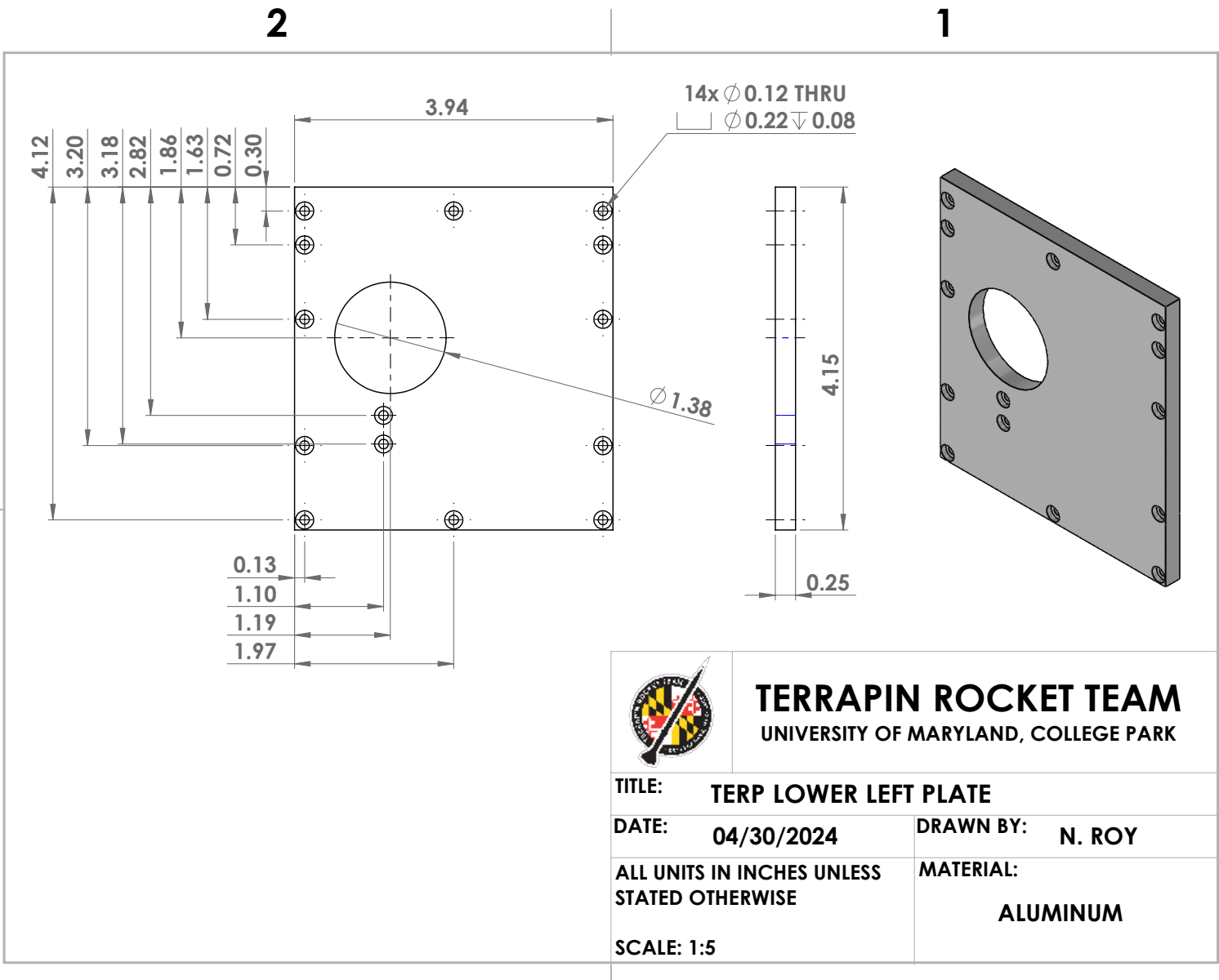
B

A

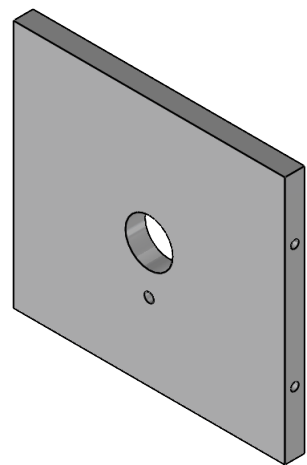
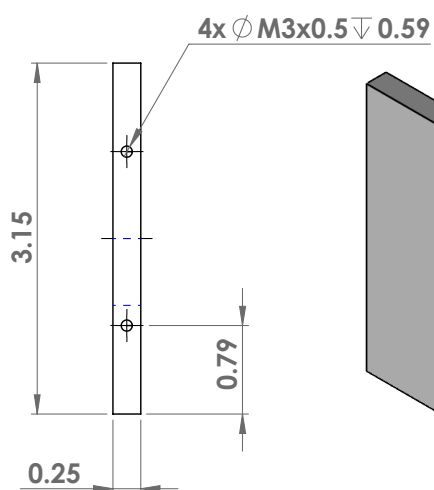
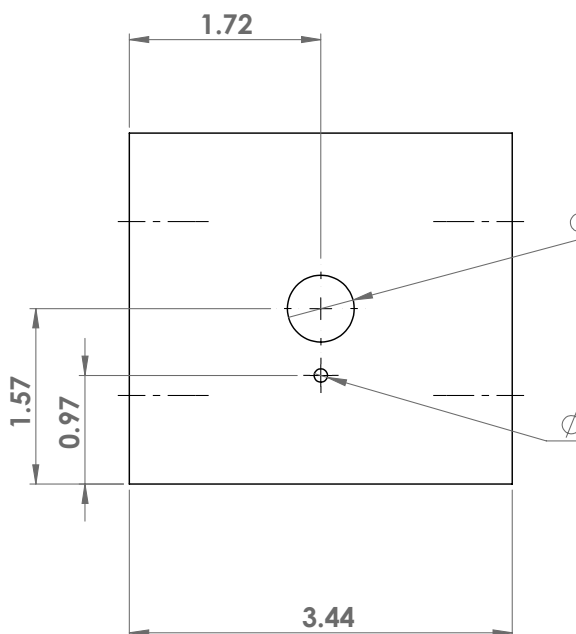


TERRAPIN ROCKET TEAM UNIVERSITY OF MARYLAND, COLLEGE PARK

TITLE: TERP LOWER RIGHT PLATE	
DATE: 04/30/2024	DRAWN BY: N. ROY
ALL UNITS IN INCHES UNLESS STATED OTHERWISE	MATERIAL: ALUMINUM
SCALE: 1:5	



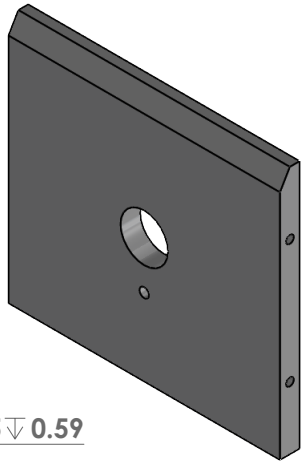
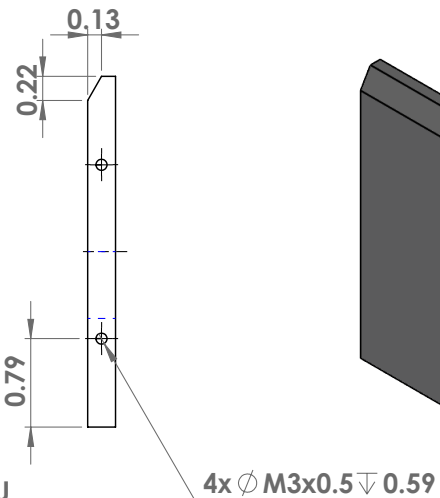
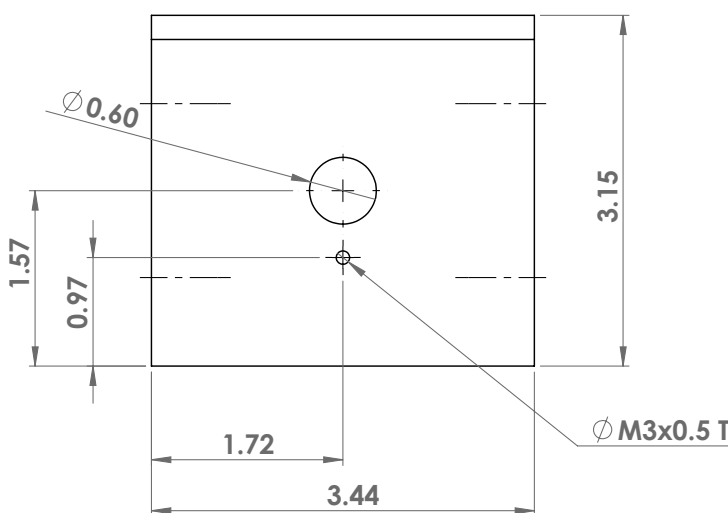
SOLIDWORKS Educational Product. For Instructional Use Only.

2**1****B****B****A**

TERRAPIN ROCKET TEAM UNIVERSITY OF MARYLAND, COLLEGE PARK

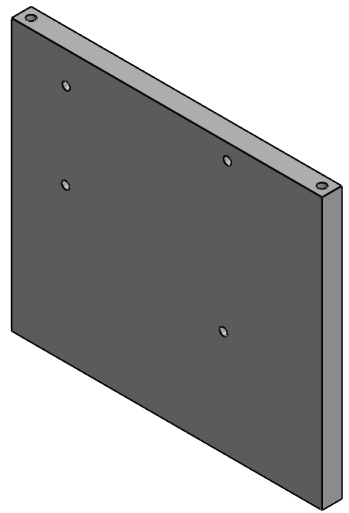
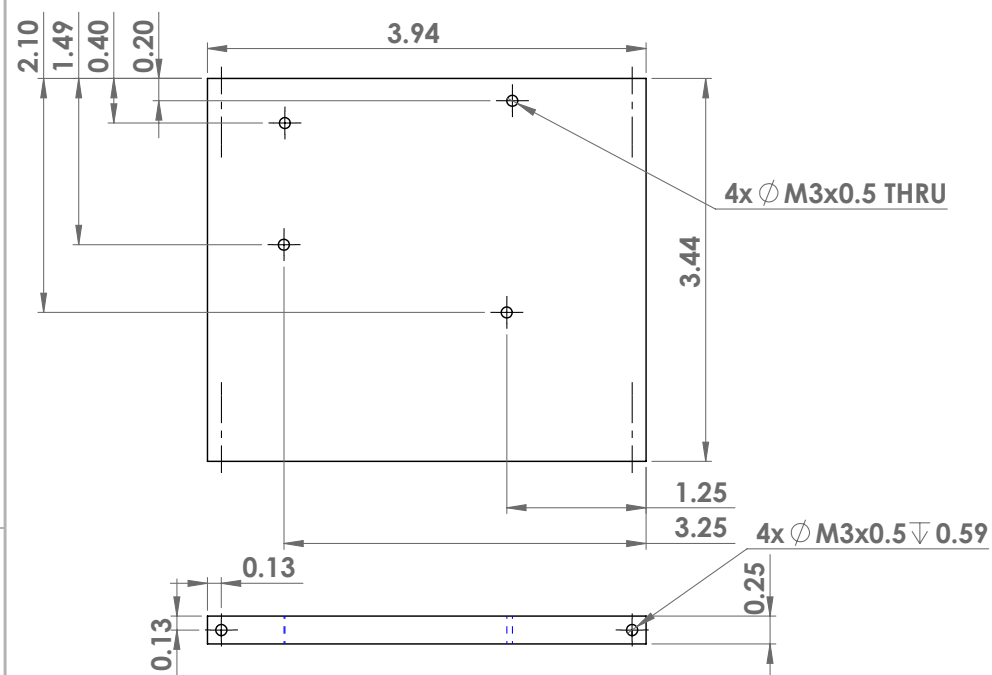
TITLE: TERP LOWER FRONT PLATE	DATE: 04/30/2024	DRAWN BY: N. ROY
ALL UNITS IN INCHES UNLESS STATED OTHERWISE	MATERIAL: ALUMINUM	
SCALE: 1:5		

A

2**1****B****B**

TERRAPIN ROCKET TEAM UNIVERSITY OF MARYLAND, COLLEGE PARK

TITLE: TERP LOWER BACK PLATE	DATE: 04/30/2024	DRAWN BY: N. ROY
ALL UNITS IN INCHES UNLESS STATED OTHERWISE		MATERIAL:
SCALE: 1:5		ALUMINUM

2**1****B****B**

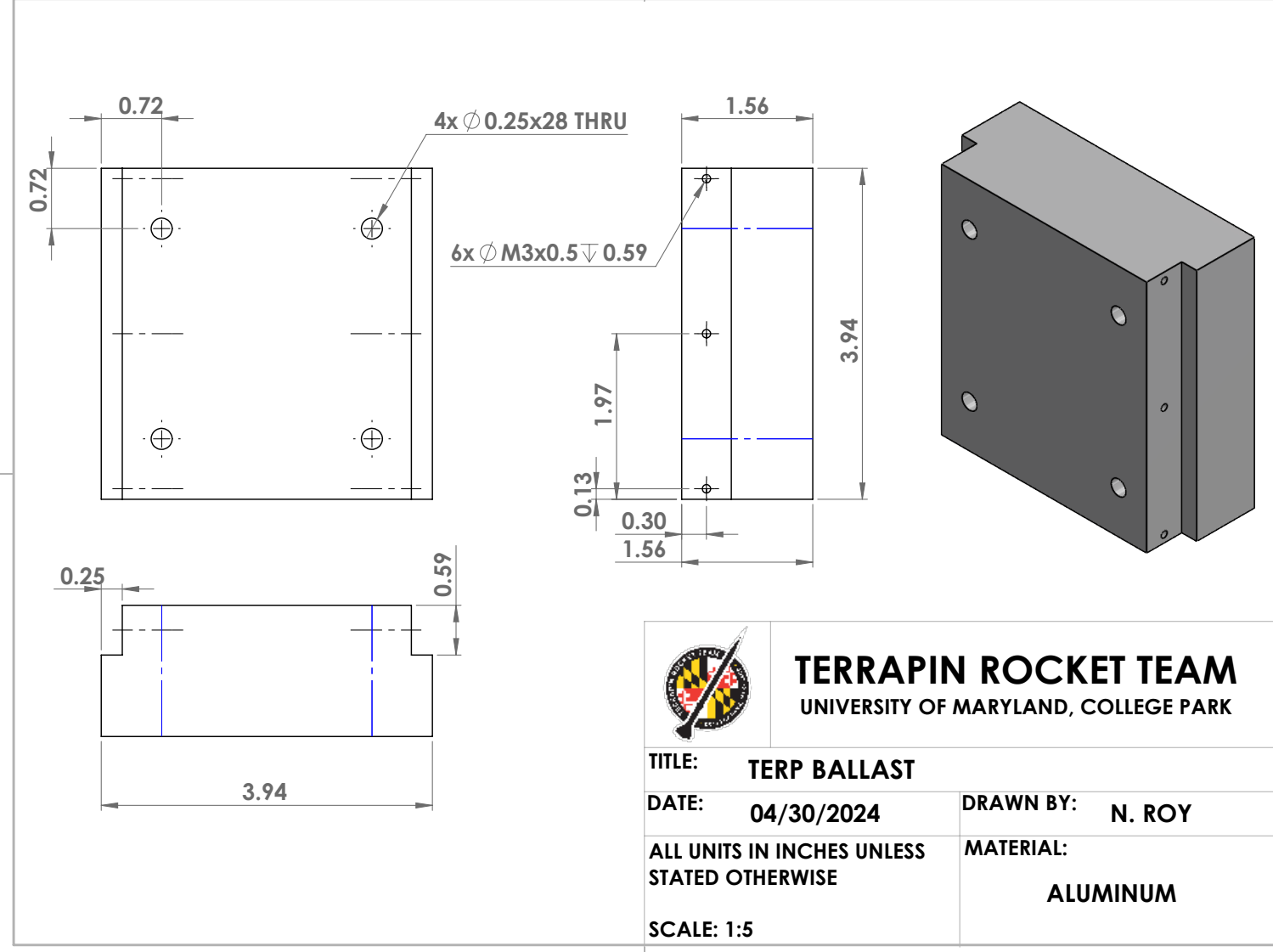
TERRAPIN ROCKET TEAM UNIVERSITY OF MARYLAND, COLLEGE PARK

TITLE: TERP BOTTOM PLATE	DATE: 04/30/2024	DRAWN BY: N. ROY
ALL UNITS IN INCHES UNLESS STATED OTHERWISE		MATERIAL:
SCALE: 1:5		ALUMINUM

2**1**

SOLIDWORKS Educational Product. For Instructional Use Only.

A**A**

2**1****B****2****1****B****A**

XI. Acknowledgements

This year would not have been possible without the support of our mentors, advisors, and donors. We have accomplished so much this year because of their generous support. First, we would like to thank our Tripoli Mentor Dennis Kingsley as well as the Maryland Delaware Rocketry Association (MDRA). Dennis has been working with us as our mentor for four years and has shared a great amount of experience with us. We'd also like to thank our solid propulsion mentor Scott Szympruch. He has provided lots of valuable advice, mixing facilities, and testing equipment for the team. MDRA has been our primary launch site and our test flights would not have been possible without such a great organization and members close by. We'd also like to thank our faculty advisor Dr. Christopher Cadou as well as Dr. Michael Kio, Bryce Liposky and Ezra Bregin for their guidance throughout the year and helpful reviews of our project.

Additionally, we would like to thank our generous donors and sponsors this year. The A. James Clark School of Engineering, The University of Maryland Student Government Association, Maryland Space Grant Consortium, Boeing, Northrop Grumman, Blue Origin, ST Engineering MRAS, VectorNav, Aerojet Rocketdyne, Kratos Space and Missile Defense Systems Inc., and LaunchUMD supporters have all been critical in our successes this year.



XII. References

- [1] Rogers, C., “The Solid Rocket Motor - Part 6 Erosive Burning Design Criteria for High Power and Experimental/Amateur Solid Rocket Motors,” 2005, pp. 33–34. URL <http://rasaero.com/dloads/Erosive%20Burning%20Design%20Criteria.pdf>.
- [2] Becker, A., “Kalman Filter Tutorial,” , 2023. URL <https://www.kalmanfilter.net/multiExamples.html>.